Proceedings of the 4th International Conference on Civil Engineering for Sustainable Development (ICCESD 2018), 9~11 February 2018, KUET, Khulna, Bangladesh (ISBN-978-984-34-3502-6)

NUMERICAL ANALYSIS OF RESPONSE OF PLATE ANCHOR UNDER COMBINED LOADING

Md. Al-Amin[1], Md. Shafiqul Islam[2], Mst. Rahanuma Tajnin[3], Grytan Sarkar[4] and Md. *Rokonuzzaman*[5]

[1]Undergraduate Student, Dept. of Civil Engineering, Khulna University of Engineering &Technology, Khulna, Bangladesh, e-mail: ashik.ghs@gmail.com
[2]Assistant Professor, Dept. of Civil Engineering, Khulna University of Engineering & Technology, Khulna, Bangladesh, e-mail: shafiq0837@gmail.com
[3]Assistant Engineer, Public Works Department (PWD), Division-2, Khulna, Bangladesh, e-mail: rtajnin@gmail.com
[4]Assistant Professor, Dept. of Civil Engineering, Khulna University of Engineering & Technology, Khulna-9203, Bangladesh, e-mail: grytan_ce04@yahoo.com
[5] Professor, Dept. of Civil Engineering, Khulna University of Engineering & Technology, Khulna, Bangladesh, e-mail: rokoncekuet@yahoo.com

ABSTRACT

Drag anchor is an economical foundation option, although its installation procedure is not understood properly. For this reason, it is necessary to define failure envelope and failure mechanism of anchor soil under combined loading. The present study focuses on the capacity of drag anchor under uni-directional vertical, horizontal and moment loading in homogeneous clay deposit. A model of deeply embedded strip anchor exposed to combined loading is analyzed by two-dimensional finite element analysis (FEA) based on swipe and probe test procedure. Numerical result reveals that the failure envelope of swipe test procedure lie inside the true failure envelope of probe test under combined loading. For normal loads lower than 45% of ultimate vertical load, parallel loading as well as moment loading, dominate the failure mechanism of the plate anchor. Moreover, in this study, some remarkable soil failure mechanisms under combined loading are produced.

Keywords: *Finite element analyses (FEA), drag anchor, combined loading and failure envelope.*

1. INTRODUCTION

Offshore structure and their foundation system are usually subjected to large vertical, horizontal load and overturning moment due to the movement of wind, wave and many other environmental loadings. Floating structures anchored to the seabed using catenary and taut-wire mooring systems are generally more technically feasible and cost effective than gravity-based platforms in these deep-water environments. Drag anchor is used widely due to its simplicity to design high economic value, low cost of installation and high pullout capacity relative to the low anchor weight in soft clay (Kim 2007). Hence, the anchor final position is important because it determine the anchor holding capacity. But, there are lot of vagueness of the anchor position during and after the installation and still a major problem for anchor design. Therefore, it is necessary and important to understand the anchor behaviour correctly during installation. The method using yield envelopes to characterize the anchor behaviour under combined loading for installation prediction is promising. This method has been used for the installation behaviour prediction of the drag embedment anchor (DEA) and vertical loaded anchor (M P O'Neill et al., 2003;Elkhatib and Randolph, 2005; Yang, et al., 2010) the prediction of keying process of suction embedded plate anchor (SEPLA) and OMNI-MAX anchor (Aubeny et al., 2008;Yang et al., 2011;Cassidy et al. 2012;Tian et al.,2012; Wei et al., 2015; Liu et al., 2016).

Due to the complex geometry of practical drag anchors, studies on drag anchors usually start from anchor plate with simplified geometry, which is similar to plate anchor. The majority of the earlier studies have focused on the plate anchor uplift capacity, which is based on analytical solutions or experimental data. Numerical studies have been conducted by (Rowe, 1978;Merifield et al., 2003;Song and Hu, 2005;Song et al., 2008 and Wang et al., 2009). However, these studies are focused only the vertical pullout capacities of plate anchor. But, the anchor plate subjected to combined vertical, horizontal and moment loading. In order to recognize the behaviour anchor plate under combined loading and analyse the failure pattern, it is essential to recognize the anchor behaviour under combined vertical, horizontal and moment loading or combination of all three. The controlling values of anchor capacity under the three uni-directional loadings with deep localized failure were studied by O ' Neill et al. (2003) , Elkhatib and Randolph (2005), Elkhatib (2006) and Wu et al. (2017).

In order to solve the above problems and to understand the correct failure mechanism, the present study emphases on the drag anchor capacity under pure vertical, horizontal and moment loading and combination of any of two loadings. The trajectory prediction using yield envelopes in current studies assumed deep anchor behaviour for the whole drag process by using yield envelope for deep anchor behaviour. Detailed analyses of swipe and probe tests are conducted to understand the behaviour of anchor under combined loading. In order to understand the failure mechanism in horizontal-moment loadings load-displacement probe tests are conducted.

2. METHODOLOGY

2.1 Finite Element Model

The objectives of this study are to improve the understanding of the fundamental mechanism of continuous pullout of horizontal anchor under combined loading condition of V, H and M. In this study, the two-dimensional finite element analysis (FEA) is carried out by commercial software ABAQUS. The strip plate anchor of width B is assumed to be deeply embedded, with localized plastic flow forming around the plate anchor and not extending to the surface, resulting in capacity factors that are not affected by overburden and soil weight (Song et al., 2008; Wang et al. 2010). Conventional small strain analysis is carried out to determine the pullout capacity of embedded anchor, where the anchor movement is limited to 0.1 times to the anchor length. The contact between the anchor and the soil is assumed to be fully bonded. In order to ensure the fully bonded condition, the interfaces between the anchor plate and soil domains are defined as (i) tangential behaviour and (ii) normal behaviour. In tangential behaviour is assumed to be rough and normal behaviour is defined as hard contact with no separation between soil and anchor when tension develops. An elastic perfectly plastic associative Mohr-Coulomb material model is used for purely cohesive soil with cohesion c=10 kPa, modulus of elasticity E=10 Mpa and the Poisson's ratio 0.49. The anchor is modelled as rigid body with young's modulus 10^7 times that of soil and Poisson's ratio 0.15 (Andersen et al., 2003). The FE analyses are based on 4-noded linear hybrid elements of type CPE4H. Figure 1 presents a typical two-dimensional finite-element mesh for a strip plate of width B=0.5m and thickness t=L/7=0.071m. The soil domain is extended to 20B in horizontal and vertical directions, respectively. Zero-displacement boundary conditions are applied to prevent out-of-plane displacements of the vertical boundaries and the base of the mesh is fixed in both horizontal and vertical coordinate directions. To obtain more accurate results, elements are kept very small (L/60) near the plate, increasing gradually in size and moving away from the plate (Nouri et al., 2017).

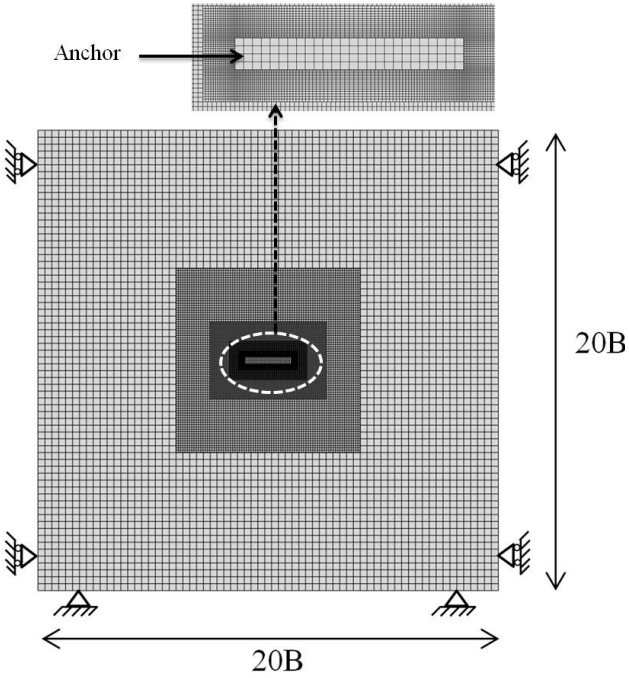

Figure 1: Finite element model used for numerical analysis

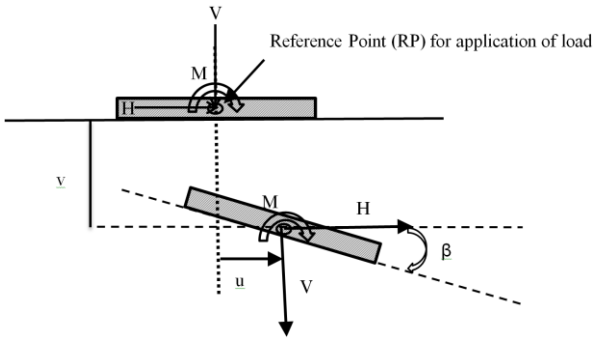

Figure 2: Load and displacement convention adopted

To determine the collapse load of the anchor, displacement-based analyses are performed. The total displacement is applied over a number of sub-steps in the reference point (RP) of anchor as shown in Figure.2. All the nodes defining the soil anchor interfaces are forced to move together either parallel to the anchor (sliding), perpendicular to the anchor (normal) and in a path corresponding to rotation of anchor plate about the centre. All results are presented here as non-dimensional forms using the factors defined as

$$N_v = \frac{V}{Bc};\ N_s = \frac{H}{Bc};\ N_m = \frac{M}{B^2 c} \quad (1)$$

Where H, V and M are the normal, parallel and rotational capacities (normal to the intended plane of loading), respectively.

2.2 Sign Convention for Load and Displacement

The centroid of anchor is used as the reference point (RP) for application of combined load components V, H and M**.** The notation used in this paper is shown in Figure.2. The V, H and M loads as well as the corresponding footing movements' v, u and β are also illustrated in Figure. 2. The sign convention for loads presented and displacements in this study obeys a right-handed rule and clockwise positive convention as proposed by Butterfield and Houlsby (1997). The anchor's ultimate pullout capacities for pure loading of one single component (i.e. for ultimate pure moment load capacity V=H=0), are de-noted as V_0, H_0 and M_0 for pure vertical, horizontal and moment loadings, respectively.

2.3 Numerical Analysis to Define the Failure Envelope

In the finite element analysis (FEA), the load is usually applied in two ways such that load-controlled method and displacement-controlled method. The benefit of displacement-controlled method is to simulate post failure phenomena's. From the load displacement response of anchor in any direction it can be concluded that the anchor is in limit equilibrium state in that direction. In this state, the slope of load displacement curve is tends to zero that means loads does not increase with the increase of load. It indicates that the ultimate load capacity (H, V and M) of anchor in that direction (v, u and β). For combination of load the

displacement controlled method is found to be more suitable instead of load controlled method (Bransby and Randolph, 1997). Constant-ratio displacement probe tests and displacement-controlled swipe tests were carried out to determine the post failure phenomena's in different loading planes, such as vertical horizontal plane (V:H, where V>0, H>0 and M=0), vertical moment plane (V:M, where V>0, M>0 and H=0) and horizontal moment plane (H:M, where H>0, M>0 and V=0).

2.3.1 Swipe test

The sideswipe test was first introduced by Tan (1990) during centrifugal modelling in sand. Many researchers have used frequently this test procedure in both experimental (Houlsby, 1994;Martin and Houlsby, 2001, Cassidy et al., 2002 and numerical (Bransby and Randolph, 1998; Gourvenec and Randolph 2003;Yang et al., 2010 and Randolph et al., 2011) studies.

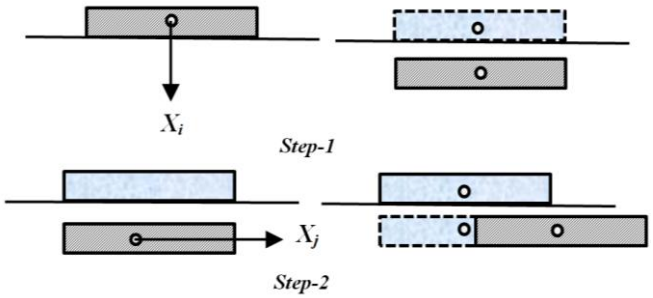

Figure 3: Example of a swipe test

Swipe tests are carried out to identify the failure envelopes in VH and VM plane, but are unsuitable for loading in the HM plane (Bransby et al., 2003). For a failure envelope in ij plane a displacement X_i is applied at the RP along i-direction from zero load state to limit equilibrium state at which ultimate load in that direction is reached. In its second step a displacement X_j is imposed in j-direction keeping constant displacement in i-direction displacement until the anchor load does not vary with the increased displacement in j-direction. The benefit of the swipe test is that a complete failure locus on a certain plane can be determined in a single test. The resultant load path is the failure envelope in ij-plane.

2.3.2 Probe analysis

Fixed displacement ratio probe test suggested by Bransby and Randolph (1997) is another way to check the accuracy of the failure envelopes obtained from the swipe tests. The probe tests give rise to load paths that move from the origin across the failure envelope, initially at gradients determined by the elastic stiffness but with the gradients changing owing to internal plastic yielding as the paths approach the failure envelop. Once the failure envelope is reached, each loading path travels around the failure envelope until it reaches a termination point where the direction of tangent to the failure envelope matches with the prescribed dis-placement ratio. However, several analyses with different displacement ratio are required to define the correct failure loci, it defines correct failure envelope specially in H:M loading plane. Fig. 4 shows the load paths for twenty Dβ/Du displacement ratios (v=0) and final termination point agrees well with the failure envelope.

3. RESULTS AND DISCUSSION

One combination of V, H and M loads causing anchor to failure is found by translating and/or rotating the anchor until a constant load state is reached in that direction. The crudest example of this is to push the anchor in vertical direction into the soil until the vertical load plateaus reached is followed by translating and/or rotation. However, to define a complete failure envelope in different plane a variety of vertical and horizontal displacement and

rotational combinations are required. In this study, total 40 probe tests were conducted to define failure envelope in three different planes. The failure envelopes in the V–H, V–M and H–M planes are found by connecting the termination points. A summary of dimensionless normal, shear and rotational capacities of anchor under pure loading is provided in Table 1.

Table 1: Bearing Capacity Factors

Bearing capacity factors	Current FEM study	API/Deepstar
$N_{v0}=V_{ult}/Bc$	11.98	11.58
$N_{s0}=H_{ult}/Bc$	4.39	4.49
$N_{m0}=M_{ult}/B^2c$	1.63	1.74

The capacity factors shown in Table 1 are compared with the API/Deepstar study (Andersen et al., 2003). Current FEM study agreed well with the API/Deepstar study. The pure normal capacity (N_{v0}) of current FEM are found 3%, higher than that of API/Deepstar study. But, pure shear (N_{s0}) and pure moment (N_{m0}) capacities are found 2% and 6%, respectively. These slight disagreements might be due to different mesh configurations and other minor details of the model.

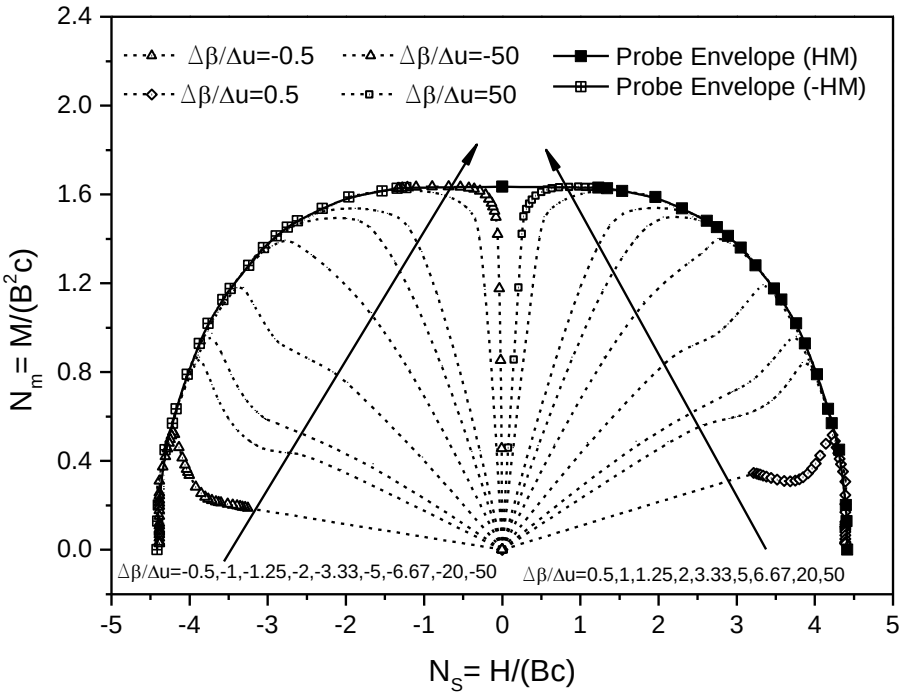

Figure 4. Loading path and failure envelope at H-M plane (V=0)

The failure envelopes for H:M loading shown in Figure. 4 is obtained from the 10 different probe tests for both HM and –HM failure. Different displacement ratios ranging from 0.5 to 50 are considered to construct complete failure envelope for both HM and –HM planes. The envelopes are symmetric, with the maximum moment M_{max} =1.63 at H=0. At a lower shear loading upto $0.45H_{ult}$, the slope of HM failure envelope is almost zero. After that, it changes abruptly and slope of the failure envelope is found to be steeper at lower value of moment. Hence, it can be concluded that at a lower shear loading moment loading dominates the failure mechanism. The Figure.5 shows the comparison of failure envelope with the previous studies (Andersen et al., 2003 and Yang et al., 2010).The solutions obtained in the present study are in good agreement with a research conducted by Yang et al. (2010), but small discrepancies upto 6% are found with the API/Deepstar.

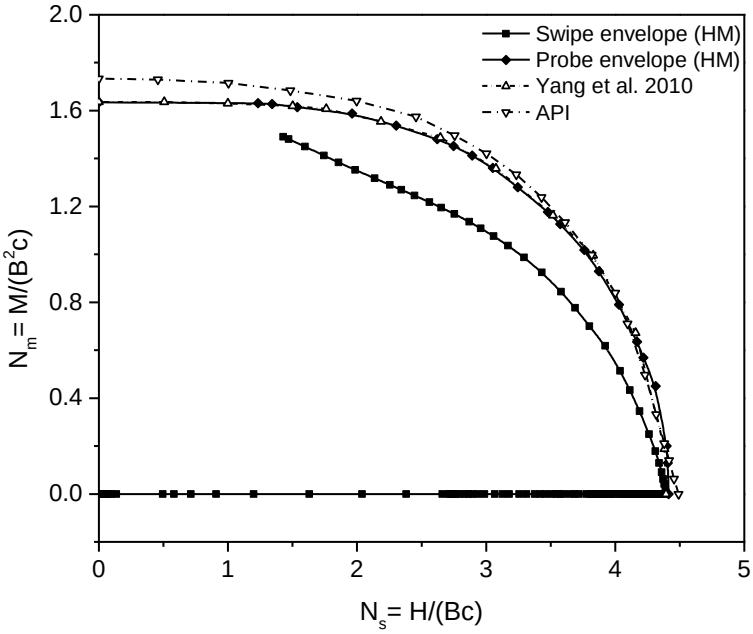

Figure 5: Compares between the failure envelope for swipe and probe tests at H-M plane

Additionally, it also compares the failure envelope found from both swipe and probe analysis. Failure envelope of swipe test lies inside the true failure envelope. If the anchor is brought to sliding failure first, and then rotated at a fixed horizontal position, the resulting load path lies significantly inside the true failure envelope (Gourvenec & Randolph, 2003).

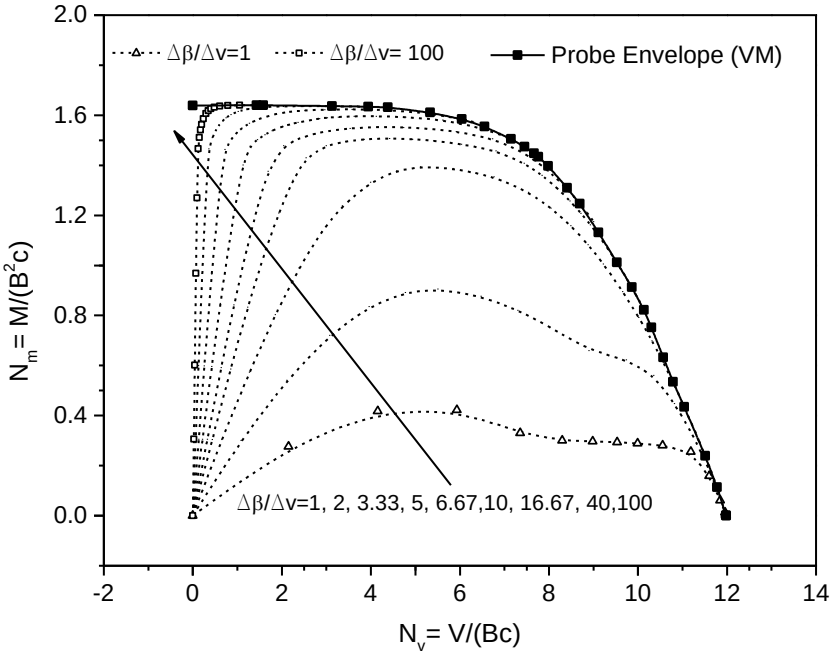

Figure 6: Loading path and failure envelope at V-M plane (H=0)

Symmetry of the problem indicates that *f*(M,H)= *f*(M,-H), *f*(V,H)= *f*(V,-H) and *f*(V,M)= *f*(V,-M), so that only positive load combinations of HM, VH and VM are required to define the complete failure envelope. The Figure.4 also represents the prove of symmetry of HM loading. For this reason, further analyses were carried out only with the positive load combinations. The Figure.5 represents the failure loci under VM loading. To construct

complete failure envelope ten probe tests (∆β/∆v) ranging from 1 to 100 are carried out as shown in Fig.6 . All probes are shown by dotted lines. It also proves that after reaching a failure all loading path travel along the failure envelope. At a lower normal loading upto $0.5V_{ult}$, moment reduces slightly and after that it changes sharply. Hence, it can be concluded that, when normal force>$0.5V_{ult}$ then vertical loading dominates the failure mechanism.

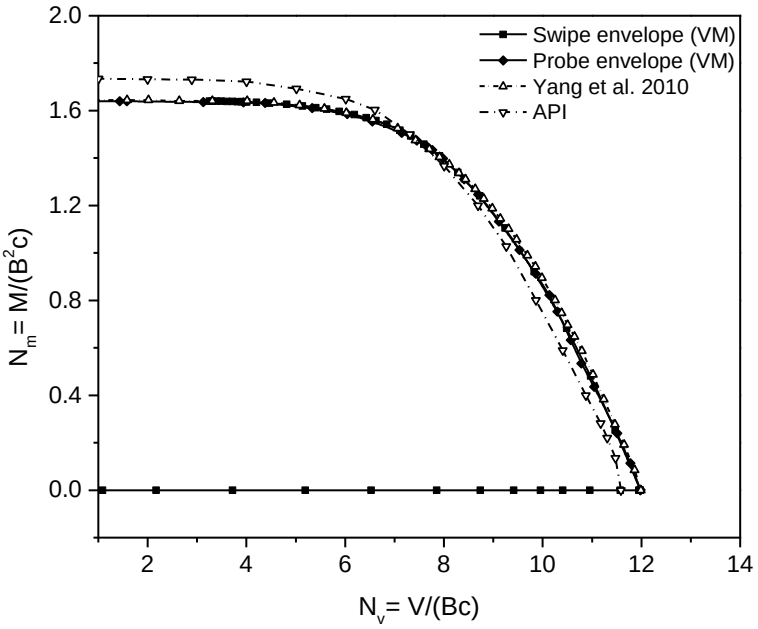

Figure 7: Compares between the failure envelope for swipe and probe tests at V-M plane

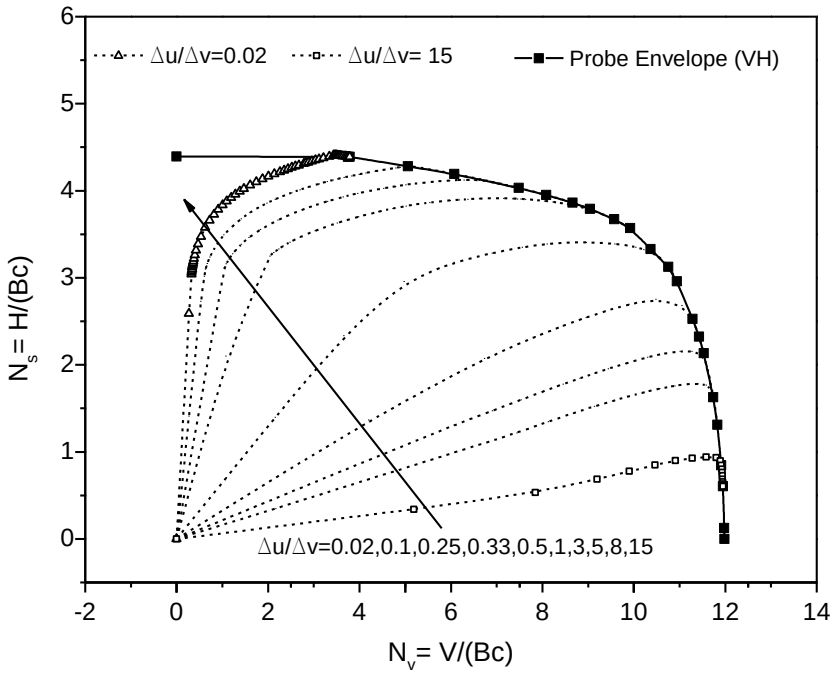

Figure 8: Loading path and failure envelope at V-H plane (M=0)

This trend found same in Andersen et al. (2003) and Yang et al. (2010) studies, as shown in Figure.7. Figure.7 also shows a good agreement of probe and swipe test in VM plane. Fig.8 represents the interaction diagram in horizontal and vertical loading plane (VH). In this study,

in order to construct complete interaction diagram, 9 probe tests were carried out. The H:V interaction curves as shown in Figure.8. The Figure.8 drop abruptly at large values of N_v implying that parallel loading has little impact on the normal capacity before it reaches $0.5H_{ult}$. In this case, normal load dominates the failure mechanism. Figure.9 shows the compares between the swipe and probe test. In the case of VH loadings, swipe envelope lies slightly inside the probe envelope. It also agreed well with the research conducted by Andersen et al. (2003) and Yang et al. (2010).

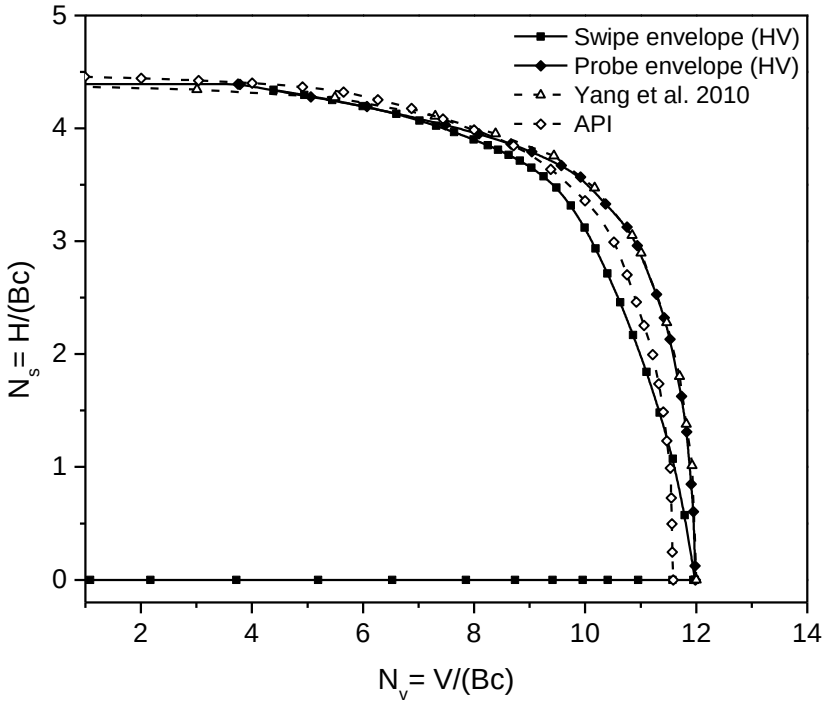

Figure 9: Compares between the failure envelope for swipe and probe tests at V-H plane

3.1 Soil failure mechanism

Soil failure mechanism under combined loading is illustrated in Figure.10 by equivalent plastic strain (ε_p) and the deformed soil shape is calculated by load-displacement probe test in HM plane. This method consists of two steps. In first step a load (say horizontal load, H) is applied directly along the horizontal direction by the load-controlled method which is less than the ultimate failure load (H_{ult}) and a failure point is gained on the failure envelope. In its second step, horizontal load along this direction is kept constant and rotational displacement is applied until the rotational failure occurs in that direction. A point, at which load value in horizontal direction can be predefined, is probed on the envelope in HM failure plane. Figure.10a represents the failure mechanism in fully bonded condition under pure shear loading. It demonstrates that, the maximum plastic strain occurs along the side of the plate. The black triangles left and right side of the plate are soil wedges that move rigidly as plate progresses and finally the plastic strain contours travel around the plate. Figure.10b represents the failure mechanism in fully bonded condition under pure vertical loading. The white rectangle is the plate anchor which is modelled as a rigid plate. The plastic yielding region of the soil progresses similarly on each side of the plate anchor such that substantial portions of soil are involved.

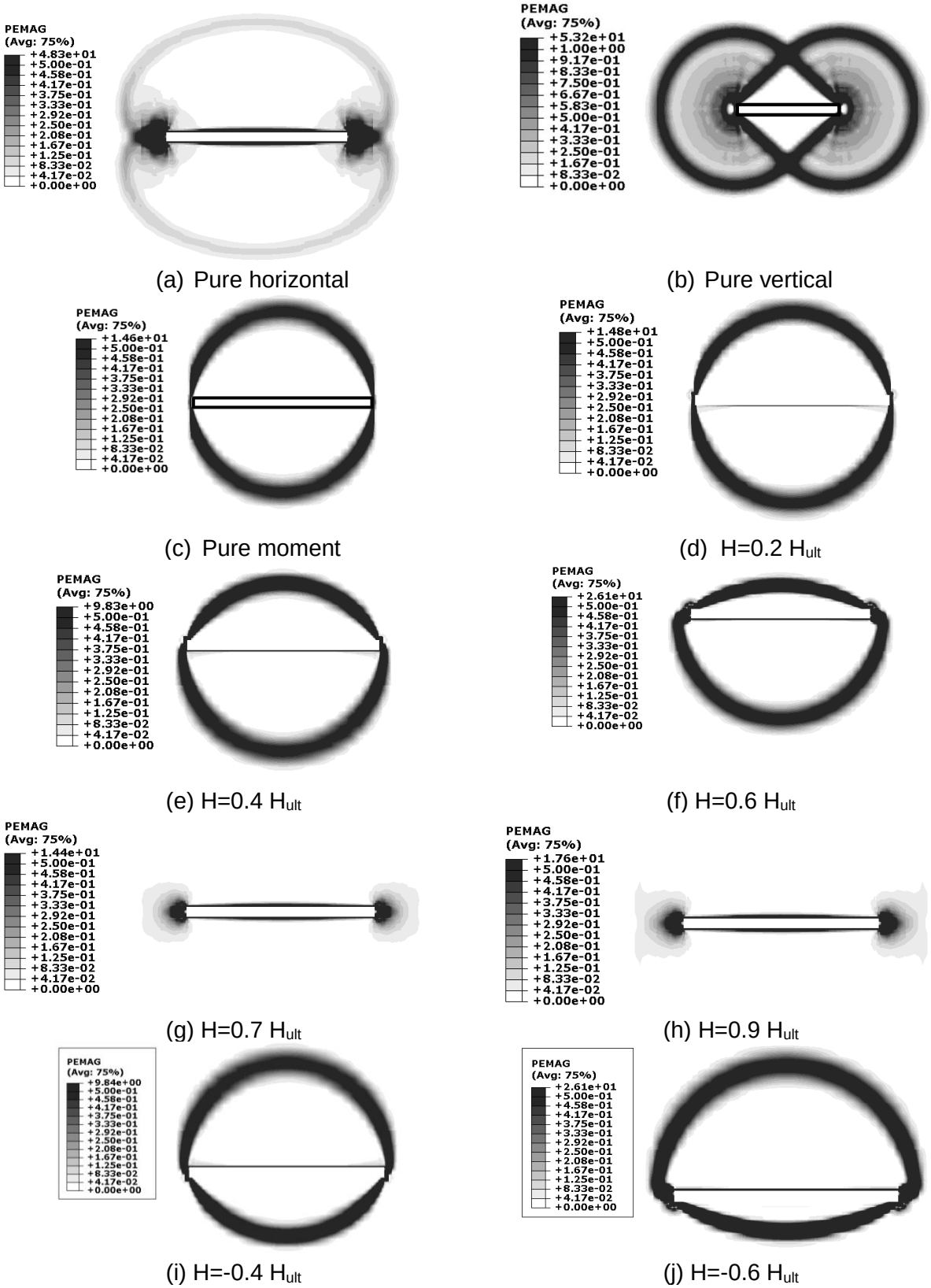

Figure 10: Distribution of plastic strain (ε_p) under combined loading.

It also shows the plastic strain where the soil is "flowing" around the plate anchor as two symmetrical circles, demonstrating a complete plastic failure mechanism has formed as the critical load is reached. The white triangles on each side of the plate are soil wedges that

move basically rigidly with the plate as it progresses. It also indicates that, the maximum plastic strain occurs along the sides of the "rigid" soil wedges (Andersen et al., 2003 and Yang et al., 2010). This is closely in consensus with classical theory. Fig.10c represents the plastic strain flow at failure under pure rotation. It illustrates that, the plastic strain start to flow along the edge of anchor and travel symmetrically. The maximum plastic strain occurs as two half circles at top and bottom of the anchor plate.

For the case of HM load combination, Figure.10d through Figure.10h represents the failure mechanism in positive HM loadings (H=left to right positive and M=clockwise positive) and Figure.10i and Figure.10j shows the failure mechanism in-HM loadings. When H=0.2 H_{ult}, soil flows symmetrically around the plate as two half circles. As the horizontal load increases, upper half circles starts to diminishing and in that case horizontal loading dominates the failure mechanism. When H>0.7 H_{ult}, then circular zone does not exist and soil starts yielding due to the horizontal loading. Plastic strain distribution of Figure.10i and Figure.10j are same as Figure.10e and Figure.10f, but reverse in direction, where, lower half circles starts to diminishing and in that case horizontal loading also dominates the failure mechanism. Hence, the total works done and ultimate failure load is same in both cases.

4. CONCLUSION

The drag anchor response under combined uni-directional horizontal, vertical and moment loadings are explored for strip horizontal anchor by FEA. In order to hypothesis the failure envelope in HM, VM and HV plane, both the swipe and probe tests were conducted. Additionally, to understand the failure mechanism in HM loading condition load-displacement probe tests were also conducted. Compared with the result of swipe and existing numerical studies it can be concluded that the probe test gives the correct prediction of the failure envelope in all loading plane. Result also reveals that the soil failure changes from symmetrical circular pattern to asymmetrical pattern due to the increase of horizontal load in HM plane.

REFERENCES

Andersen, K. H., Murff, J. D., & Randolph, M. F. (2003). "Deepwater anchor design practice-vertically loaded drag anchors." *Phase II Report to API/Deepstar, Norwegian Geotechnical Institute, Norway, Offshore Technology Research Center, USA and Centre for Offshore Foundation Systems, Australia*.

Bransby, M. F., & Randolph, M. F. (1997). "Shallow foundations subject to combined loadings." *In 9th International Conference of the International Association for Computer Methods and Advances in Geomec*, (Vol. 3, pp. 1947–1952.

Bransby, M. F. & Randolph, M. F. (1998). "Combined loading of skirted foundations." *Geotechnique*, 48(5), 637–655.

Butterfield R, Houlsby GT, G. G. (1997). "Standardized sign conventions and notation for generally loaded foundations." *Geotechnique*, 47(5), 1051–4.

Cassidy, M. J., Byrne, B. W., & Houlsby, G. T. (2002). "Modelling the behaviour of circular footings under combined loading on loose carbonate sand." 705–712.

Cassidy, M. J., Randolph, M. F., and Wong, P. . (2012). "A plasticity model to assess the keying of plate anchors." *Géotechnique*, 62(9), 825.

Tian, Y., Gaudin, C., Cassidy, M. J., & Randolph, M. F. (2012)."Considerations on the Design of Keying Flap of Plate Anchors." (2013). *Journal of Geotechnical and Geoenvironmental Engineering*, 139(7), 1156–1164.

Elkhatib, S. (2006). *The behaviour of drag-in plate anchors in soft cohesive soils*. (Ph.D. thesis), University of Western Australia, Australia.

Elkhatib, S., and Randolph, M. F. (2005). "The effect of interface friction on the performance of drag-in plate anchors." Perth, Western Australia: Taylor & Francis., pp.171-177.

Gourvenec, S. & Randolph, M. F. (2003). “Effect of strength non-homogeneity on the shape and failure envelopes for combined loading of strip and circular foundations on clay.” *Geotechnique*, 53(6), 575–586.

Houlsby, G. T. (1994). “Physical and numerical modelling of offshore foundations under combined loads.” *(Doctoral dissertation, University of Oxford)*.

Kim, B. M. (2007). *Upper bound analysis for drag anchors in soft clay*. (Ph.D. thesis),Texas A&M University.

Liu, J., Lu, L., and Hu, Y. (2016). “Keying behavior of gravity installed plate anchor in clay.” *Ocean Engineering*, 114, 10–24.

M P O’Neill, M F Bransby, and M F Randolph. (2003). “Drag anchor fluke-soil interaction in clays.” *Canadian Geotechnical Journal*, 40(1), 78–94.

Martin, C. M., & Houlsby, G. T. (2001). “Combined loading of spudcan foundations on clay: numerical modelling.” *Géotechnique*, 51(8), 687–700.

Nouri, H., Biscontin, G., and Aubeny, C. P. (2017). “Numerical prediction of undrained response of plate anchors under combined translation and torsion.” *Computers and Geotechnics*, 81, 39–48.

Aubeny, C. P., Murff, J. D., & Kim, B. M. (2008).“Prediction of Anchor Trajectory During Drag Embedment In Soft Clay.” (2008). *International Journal of Offshore and Polar Engineering*, 18(4).

Randolph, M. F., G audin, C. , Gourvencec, S. M., Whi te, D. J ., Boylan, N., and and Cassidy, M. J. (2011). “Recent advances in offshore g eotech-nics for deep w ater oi l and gas developments.” *Oc ean Eng. ,* 38(7), 818–834.

Rowe, R. K. (1978). “Soil structure interaction analysis and its application to the prediction of anchor plate behaviour.” *(Doctoral dissertation)*.

Song, Z., Hu, Y., & Randolph, M. F. (2008). “Numerical Simulation of Vertical Pullout of Plate Anchors in Clay.” *Journal of Geotechnical and Geoenvironmental Engineering*, 134(6), 866–875.

Song, Z., and Hu, Y. (2005). “Vertical pullout behaviour of plate anchors in uniform clay.” Perth, Western Australia: Taylor & Francis.

Wang, D., Hu, Y., & Randolph, M. F. (2009).“Three-Dimensional Large Deformation Finite-Element Analysis of Plate Anchors in Uniform Clay.” (2010). *Journal of Geotechnical and Geoenvironmental Engineering*, 136(2), 355–365.

Merifield, R. S., Lyamin, A. V., Sloan, S. W., & Yu, H. S. (2003) “Three-Dimensional Lower Bound Solutions for Stability of Plate Anchors in Clay.” (2003). *Journal of Geotechnical and Geoenvironmental Engineering*, 129(3), 243–253.

Wei, Q., Cassidy, M. J., Tian, Y., and Gaudin, C. (2015). “Incorporating Shank Resistance into Prediction of the Keying Behavior of Suction Embedded Plate Anchors.” *Journal of Geotechnical and Geoenvironmental Engineering*, 141(1), 4014080.

Yang, M., Murff, J. D., & Aubeny, C. P. (2010). “Undrained capacity of plate anchors under general loading.” *Journal of geotechnical and geoenvironmental engineering*, 136(10), 1383–1393.

Proceedings of the 4th International Conference on Civil Engineering for Sustainable Development (ICCESD 2018), 9~11 February 2018, KUET, Khulna, Bangladesh (ISBN-978-984-34-3502-6)

EFFECT OF INTERPARTICLE FRICTION ON THE SMALL STRAIN STIFFNESS OF GRANULAR MATERIALS BY DEM

Md. M Sazzad[1] and Md. S Islam[2]

[1] *Professor, Department of Civil Engineering, Rajshahi University of Engineering & Technology, Bangladesh, e-mail: mmsruet@gmail.com*
[2] *Undergraduate Student, Department of Civil Engineering, Rajshahi University of Engineering & Technology, Bangladesh, e-mail: sharif.ruet12@gmail.com*

ABSTRACT

Interparticle friction plays a crucial role in the stability of granular materials such as sand during shear. In this study, the effect of interparticle friction angle at a very small strain level (less than 0.001% strain) is examined using the Discrete Element Method (DEM). DEM is used because it is not easy to compute the small strain stiffness of granular materials for varying interparticle friction angle experimentally. A numerical sample consisting of 9826 spheres similar to dry Grade chrome steel balls was prepared numerically. The sample was then subjected to shear for varying interparticle friction angle ranging from 1 to 50 degrees. The stress-strain behavior obtained from the numerical simulation was compared with the experimental results to warrant the validity of the simulation. The small strain stiffness was computed for varying interparticle friction angle and a relationship between the friction angle and small strain stiffness was established. It is noted that small strain stiffness is a function of interparticle friction angle for its lower value.

Keywords: *Small strain stiffness, interparticle friction, granular materials, discrete element method.*

1. INTRODUCTION

Interparticle friction angle is a dominant parameter that controls the mechanical behaviour of granular materials such as sand. The interparticle friction angle can be defined with the help of Figure 1, where f_n indicates the normal force exerted on the contact points between two particles, f_s indicates the shear force developed at the contact points between two particles, f indicates the force exerted on the contact points between two particles and ϕ indicates the interparticle friction angle. Experimentally, the effect of interparticle friction angle was reported by Skinner (1969). By shearing a random assembly of spherical particles, he depicted that both the effective angle of shearing resistance at constant volume and at peak stress state for a given initial porosity do not increase monotonically with the increase of the interparticle friction angle. Numerical studies using the particulate approach depicted that the characteristics of grain-scale level responses are severely affected by the interparticle friction angle (e.g., Hu & Molinary, 2004; Sazzad & Islam, 2008; Sazzad & Suzuki, 2011). The stability of a system depends on the values of the interparticle friction angle. A dense sample can behave like a loose sample for lower values of interparticle friction angle and can behave even like a fluid when the interparticle friction angle is almost zero (Sazzad & Islam, 2008). It was also reported that the macro-scale behaviors were significantly influenced by the variation of interparticle friction angle, in particular, at peak stress state (Sazzad et. al., 2017). Since the deformation properties of granular materials at small strain levels play an important role in predicting the short-term residual deformation of the ground and structural displacement, it is intended to study the macroscopic response at a very small strain level (lesser than 0.001%) due to the variation of interparticle friction angle. Earlier studies reported that the soil behavior observed by applying many small unload/reload cycles of axial stress statically in the laboratory tests is linear (e.g., Tatsuoka, Iwasaki,

Fukushima & Sudo, 1979; Enomoto, 2016). It should be noted that the experimental device should be extremely precise with a higher degree of accuracy to measure the small strain stiffness. Conventional experimental facilities may not be able to measure the strain at such a very small strain level. Numerical methods such as the discrete element method (DEM) pioneered by Cundall and Strack (1979) can be used instead. So far, only a limited number of studies were reported in the literature that considered the DEM to estimate the small strain stiffness parameters (Sazzad et. al., 2017).

So, the objective of the present study is firstly to simulate the laboratory stress-strain response of conventional triaxial compression (CTC) tests carried out using the steel balls (i.e. spheres) and secondly to observe the effect of the variation of interparticle friction angle on the small strain stiffness parameter (i.e elastic modulus) of granular materials. To do this, the laboratory based conventional triaxial compression (CTC) test reported in Cui, O'Sullivan & O'Neil (2007)] and O'Sullivan, Cui & O'Neil (2008) on dry grade chrome steel balls under vacuum confinement of 80 kPa was simulated using the discrete element method. A numerical sample consisting of 9826 spheres was randomly generated without any initial interparticle contact. The generated numerical sample was compressed in different stages to attain a confining pressure of 80 kPa. During the compression, the periodic boundary condition was applied. The simulation of the CTC test was carried out under the strain control condition using the DEM. A very small strain increment was assigned so that the quasi-static condition could be attained and the effect of numerical damping became minimum. The simulated data were recorded at required intervals for the post analysis. The stiffness parameter at a very small strain range smaller than 0.001% was carefully measure for varying interparticle friction angle.

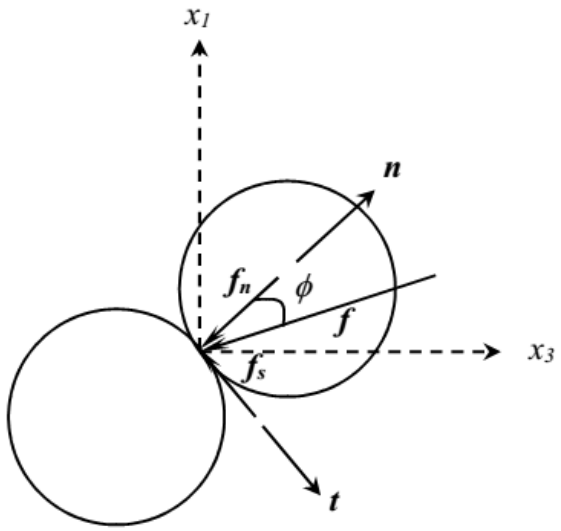

Figure 1: Interparticle friction angle, ϕ with force vectors in x_1-x_3 plane

2. DISCRETE ELEMENT METHOD AND OVAL

Discrete element method (DEM), also called distinct element method, is a family of numerical methods for computing the motion of large number of small particles. DEM is a numerical technique where Newton's second law of motion is applied. The translational and rotational accelerations of a 3D particle in DEM are computed using the Newton's second law of motion and are expressed as follows:

$$m\ddot{x} = \Sigma f_i \qquad i = 1-3 \tag{1}$$

$$I\ddot{\theta} = \Sigma M \tag{2}$$

where f_i are the force components, M is the moment, m is the mass, I is the moment of inertia, $\ddot{x}_i$ are the translation acceleration components and $\ddot{\theta}$ is the rotational acceleration of the particle. Velocities and displacements of particles are obtained by integrating the accelerations over time successively. For basics of DEM, readers can refer to Cundall and Strack (1979). Computer program OVAL is used to analyse the particulate assemble using the DEM. The effectiveness of OVAL has already been recognized (Kuhn, 1999; Sazzad & Suzuki, 2010; Sazzad & Suzuki, 2013; Sazzad, 2014). In the present study, Hertz-Mindlin contact model is used. The normal force of a Hertz-type contact is computed as follows (Sazzad, Sneha, & Rouf, 2017):

$$F^n = \frac{\bar{E} a^3}{R} \tag{3}$$

$$\bar{E} = \frac{8G}{3(1-\nu)} \tag{4}$$

$$a = \sqrt{\frac{d \times R}{2}} \tag{5}$$

$$R = \frac{2R_1 R_2}{R_1 + R_2} \tag{6}$$

Here, $\bar{E}$ is the elastic constant, a is the contact radius, d is the overlap between the contacting particles, R is the effective radius of curvature, R_1 and R_2 are the radii of curvatures of two particles at contact.

3. NUMERICAL SAMPLE PREPARATION

In the present study, the laboratory based conventional triaxial compression (CTC) test reported in Cui, O'Sullivan & O'Neil (2007) and O'Sullivan, Cui & O'Neil (2008) on dry grade chrome steel balls under vacuum confinement of 80 kPa was used to compare with that of DEM to depict the authentication of DEM based simulated results. Three types of spheres having the radii of 2 mm, 2.5 mm and 3 mm, respectively, having a mixing ratio of each type particle of 1:1:1 (a sample height to width ratio of two) were used in the laboratory test. The void ratio of nonuniform sample used in the experiment was 0.603. The characteristics of the spheres used in the CTC tests as reported in Cui, O'Sullivan & O'Neil (2007) and O'Sullivan, Cui & O'Neil (2008) are shown in Table 1. For numerical study, a numerical sample consisting of 9826 spheres similar to the experimental study was randomly generated without any initial contacts among spheres. The spheres were modeled as particles. This is because it simplifies the contact detection algorithm and thus, it reduces the computational cost of the simulation. The radii of spheres used to make the numerical samples were same as the experiment (i.e. 2 mm, 2.5 mm and 3 mm), respectively with a mixing ratio of 1:1:1. The initial sample is surrounded by the periodic boundaries, a boundary condition in which the periodic cells are surrounded by the identical cells. The generated numerical sample was compressed in different stages to attain a confining pressure of 80 kPa. The consolidation of the initially generated sparse sample was carried out using the strain control condition. After the end of isotropic compression, the void ratio of the numerical sample became 0.626. The void ratio of the numerical sample is a bit higher than that of the experiment. However, it is expected that this very small difference of the void ratio between the experiment and numerical sample has very little effect on the shear behavior.

Table 1: Characteristics of dry grade chrome steel balls used in the CTC test (after Cui, O'Sullivan & O'Neil 2007)

Properties	**Values**
Density of spheres (kg/m^3)	7.8 ×10^3
Shear modulus (Pa)	7.9 ×10^3
Poisson's ratio	0.28
Interparticle friction angle (degree)	5.5
Boundary friction coefficient	0.228

4. NUMERICAL SIMULATIONS

The simulation of the CTC test was carried out under the strain control condition using DEM. A very small strain increment was assigned during shear. The material properties and DEM parameters used in the simulation are shown in Table 2. It should be noted that the properties of particles used in DEM simulation are same as that of grade chrome steel balls used in the experiment (CTC test). To monitor the quasi-static condition, a non-dimensional index is defined as follows (Sazzad, Sneha, & Rouf, 2017; Sazzad, 2014):

$$I_{uf} = \sqrt{\frac{\sum_{1}^{N_p} F_{ubf}^2 / N_p}{\sum_{1}^{N_c} F^2 / N_c}} \times 100\,(\%) \tag{7}$$

where F_{ubf} , F , N_p and N_c denote the unbalanced force, contact force, number of particles and number of contacts, respectively. Index I_{uf} is directly related to the accuracy of the simulation. Lower the value of I_{uf} , higher the accuracy of the simulation.

Table 2: Material properties and DEM parameters used in the present study

Properties	**Values**
Density of spheres (kg/m^3)	7.8 ×10^3
Shear modulus (Pa)	7.9 ×10^3
Poisson's ratio	0.28
Interparticle friction angle (degree)	1 to 50
Increment of time step (s)	1.0 ×10^{-6}
Damping coefficients	0.10

5. VALIDATION OF SIMULATED RESULTS

The simulation of the CTC test was carried out under the strain control condition using DEM. The Simulated stress-strain behavior is compared with the laboratory CTC test as reported in Cui, O'Sullivan & O'Neil (2007) and depicted in Figure 2 The normalized deviatoric stress, q in Figure 2 is defined as $q = (\sigma_1 - \sigma_3)/\sigma_3$, σ_1 and σ_3 are the stresses in vertical and lateral directions, respectively. It is noted that the stress-strain behavior by DEM has excellent agreement with the laboratory CTC test reported in Cui, O'Sullivan & O'Neil (2007). This quantitative validation of the simulated results with the experiment depicts the versatile

nature of the present study by DEM and proofs that DEM can successfully replicate the behavior of granular materials quantitatively.

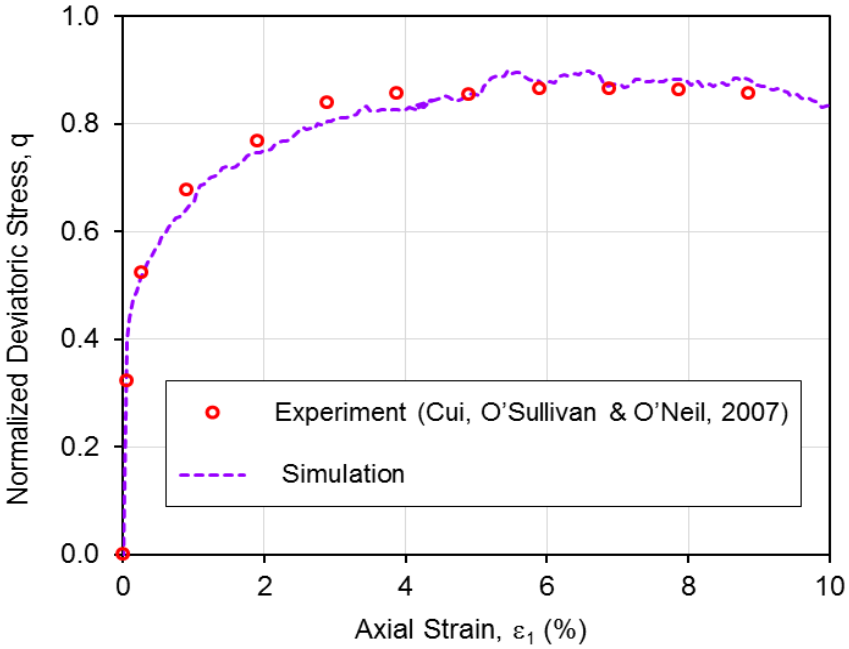

Figure 2: Comparison of the simulated stress-strain behavior using DEM with the experiment reported in Cui, O'Sullivan & O'Neil (2007)

6. EFFECT OF INTERPARTICLE FRICTION ANGLE

The effect of interparticle friction angle is studied in this section. For this reason, several CTC tests were simulated for varying interparticle friction angles ranging from 1 to 50 degrees. Figure 3 shows the stress-strain behavior of granular materials for three different interparticle friction angles (i.e. 5, 25 and 45 degrees) during shear. It is observed that the interparticle friction angle has severe effect on the stress-strain behavior. The peak stress increases with the increase of the interparticle friction angle. Same behavior is also reported in earlier DEM studies (Sazzad and Islam, 2008; Sazzad, Alam & Rowshan, 2017). The evolution of the volumetric strain with axial strain is depicted in Figure 4.

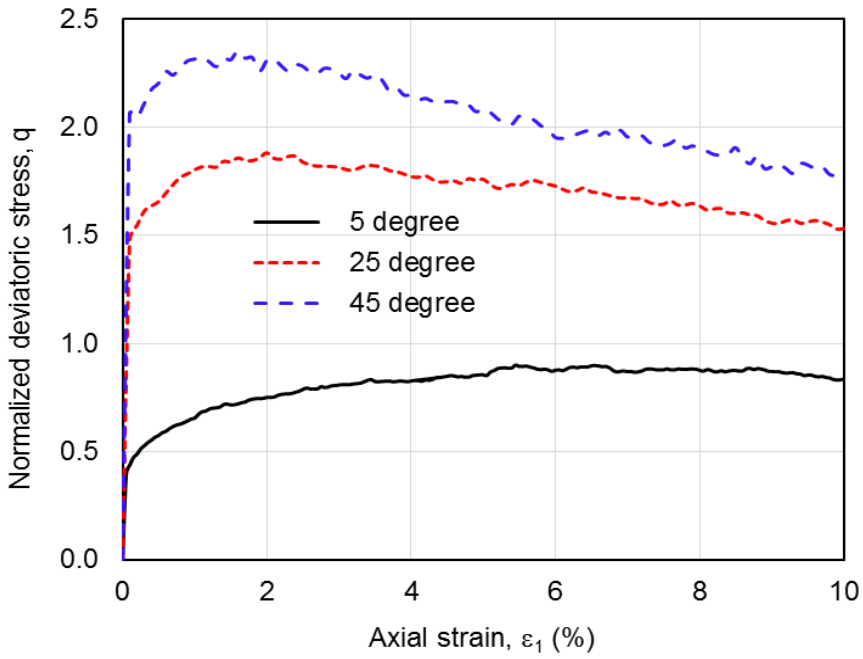

Figure 3: Stress-strain relationship for varying interparticle friction angle

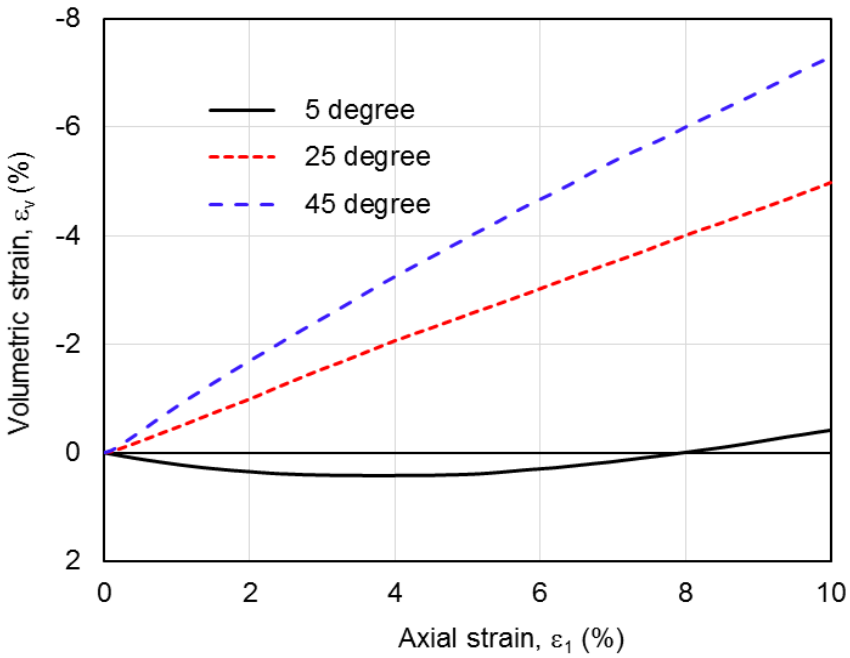

Figure 4: Evolution of volumetric strain for varying interparticle friction angle

The volumetric strain is defined as $\varepsilon_v = \varepsilon_1 + 2\varepsilon_3$, where ε_1 is the strain in x_1- direction and ε_3 is the strain in x_3- direction. The positive value of strain indicates compression while the negative value indicates dilation. It is observed that dilation of the sample increases with the increase of interparticle friction angle. The relationship between the elastic modulus and interparticle friction angle at small strain lower than 0.001% is depicted in Figure 5.

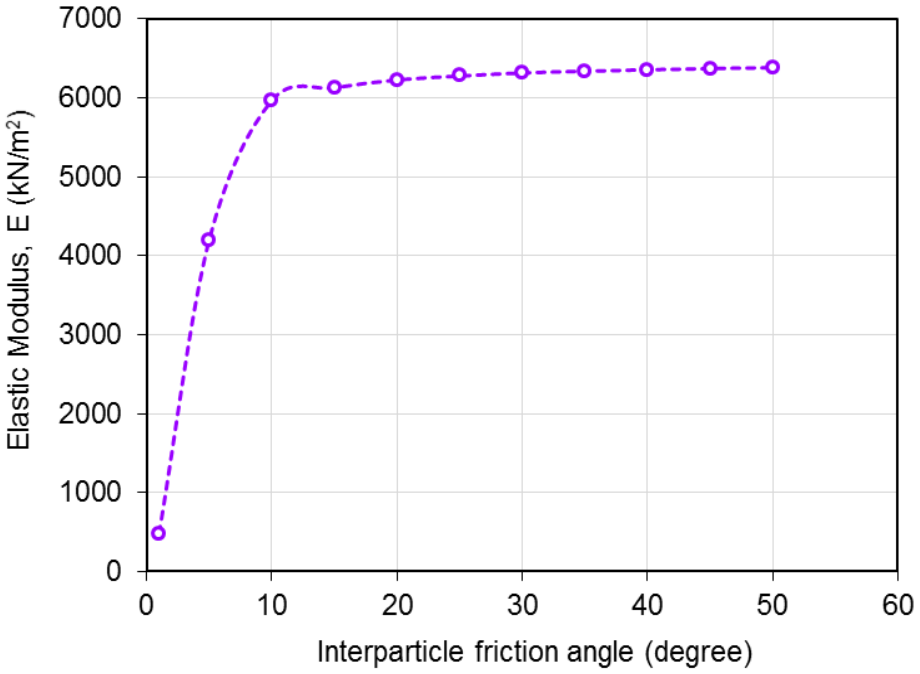

Figure 5: Relationship between the elastic modulus and interparticle friction angle at small strain range lower than 0.001%

The elastic modulus increases sharply with the increase of the interparticle friction angle up to 10 degree and beyond that the elastic modulus becomes almost constant with the further increase of interparticle friction angle. So, it can be concluded that elastic modulus is the function of the interparticle friction angle for the lower range of interparticle friction angle only.

7. CONCLUSIONS

This study simulated the stress-strain behavior of a numerical sample consisting of 9826 spheres similar to dry Grade chrome steel balls reported in Cui, O'Sullivan & O'Neil (2007). An excellent agreement between the simulated and experimental stress-strain behavior was observed. This illustrates the accuracy and perfectness of the simulation using DEM. The effect of the variation of the interparticle friction angle on the stress-strain-dilative behavior was investigated. It is observed that interparticle friction angle severely affects the stress-strain behavior at peak stress state. Peak stress increases with the increase of the interparticle friction angle. The dilation also increases with the increase of the interparticle friction angle. The stiffness parameter i.e. the elastic modulus is also calculated at a very at small strain range lower than 0.001%. The relationship between the elastic modulus and the interparticle friction angle is illustrated. It is noted that the value of elastic modulus increases with the increase of interparticle friction angle for lower values of interparticle friction angle. So it can be concluded that elastic modulus is the function of the interparticle friction angle for its lower value only.

REFERENCES

Cui, L., O'Sullivan, C., & O'Neil, S. (2007). An analysis of the triaxial apparatus using a mixed boundary three-dimensional discrete element model. *Geotechnique*, 57(10), 831–844.

Cundall, P.A. (1971). A computer model for simulating progressive, large scale movement in blocky rock systems. *Proc. Symp. Int. Soc. Rock Mech., Inst. Civ. Engrg*., 2(8), 129-136.

Enomoto, T. (2016). Effects of grading and particle characteristics on small strain properties of granular materials. *Soils and Foundations,* 56(4), 745–750.

Hu, N., & Molinari, J. F. (2004). Shear band in dense metallic granular materials. *Journal of Mechanics and Physics of Solids*, 52(3), 499-531.

Kuhn, M.R. (1999). Structured deformation in granular materials. *Mechanics of Materials*, 31(6), 407-429.

Mechanics and Physics of Solids, 52, 499-531

Mechanics and Physics of Solids, 52, 499-531

O'Sullivan, C., Cui, L., & O'Neill, S. (2008). Discrete element analysis of the response of granular materials during cyclic loading. *Soils and Foundations,* 48(4), 511-530.

Sazzad, M. M. & Islam, M. S. (2008). Macro and micro mechanical responses of granular material under varying interparticle friction. *Journal of Civil Engineering*. 36(2). 87-96.

Sazzad, M. M. & Suzuki, K. (2010). Micromechanical behavior of granular materials with inherent anisotropy under cyclic loading using 2D DEM. *Granular Matter*, 12(6), 597–605.

Sazzad, M. M. & Suzuki, K. (2011). Effect of Interparticle Friction on the Cyclic Behavior of Granular Materials Using 2D DEM. *Journal of Geotechnical and Geoenvironmental Engineering*, ASCE, 137(5). 545-549.

Sazzad, M. M. & Suzuki, K. (2013). Density dependent macro-micro behavior of granular materials in general triaxial loading for varying intermediate principal stress using DEM. *Granular Matter*, 15(5), 583-593.

Sazzad, M. M. (2014). Micro-scale behavior of granular materials during cyclic loading. *Particuology*, 16, 132–141, 2014.

Sazzad, M.M., Alam, A.A., & Rowshan, M.N.A. (2017). Effect of interparticle friction angle on the stress-dilatancy responses of granular materials by DEM. *Journal of Engineering Science*, 8(1), 41-50.

Sazzad, M.M, Islam, M.S., & Hossain, M.S. (2017). Measurement of Small Strain Stiffness Parameters of Granular Materials. *International Conference on Mechanical, Industrial and Materials Engineering*, RUET, Rajshahi, Bangladesh.

Sazzad, M.M., Sneha, E., & Rouf, R.B. (2017). Comparison of stress-stain behavior of CTC test using DEM simulation. *International Conference on Planning, Architecture and Civil Engineering*, Rajshahi, Bangladesh, 194-199.

Skinner, A.E. (1969). A note on the influence of interparticle friction on the shearing strength of a random assembly of spherical particles. *Geotechnique*, 19(1), 150-157.

Tatsuoka, F., Iwasaki, T., Fukushima, S., & Sudo, H. (1979). Stress conditions and stress histories affecting shear modulus and damping of sand under cyclic loading. Soils and Foundation, 19(2), 29–43.

Proceedings of the 4th International Conference on Civil Engineering for Sustainable Development (ICCESD 2018), 9~11 February 2018, KUET, Khulna, Bangladesh (ISBN-978-984-34-3502-6)

NEGATIVE SKIN FRICTION INDUCED ON SINGLE PILE IN COLLAPSIBLE SOILS DUE TO TOP INUNDATION

Roy, C.[1], Noor, S.T.[2], Niloy, T.M.[3], Trisha, A.H.[4], Rana, M.[5] and Aziz, T.[6]

[1] Graduate Student, Department of civil engineering, University of Asia Pacific, Bangladesh, e-mail: chiranjib.uap@gmail.com
[2] Associate Professor, Department of civil engineering, University of Asia Pacific, Bangladesh, e-mail: sarah@uap-bd.edu
[3,4,5,6] Graduate Student, Department of civil engineering, University of Asia Pacific, Bangladesh, e-mail: tmniloy@gmail.com

ABSTRACT

The collapsible soil is known as problematic soil, which possesses considerable strength when it is dry and loses its strength and experience excessive settlement when inundated. Moreover, Inundation of any soil is practically unavoidable, as it could take place either naturally or accidentally. Top inundation comes about due to surface runoff, percolation of rain-water, poor drainage, flood etc. Practicing engineers face enormous challenges when they build on/in collapsible soil and as there is lack of sufficient and reliable methods for predicting negative skin friction (NSF) and drag force on piles embedded in collapsible soils, the foundation design in collapsible soil is still based on conventional soil mechanics, which yields unsafe design values. From this paper, however, they will get an insight into the problematic behavior of collapsible soil and associated foundation problems during inundation. This thesis work also attempted to perform a parametric study to establish the effect of the governing parameters that may affect the performance of a single pile in collapsible soil subjected to inundation. In this study, an extensive numerical investigation was carried out using the numerical model to predict NSF exerted on the pile for a given soil and pile conditions due to soil inundation. An analytical model was developed based on the numerical results obtained from the previous investigation to calculate the drag load as well. The results revealed that the value of the average negative shear stress usually varied between 12 to 30 KPa. Whereas, the unit NSF ($Q_n/\pi D$) already reaches its maximum value due to the wetting of 7 m radius front. Beyond this level, the soil becomes detached from the pile. Therefore, any increase in the radius of wetting front and the collapse potential could not further increase the value of NSF.

Keywords: *Collapsible Soil, Top Inundation, Negative Skin Friction, Drag Load and Analytical Modeling.*

1. INTRODUCTION

In recent years, several landslides were experienced suddenly after heavy rainfall in Chittagong hill tracts, Bangladesh, while significant soil settlements near riverside zones have also been reported. Though the causes of both types of disasters have not yet been studied, the consequences resemble inundation induced collapse problem that is commonly observed in arid and semi-arid climatic zones of USA, China, Algeria, Egypt, Russia, etc. Collapsible soils are known to experience significant volume decrease due to the increase of soil moisture content, without an increase in the in-situ stress level. Such soil response (i.e., landslides or significant soil settlements) to inundation could not be predicted beforehand, based on the knowledge of saturated soil mechanics and the experiences with non-problematic or other kinds of problematic (for example, expansive soil and sensitive clay) soils as well. The irrecoverable volume reduction (under constant stress level and only due to the inundation) of collapsible soil takes place so fast and hasty that no measures can be taken to forefend the problem once it initiates.

The problem of negative skin friction (NSF) is the most common problem in the design of pile foundations in soft ground (Lee, Bolton & Al-Tabaa, 2001). In the literature, several reports can be found dealing with negative skin friction on pile foundations, the majority of them dealing with soft soils, while few address the case of collapsible soils, and accordingly, there is a high level of uncertainty for predicting negative skin force on these piles in collapsible soil subjects to top inundation. Negative skin friction mobilizes on piles when the surrounding soil's settlement is faster than the settlement of the pile, resulting in friction force acting downward on the pile shaft (Chen, Huang, Qin & Fang, 2008). The collapsible soil is known as problematic soil that is susceptible to a large and sudden reduction in volume upon wetting. However, inundation of any soil is practically unavoidable, since it could take place either naturally (due to rainfall) or accidentally (e.g., leakage from underground waterlines). Likewise, the most significant, top inundation is brought about due to surface runoff, percolation of rain-water, poor drainage, flood etc. Therefore, piles installed in collapsible soils are subjected to negative skin friction due to the excessive settlement accompanied during inundation from the top. The collapse behavior is governed by some parameters including the collapse potential, the method of inundation and the thickness of the collapsible layer. In this investigation, a prototype experimental model was built to measure negative skin friction forces acting on an end-bearing pile embedded in the collapsible soil during top inundation. The drag load on the pile shaft was also measured as the governing parameters.

Drag load that is induced on the pile as an additional load due to negative skin friction conventionally develops on the pile surface, which needs to be considered in pile design (Noor, Hanna & Mashhour, 2013). If drag load is not considered in the design, it may cause serious damage to structures and might have even lead to catastrophic failure. Piles in the collapsible soil, soft clay, and liquefiable soil may experience drag load due to inundation (Chen, Zhou & Chen, 2009), consolidation (Hanna & Sharif, 2006) and liquefaction (Fellenius & Siegel, 2008), respectively. Lowering of the ground water table around the pile shaft can also cause drag load (Lee, Chen & Wang, 1998). In such cases, pile foundation is often considered the only alternative to transfer loads to the stable soil strata. This is because different soil improvement measures are available, but the extent to which the soil improvement attained in the field condition would adequately minimize the problem of foundation settlement has not been revealed. Previous studies investigated the negative skin friction developed on the pile surface due to inundation of collapsible soil at depth (Hanna and Mashour, 2016; Noor, 2017a and Noor 2017b).

In this study, the effect of inundation of collapsible soil existing near the ground on the development of negative skin friction has been studied. An extensive numerical investigation was carried out to identify the parameters (such as collapse potential, the radius of wetting etc.) and the effects of such parameters on the development of NSF resulting from the full inundation of a given collapsible layer in a single event as well. This paper has also introduced the analytical models, developed by Noor (2011), to predict the drag load on pile due to NSF, caused by the inundation of collapsible soil around the pile. Therefore, by this study, the practicing geotechnical engineers will get an insight about the pile design problems in collapsible soil subject to inundation and thus take part in sustainable development in construction works in our country by addressing these problems.

2. METHODOLOGY

2.1 Numerical Modeling

An axisymmetric finite element model of a single vertical pile was developed to predict negative skin friction for quantifying the drag load. The vertical boundaries were restrained in the horizontal direction, but free to move in the vertical direction. The bottom of the mesh was restrained in both the horizontal and the vertical directions. Therefore, the vertical

settlements of the pile and the soil can occur because of external load and/or the occurrence of inundation of collapsible soil. The centerline of the mesh coincides with the axis of the pile. Both the soil and the pile clusters were meshed with the 15-node triangular element, giving a fourth order interpolation for displacements. Five-node line elements were used at the pile-soil interface to account for the relative pile-soil movement. Figure 1(a) presents the applied boundary condition of the axisymmetric model of a pile embedded in a deep soil bed. The generated mesh, as shown in Figure 1(b), was of medium coarseness using the software *PLAXIS, 2D*.

Important mesh parameters, including size and types of elements and mesh coarseness, were provided to generate mesh automatically, skipping a laborious job of defining thousands of nodes and elements manually. Some important issues were given special attention in generating mesh. First of all, very coarse and very fine meshes were not created to avoid large errors in results and to reduce excessive computational time, respectively. Based on the experience, global fine mesh was considered inappropriate for the problem in hand, as it also involves excessive number of total DOFs. On the other hand, an acceptable mesh demands relatively large number of nodes in the vicinity of the pile‘s shaft, as deformations and stresses generally vary significantly around the pile and at the interface, respectively, as the objective of this modeling is to investigate shear stress distribution at the pile-soil interface.

Mesh is considered acceptable, if it does not include any elongated element and aspect ratio ranges within the reasonable range. However, medium global coarseness applied all over cannot dispense the accuracy in results up to the mark. Therefore, considering the mesh dependency of the FEM results, mesh refinement technique was adopted in this study. A zone, 3 m horizontally from the pile axis and 1.5 L from the ground, was considered for this local mesh refinement. Secondly, any quick transition of element size (between the global elements and those in the refined mesh zone near the outer boundary of the refined mesh zone) was eliminated as the initial mesh was generated with medium global coarseness. Thirdly, the graphical display of the generated mesh was visually inspected for any possible errors, related to the shape of elements and the aspect ratio. If any element is distorted and/or elongated, the shape of the element is adjusted by refining adjacent geometry lines.

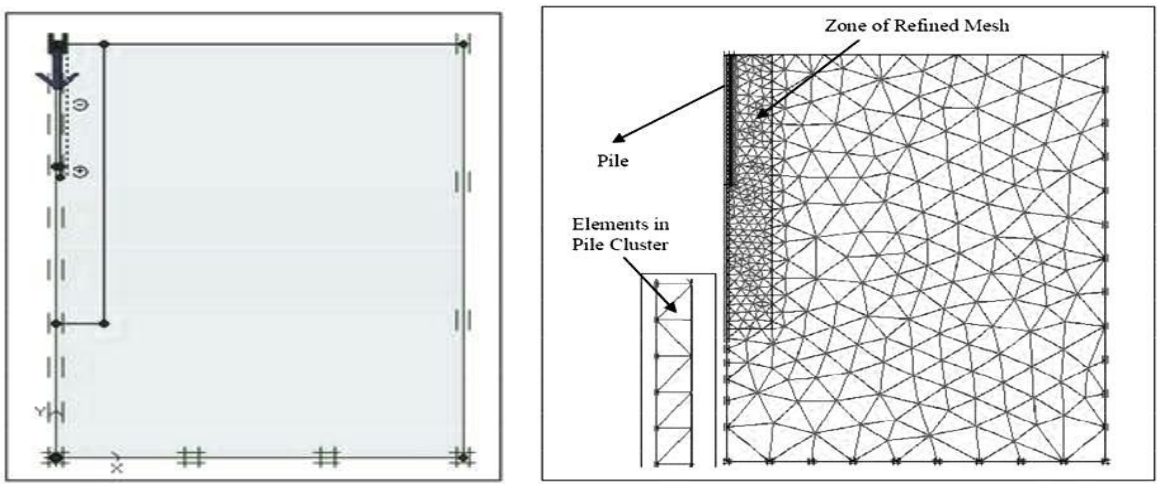

Figure 1: (a) Boundary condition & (b) Generated Mesh in an axisymmetric model.

Pile material was modeled as a non-porous material with Linear-Elastic (isotropic) constitutive relationship, requiring only two input parameters: Young’s modulus (E_p) and Poisson’s ratio (u_p). The constitutive law of the soil was defined by Mohr-Coulomb (MC) failure criterion, requiring five material parameters; including cohesion (c), the angle of

internal friction (φ), the angle of dilatancy (ψ), modulus of elasticity (E) and Poisson's ratio (υ). The behavior of the pile-soil interface was also defined by the MC Model.

In simulating the inundation of collapsible soil, the procedure given in (Noor et al., 2013) proposed to carry out the finite element calculation in three steps [Steps 1, 2*a* and 2*b*]. Step 1 was for the installation of the pile, step 2*a* was to incorporate the effect of strength reductions due to inundation, and Step 2*b* was to simulate volume reduction of collapsible soil subjected to inundation. While detailing out Step 2*a*, that study addressed only the soils that underwent significant reductions in the initial shear strength parameters.

As the present study simulates the scenario of inundation taking place within the collapsible soil layer (in contact with the pile shaft), the changes in the aspects of collapsible soil due to inundation are considered in developing the numerical model. It is to note that the values of c and φ (*i.e.*, two input parameters) decrease, as matric suction decreases during inundation. Moreover, the friction angle (δ) between the pile and the soil that is the main factor to control the magnitude of pile skin friction also decreases during inundation. In the simulation of the present study, these two aspects were addressed in two steps [Step *2a-1* and Step *2a-2*], as shown in Figure 2. Step *2a-1* is to address the strength reduction of unsaturated soils due to inundation. It was previously noted that reduction in φ value of the soil adjacent to the pile shaft has a minor influence on the magnitude of drag load, as calculated from the *PLAXIS* output. Therefore, Step *2a-2* is necessary to incorporate the required adjustment of the input parameters' values for pile interface elements to address the changes in the value of the friction angle (δ).

The above numerical model was employed to derive the mathematical functions that define the coefficients of analytical models developed in this study. Hence, the case of a single-vertical pile was modelled for different pile dimensions, soil properties, and inundation conditions, as listed in Table (1). However, in order to develop charts, the study has choosen the ranges of different parameters by giving considerations to the properties of collapsible soil identified by previous researchers.

Table 1: List of Variable Parameters of Collapsible Soil Properties.

Parameters	Unit	Range
Cohesion (c) of collapsible soil	kPa	20
Angle of internal friction (φ_{cs}) of collapsible soil	°	20–40
Collapse potential (C_p)	%	5–15
Angle of internal friction (φ) of dense sand	°	40
Thickness of collapsible soil layer (H)	m	8–15
Depth of collapsing soil (H_s)	m	4–7.5
$x = H_s/H$	-	0.5
Length of pile (L)	m	12–30
Diameter of pile (D)	m	0.2–1
Pile length-to-diameter ratio (L/D)	-	20–75
Embedded pile length into noncollapsible soil-to-full pile length ratio (L_e/L)	-	0.3–0.75
Radius of wetting (h)	m	3–10
Interface strength reduction factor (ISRF)	-	0.6–0.9

(Noor, 2017)

2.2 Validation of Numerical Model

Firstly, the performance of the developed model and the generated mesh has been tested in terms of ultimate pile capacity, shaft resistance and base resistance of a single pile in dense, medium dense and loose sands using finite element analysis, and the numerically obtained results compare well with those predicted from empirical formulae. Secondly, the validation of the numerical model has been verified by simulating the pile load test in Volgodon experimental region -2 in constant moisture condition. The soil properties of test site have been given in Table (2). The results obtained from numerical analysis have also been found in good agreement (Table 3). Thirdly, the performance of the model in predicting drag load due to negative skin friction due to inundation from the top, was found efficacious with respect to the results of full-scale pile load test in Nikopol region from Grigoryan (1997). Table 4 presents the soil properties used for validation of the numerical model. The comparisons between numerical and experimental results have been given in Table 3. The length-to-diameter ratio (L/D) was 18 and 44 for the piles at Volgodon-2 and at Nikopol, respectively. The collapse potential of the soil up to 6 m below the ground level was 7 %.

Table 2: Soil Properties (Volgodon-2)

Depth (m)	w_n (%)	γ_{bulk} (kN/m^3)	G_s	e	S %	c (kPa)	υ (º)	Remarks
0 – 6	13.8	16.95	2.68	0.78	51	15	19	Collapsible
6 – 15	15	17.5	2.69	0.73	56	24	17	Collapsible
15 - 25	17.9	18.82	2.69	0.62	73	33	19	Non-Collapsible, unsaturated
25-35	23.0	19.6	2.69	0.62	100	33	19	Non-Collapsible, saturated

Table 3: Comparison of Results: Collapsible Soil without inundation condition.

Pile Resistances	Present study	Experimental (Grigoryan, 1997)
Ultimate Pile Capacity, Q_u (kN)	3204	3240
Shaft Resistance, Q_s (kN)	2930	2948
End Resistance, Q_b (kN)	274	292

Table 4: Soil Properties (Nikopol)

Depth (m)	w_n (%)	Void Ratio $e_{initial}$	w_{sat} (%)	γ_{sat} (kN/m^3)	c (kPa)	υ (˚)
0 – 8	7	0.91	28.7	17.57	5	20
8 – 23	4.3	0.86	30.82	18.34	6	16
23 - 30	11.3	0.71	21.2	18.4	5	18

The pile, tested in Nikopol, was equipped with three strain gauge dynamometers at 9.2 m, 12.3 m and 22 m (pile tip) from the pile head. The strain gauge dynamometer was specially

designed with electrical sensors, developed at the Central Scientific Research Institute (TsNIIK in Russian). The dynamometer was installed within the pile stem, so that the full longitudinal force could pass through it. The principle component of a strain gauge dynamometer was the elastic ring, made of high strength steel. The elastic ring was placed between two steel plates of 10 mm thick. The steel plates, with the elastic ring inside, were covered by rubber casings, of 3–4 mm thick. The rubber casing was used for the protection of the steel plates and the elastic ring. Individual pile section was welded to the steel plates. Each cable (wire) attached to the elastic ring was brought to the ground through separate pipe. Pipes were covered with bitumen to prevent cohesion 96 between the pipe and the concrete. In the laboratory, the gauge reading showed no effect of moisture and temperature variations, insulation condition of conductors and oxidation of contacts. Dynamometer measures deformation gave the magnitude of the axial load at the point where it was installed. This dynamometer was calibrated in the laboratory and recalibrated after the pile installed in the ground. The calibration was made up to a load of 1000 kN. The pile was acting under 600 kN load applied at the pile head. The drag load acting on the pile in Nikopol region was 180 kN as measured during field test. The drag load of 186 kN was estimated by numerical analysis of the test pile at Nikopol.

2.3 Analytical Modeling

In this study, the analytical models (developed by Noor, 2011) were employed to predict the drag load (Q_n) due to negative skin friction resulting from the inundation of collapsible soil from the top. Based on the numerical results, unit negative skin friction ($Q_n/\pi D$) has a linear relationship with Hs/D, as defined by Equation (1).

$$Q_n/\pi D = I_a * (H_s/D) + I_b \quad (1)$$

The values of I_a and I_b depend on the collapse potential (C_p), as $Q_n/\pi D$ shows different slopes for different collapse potential (varies between 5–15%) for a given H_s/D ratio. The values of I_a and I_b depend on H_s/D ratio, as shown in Figure 2 and Figure 3.

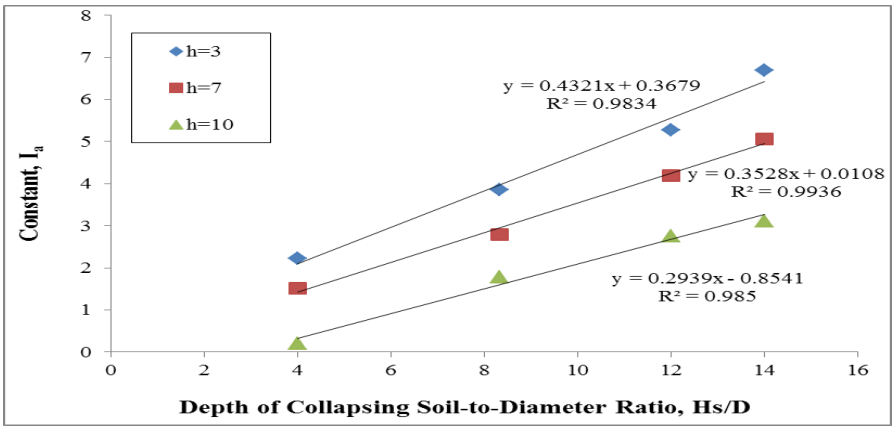

Figure 2: Value of Ia for different Hs/D and h, when Cp between 5–15%.

The value of I_a can be found from Equation (2) – Equation (4) as below.

For h = 3 m

$$I_a = 0.432\ (Hs/D) + 0.368 \quad (2)$$

For h = 7 m

$$I_a = 0.353\ (Hs/D) + 0.011 \quad (3)$$

For h = 10 m

$$I_a = 0.294\ (Hs/D) + 0.854 \quad (4)$$

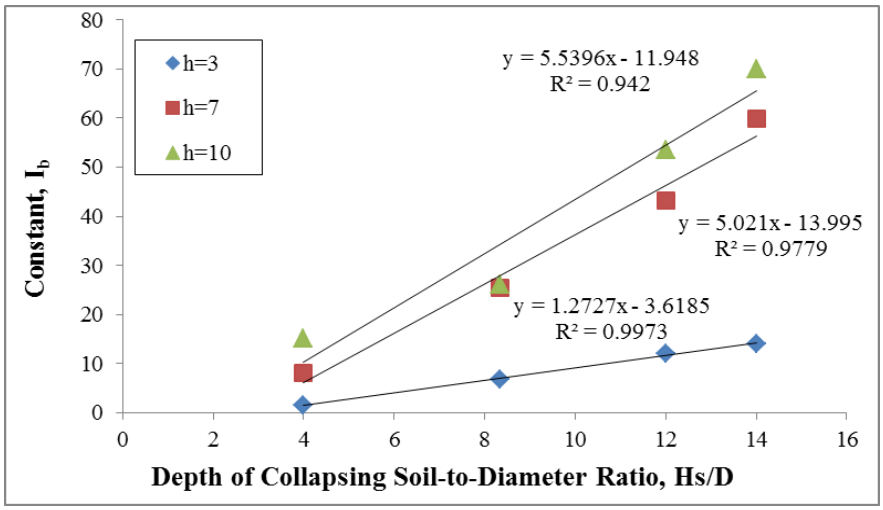

Figure 3: Value of Ib for different Hs/D and h, when Cp between 5–15%.

The value of I_b can be found from Equation (5) – Equation (7) as below.

For h = 3 m
Ib = *1.273* *(Hs/D)* – *3.619* (5)

For h = 7 m
Ib = *5.021* *(Hs/D)* – *13.995* (6)

For h = 10 m
Ib = *5.539* *(Hs/D)* – *11.948* (7)

Therefore, the indirect load is also known as drag load (Q_n) due to NSF (at ISRF 0.8) can be predicted from the value of the unit negative skin friction using Equation (1) multiplied by the perimeter (πD) of the pile for the case of inundation from the top.

3. RESULTS AND DISCUSSION

The shear stress distribution at the pile interface for a given collapsible soil layer (h=3m) of different collapse potential (Cp) has been illustrated in Figure 4. It is observed that during soil collapse, both the negative shear stress (due to NSF) and the positive shear stress (due to positive skin friction) take place simultaneously. A significant influence of collapse strain (i.e. volume reduction) was also observed due to inundation, such as for greater collapse strain, Q_n increases, because of the increase in the area bounded by the negative part of the shear stress distribution.

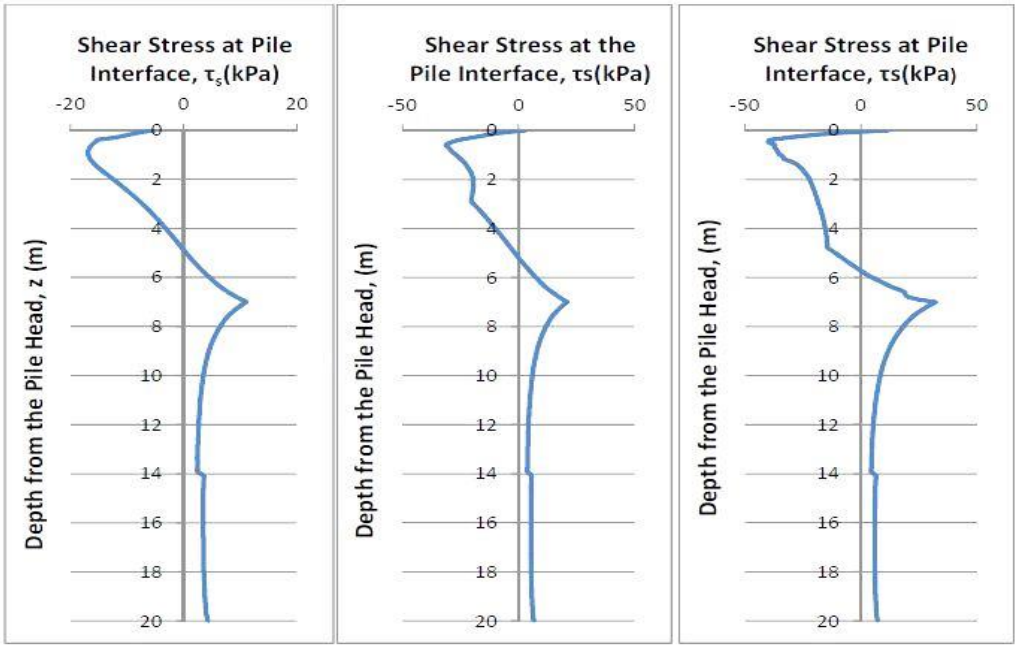

Figure 4: Shear stress distribution, when h = 3m, (a) Cp = 5%, (b) Cp = 10% and (c) Cp = 15%.

The effects of the radius of wetting front (h) on the shear stress distribution were also examined in Figure 5 for the cases of inundation from top. It was investigated that the area bounded by the negative part of the shear stress distribution increases with the increase of the radius of wetting front, and hence, the indirect load (Q_n) due to NSF also increases, accordingly.

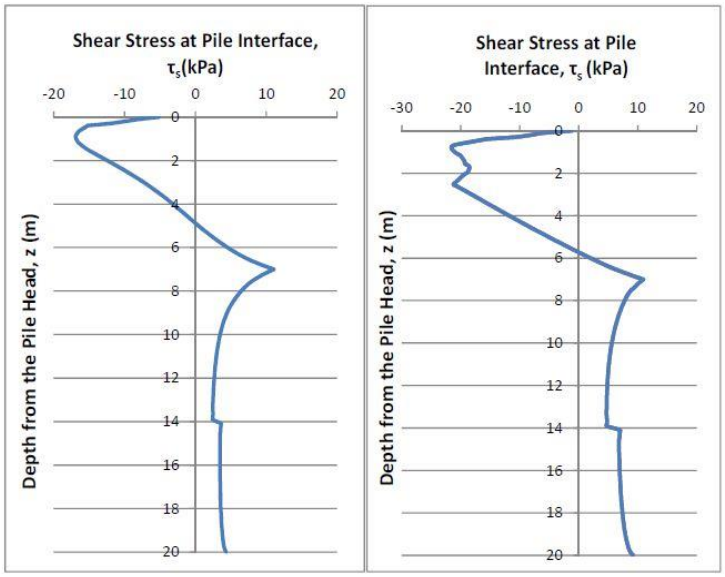

Figure 5: Shear stress distribution, when C_p = 5%; (a) h = 3m, and (b) h =7m.

The effect of the depth of collapsing soil-to-pile diameter ratio (Hs/D) on negative skin friction has been depicted in Figure 6- Figure 8 by turns for different depth of collapsible soil layer, where the unit negative skin friction ($Q_n/\pi D$) shows linear variation with the increase of H_s/D ratio. High collapse potential of the collapsing soil and wide wetting front were also found to increase the intensity of the effect of Hs/D ratio on $Q_n/\pi D$.

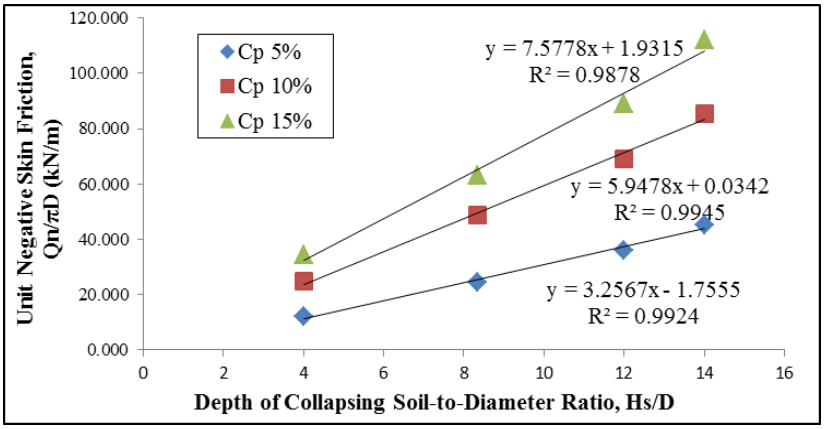

Figure 6: Unit negative skin friction (Qn/πD) vs. Hs/D ratio, when h = 3m.

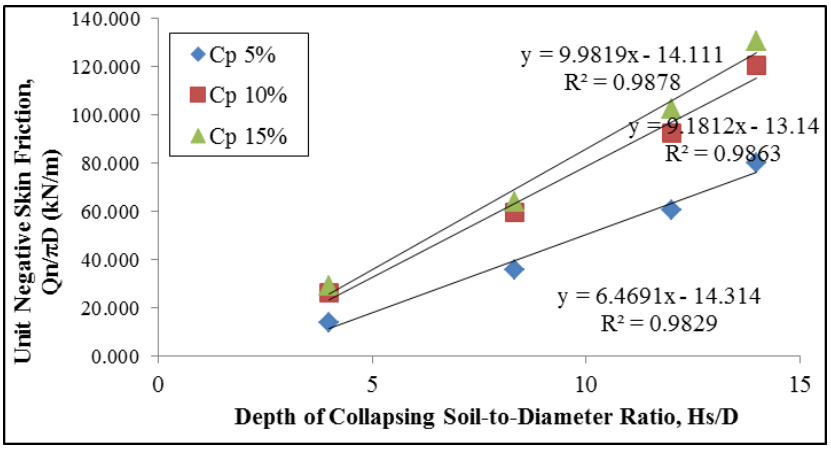

Figure 7: Unit negative skin friction (Qn/πD) vs. Hs/D ratio, when h = 7m.

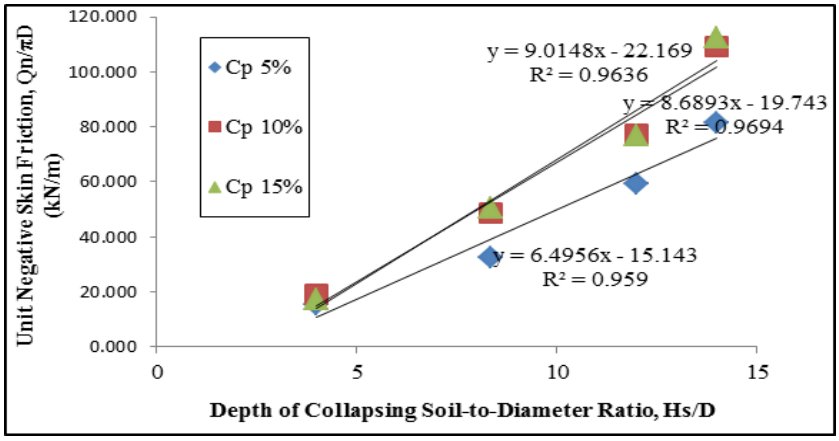

Figure 8: Unit negative skin friction (Qn/πD) vs. Hs/D ratio, when h = 10m.

The effect of the radius of wetting front on Qn/πD for different Hs/D ratio and Cp has been shown in Figure 9- Figure 11 as below. It is found that Qn/πD does not increase infinitely with the increase of h. Figure 11 has demonstrated that $Q_n/\pi D$ attains its maximum value due to 7 m of the radius of wetting front. Beyond this level, the soil becomes detached from the pile. Therefore, any increase in the radius of wetting front and the collapse potential could not further increase the value of $Q_n/\pi D$.

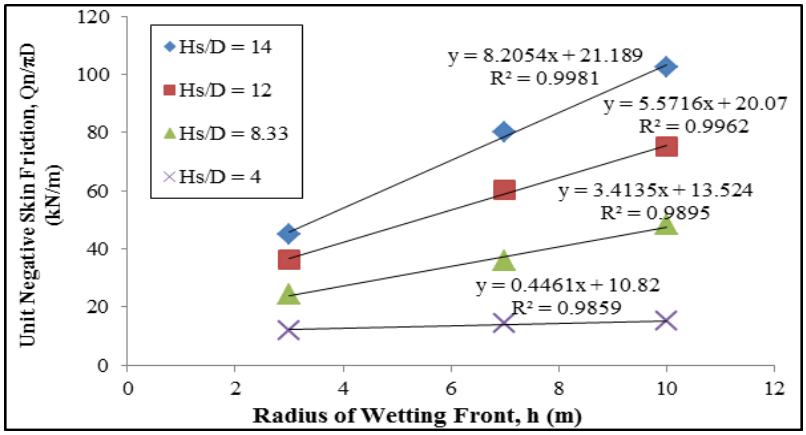

Figure 9: Effect of radius of wetting front (h) on ($Q_n/\pi D$), when C_p = 5%.

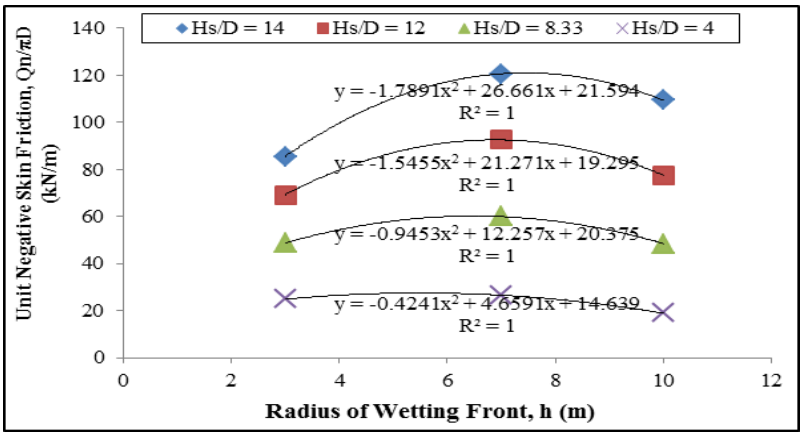

Figure 10: Effect of radius of wetting front (h) on ($Q_n/\pi D$), when C_p = 10%.

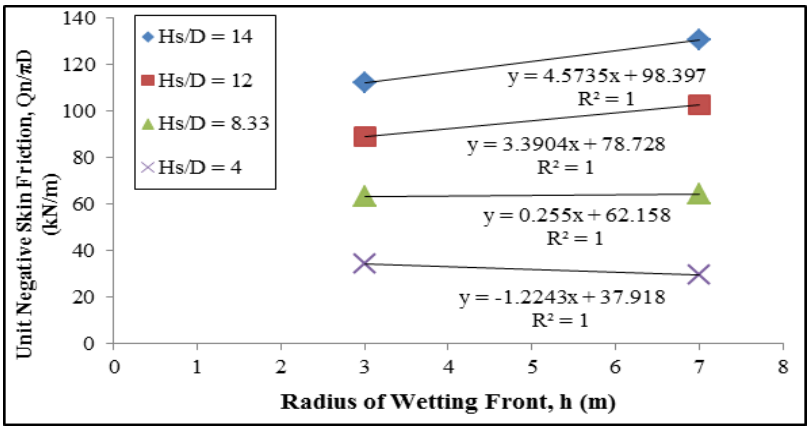

Figure 11: Effect of radius of wetting front (h) on ($Q_n/\pi D$), when C_p = 15%.

The effect of collapse potential (C_p) on $Q_n/\pi D$, for different Hs/D ratio and h, has been demonstrated in Figure 12 - Figure 14. It is noted that there exists a linear relation between average negative shear stress (q_n) and collapse potential (C_p) in each case. For a given radius of wetting front (h), the straight line in q_n vs C_p plot passes through origin. The investigated result reveals that between 5–10% of collapse potential, the effect of C_p is more pronounced than any other condition beyond this range. It can also be noted that the proportional coefficient relating q_n and C_p varies with H_s/D. The value of proportional coefficient also increases if the H_s/D ratio is less than 14, for a given radius of wetting.

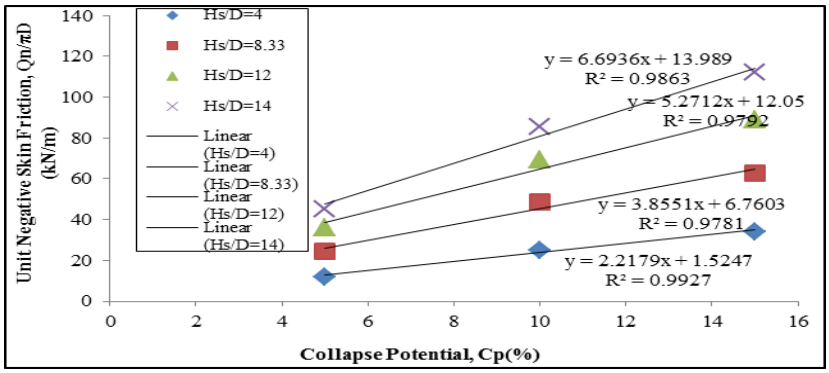

Figure 12: Effect of collapse potential (C_p) on ($Q_n/\pi D$), when h = 3 m.

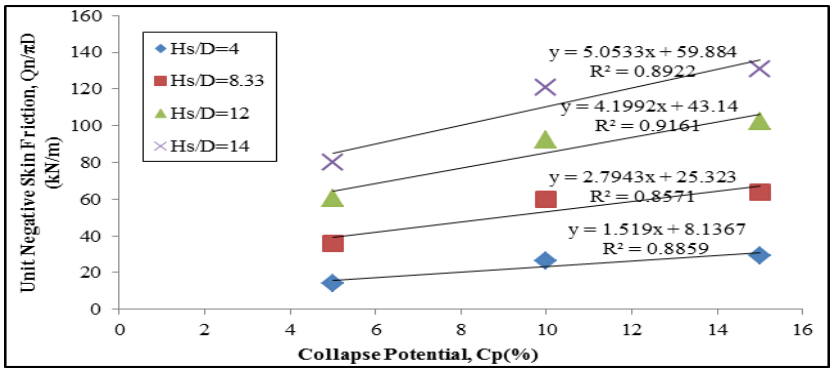

Figure 13: Effect of collapse potential (C_p) on ($Q_n/\pi D$), when h = 7 m.

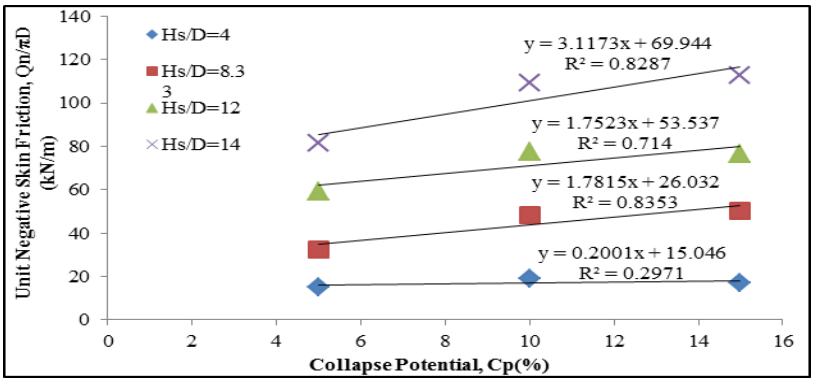

Figure 14: Effect of collapse potential (C_p) on ($Q_n/\pi D$), when h = 10 m.

However, based on the numerical results, collapse potential (C_p), radius of wetting (h), direction of wetting (from bottom or top) and interface strength reduction factor were found to have significant influence on the shear stress developed on the pile interface during inundation of collapsible soil around the pile. Instead, the angle of soil internal friction (φ), L_e/L and L/D ratios have no effect on average negative shear stress (q_n). Furthermore, H_s/D ratio governs the magnitude of average negative shear stress.

4. CONCLUSIONS

The magnitude of the drag load caused by inundation-induced soil collapse adjacent to the pile shaft depends on several parameters, while most of these parameters are not related to the development of drag load due to consolidation or liquefaction. In this study, numerical model is developed considering all the parameters influencing the magnitude of drag load

and the fact that negative skin friction is a kinetic type of friction. The analytical models are developed to quantify the drag load at the design stage. Moreover, the following conclusions could also be summarized based on the scope of this study:

- Unit negative skin friction ($Q_n/\pi D$) has linear relation with H_s/D ratio in a semi logarithmic plot, for given h and C_p.
- Unit negative skin friction ($Q_n/\pi D$) does not increase infinitely due to the increase of h.
- Collapse potential (C_p) influences unit negative skin friction ($Q_n/\pi D$) more than the depth of neutral axis (N.A.).
- The design guideline, presented in this paper, will allow the foundation designers to optimize the pile design diameter.

ACKNOWLEDGEMENTS

The information used in this paper has been adapted from several international journals, conference papers, and both M.Sc. & undergraduate thesis papers. The authors of this paper are indebted to the lab stuff for their nice cooperation. This thesis work was conducted with the financial support and laboratory facilities provided by University of Asia Pacific, Dhaka, Bangladesh under a sustainable project in Dhaka city.

REFERENCES

Chen, Z. H., Huang, X. F., Qin, B., Fang, X.W. & Guo, J. F., (2008). Negative skin friction for cast-in-place piles in thick collapsible loess. In: D.G. Toll, C.E. Augrade, D. Gallipoli, and S.J. Wheeler, Eds., *Unsaturated Soils. Advances in Geo-Engineering.,* Taylor and Francis: London, UK, pp. 979-985.

Chen, R.P., Zhou, W.H., & Chen, Y.M., (2009). Influences of soil consolidation and pile load on the development of negative skin friction of a pile. *Comput. Geotech.,* vol. 36, pp. 1265-1271. Retrieved from http://dx.doi.org/10.1016/j.compgeo.2009.05.011.

Fellenius, B.H. & Siegel, T.C. (2008). Pile drag load and downdrag in a liquefaction event. *J. Geotech. Geoenviron. Eng.,* vol. 134, pp. 1412-1416. Retrieved from http://dx.doi.org/10.1061/(ASCE)1090-0241(2008)134:9(1412).

Grigorian, A.A., (1997). *Pile foundations for buildings and structures in collapsible soil.,* A.A. Balkema Publishers: Brookfield, VT.

Hanna, A.M. and Sharif, A., (2006), "Drag force on a single pile in clay subjected to surcharge loading", *Int. J. Geomech.,* vol. 6, pp. 89-96. Retrieved from http://dx.doi.org/10.1061/(ASCE)1532-3641(2006)6:2(89).

Lee, C.J., Bolton, M.D., & Al-Tabaa, A. (2001, April). Recent findings on negative skin friction in piles and pile groups in consolidating ground. Proceedings of the 5th International Conference on Deep Foundation Practice. Singapore. pp. 273-280.

Lee, C.J., Chen, H.T. & Wang, W.H., (1998). Negative skin friction on a pile due to excessive ground water withdrawal. Proceedings of the International Conference. Centrifuge, New York. pp. 513-518.

Noor, S.T., Hanna, A.M., & Mashhour, I., (2013). Numerical modeling of piles in collapsible soil subjected to inundation. *Internatioal Journal on Geomech.,* vol. 13, pp. 514-526. Retrieved from http://dx.doi.org/10.1061/(ASCE)GM.1943-5622.0000235.

Noor, S.T., (2017). Numerical and Analytical Modeling for Predicting Drag Load Induced on Pile in Collapsible Soil because of Inundation. *The Open Civil Engineering Journal*, August, 2017, *11*, pp.664-675. DOI: 10.2174/1874149501711010664. Retrieved from www.benthamopen.com/TOCIEJ/.

PLAXIS 2D 8.6 [Computer Software]. Delft, Netherlands, PLAXIS.

Proceedings of the 4th International Conference on Civil Engineering for Sustainable Development (ICCESD 2018), 9~11 February 2018, KUET, Khulna, Bangladesh (ISBN-978-984-34-3502-6)

INVESTIGATION OF GEOTECHNICAL PROPERTIES OF COAL MINE WASTE: A CASE STUDY FOR BARAPUKURIA COAL MINE

Md. Belal Hossain[1], Md. Kumruzzaman[2] and Md. Roknuzzaman[3]

[1] *Assistant Professor, Department of Civil Engineering, Hajee Mohammad Danesh Science and Technology University, Bangladesh, e-mail: mbh.civil@hstu.ac.bd*
[2] *Professor, Department of Civil Engineering, Rajshahi University of Engineering & Technology, Bangladesh, e-mail: kzzaman@hotmail.com*
[3] *Lecturer, Department of Civil Engineering, Hajee Mohammad Danesh Science and Technology University, Bangladesh, e-mail: mrz.civil@hstu.ac.bd*

ABSTRACT

The byproducts generated during mining and processing of coal, generally known as coal mine wastes, are usually dumped near the mining area causing several environmental and aesthetic problems. The present study is aimed to investigate engineering properties of coal mine waste generated from the Barapukuria coal mine, Dinajpur and to evaluate the possibility of using them in the field of geotechnical engineering such as a replacement of road subgrade. Laboratory tests like specific gravity test, grain size analysis, Atterberg limit test, proctor test, unconfined compression test and California Bearing Ratio test were carried out on fresh coal mine waste collected from the Barapukuria coal mine. Test results indicate that the mine waste behaves like a poorly graded inorganic soil which falls in the category "sandy lean clay" with a maximum dry density of 18.13 kN/m3. Unconfined compressive strength was determined as low as 39.99 kN/m2 and hence the waste itself was found to be unsuitable for using as a supplementary engineering material for geotechnical structures. It was concluded that the fresh coal mine waste must be improved with strengthening admixture before using them as an engineering material for structures. In addition, chemical analysis of the waste detected lead content as 0.026 ppm that indicated the requirement of precautions for the areas with high ground water table.

Keywords: *Coal Mine Waste, Barapukuria Coal Mine*

1. INTRODUCTION

Coal is one of the primary sources of energy in Bangladesh and there is an increase in demand for coal production to meet the requirements of the industries. The amount of waste generated from coal mining and processing operation is increasing alarmingly. At present, with the exception of some small scale underground waste disposal operations in abandoned coal mines, most of these wastes are disposed at the surface, which inevitably requires excessive planning and control to minimize the environmental impact of mining. It also results in non-productive use of land, air and water pollution, possible failure of waste embankments, and the loss of aesthetic value of the land. It is high time to find out alternative ways to utilize the coal mine wastes. Before planning such alternate use in the field of engineering, it is essential to know several physical, chemical and engineering properties of the waste. The present study is focussed on investigating the properties of coal mine waste so that they can be used in the field of geotechnical engineering. The Barapukuria Coal Mine, the only natural coal mine reserve that is in operation, is taken under consideration.

Various research and studies on coal mine waste have been conducted in recent years to analyse the possibility of utilization of these wastes, to find out ways to store these wastes safely without causing any pollution and also to find out the methods by which these wastes can be used to prevent various kinds of environmental pollution. A research about Re-Use of

Mine Waste Materials Amended with Fly Ash in Transportation Earthwork Projects revealed that mine waste materials mixed with fly ash can be used in transportation projects bringing some environmental benefits by decreasing energy consumption, raw material use, and greenhouse gas emissions (Christopher, 2013). Another investigation on the use of coal mine refuse for sub-base material and embankment fill in south Dakota showed that coal mine refuse sampled at an abandoned mine site in South Dakota can be used as embankment fill material and can provide limited uses for sub-base applications (Uckert et al., 2006). A geotechnical investigation of coal mine refuse was conducted to assess the fill's ability to act as a ground support material and to study the physical and mechanical properties of coal mine refuse where samples were collected from different mines of Mahanadi Coalfields Ltd (MCL), Hindalco, and South Eastern Coalfields Ltd (SECL). The different tests were performed like triaxial test, slake durability test, liquid limit test, standard proctor compaction test and permeability test. It was found that only coal refuse sample can be used for the purpose of backfilling without much treatment. But all other samples need some treatment such as removal of some fine particles, mixing with some amount of cement or some other binding material so that its strength increases and it does not deteriorate when subjected to wetting and drying cycles (Agarwal, 2009). In another study the physical and mechanical properties of coal mine waste from different sites were described and the effects of these properties on the duty requirements of fill materials were assessed. It was concluded in that study that if improving ground control is the only reason for backfilling, coal refuse alone does not appear to be a suitable stowing material. If coal-refuse disposal is also a consideration, then it may be more attractive stowing and backfilling material (Karfakis et al., 1996). There are also few number of studies carried out on Barapukuria Coal Mine. A research titling "an Assessment of the Underground Roadway Water Quality for Irrigation Use around the Barapukuria Coal Mining Industry" was carried out to investigate the effect of coal mining work on irrigation water (Howladar et al., 2014). The effect of long-wall mining on groundwater for underground coal extraction in Barapukuria was also studied (Kibria et al., 2012). However, the possibility of using Barapukuria coal mine waste as an engineering material was never analyzed by any researchers. The wastes generated from Barapukuria coal mine are not disposed in an authority controlled safe zone. Also they are not generally used for any engineering purpose. Hence, this study about analyzing the geotechnical properties of coal mine wastes collected from the Barapukuria Coal Mine is justified and a well-demanded work.

2. METHODOLOGY

A number of laboratory tests are carried out in order to accomplish this work. Coal mine wastes were collected several times from nearby coal mine. The tests were carried out following the methods and procedures described in ASTM standard.

2.1 Collection of Sample

For this research work, Coal mine waste was collected from Barapukuria coal mine situated at Chowhati village of Phulbari upozilla, Dinajpur. Sample was collected from the dumping site removing the top layers.

Figure 1: Dumped coal mine waste at Barapukuria Coal Mine

2.2 Laboratory Tests of Waste

The entire laboratory testing on coal mine waste was carried out in accordance with ASTM designation. Laboratory tests such as specific gravity test, grain size distribution test (by sieving and hydrometer), standard proctor test, Atterberg limit test, unconfined compression test and California Bearing Ratio (CBR) tests were performed.

2.2.1 Specific Gravity Test

ASTM D 854-00 – Standard test for specific gravity of soil solids by water Pycnometer was adopted for determining specific gravity of coal mine waste sample. The value of specific gravity roughly indicates soil behaviour.

2.2.2 Grain Size Analysis

ASTM D 422 - Standard test method for particle size analysis of soils was adopted for identifying soil type and gradation of fresh coal mine waste.. The Unified Soil Classification System (USCS) was used to classify the waste as a particular soil type based on its grain size analysis data.

2.2.3 Atterberg Limit Tests

ASTM D 4318 - standard test method for liquid limit, plastic limit, and plasticity index of soils was applied for the determination of Atterberg limits of the waste sample. Liquid limit, plastic limit and plasticity index was calculated. Based on the plasticity index and sieve analysis result USCS soil classification was applied in accordance to the plasticity chart.

2.2.4 Standard Proctor Tests

ASTM D 698 - Standard test methods for laboratory compaction characteristics of soil using standard effort (12,400 ft-lbs/ft3) was applied for the determination of optimum moisture content and maximum dry density of the waste sample.

2.2.5 Unconfined Compression Test

ASTM D 2166 - Standard test method for unconfined compressive strength of cohesive soil was adopted for the determination of unconfined compression strength of the waste. This test reveals strength characteristics of the sample. Das (1994) suggested the general relationship between unconfined compressive strength and the quality of the subgrade soils used in pavement applications as in Table 1.

Table 1: Relationship between unconfined compressive strength and the quality of the subgrade (Das, 1994)

UCS value (psi)	Quality of Subgrade
<3.625	Very soft
3.625-7.25	Soft
7.25-14.50	Medium
14.50-29.00	Stiff
29.00-55.10	Very stiff
>55.10	Hard

2.2.6 California Bearing Ratio Test

ASTM D 1883 - Standard test method for determination of California bearing ratio of soil was adopted for the determination of CBR value of the waste. This test evaluates the potential of the waste to be used as a road pavement material.

2.2.7 Chemical Analysis

Standard X-ray Fluorescence chemical tests were performed on fresh coal mine waste to find-out the existence of possible toxic or harmful content in the sample. An EDF3600B model EDXRF (Energy Dispersive X-ray Fluorescence) spectrometer was used. The test result was obtained by ORE work curve method from the attached computer.

3. RESULTS AND DISCUSSIONS

3.1 Specific Gravity

The value of specific gravity was found to be 2.59. This value lies within the range 2.6 to 2.8 which indicates that the fresh coal mine waste resembles like an inorganic soil (Aurora 2006).

3.2 Grain Size

Both sieve analysis and Hydrometer test were carried out for the waste and combining sieve analysis and hydrometer analysis data, a grain size distribution curve is plotted as shown in Figure 2.

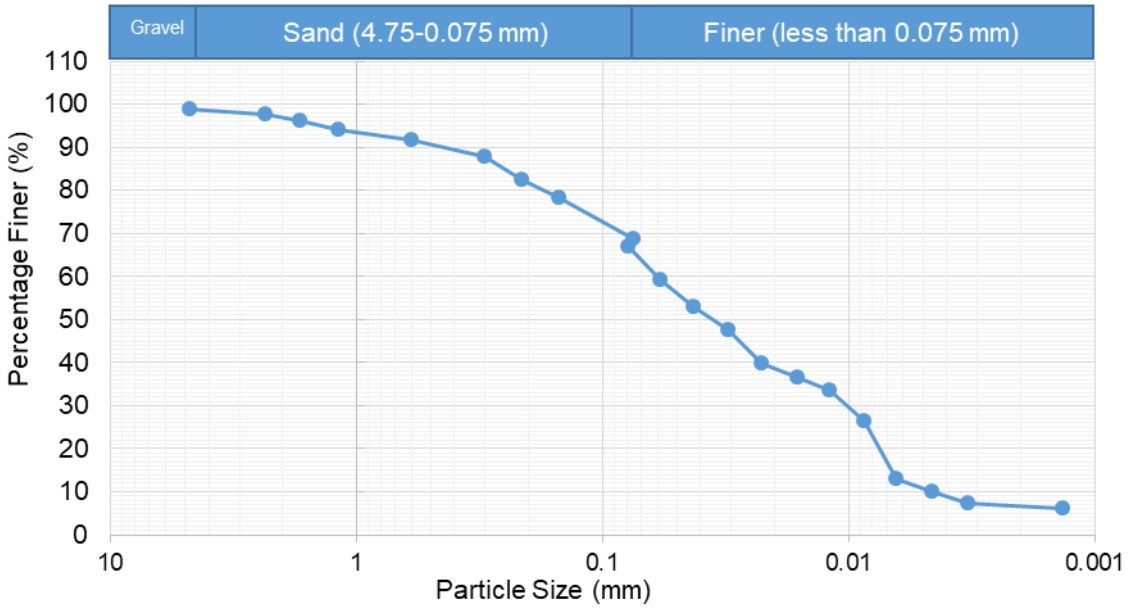

Figure 2: Grain size distribution curve for fresh coal mine waste

Analyzing the grain size distribution curve, the uniformity coefficient (C_u) was found to be 13.33 and Coefficient of Curvature (C_c) was found to be 0.37. A soil sample is said to be well graded if the criteria $C_u \geq 6$ and $1 < C_c < 3$ are satisfied (Holtz and Kovacs 1981). In case of fresh coal mine waste criteria for C_u is met, but C_c lies below unity and hence the soil is poorly graded (Arora, 2006).

3.3 Atterberg Limits and Soil Classification

The liquid limit of waste sample was found to be 32.30% and plastic limit was 13.56%. Plasticity index was calculated as 18.74%. Based on the criteria of the unified soil classification system (USCS), Since in sieve analysis, more than 70% sample Passes No. 200 Sieve and from Atterberg limit test PI > 7 and plots above "A" line in the plasticity chart; So, the sample is of CL group & classified as “Sandy Lean Clay” (inorganic clay of low to medium plasticity). The plasticity chart is shown in Figure 3.

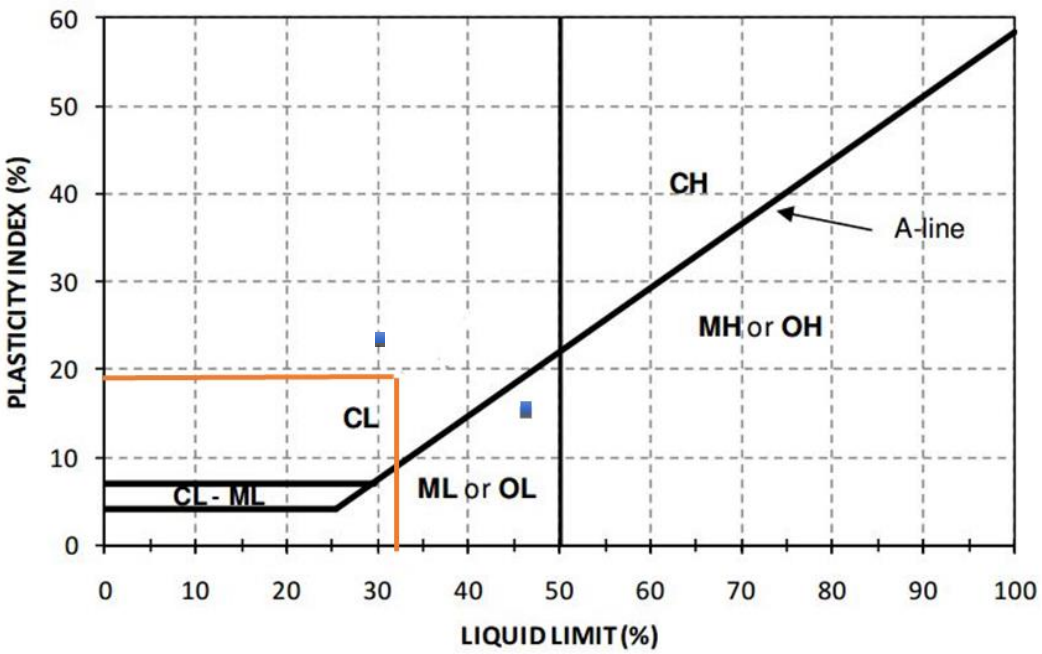

Figure 3: Determination of soil type of waste sample from plasticity chart (USCS)

3.4 Compaction Parameters

By performing standard Proctor test, optimum misture content was found to be 7.5% and maximum dry density was obtained as 18.13 kN/m^3. Corresponding graph for the determination of optimum moisture content (OMC) and maximum dry density (MDD) are presented in Figure 4.

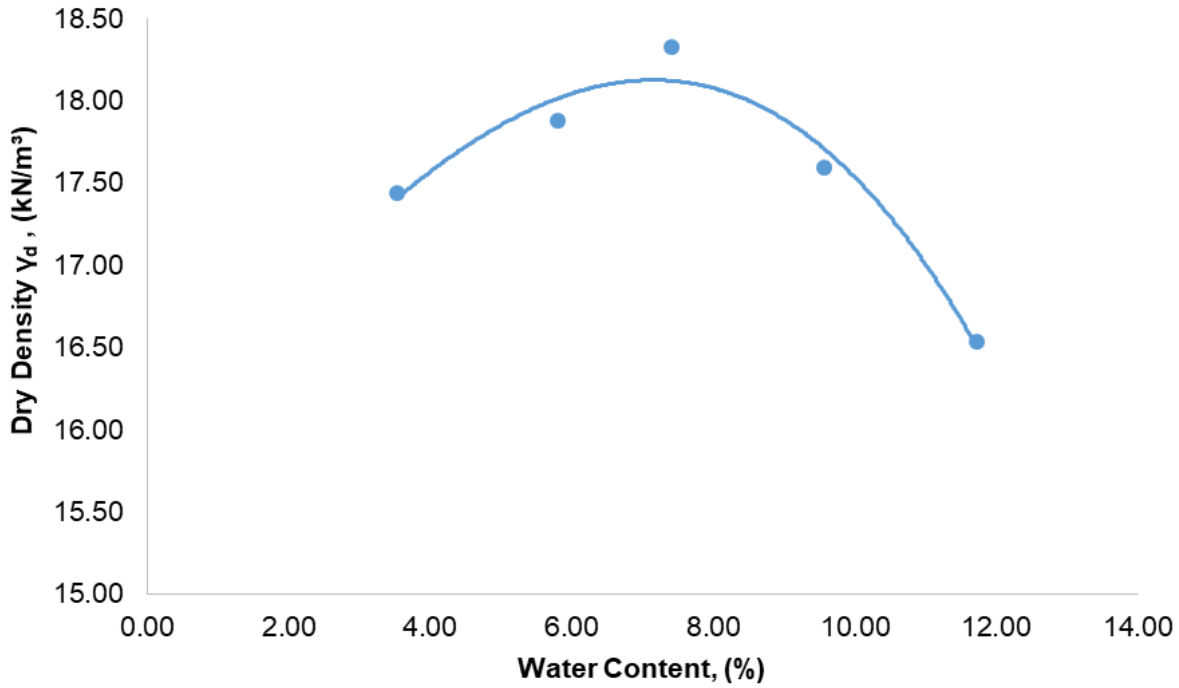

Figure 4: Relationship between dry density (kN/m^3) and water content (%)

3.5 Unconfined Compression Strength

Using unconfined compression test data, the relation between axial stress and axial strain are presented in Figure 5.

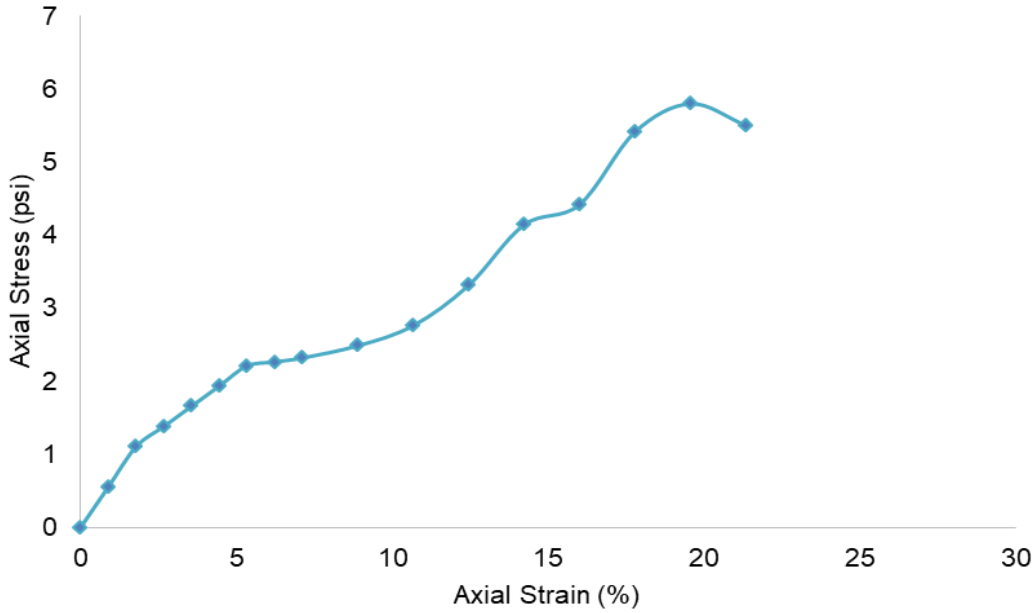

Figure 5: Relationship between axial stress (psi) vs. axial strain (%) for different mixes

The unconfined compression strength was found to be 5.8 psi only and the waste falls in the category “very soft” according to USCS classification system.

3.6 California Bearing Ratio

The relation between unit load and penetration for both unsoaked and soaked CBR test are shown in Figure 6.

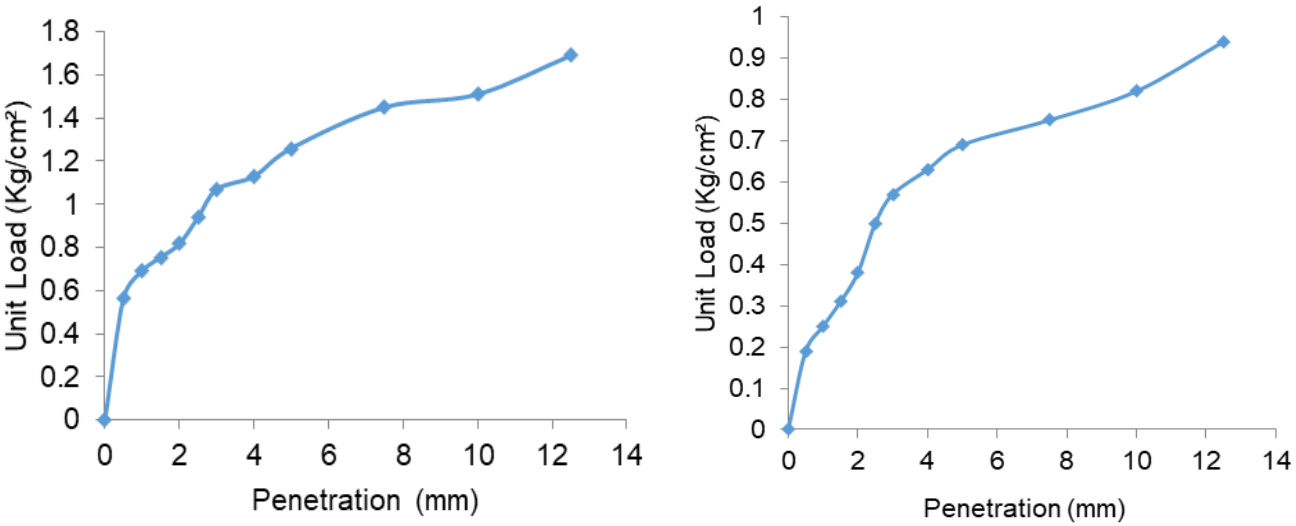

(a) Unsoaked Sample (b) Soaked Sample

Figure 7: Relationship between unit load and penetration

CBR value and expansion ratio is presented in table 2.

Table 2: CBR test result

Sample Condition	Penetration	
	2.5mm	**5.0mm**
Un-soaked	1.34	1.2
Soaked	0.71	0.66
Expansion ratio	1.51	

A large expansion ratio was obtained for the waste sample which indicates its inferiority as a road material.

3.7 Chemical Analysis Report

The chemical analysis report for the waste sample is presented in Table 3.

Table 3: XRF test result for fresh coal mine waste

Element	Content in Sample-1 ppm	Content in Sample-2 ppm	Content in Sample-3 ppm	Average Content ppm
Al	1.625	1.287	1.458	1.456
Si	5.570	4.455	4.981	5.002
P	0.002	0.000	0.000	0.001
S	0.055	0.036	0.041	0.044
K	0.297	0.211	0.244	0.251
Ca	0.034	0.022	0.030	0.029
Ti	0.081	0.087	0.067	0.078
Mn	0.010	0.008	0.007	0.008
Co	0.003	0.004	0.004	0.003
Fe	2.669	2.563	2.552	2.595
Cu	0.011	0.011	0.011	0.011
Zn	0.019	0.020	0.021	0.020
Sn	0.046	0.041	0.044	0.043
Pb	0.019	0.024	0.035	0.026
Rb	0.005	0.004	0.004	0.004
Nb	0.001	0.005	0.001	0.002
Mo	0.022	0.015	0.017	0.018

The tested lead level of the waste samples is obtained 0.026 ppm. No level of lead is considered safe in drinking water; although an action level of 0.015 ppm at the tap can be used to identify highly impacted water. Therefore the lead content of waste may be potentially harmful for ground water, if the waste is dumped on ground, particularly in the areas with high ground water table.

4 CONCLUSIONS

The laboratory tests carried out on the coal mine waste sample collected from Barapukuria coal mine revealed its inferior quality as an engineering material. The waste sample possesses very low strengths with a large expansion ratio (>1) which makes it unfit to use even as a road subgrade materials (Road pavement design manual, 1999). The fresh coal mine waste must be improved with proper additives in order to make it usable in an engineering work. Strength and plasticity of the fresh waste can be significantly improved by mixing it with a certain portion of improving agent such as cement. However, extensive study with cost-benefit analysis is recommended for such improvement.

ACKNOWLEDGEMENTS

Authors would like to express their gratitude to the Department of Civil Engineering, Rajshahi University of Engineering and Technology for financing this research work. Authors are also grateful to the authority of Barapukuria Coal Mine for their cooperation. They give thanks to the staff and assistants of soil lab, RUET.

REFERENCES

Agarwal, V. K., (2009). Geotechnical investigation of coal mine refuse for backfilling in mines. Undergraduate thesis submitted to department of mining engineering National institute of technology, Rourkela – 769 008.

Arora K. R., (2006).Soil Mechanics and Foundation Engineering. 6th Edition, ISBN: 81-8014-028-8.

ASTM D 422 - Standard test method for particle size analysis of soils.

ASTM D 698 - Standard test methods for laboratory compaction characteristics of soil using standard effort (12,400 ft-lbs/ft3).

ASTM D 854-00 – Standard test for specific gravity of soil solids by water Pycnometer.

ASTM D 854-92 – Specific gravity of solid determination.

ASTM D 1883 - Standard test method for determination of California bearing ratio of soil.

ASTM D 2166 - Standard test method for unconfined compressive strength of cohesive soil.

ASTM D 4318 - standard test method for liquid limit, plastic limit, and plasticity index of soils.

Christopher A. B., (2013). Re-Use of Mine Waste Materials Amended with Fly Ash in Transportation Earthwork Projects.MPC- 411. January 1, 2013- December 31, 2013.

Classification of Soils for Engineering Purposes: Annual Book of ASTM Standards, D 2487-83, 04.08, American Society for Testing and Materials, 1985, pp. 395–408.

Das B., (1994).Principles of Geotechnical Engineering. PWS-Kent Publishing Company, Boston.

Holtz, R., and Kovacs, W., (1981). An Introduction to Geotechnical Engineering.Prentice-Hall, Inc. ISBN 0-13-484394-0.

Howladar, M. F., Deb, P. K., Shahidul, A. T. M., and Miah, M., (2014).An Assessment of the Underground Roadway Water Quality for Irrigation Use around the Barapukuria Coal Mining Industry Dinajpur, Bangladesh. International Conference on Mechanical, Industrial and Energy Engineering 2014, Khulna, Bangladesh.

Karfakis , M. G., Bowman, C. H., and Topuz, E., (1996). Characterization of coal-mine refuse as backfilling material. Volume-14, Geotechnical and Geological Engineering, pp. 129-150.

Kibria, M. G., Quamruzzaman, C., Ullah, A. S. M. W., and Kabir, A. K. M. F., (2012).Effect of longwall mining on groundwater forunderground coal extraction in Barapukuria, Bangladesh.Journal of mines, metals & fuels, pp. 60-66.

The Technical Working Group, LGED, 1999: “Road Pavement Design Manual”.

Uckert, R. S., and Jones, A. L., (2006).The investigation of the use of coal mine refuse for sub-base material and embankment fill in south Dakota. BLRS and ASMR, R.I. Barnhisel (ed.) 3134 Montavesta Rd., Lexington, KY 40502.

Proceedings of the 4th International Conference on Civil Engineering for Sustainable Development (ICCESD 2018), 9~11 February 2018, KUET, Khulna, Bangladesh (ISBN-978-984-34-3502-6)

NUMERICAL ANALYSIS OF REINFORCED SLOPE USING LIMIT EQUILIBRIUM METHOD

Md. M Sazzad[1] and T Rahat[2]

[1]*Professor, Department of Civil Engineering, University of Engineering & Technology, Bangladesh, e-mail: mmsruet@gmail.com*
[2]*Department of Civil Engineering, University of Engineering & Technology, Bangladesh, e-mail: tasnimrahat10@gmail.com*

ABSTRACT

Over the past few decades, the limit equilibrium method has dominated the usage of any other method for slope stability investigations for its case in use. High and steep cut slopes due to excavation are a common sight in building high-grade throughways. Such steep slope often requires reinforcement to stabilize it. In this study, GEO5 software was used to investigate the behavior of soil slope under different reinforcement conditions. The use of steel bars as reinforcement is increasingly becoming widespread in engineering practice. Consequently, this paper studies the effect of the incorporation of steel reinforcement in different manners using the limit equilibrium method. The parametric modeling was done to determine the effect of the inclination angle of reinforcing bars and their individual spacing on the factor of safety. From the analysis, it is observed that factor of safety of slope decreases due to the increase of slope angle.The effect of bar inclination angle in the reinforced slope is studied as well and it is noted that factor of safety of reinforced slope becomes maximum when the reinforcing bar inclination angle becomes 10°. It is also observed that factor of safety increases up to an optimum number of reinforcement layers and beyond this, factor of safety decreases even though the number of reinforcing bar layers increases. Higher values of factor of safety are obtained when equal spacing rather than random spacing of bar is used in the reinforced slope.

Keywords: *Slope stability, reinforcing bar, slope angle, reinforcing bar inclination angle, spacing.*

1. INTRODUCTION

Slope stability analysis is an enormously important deliberation in the design and construction of earth dams, embankments, bridge abutments, retaining walls and various other civil engineering structures. It may fail due to heavy rainfall, changes in topography, external forces, loss of shear strength, increase in ground water table, change in stress condition, etc. (Sazzad, Hie & Hossain, 2016). So, it is a big challenge to both researchers and professionals to estimate accurately the factor safety of slopes. Due to its engineering significance, it draws attentions to many researchers and numerous research works have been reported in the literature (Wei & Cheng, 2010; He & Zhang, 2012; Sazzad & Moni, 2017, Sazzad & Rahat, 2017). The reinforced soil is a decent technique and an economical alternative to stabilize the natural or artificial slopes as a part of civil engineering projects. It is in some cases used to construct stable slopes at much steeper angles than would otherwise be possible without reinforcing the slope. Previous studies depicted that the shear strength of soil can be improved by using steel nails (Wei & Cheng, 2010; He, Ouyang & Luo, 2012; Sazzad, Hie & Hossain, 2016). The stability of slope using soil reinforcing technique can be analyzed by using the conventional limit equilibrium methods or by using the finite element method (FEM). For example, a parametric study on the reinforced slope to investigate the effect of slope angle, inclined reinforcement bars and random and group spacing was carried out by Sazzad, Hie & Hossain (2016) using the FEM.

In this paper, the numerical analysis is carried out by using the limit equilibrium method (LEM) for its simplicity. The limit equilibrium method is used to analysis the stability of slope using soil reinforcing technique. Limit equilibrium methods have been widely adopted for slope stability analysis. A potential sliding surface is assumed prior to the analysis and a limit equilibrium analysis is then performed with respect to the soil mass above the potential slip surface. Many methods based on this approach are available in the literature. For example, the methods reported by Bishop (1955), Janbu (1957), Morgenstern and Price (1965), Spencer (1967) and so on are based on LEM. Although the approach is straightforward, these methods will not consider the stress–strain behavior of the soil mass while calculating the stresses. This paper aims at performing a comprehensive numerical study of the stability of the reinforced soil slope. The influence of the variation of the reinforcing bar inclination angle along with the variation of the reinforcing bar number and spacing of reinforcing bar on the factor of safety of slope by LEM is studied using GEO5. The effect of regular and random spacing of reinforcing bars has been investigated. An attempt has also been made to find the optimum spacing and number of bar for the application of soil reinforcement in slope stability. The consequences of using different factors in the LEM based study have been investigated and the numerical results have been reported.

2. METHODOLOGY

2.1 Limit Equilibrium Method

Limit equilibrium method (LEM) is a powerful numerical tool for solving many problems of engineering and mathematical physics. Several limit equilibrium methods (LEM) have been developed for slope stability analysis. Fellenius (1936) introduced the first method, referred to as the Ordinary or the Swedish method, for a circular slip surface. Bishop (1955) advanced the first method introducing a new relationship for the base normal force. The equation for the factor of safety hence become non-linear. At the same time, Janbu (1954) developed a simplified method for non-circular failure surfaces, dividing a potential mass into several vertical slices. The generalized procedure of the same time as a further development of the simplified method was proposed by Janbu (1973). Later, Morgenstern-Price (1965), Spencer (1967) and several others made future contributions with different assumptions for the interslice forces. A procedure of general limit equilibrium was developed by Chuge (1986) as an extension of the Spencer and Morgenstern-Price methods, satisfying both moment and force equilibrium conditions (SLOPE/W, 2004 and Abramson et al., 2002). All limit equilibrium methods (LEMs) are based on certain assumptions for the interslice normal (E) and shear (T) forces, and the basic difference among the methods lies in how these forces are determined or assumed.

2.2 Brief Description of GEO5

The numerical study of the reinforced slope has been carried out by GEO5 (2017) based on limit equilibrium Method. This software enables the linear or nonlinear, time-dependent and anisotropic behavior of soil or rock from the most basic to the most advanced constitutive models. The effectiveness of GEO5 has already been recognized (e.g., Sazzad, Hie & Hossain, 2016; Sazzad & Moni, 2017). For further details, readers are referred to GEO5 (2017).

3. GEOMETRIC MODELING

The geometric model used in the present study is depicted in Figure 1 where β is the sloping angle and θ is the reinforcing bar inclination angle with the horizontal axis. All the dimensions in the model slope are given in meter. After the generation of model and assignment of the properties of soil and reinforcing bar, the stability analysis is performed.

The stability analysis is carried out by using five basic methods of LEM. Eleven layers of steel bar are reinforced in slope keeping the relative spacing same.

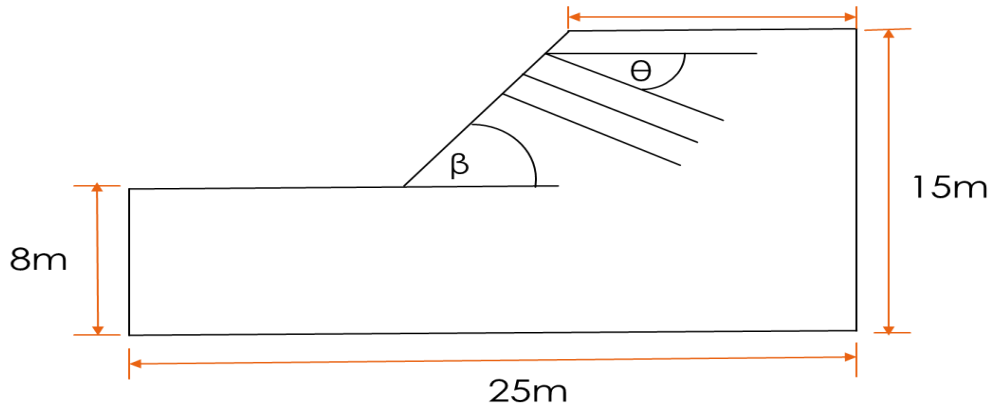

Figure 1: Geometric model of soil slope

Table 1: Properties of steel bar used in the present study

Properties of steel bar	**Values**
Stiffness of bar (kN/m)	60
Coefficient of interaction	0.80
Total length of reinforcement bar in 1m width of slope (m)	121

Table 2: Properties of soil used in the present study

Soil properties	**Values**
Dry unit weight (kN/m^3)	18
Cohesion of soil (kPa)	7
Angle of friction (°)	25
Saturated unit weight (kN/m^3)	21

4. NUMERICAL RESULTS AND DISCUSSION

4.1 Effect of the variation of slope angle in reinforced slope

The stability of slope was analysed with the help of GEO5 software. Different slope angles (45°, 49° and 54°) were considered during the numerical analysis. In this study, eleven rows of soil reinforcement (steel bar), each 11m length having stiffness of 60 kN/m, are placed at a regular interval in the slope. For each slope angle (β), different Limit Equilibrium Methods such as Bishop (1955), Fellenious (1936), Spencer (1967), Janbu (1957) and Morgenstern and Price (1965) were used to obtain the factor of safety of slope with a fixed bar inclination angle (θ). This will help to compare the factor of safety of slope obtained by different methods for a particular slope angle and bar inclination angle. It is observed that Fellenious (1936) method gives the lowest factor of safety regardless of the slope angle for a constant

value of bar inclination angle. On the other hand, the higest values of factor safety are obtained when either Spencer (1967) or Janbu (1957) or Morgenstern and Price (1965) method is used. It should be noted that the increase of the bar inclination angle has negligible effect on the development of the above discussed pattern. It is interesting to note that factor of safety of slope is the highest when the bar inclination angle is 10° regardless of the values of slope angle.

Table 3: Factor of safety of reinforced soil slope with varying slope and bar inclination angles

Bar inclination	Slope angle (°)														
	45					49					54				
	Bishop	Fellenious	Spencer	Janbu	Morgenster-price	Bishop	Fellenious	Spencer	Janbu	Morgenster-price	Bishop	Fellenious	Spencer	Janbu	Morgenster-price
0	1.59	1.51	1.77	1.77	1.77	1.17	1.14	1.22	1.22	1.19	1.20	1.15	1.12	1.12	1.12
5	1.82	1.73	1.98	1.98	1.98	1.43	1.34	1.48	1.48	1.48	1.59	1.49	1.61	1.61	1.61
10	1.76	1.69	1.81	1.81	1.81	1.72	1.64	1.89	1.89	1.89	1.73	1.64	1.80	1.80	1.80
15	1.74	1.68	1.81	1.81	1.81	1.63	1.56	1.71	1.71	1.71	1.68	1.65	1.72	1.71	1.72
20	1.61	1.54	1.79	1.78	1.78	1.45	1.36	1.52	1.52	1.52	1.44	1.37	1.45	1.54	1.55
25	1.47	1.32	1.54	1.54	1.54	1.11	1.06	1.12	1.12	1.12	1.17	1.15	1.08	1.08	1.08

4.2 Effect of the number of reinforcement layer

The effect of the number of reinforcement layer number is studied in this section. It sholud be noted that the total length of bar (11@11 m =121 m) is kept conatant while studing the effect of the number of reinforcing layer on the stability of slope. The total bar length is kept constant because it otherwise may have effect on the overall result. The bar inclination angle is also fixed at 10°. This is because the bar inclination angle of 10° gives the highest factor of safety. Since the total length of the reinforcing bar is fixed, the increase in the number of reinforcing layer decreases the length of each reinforced bar as also noticed in Table 4. It is interesting to note that the factor of safety of reinforced slope becomes maximum when 13 no. of bars with a bar length of 9.30 m each is used.

Table 4: Factor of safety of reinforced slope for the variation of the number of reinforcement layer

Numbers of layer	Length of each bar	Factor of safety				
		Bishop	Fellenious	Spencer	Janbu	Morgenster-price
10	12.10	1.18	1.12	1.33	1.33	1.34
11	11.00	1.31	1.27	1.47	1.47	1.47
12	10.08	1.44	1.41	1.59	1.59	1.59
13	9.30	1.77	1.69	1.83	1.83	1.83
14	8.64	1.74	1.62	1.81	1.81	1.81
15	8.10	1.68	1.57	1.74	1.75	1.74
16	7.56	1.59	1.44	1.62	1.62	1.62
17	7.10	1.54	1.47	1.59	1.59	1.61
18	6.72	1.46	1.42	1.54	1.53	1.53

4.3 Effect of the spacing of reinforcing bar

The effect of different spacing styles such as equal spacing and random spacing for reinforced slope is given in Table 5. It is noted that the elevated values of factor of safety is obtained when equal spacing rather than random spacing of bar is used in the reinforced slope.

Table 5: Factor of safety for the variation of bar spacing

Type of Spacing	Factor of safety				
	Bishop	**Fellenious**	**Spencer**	**Janbu**	**Morgenster-price**
Equal spacing	1.76	1.65	1.82	1.81	1.81
Random spacing	1.44	1.34	1.54	1.53	1.54

5. CONCLUSIONS

Different Limit Equilibrium Methods were used in this study to evaluate the factor of safety of slope with varience of slope angle, bar inclination angle and spacing style. Some of the important findings of the study are summarized below:

i. The factor of safety of reinforced slope decreases with the increase of slope angle regardless of the values of reinforcing bar inclination angle.
ii. Fellenious (1936) method gives the lowest factor of safety regardless of the slope angle for a constant value of bar inclination angle.
iii. The factor of safety of the reinforced slope becomes maximum when the reinforcing bar inclination angle becomes 10° regardless of the value of slope angle.
iv. Factor of safety increases up to an optimum number of reinforcement layer and beyond this, factor of safety decreases even though the number of reinforcing bar layers increases.
v. Elevated values of factor of safety is obtained when equal spacing rather than random spacing of bar is used in the reinforced slope.

REFERENCES

Abramson, L.W., Lee T.S., Sharma, S. and Boyce, G.M. (2002) “Slope Stability and Stabilization Methods.” *John Wiley & Sons, Inc,* New York, USA

Bishop, A.W. (1955). “The use of slip circles in stability analysis of slopes”, *Geotechnique*, 5(1), 7_17.

Fellenius, W. (1936). “Calculation of the stability of earth dams”, P*roc. of the 2nd congress on large dams*, Washington, D.C., 4, U.S. Government Printing Office.

GEO5 v19. (2017). User’s manual. *Fine software company*, Czech Republic.

He, B. and Zhang, H. (2012). “Stability analysis of slope based on finite element method.”, *International Journal of Engineering and Manufacturing*, 3, 70-74.

He, S., Ouyang, C. and Luo, Y. (2012). “Seismic stability analysis of soil nail reinforced slope using kinematic approach of limit analysis.”, *Environmental Earth Sciences*, 66(1), 319-326.

Janbu, N. (1954) “Application of composite slip surface for stability analysis”, *European Conference on Stability Analysis*, Stockholm, Sweden.

Janbu, N., (1973). “Slope stability computations.” *Embankment Dam Engineering, John Wiley and Sons.*

Morgenstern, N.R., and Price, V.E. (1965). “The analysis of the stability of general slip surfaces”, *Geotechnique*, 15(1), 77_93.

Sazzad, M.M. and Moni. M.M. (2017). “Stability analysis of slopes for homogeneous and layered soil by FEM. *Journal of Engineering Science*. 8(1). 51-62.

Sazzad, M.M. and Rahat, T. (2017). Response of reinforced soil slope against earthquake by LEM. *International Conference on Disaster Risk Mitigation, At Dhaka, Bangladesh*

Sazzad, M.M., Hie, A.B.K.M.A., Hossain, M.S. (2016). “Stability analysis of reinforcement slope using FEM”, *International Journal of Advanced Structures and Geotechnical Engineering*, 05(2), 83-88.

SLOPE/W (2004) “Slope Stability Modeling with SLOPE/W, An Engineering Methodology.” *GeoSlope Office*, Canada

Spencer, E. (1967) “A method of analysis of the stability of embankments assuming parallel interslice forces”, *Geotechnique*, 17(1), 11–26.

Wei, W. B. and Cheng, Y. M. (2010). “Soil nailed slope by strength reduction and limit equilibrium Methods.”, *Computers and Geotechnics*, 37, 602-618

Proceedings of the 4th International Conference on Civil Engineering for Sustainable Development (ICCESD 2018), 9~11 February 2018, KUET, Khulna, Bangladesh (ISBN-978-984-34-3502-6)

ARTIFICIAL NEURAL NETWORK BASED PULLOUT CAPACITY PREDICTION FORMULA FOR PLATE ANCHORS IN SAND

Bayshakhi Deb Nath[1] and Md. Rokonuzzaman[2]

[1] Lecturer, Department of Civil Engineering, Khulna University of Engineering & Technology,, Bangladesh, E-mail: bayshakhidebnath@yahoo.com
[2] Professor, Department of Civil Engineering, Khulna University of Engineering & Technology, Bangladesh, E-mail: rokoncekuet@yahoo.com

ABSTRACT

The problem of estimating the pullout capacity of plate anchors on sand is very complex and not yet entirely understood. Most of the existing theories for the prediction of pullout capacity of anchor foundation are based on the assumptions of the failure surface. The failure surfaces have been simplified by the investigators to simplify the computation of pull out capacity. Hence, the theoretical result shows great deviation and experimental result. In this study, artificial neural network is used for the prediction of pullout capacity of plate anchors on the sand and have been found to outperform the most commonly-used traditional methods. This paper presents a new hand-calculation design formula for the prediction of pullout capacity of plate anchors on sand based on a more accurate pullout capacity prediction model using artificial neural network. A large database of 583 individual cases of laboratory and field measurements is used to develop and verify the ANN model. Random data division technique is used to divide the data into three subsets: training, testing, and validation sets containing a different percentage of data. Feed Forward Backpropagation algorithm is used to train the network. The ANN geometry (no. of hidden neurons, no. of hidden layers, and training functions) were also varied to optimize the network weight i.e. minimum error and maximum correlation coefficient value. Finally based on the optimum weight combination a design formula is proposed from which pullout capacity can be calculated easily without the need for computers.

Keywords: *Plate anchor, ANN, Back propagation*, *Pull out capacity, Correlation*

1. INTRODUCTION

Anchors are lightweight foundation systems designed and constructed to resist vertical or horizontal uplift resistance or overturning moment acting on structures such as transmission towers, sheet piles, retaining walls, deepwater offshore developments, airport hangars, wind loads on tall structures, buoyancy forces on buried pipelines under water, earthquake, ice forces (Hanna et al. 2014). The pullout capacity of soil anchors is mainly influenced by anchor geometry and local soil conditions. Several researchers have investigated the effect of anchor geometry on the pullout capacity of plate anchor (Hanna et al. 2011). Kumar and Kouzer (2008) have studied the effect of embedment ratio and frictional angle on the pullout capacity of plate anchor in the sand and found that the pullout capacity increases with the increase in the embedment ratio and the frictional angle.

Plate anchor could be installed vertically, horizontally as well as with different inclination to meet the field requirements. Horizontal anchors are generally used to resist vertical uplift forces, while vertical anchors are often used to resist passive resistance in retaining walls, sheet piles, and bulkheads. Hanna et al. (1988) has conducted both experimental and analytical investigation on the pullout capacity of shallow strip inclined plate anchor in the sand and recommended a design procedure for the practicing engineers. However, these methods are inconsistent with each other and with the experimental results.

In the last few years, ANNs have been employed for the solution of a wide range of problems in Geotechnical Engineering. Shahin et al. (2001) have summarized the application of ANN to problems in geotechnical engineering such as bearing capacity of piles, settlement predictions, liquefaction and slope stability. Padmini et al. (2008a) have developed models using ANN, Fuzzy and Neurofuzzy techniques that have been used successfully for the prediction of the ultimate bearing capacity of shallow foundations on cohesionless soils. Wojciechowski (2011) has investigated the application of Artificial Neural Network in soil parameter identification for deep excavation. Padmini et al. (2008b) have applied ANN to predict the pullout capacity of the circular anchor.

This work will present the development of ANN model for the prediction of pullout capacity of plate anchor in sand. The conventional Back Propagation Algorithm is used for training the network. The performance of the ANN model is compared with some of the most commonly used traditional methods. Finally, based on the ANN model an equation is proposed to predict the pullout capacity of plate anchor.

2. METHODOLOGY

The steps used to develop the ANN model to predict the pullout capacity of anchor foundation include the preparation of the database, selection of model inputs, data division and preprocessing, determination of the ANN architecture, model optimization, stopping criteria and model validation.

2.1 Database Preparation

A database consisting of 583 individual cases is used to develop and validate the model. The database includes both chamber, centrifuge model test and field test data. The data cover a wide range of variation in anchor geometry and soil properties. The datasets are collected from the published journals and conference papers. The personal computer based software MATLAB 2015 is used in this work to simulate the ANN operation.

2.2 Selection of Model Inputs

Thorough investigation of the factors affecting the pullout capacity of anchor foundation is very important to propose a successful prediction model. The anchor geometry (L/B), unit weight of soil (γ), friction angle of soil (φ) and anchor width (B) are the most important factors affecting the bearing capacity of shallow foundation in cohesionless soils (Burland and Burbridge 1985). Murray and Geddes (1989) carried out laboratory model tests on both horizontal, vertical and inclined anchors and showed that the embedment ratio (H/B) and the anchor rotation (θ) has also a significant effect on the pullout capacity of anchor foundation. Thus the anchor geometry (L/B), anchor embedment ratio (H/B), unit weight of soil (γ), friction angle of soil (φ), anchor rotation (θ) and anchor width (B) is used in the ANN model as the input variables while the dimensionless pullout capacity factor (N_q) is the single output variable. The data range used to investigate the pullout behavior of plate anchor in sand is presented in Table 1.

Table 1: Data ranges of the input variables used to train the model.

	H/B	L/B	B (mm)	θ (°)	γ (kN/m^3)	φ (°)
minimum	0.47	1	18	0	12.99	30
maximum	12	10.5	2350	90	18.32	48

2.3 Data Division

Data division is one of the most important features that affect the model performance of ANN model. However, there is no precise rule for the data division. Though different investigators

have used different methods of data division the most common practice is to divide the data into two subsets: a training set and validation set. The training data set is used to construct the prediction model and the validation data set is used to justify the performance of the model (Twomey and Smith 1997). However, dividing the data into two subsets may lead to overfitting the model (Shahin et al. 2002). In order to avoid overfitting, Stone (1974) suggested using cross-validation as stopping criteria, when sufficient datasets are available. In this investigation, cross-validation was used as stopping criteria. Thus the total dataset was divided into three subsets: training, testing, and validation. There is no clear relationship between the proportions of data used for training, testing, and validation and the model performance (Shahin et al. 2004). Therefore, to obtain the optimum ratio of training, testing, and validation dataset, several random combinations of the three data sets are tried and finally, the proportions of the data points are selected based on the best model performance.

2.4 Data Pre-processing

It is important to preprocess the input and output variables to ensure that all variables receive equal attention during the training process. It aims at transforming the data into a better form for the network to use and reduce the chances that the ANN gets stuck in a local minimum (Demuth 2008). It is essential, as they have to be equal with the limits of the transfer functions used in the output layer. As the pureline and tansigmoid transfer functions are used in the input-hidden and hidden-output layer, respectively. In this investigation input and output variables are scaled between -1.0 and +1.0 using the following equation.

$$x_n = 2\frac{x - x_{\min}}{x_{\max} - x_{\min}} - 1 \qquad (1)$$

Where, x_{min} and x_{max} are the minimum and maximum value of each input variable, respectively.

2.5 ANN Model Architecture

Construction of network architecture is one of the most essential and tedious jobs in ANN model development. It is usually achieved by fixing the number of hidden layers and number of nodes in each layer. The number of nodes used in the input and output layers is restricted by the number of input and output parameters, respectively. Hence the input layer consist of 6 nodes, includes H/B, L/B, B,γ, θ and φ, while the output layer consists of one node representing N_q. Trial and error techniques are used to obtain the optimum number of hidden layers.

Shahin (2002) mentioned that the number of hidden layer nodes should be determined in such a way that the relationship obtained by the ANN can be interpreted in the physical sense. Therefore, the model should have sufficient free parameters (weights) to be able to approximate the functions with the desired minimum error and not having too many so as to avoid overtraining. In order to obtain the optimum network geometry, the model is trained several times by changing the number of hidden layer nodes. Finally, the number of hidden layers and the number of hidden layer nodes are selected based on the best model performance.

2.6 Model optimization

To obtain a model with the best performance and maximum generalization ability, the connection weights between the input–hidden–output neurons are adjusted. The most popular method for finding the optimum weight combination is feedforward back-propagation neural network. Back-propagation neural network can be trained with a wide range of training algorithms available in the literature. In this study, the model is trained using a number of training algorithms and finally, the training algorithm is selected based on the model performance.

2.7 Stopping Criteria

In this study, cross-validation is used as the stopping criteria for training. Smith & Davey, (1993) mentioned that, cross-validation is the most valuable tool to avoid overfitting when sufficient data are available to create training, testing and validation sets. The training set is used to adjust the connection weights and the testing set is used to measure the ability of the model to generalize.

2.8 Model Validation

The performance of the model is validated to ensure that the model has the ability to generalize within the ranges defined by the training data. The coefficient of correlation (r), root mean squared error (RMSE) and mean absolute error (MAE) are used to validate the model performance. The coefficient of correlation is used to determine the relative correlation and the goodness-of-fit between the expected and experimental data. It is a measure of linear relationship between the predictions and the actual values. The most commonly used measure of error is the root-mean-squared error (RMSE) which has the advantage that large errors receive greater attention than smaller ones (Hecht-Nielsen 1990) and the Mean Absolute Error (MA*E*) is a measure of closeness of predictions to actual values.

2.9 Traditional Methods for Pullout Capacity Prediction

It is essential to verify experimental results with theoretical solutions wherever possible as the results obtained from laboratory testing alone are typically problem specific. Besides, it is difficult to perform laboratory tests on each and every field problem combination, so it is necessary to be able to predict soil uplift resistance theoretically for the purposes of design. Many traditional methods are available in the literature to predict the pullout capacity of horizontal and vertical anchors but the traditional methods available to predict the pullout capacity of the inclined anchor is very limited. Among all these traditional methods some most commonly used methods are recalled here to assess the relative performance of ANN.

3. RESULTS AND DISCUSSION

3.1 Effect of Data Division

The performance of the model using different data proportions for training, testing, and validation of the model are presented in Table 2. The first, second and third Figure in the second column of Table 2 is the data proportions assigned to the validation, testing and training sets respectively. This Table shows that the effect of the ratio of training, testing and validation subsets on the model performances is not very significant but the best possible performance is obtained when 70% of the available data is used for the training, 15% for the testing and 15% for the validation of the model. So this ratio is used for the final development of the model. As ANN cannot extrapolate beyond the ranges of data used for training of the model, so the datasets used for testing and validation of the model is kept within the limit of the training datasets. Besides, the Artificial Neural Networks cannot extrapolate beyond the ranges of their training data, so to achieve the best possible model the datasets used for testing and validation sets is kept within the ranges of training datasets.

Table 2: Performance of the ANN model for different data proportions

Category No.	Data proportion and data set	RMSE	MAE	r
1	**80 10 10**			
	Training	8.148	5.350	0.920
	Testing	7.244	4.656	0.908
	Validation	7.470	5.297	0.960
	Overall	7.997	5.276	0.925
2	**70 20 10**			
	Training	7.293	4.216	0.931
	Testing	7.873	4.018	0.933
	Validation	6.498	3.993	0.965
	Overall	7.339	4.154	0.934
3	**60 30 10**			
	Training	7.550	4.583	0.922
	Testing	7.482	4.533	0.940
	Validation	6.221	3.826	0.970
	Overall	7.408	4.493	0.933
4	**70 10 20**			
	Training	7.256	4.179	0.932
	Testing	7.048	3.350	0.911
	Validation	7.586	4.369	0.953
	Overall	7.303	4.135	0.935
5	**60 20 20**			
	Training	7.519	4.598	0.923
	Testing	7.948	4.777	0.932
	Validation	6.398	4.172	0.958
	Overall	7.398	4.548	0.933
6	**50 30 20**			
	Training	7.657	4.285	0.910
	Testing	6.908	3.866	0.953
	Validation	7.129	4.353	0.952
	Overall	7.334	4.173	0.935
7	**50 25 25**			
	Training	7.657	4.285	0.910
	Testing	7.036	3.930	0.953
	Validation	6.958	4.192	0.952
	Overall	7.334	4.173	0.935
8	**70 15 15**			
	Training	7.242	4.169	0.932
	Testing	7.902	4.624	0.951
	Validation	6.951	3.494	0.934
	Overall	7.302	4.136	0.935
9	**60 10 30**			
	Training	7.492	4.558	0.923
	Testing	7.594	4.268	0.901
	Validation	7.084	4.437	0.954
	Overall	7.382	4.493	0.934
10	**50 20 30**			
	Training	7.657	4.285	0.910
	Testing	7.153	3.977	0.946
	Validation	6.892	4.117	0.957
	Overall	7.334	4.173	0.935
11	**40 30 30**			
	Training	7.983	4.946	0.902
	Testing	7.788	4.935	0.938
	Validation	7.752	4.894	0.936
	Overall	7.856	4.927	0.925

3.2 Effect of ANN Model Geometry

This section includes determining the most suitable training function and an optimum number of hidden layers and neurons for the available dataset.

3.2.1 Effect of Training Function

Literature reveals that different types of training functions are available in backpropagation algorithm. To select the appropriate training function for the problem, the performance of the model is checked by training the network with different types of training functions. The training functions used in this study to check the performance of the model is presented in Table 3. The performance of the model using different training functions are presented in Table 4. From this table, it is clear that the Levenberg-Marquardt (LM) training function can produce a better correlation between the observed and predicted pullout capacity factors than any other training functions, as the obtained value of correlation coefficient is very close to 1. The error criteria (RMSE and MAE) for this training function is also the lowest one. So, LM is the most appropriate training function for the available database.

Table 3: Training functions used in backpropagation algorithm

Acronym	Algorithm	
LM	trainlm	Levenberg-Marquardt
BFG	trainbfg	Quasi-Newton
SCG	trainscg	Scaled Conjugate Gradient
CGF	traincgf	Fletcher-Powell Conjugate Gradient
CGB	traincgb	Conjugate Gradient with Powell/Beale Restarts
CGP	traincgp	Polak-Ribiére Conjugate Gradient
OSS	trainoss	One Step Secant
RP	trainrp	Resilient Backpropagation

Table 4: Performance of ANN models with different Training Function

Training Function	RMSE				MAE				Correlation Coefficient (R)			
	Training	Testing	Validation	Overall	Training	Testing	Validation	Overall	Training	Testing	Validation	Overall
LM	7.29	7.19	7.31	7.28	4.21	4.31	4.16	4.22	0.94	0.92	0.92	0.94
BFG	11.79	8.49	10.08	11.11	6.75	5.14	6.01	6.40	0.85	0.86	0.84	0.84
SCG	9.36	9.07	7.77	9.09	5.33	5.51	4.32	5.21	0.88	0.93	0.91	0.90
CGF	11.14	9.61	8.98	10.62	6.33	5.65	4.87	6.01	0.84	0.92	0.89	0.86
CGB	8.05	7.69	7.57	7.92	4.95	4.73	4.39	4.83	0.91	0.96	0.92	0.92
CGP	8.17	7.81	7.64	8.04	4.95	4.76	4.31	4.83	0.91	0.95	0.92	0.92
OSS	9.11	8.47	7.48	8.79	5.69	5.62	4.68	5.53	0.89	0.94	0.92	0.91
RP	8.84	8.77	7.36	8.62	5.13	5.20	4.15	5.00	0.90	0.94	0.93	0.91

3.2.2 Effect of the No. of Hidden Layer

The selection of the number of hidden layers (s) is the most challenging part of the total network development process (Noorzaei et al. 2008). Unfortunately, there are no fixed guidelines available for this purpose and hence this is done by the trial-and-error method (Kartalopoulos 2002). The variation of RMSE, MAE and correlation coefficient (r) with the number of hidden layers are shown in Figure 1(a), (b) and (c) respectively. These Figures indicate that the network having one hidden layer produces minimum errors and shows the best correlation between the measured and predicted pullout capacity factor for both training, testing, and validation subsets. Besides, Hornik et al. (1989) have shown that a network with one hidden layer can approximate any continuous function. Therefore, the network with one hidden layer is the optimal network for the available dataset.

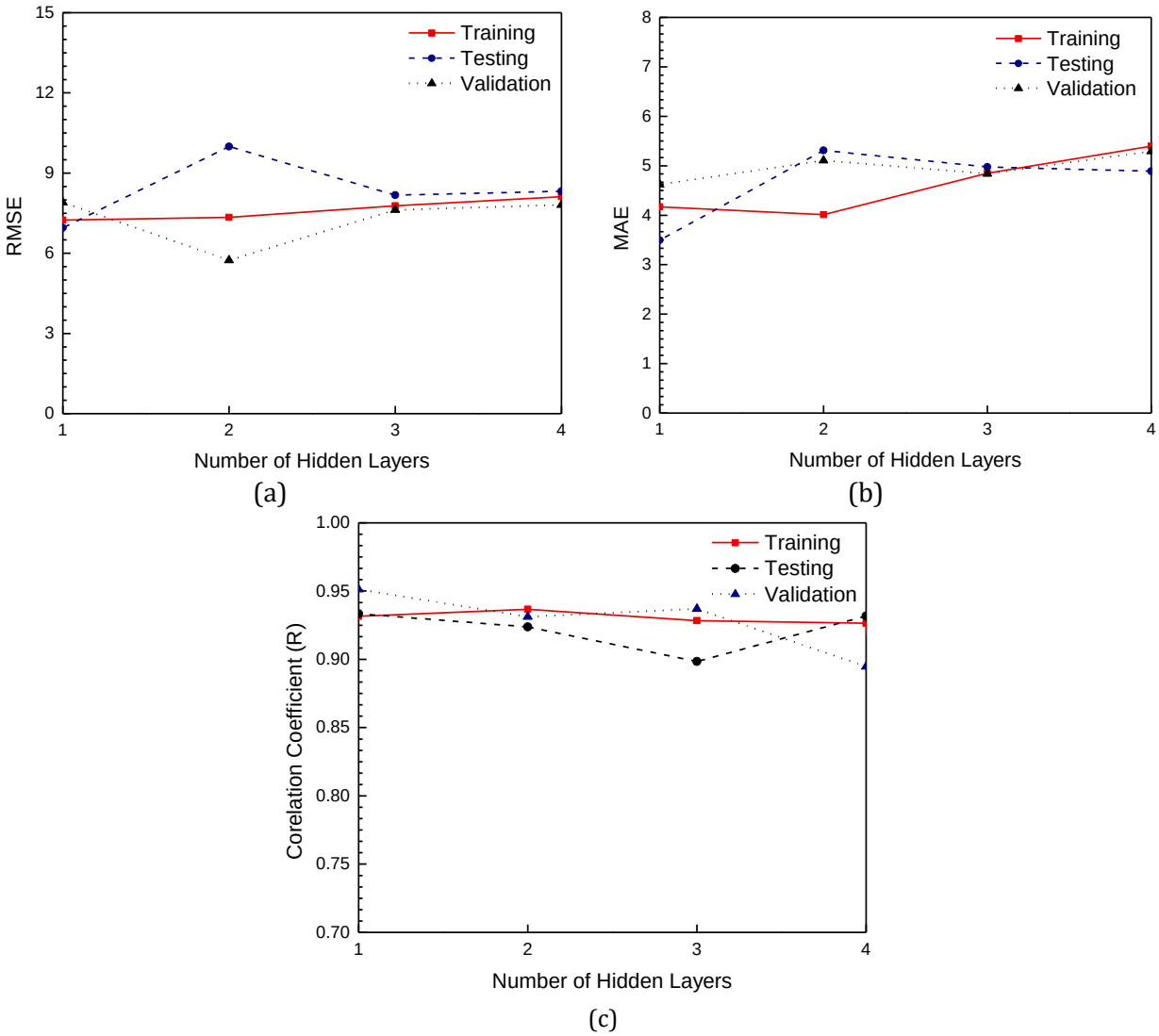

Figure 1: Performance of ANN models with different hidden layers for testing data set (two hidden nodded network)

3.2.3 Effect of No. of Hiddn Neurons

The number of hidden layer nodes should be determined so that the model has sufficient parameters to be able to approximate the functions with the desired minimum error. To achieve this, the model network is trained several times with different numbers of hidden neurons using the Levenberg–Marquardt training algorithm, which is a modification of the Newton method (Martin and Green 1995). The performance of the model using a different number of hidden neurons is presented in Figure 2. It can be observed that the number of hidden layer nodes has a very little impact on the model performance. The RMSE and MAE of the model changes in almost zig-zag ways with the number of hidden neurons. Figure 2 indicates that the network having eight hidden layer nodes has the lowest prediction error in most of the cases but the network having two hidden layer nodes is considered optimal, as the prediction error of the network having two hidden layer nodes is very close to that of the network having eight hidden layer nodes and it can easily be physically interpreted.

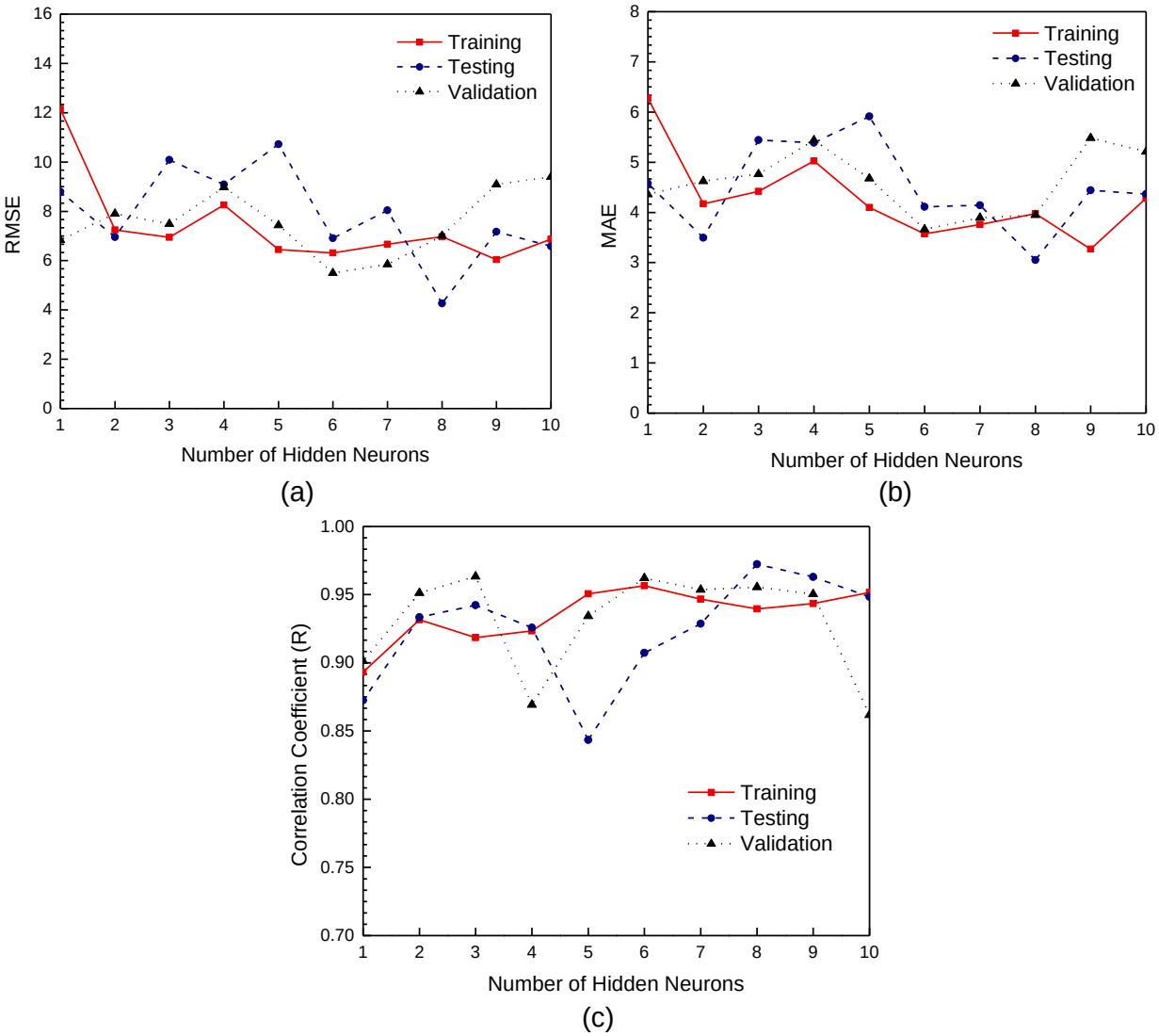

Figure 2: Performance of ANN model with different number of hidden layer neurons for the testing dataset

3.3 Performance of proposed ANN Model

Finally, the 6-2-1 network (6 input layer nodes, 2 hidden layer nodes, and 1 output layer node) with the LM training algorithm is selected as the optimal network. The predictive performance of the optimal ANN model is presented in Table 4. This table indicates that the ANN model performs reasonably well with a coefficient of regression of 0.934, RMSE of 3.494 and MAE of 6.951 for the validation dataset. Besides, the performance of the model is also consistent with the training, testing and validation dataset which indicates the good generalization ability of the proposed model.

Table 4: Performance of the ANN model.

Dataset	MAE	RMSE	r
Training	7.242	4.169	0.932
Testing	7.902	4.624	0.951
Validation	6.951	3.494	0.934
Overall	7.302	4.136	0.935

3.4 Comparison of the ANN model with the Traditional Methods

To increase the reliability of the model, the performance of the model is also compared with some of the most commonly used traditional methods which are presented in Figure 3. To provide an evaluation of the model's predictive abilities, quantitative assessments of the degree to which the model simulations match the actual output are very necessary. The linear correlation between the actual and predicted pullout capacity factors of horizontal, vertical and inclined anchors are shown in Figure 3(a), (b) and (c) respectively. It is seen that the prediction of the ANN model is more close to the measured pullout capacity factor compared to the commonly used traditional methods.

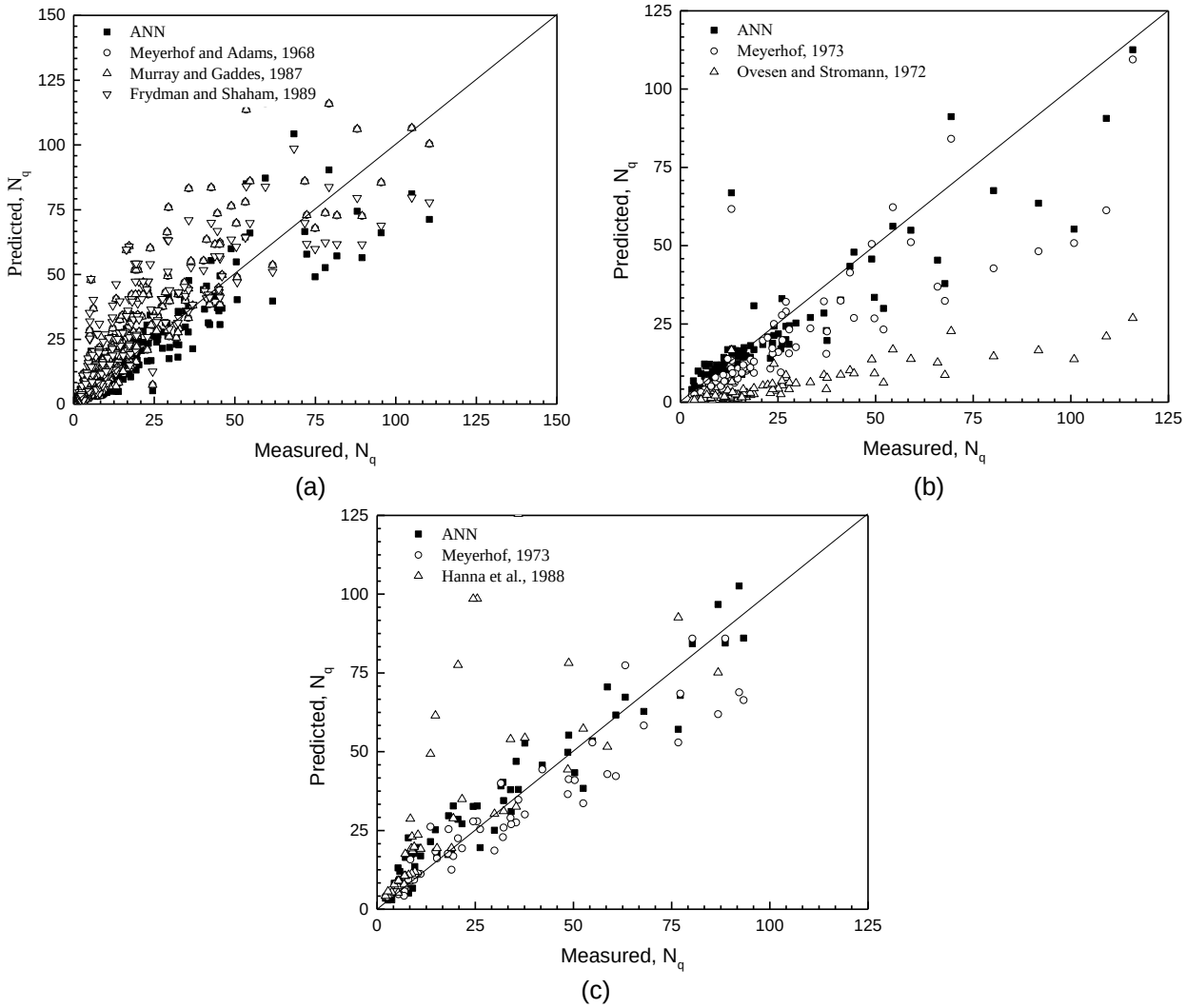

Figure 3: Comparison between the predicted and measured pullout capacity factor of (a) horizontal anchor (b) vertical anchor and (c) inclined anchor.

3.5 ANN Based Formulation:

The pullout capacity factor of anchor foundation can be calculated based on the validated artificial neural network model using the following procedure-

The structure of the optimal Artificial Neural Network architecture is presented in Figure 4. Using this network an equation is developed to predict the pullout capacity factor directly. The input-hidden and hidden-output layer connection weights and the threshold values obtained from the proposed model are summarized in Table 5.

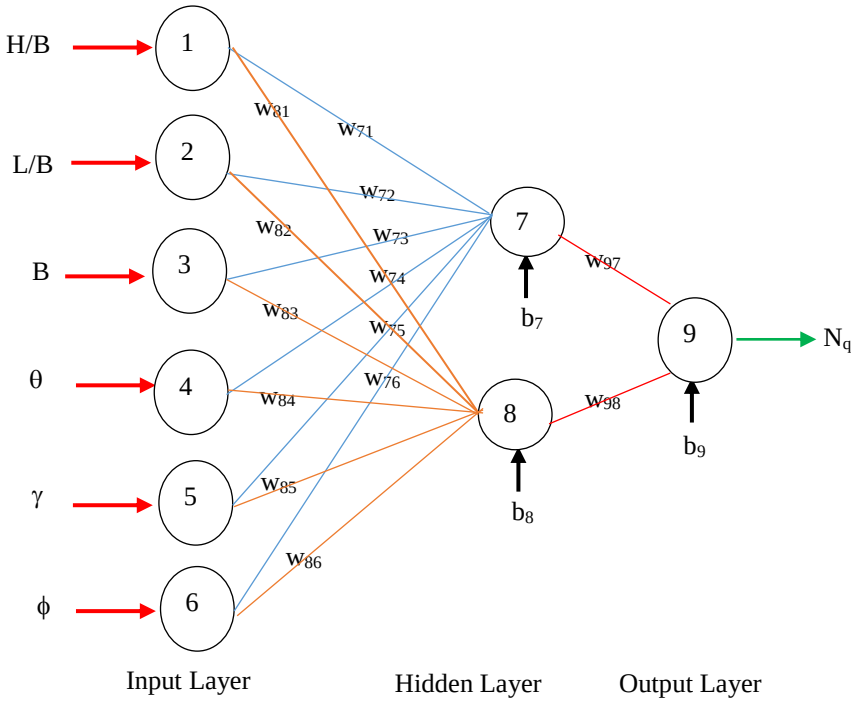

Figure 4: Structure of the proposed Artificial Neural Network

Table 5: Weights and threshold values for the ANN model

Hidden layer nodes	w_{ji} (weight from node i in the input layer to node j in the hidden layer)						Hidden layer threshold (b_j)
	i=1	i=2	i=3	i=4	i=5	i=6	
j=7	-1.340	4.164	0.143	-0.140	-0.214	-1.523	5.184
j=8	0.399	-0.085	-0.012	0.184	0.075	-0.031	-0.966
Output layer nodes	w_{ji} (weight from node i in the hidden layer to node j in the output layer)						Output layer threshold (b_j)
	i=7	i=8	--	--	--	--	
j=9	-0.645	1.000	--	--	--	--	0.559

The small number of connection weights of the neural network enables the ANN model to be translated into a relatively simple formula. As tanh and purelin activation functions are used in the hidden-output and input-hidden layer respectively the pullout capacity factor can be expressed as follows (Equation 2):

$$N_q = b_9 + w_{97}\tanh(x_1) + w_{98}\tanh(x_2) \quad (2)$$

Where,

$$x_1 = b_7 + w_{71}\frac{H}{B} + w_{72}\frac{L}{B} + w_{73}B + w_{74}\theta + w_{75}\gamma + w_{76}\varphi \quad (3)$$

$$x_2 = b_8 + w_{81}\frac{H}{B} + w_{82}\frac{L}{B} + w_{83}B + w_{84}\theta + w_{85}\gamma + w_{86}\varphi \quad (4)$$

It should be noted that, before using Equations 3 and 4, all input variables (i.e. H/*B*, L/B, *B*, θ, γ and φ) are needed to be scaled between -1.0 and +1.0 using equation 1 within the data ranges given in Table 1. As the predicted pullout capacity factor obtained from Equation 2 is scaled between -1.0 and +1.0 and in order to obtain the actual value, this pullout capacity factor has to be rescaled.. Using such a procedure for scaling and substituting the values of weights and threshold levels from Table 5, Equations 2, 3 and 4 can be rewritten as follows:

$$N_q = 99.317 - 40.548\tanh(x_1) + 62.865\tanh(x_2) \quad (5)$$

and,

$$x_1 = 9.45 + 10^{-2}\left[-23.24\left(\frac{H}{B}\right) + 87.66\left(\frac{L}{B}\right) + 0.01(B) - 0.31(\theta) - 8.05(\gamma) - 16.92(\varphi)\right]$$

(**Error! No text of specified style in document.**)

$$x_2 = -1.77 + 10^{-2}\left[6.93\left(\frac{H}{B}\right) - 1.79\left(\frac{L}{B}\right) - 0.001(B) + 0.41(\theta) + 2.81(\gamma) - 0.34(\varphi)\right] \quad (7)$$

It should be noted that these equations are valid only for the ranges of values of *H/B, L/B, B,* θ, γ and φ given in Table 1. This is due to the fact that ANNs should be used only in interpolation and not extrapolation (Minns and Hall 1996).

4. CONCLUSIONS

Though a number of traditional methods are available to predict the pullout capacity of anchor foundation, the results of all these methods are inconsistent with each other as well as with the experimental results. As the ANN model is developed based on the experimental results, it is found to outperform most of the traditional methods. The following conclusions can be drawn from the results of the above study.

i) Random data division technique is used to divide the data into training, testing and validation of the model. The optimum model performance is obtained when 70% data is used for training, 15% data is used for testing and 15% data is used for validation of the model.

ii) The 6-2-1 network (6 input nodes, 2 hidden layer nodes, and 1 output node) with the LM (Levenberg–Marquardt) training algorithm is obtained as the optimum ANN geometry as it shows a better correlation with minimum errors than any other network.

iii) From the comparison between the experimental results and the prediction of the ANN model, it was obtained that the ANNs has the ability to predict the pullout capacity of anchor foundations with sufficient reliability (r=0.935, RMSE=4.136 and MAE=7.302).

iv) Comparison between the predictions of the ANN model and the most commonly used traditional methods has shown that the prediction of the ANN model matched more closely with the experimental results than the prediction of traditional methods for both horizontal, vertical and inclined anchors.

v) Finally, a tractable and relatively simple formula is proposed for the design engineers to predict the pullout capacity of anchor foundation more easily based on the ANN model which is suitable for hand calculation.

The main limitation of the ANN-based proposed formula is that, as the ANN model is based on experimental data and is suitable for use in an interpolative sense, it may not perform well in all design situations. The range of applicability of the ANN-based design formula is constrained by the data used in the model training phase and in order to update the model and make it more accurate in the future, it would be desirable to include additional data so that the model can be re-trained. Despite of having some limitations, the proposed formula can be considered as a powerful, quick and practical tool for prediction of the pullout capacity of anchor foundations on the cohesionless soils as the above study showed that the ANN method can outperform any other traditional methods within the data ranges used to train the model. Besides the predictions of ANNs are based on the experimental results, so there is no need to consider any assumptions. Whereas most of the traditional methods are based on different assumptions.

REFERENCES

Burland, J. B., and Burbridge, M. C. (1985). “ettlement of foundations on sand and gravel.” *In Institution of Civil Engineers, Proceedings*.

Demuth, H. (2008). *Neural Network Toolbox ™ 6 User ’ s Guide*. *MATLAB*.

Hanna, A., Foriero, A., and Ayadat, T. (2014). “Pullout Capacity of Inclined Shallow Single Anchor Plate in Sand.” *Indian Geotechnical Journal*, 45(1), 110–120.

Hanna, A. M., Das, B. M., and Foriero, A. (1988). “Behavior of Shallow Inclined Plate Anchors in Sand,.” *Geotech. Spec. Tech, ASCE*, 16, 54–72.

Hanna, A., Rahman, F., and Ayadat, T. (2011). “Passive earth pressure on embedded vertical plate anchors in sand.” *Acta Geotechnica*, 6(1), 21–29.

Hecht-Nielsen, R. (1990). “On the algebraic structure of feedforward network weight spaces.” *Advanced Neural Computers*, 129–135.

Hornik, K., Stinchcombe, M., and White, H. (1989). “Multilayer feedforward networks are universal approximators.” *Neural networks*, 2(5), 359–366.

Kartalopoulos, S. V. (2002). “Elastic bandwidth [optical-fiber communication.” *IEEE Circuits and Devices Magazine*, 18(1), 8–13.

Kumar, J., and Kouzer, K. M. (2008). “Vertical uplift capacity of horizontal anchors using upper bound limit analysis and finite elements.” *Canadian Geotechnical Journal*, 45(5), 698–704.

Martin, S. J., and Green, D. R. (1995). “Protease activation during apoptosis: death by a thousand cuts?” *Cell*, 82(3), 349–352.

Minns, A. W., and Hall, M. J. (1996). “Artificial neural networks as rainfall-runoff models.” *Hydrological sciences journal*, 41(3), 399–417.

Murray, E. J., and Geddes, J. D. (1989). “Resistance of Passive Inclined Anchors.” *Geotechnique*.

Noorzaei, J., Hakim, S. J. S., and Jaafar, M. S. (2008). “An approach to predict ultimate bearing capacity of surface footings using artificial neural network.” *Indian Geotechnical Journal,* 38(4), 515–528.

Padmini, D., Ilamparuthi, K., and Sudheer, K. P. (2008a). “Pullout Capacity Prediction of Circular Plate Anchors in Cohesionless Soils using Artificial Neural Networks.” *12th International Conference of International Association for Computer Methods and Advances in Geomechanics (IACMAG)*, Goa, India, India, 1818–1826.

Padmini, D., Ilamparuthi, K., and Sudheer, K. P. (2008b). “Ultimate bearing capacity prediction of shallow foundations on cohesionless soils using neurofuzzy models.” *Computers and Geotechnics*, 35(1), 33–46.

Shahin, M. A., Jaksa, M. B., and Maier, H. R. (2001). “ARTIFICIAL NEURAL NETWORK APPLICATIONS IN GEOTECHNICAL ENGINEERING.” *Australian Geomechanics*, 49–62.

Shahin, M. A., Maier, H. R., and Jaksa, M. B. (2002). “Predicting Settlement of Shallow Foundations using Neural Networks.” *Journal of Geotechnical and Geoenvironmental Engineering*, 128(9), 785–793.

Shahin, M. A., Maier, H. R., and Jaksa, M. B. (2004). “Data Division for Developing Neural Networks Applied to Geotechnical Engineering.” *Journal of Computing in Civil Engineering*, 18(2), 105–114.

Smith, P., and Davey, S. (1993). “Evidence for the competitive exclusion of Aeromonas salmonicida from fish with stress-inducible furunculosis by a fluorescent pseudomonad.” *Journal of Fish Diseases*, 16(5), 521–524.

Stone, M. (1974). “An asymptotic equivalence of choice of model by cross-validation and Akaike’s criterion.” *Journal of the Royal Statistical Society. Series B (Methodological)*, 44–47.

Twomey, J. M., and Smith, A. E. (1997). “Validation and verification.” *Artificial neural networks for civil engineers: Fundamentals and applications*, 44–64.

Wojciechowski, M. (2011). “Feed-forward neural network for python.” *Technical University of Lodz (Poland), Department of Civil Engineering, Architecture and Environmental Engineering*.

Proceedings of the 4th International Conference on Civil Engineering for Sustainable Development (ICCESD 2018), 9-11 February 2018, KUET, Khulna, Bangladesh(ISBN-978-984-34-3502-6)

BEARING CAPACITY OF SMOOTH AND ROUGH SQUARE AND RECTANGULAR FOOTINGS ON CLAY

Jubayer[1], Shafiqul Islam[2] and Rokonuzzaman[3]

[1]*Student, Khulna University of Engineering & Technology, Bangladesh,*
e-mail: jubayer92bayezid@ gmail.com.
[2]*Assistant Professor, Khulna University of Engineering & Technology, Bangladesh,*
e-mail: sumon2k8@yahoo.com.
[3]*Professor, Khulna University of Engineering & Technology, Bangladesh,*
e-mail: rokoncekuet@yahoo.com.

ABSTRACT

The Uniaxial Vertical bearing capacity of smooth and rough square and rectangular footings resting on homogeneous undrained clay is investigated with finite element analyses. The results are compared with the conventional and available analytical and numerical solutions. Finally a best estimate of bearing capacity and shape factor are derived as a function of aspect ratio. The bearing capacity of rough square footing is 5.36% greater than the bearing capacity of smooth square footing.

Keywords: *Bearing capacity, Square footings, Rectangular footings, Aspect ratio.*

1. INTRODUCTION

Traditional bearing capacity theory, developed based on conditions of plane strain (Terzaghi 1943), is suitable for strip footings where the length of the footing is “long” relative to its breadth. Many shallow foundations, particularly those used off shore, have a lower aspect ratio with a rectangular or square foot print. Edge effects improve bearing capacity (per unit area) of a three-dimensional footing compared to a strip footing as slip planes must develop around the perimeter of the three dimensional footing as opposed to only adjacent to the “long” edge under conditions of plane strain.

For the bearing capacity of square and rectangular footing no exact solution exists, even for the simple case of a surface footing resting on an isotropic, homogeneous deposit obeying an undrained failure criterion. However, the bearing capacity factors and shape factors for square and rectangular footings are bracketed with respect to strip footing.

Some studies have been carried out for bearing capacity of square and rectangular footings. Shield and Drucker(1953) proposed an upper bound solution for the ultimate limit state under uniaxial vertical loading for smooth rectangular footings, which gave a bearing capacity factor for a square footing of N_c=5.71. Later Michalowski and Dwason(2002) proposed a lower bearing capacity factor of N_c=5.43 based on finite difference analyses.

Michalowski (2001) proposed an upper bound solution for a rough square footing, giving a bearing capacity factor N_c=6.56 which is higher than the bearing capacity factor for square and rectangular footings.

The paper presents finite element analyses for smooth and rough square footings and proposes best estimates of the bearing capacity factors for rough rectangular footings of varying aspect ratio. The kinematic failure mechanism of square and rectangular footings observed are also

presented. For a square footing the failure mechanism indicates fourfold symmetry with displacement orthogonal to the edges. But it can be said that this analyses will provide a useful starting point for a better alternative upper bound solution.

2. METHODOLOGY

All the finite element analyses were carried out using the software ABAQUS. Two dimensional model was developed for strip footing analysis and three dimensional footing was developed for both square and rectangular rough and smooth footing. For two dimensional footing and three dimensional footing meshing, materials and load path was different.

Two dimensional footing was modeled for strip footing where length is relatively long than breadth. On surface footing at first we performed element study to fix the element size and meshing as well as displacement. The fixation of mesh element size is an important part of modeling because it determines the amount of element number and time required for the analysis of the model. After fixation of the element size, the type element also selected whether it is linear, quadratic or triangular. The quadratic element shows more accurate result and load-displacement curve become constant very quickly. Although triangular element shows more accurate result compared to quadratic but to avoid time for the analysis we used quadratic element. The load applied on the footing loaded area and gravity load all over the model element. For smooth footing the displacement occurred both vertically and laterally and no lateral displacement are restrained to zero. On the other hand for rough footing lateral displacement are restrained to zero and only vertical displacement occurred. Time increment for the analysis of two dimensional model was varied with different steps.

Two dimensional footings are also checked to investigate the results changing with the width. The footing was analyzed for footing width 0.5m, 1m, 2m, and 5m and found the bearing capacity results comparing with each other. Footing was also analyzed by changing the ratio of E_u/s_u =100, 250, 500, 2000, 5000, 10000, 30000 to compare the results to check whether the results vary or not.

After completed the data check then the model was submitted for the analysis. After completed the analysis of the model the failure diagram for the undeformed shape was viewed and load-displacement curve plotted with the output data. With the output data we calculated the ultimate bearing capacity (Qu) as well as bearing capacity factor. From three dimensional model analysis for both rough and smooth square and rectangular footing the kinematic failure mechanism was compared and best fit equation was developed for footing shape factor. Although three dimensional footing analysis required more time than the two dimensional footing as the number of element was high in three dimensional compared to the two dimensional footing. If the meshing is not good enough the element becomes distorted which will hamper the results as well as affect the exactness of the best estimate equation. The more the meshing finer the more it gives smooth failure pattern as well as give more accurate result.

2.1 Mesh

The two-dimensional finite element mesh used for analysis of a strip footing of width *B* and Length zero considered. The mesh extended 10*B* from the edges of the footing and 10*B* beneath the footing.

A number of mesh densities were investigated to achieve a time efficient model without maintaining accuracy and mesh element type was a 4-node bilinear plane strain quadrilateral,

reduced integration and hourglass control. Meshing was done for linear, quadratic and triangular element to fix the element for the model and to determine which provide more accurate results.

Six three-dimensional models were modeled to investigate the effect of varying footing length to breadth aspect ratio on bearing capacity of L/B=1(square), 2, 3, 4, 5, and 10. For the longer footings more elements were used in the longitudinal direction to maintain uniform element size across the models. For example the mesh for the *L=B* comprises 11700 and the mesh for the *L=5B* footing comprises 25200 linear hexahedral element (more than twice as many as the square footing mesh) shown in Figure 1.

2.2 Load Path

All the finite element analysis were carried out to investigate the ultimate load (Qu). Ultimate load Q_u= ∑sum of vertical reaction force at all nodes (RF_2)/ Footing area.The presence of rigid footing is modeled by applying uniform vertical downward displacements at the nodal points at the top surface. Horizontal displacement at the footing-soil interface were restrained to zero for rough footing U_1=0 U_2=prescribed displacement at the contact nodes, U_3=0 (for rough footing) and free for smooth footing where, U_1 ≠0 U_2=prescribed displacement at the contact nodes, U_3 ≠0.

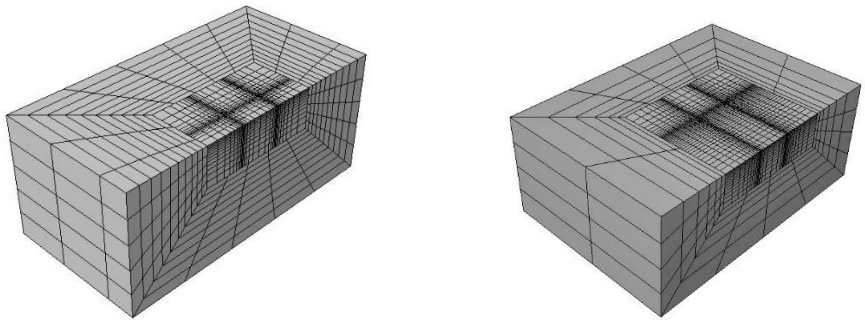

(a) (b)

Figure 1: Finite element meshes (a) square footing (L=B); (b) rectangular footing (L=5B).

3. ILLUSTRATIONS

3.1 Comparison of bearing capacity as function of footing aspect ratio

In addition to the square footing analyses, six analyses were carried out on rectangular footings to investigate the effect of aspect ratio (Length to breadth, L/B). All the rectangular footing analyses were modeled for a rough interface on the underside of the footing.

Figure 2represents comparison of bearing capacities as a function of aspect ratio for square and rectangular footings with a rough and smooth interface from the finite element results from this study with Skempton's empirical expression and other available bound solutions. Here, we see that the more the aspect ratio increases the more the difference between square and rectangular footing increases. That means for square footing the difference between bearing capacity of smooth and rough footing is maximum and the more the footing tends to strip footing the difference becoming lesser. The most visible thing is that the bearing capacity of rough and smooth based square and rectangular footings are lies in between the lower bound and upper bound solutions.

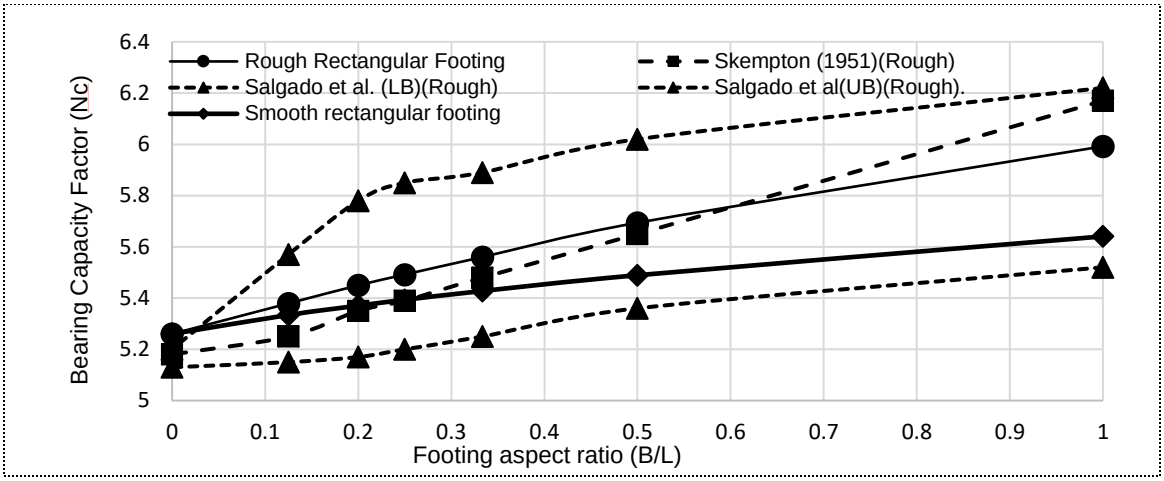

Figure 2: Comparison of Bearing Capacity Factor as function of Footing aspect ratio with available published data by Finite Element Analyses.

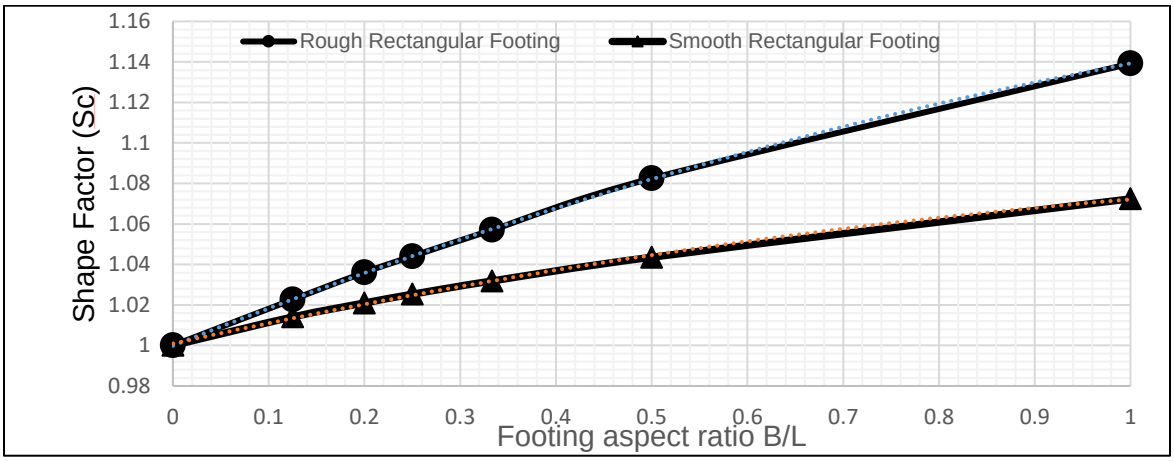

Figure 3: Best-estimate shape factors for square and rectangular footings.

The best estimate shape factors for square and rectangular footings are obtained from the Figure 3. It is clearly visible that the difference between smooth and rough square and rectangular footings decrease with the decrease of aspect ratio. The shape factor define as the ratio of bearing capacity of rectangular footing to the bearing capacity of strip footing. The relationship obtained between footing aspect ratio and shape factor from the finite element results can express through simple quadratic equations. The equations gives comparatively higher shape factor for slender footing and reduced shape function for square and rectangular footing for lower aspect ratio.

Kinematic Failure Mechanisms of Rough Footing Interface

Figure 4 represents the contours of resultant soil displacement at failure for each of the footings modeled. As the footings becomes larger the wedge underneath the footing becomes deeper and additional sliding wedge developed. At the same time the central wedge is getting sharper and smaller.

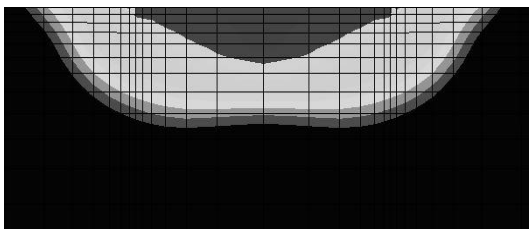

(a) L/B=1

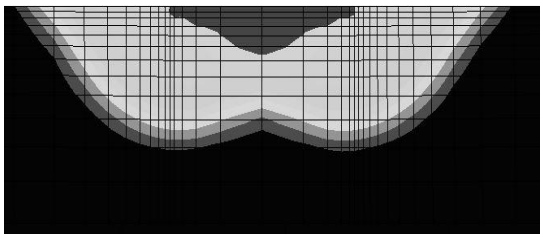

(b) L/B=2

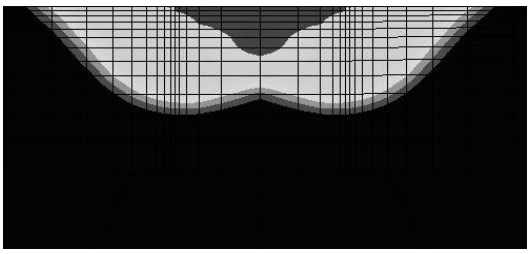

(c) L/B=3

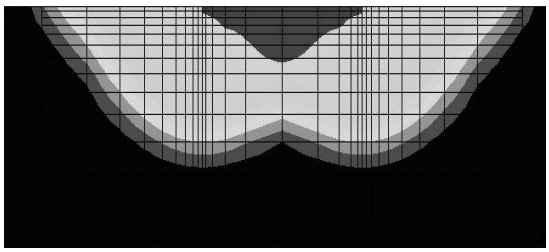

(d) L/B=4

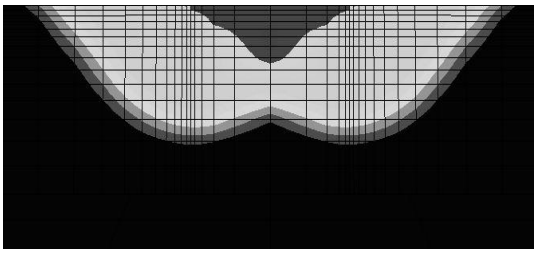

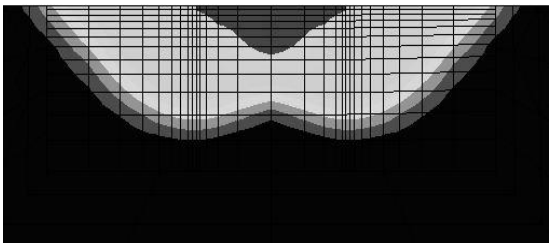

(e) L/B=5(f) L/B=8

Figure 4: Kinematic failure mechanisms of footings of various aspect ratio (rough interface)

(a) L/B=1; (b) L/B=2; (c) L/B=3; (d) L/B=4; (e) L/B=5; and (f) L/B=8.

Consideration of the regions of displaced soil, viewed in plan as illustrated in Figure.5 (a–f), shows the failure mechanism extender in the longitudinal direction i.e., along the long axis is independent of footing aspect ratio, and equal to approximately0.6*B*. Diagonal symmetry for the square footing of the failure mechanism is also clearly illustrated by the displacement contours shown in Figure.5.It could also be surmised from the displacement contours in Figure.6 that plane strain conditions prevail approximately 1.5*B*from the end of the footing, measured along the long axis.

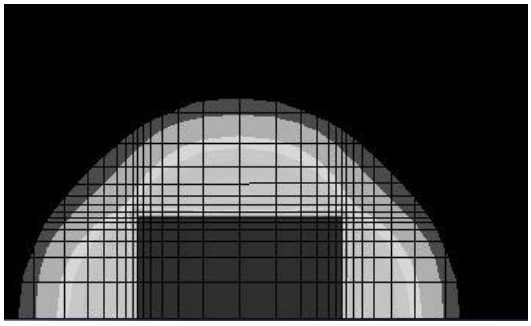

(a)L/B=1

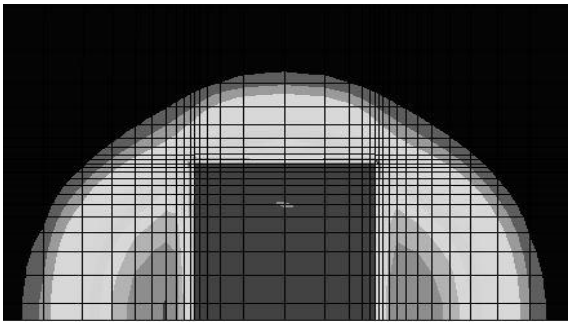

(b) L/B=2

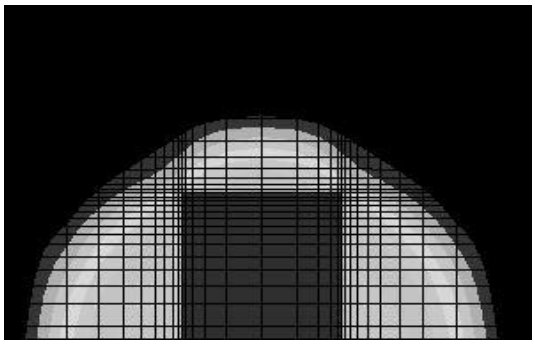

(c)L/B=3

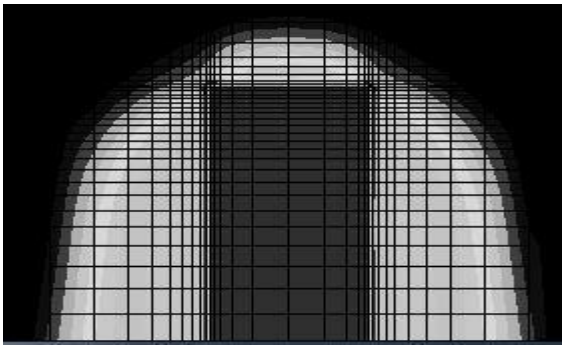

(d) L/B=4

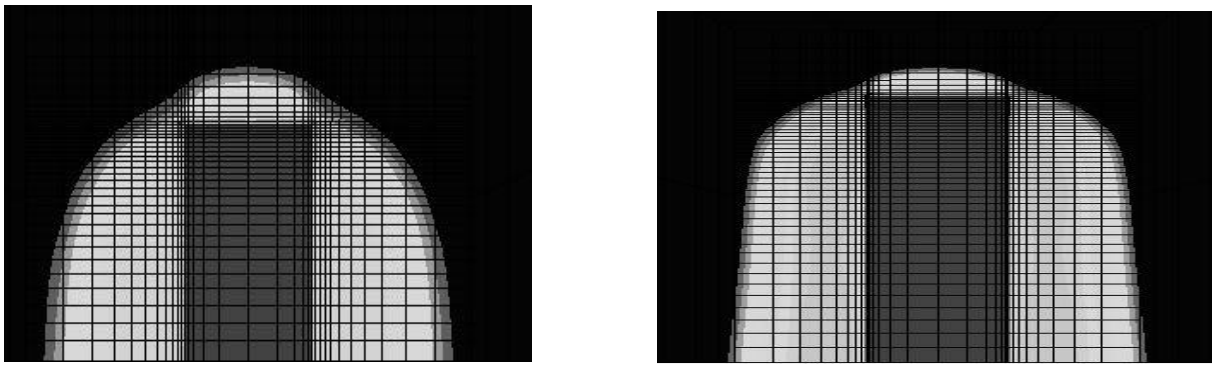

(e) L/B=5 (f) L/B=8

Figure 5: Plan view of failure mechanisms (rough footings) (a) L/B=1; (b) L/B=2; (c) L/B=3; (d) L/B=4; (e) L/B=5; and (f) L/B=8.

Smooth footing Interface

The kinematic mechanism of failure observed in the finite element analysis for the smooth square footing indicating double wedge hill type mechanism where no central edge is evident in the Figure 7 and the slip taking place underneath footing moving towards the outer edge at an angle α (Figure 6). Some soil movement occurred directly below the center of the footing.

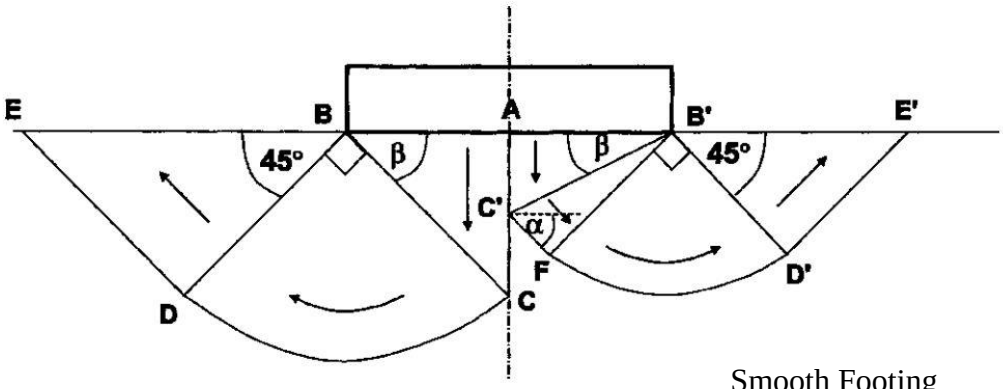

Figure 6: Typical kinematic failure mechanism of rough and square footing

The failure depth or influence zone of rough square footing is much higher than smooth square footing. It represents that the bearing capacity of rough square footing is higher than the smooth square footing. The central edge is clearly visible for rough square footing which is absent in smooth square footing. As the uniform vertical load applied at the rough footing only one direction so central edge developed but for smooth square footing the displacement freed to all directions so no central edge developed.

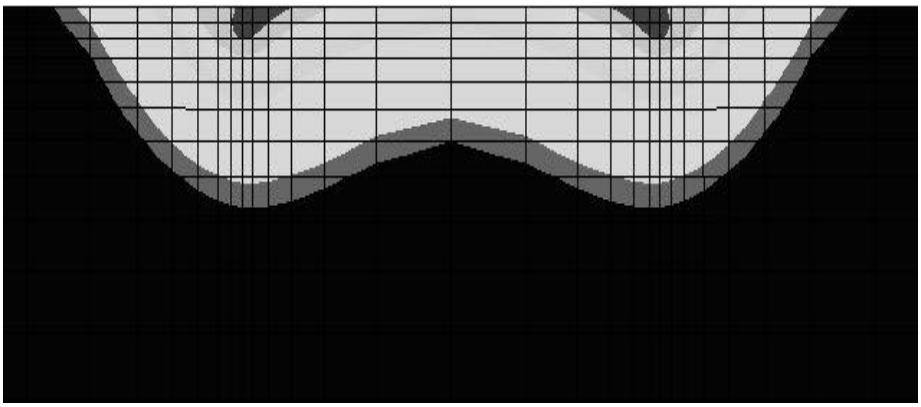

Figure 7: Kinematic Failure mechanism of smooth square footing

Contours of resultant displacement viewed in plan over therough and smooth square footings are shown in Figure 8. Thesealso illustrate the variation in nature of the soil displacement depending on interface roughness. The footings are subjected to auniform vertical displacement; the contours of resultant displacement beneath the rough footing show that the soil moves uniformly vertically downwards with no relative soil movement onthe underside of the footing. The contours beneath the smoothfooting show a variation of soil displacement across the footingarea, the maximum soil movement occurring at the footing periphery with less displacement beneath the center.

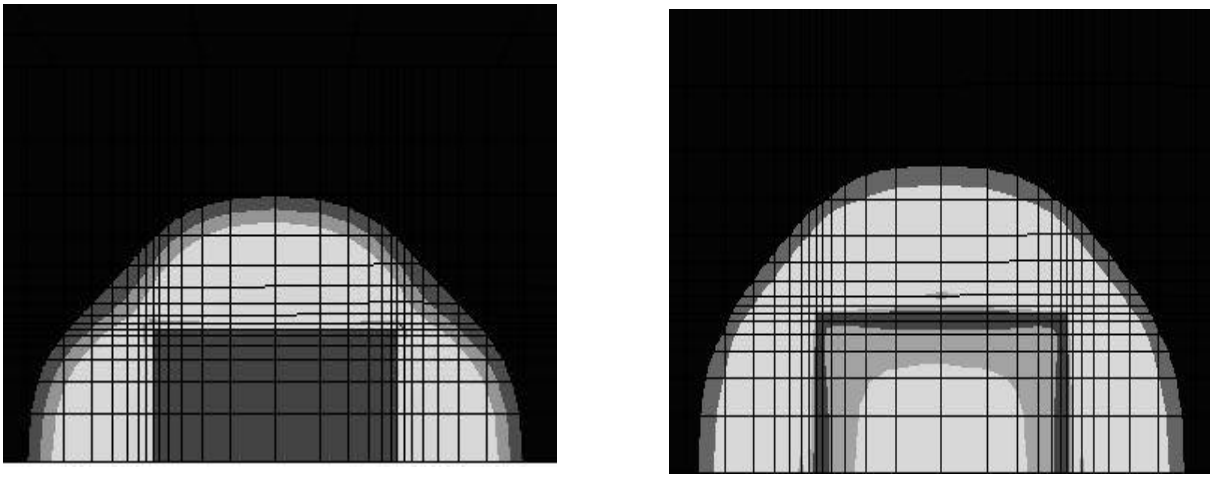

(a) Rough (b) Smooth

Figure 8: Displacement contours at failure for square footings (a) rough; (b) smooth.

3.2 Equations

The best estimate equation between shape factor and footing aspect ratio for rough rectangular footingis shown on equation (1) and for smooth rectangular footing is shown on equation (2).

$$S_c = 0.999 + 0.1896(B/L) - 0.0502(\frac{B}{L})^2 \quad (1)$$

Where, R^2=1,S_c= Shape factor of footing, B/L= Aspect ratio

And for smooth rectangular footing is,

$$S_c = 1.009 + 0.1035(B/L) - 0.0323(\frac{B}{L})^2 \quad (2)$$

Where, R^2=0.99, S_c =Shape factor.

3.3 Tables

Comparison of Undrained Bearing Capacity and Shape Factors results of the finite element analyses is shown on Table 1 with the results obtained by Skempton (1951) and Salgado et al.

Table 1: Comparison of Undrained Bearing Capacity and Shape Factors for Smooth and Rough Based Rectangular Footings

L/B	Rough Footing		Smooth Footing		Skempton(1951)		Salgado et al.		
	Nc	*Sc*	*Nc*	*Sc*	*Nc*	*Sc*	*LB*	*UB*	*Avg*
1	5.99	1.14	5.64	1.07	6.17	1.20	5.52	6.22	5.87
2	5.69	1.08	5.48	1.04	5.65	1.10	5.36	6.02	5.69
3	5.56	1.06	5.42	1.03	5.48	1.07	5.25	5.89	5.57
4	5.49	1.04	5.39	1.03	5.39	1.05	5.2	5.85	5.525
5	5.44	1.04	5.37	1.02	5.35	1.04	5.17	5.78	5.475
8	5.37	1.02	5.33	1.01	5.25	1.02	5.15	5.57	5.36

4. CONCLUSIONS

- Bearing capacity of rough square footing is 5.36% greater than smooth square footing and rough based rectangular footing has larger bearing capacity factor and shape factor with greater aspect ratio. Bearing capacity of smooth footing is 3.66% lower than rough rectangular footing.
- The best fit equation from the relationship between shape factor and aspect ratio for rough and smooth rectangular footing is derived.
- The difference of bearing capacity between rough and smooth square and rectangular footing decreases with the decrease of footing aspect ratio. The more the footing strip the minimum the difference of bearing capacity and shape factor.

ACKNOWLEDGEMENTS

I would like to thank assistant professor Md. Shafiqul Islam who inspired and helped me in the whole works and professor Md. Rokonuzzaman who guided me as a supervisor completing the works properly.

REFERENCES

Cox, A. D., Eason, G., and Hopkins, H. G. 1961. “Axially symmetric plastic deformation in soils.” *Proc. R. Soc. London, Ser. A*, 254, 1–45

De Beer, E. E. 1970. “Experimental determination of the shape factor and the bearing capacity factors for sand.” *Geotechnique*, 204, 387–411. *Geotechnique*, 519, 787–798.

Hansen, B. J. 1970. “A revised and extended formula for bearing capacity.” *Bulletin 28*, Danish Geotechnical Institute Copenhagen,Denmark.

Levin, E. 1955. “Indentation pressure of a smooth circular punch.” *Q.Appl. Math.*, 132, 133–137.

Micahlowski, R. L., and Dawson, E. M. 2002. “Three-dimensional analysis of limit loads on Mohr–Coulomb soil.” *Foundations of civil and environmental engineering*, Vol. 1, Poznan University of Technology Press, Poland,

Michalowski, R. L. 2001. “Upper bound load estimates on square andrectangular footings.”

Salgado, R., Lyamin, A. V., Sloan, S. W., and Yu, H. S. 2004. “Twoand three-dimensional bearing capacity of foundation in clay.” *Geotechnique*, 545, 297–306. Shield, R. T., and Drucker, D. C. 1953. “The application of limit analysis to punch indentation problems.” *J. Appl. Mech.*, 20, 453–460. Skempton, A. W. 1951. “The bearing capacity of clays.” *Proc., Building andResearch Congress*, Vol. 1, London, 180–189.

Shield, R. T., and Drucker, D. C. 1953. “The application of limit analysis to punch indentation problems.” *J. Appl. Mech.*, 20, 453–460

Skempton, A. W. 1951. “The bearing capacity of clays.” *Proc., Building and Research Congress*, Vol. 1, London, 180–189.

Terzaghi, K. 1943. *Theoretical soil mechanics*, Wiley, New York. 37–147.

Proceedings of the 4th International Conference on Civil Engineering for Sustainable Development (ICCESD 2018), 9~11 February 2018, KUET, Khulna, Bangladesh (ISBN-978-984-34-3502-6)

STABILIZATION OF SOIL BY MIXING WITH DIFFERENT PERCENTAGES OF LIME

M A Ashraf[1], M A Hossen[2], M A Ali[3] and B P Chakaraborty [3]

[1]*Professor, Southern University Bangladesh, Bangladesh, e-mail: ashraf.engr.66@gmail.com*
[2] *Lecturers, Southern University Bangladesh, Bangladesh, e-mail: arifhossen0101@gmail.com*
[3] *Students, Southern University Bangladesh, Bangladesh, e-mail: ajghar12sub@gmail.com*

ABSTRACT

Increasing urbanization in our cities has created a tremendous demand for developable land especially in the periphery of our cities and towns. We have found several researches dealing with soil-cement and soil-lime stabilization but none has dealt with the specific type of soils which are found in and around the city of Chittagong. We have found from the past researches that cement performs better with sandy soil while lime performs better with silty/clayey soil. In this research, we have tried to check the performance of lime with two different types of soils: hilly soil from Khulshi area and paddy land soil from South Salimpur within the city. Lime-stones were procured from local market. For the ease of measurement and for easy and uniform spreading over soil before mixing, it was converted into powder by sprinkling water on it. It was found that the lime stone procured from the local market had a lime content of 63.2%. Lime-powder in variable percentages of 0%, 2%, 4%, 6%, 8%, 10%, 12%, and 14% were used as stabilizer. The compressive strengths of lime stabilized soil were evaluated for different curing period: 7 days, 14 days, 28 days and 60 days. It was found that the load bearing capacity of soil increased with the increase in percentage of lime to a certain limit. It was, also, found that strength increases with the increase in curing period. At 8% lime content, maximum compressive strength were found in paddy land soil while at 6% lime content maximum compressive strength were found in hilly soil. Hilly soils are generally sandy while the paddy land soils are silty / clayey. It was found that less limes were necessary for stabilizing sandy hilly soil compared to silty paddy land soil. Since lime is cheaper compared to cement, it may become a viable alternative of cement for soil stabilization. Before arriving at a definite conclusion on the use of lime stabilized soil, further researches with lime using all different varieties of soils in and around the City of Chittagong will be necessary.

Keywords: *Quick Lime, hydrated lime; curing period; soil compressive strength, soil-lime stabilization*

1. INTRODUCTION

1.1 Background Information

In the last few decades, world population has increased rapidly especially in developing countries like Bangladesh. Buildings are being built and roads are constructed by encroaching into paddy land. Hills in Chittagong are continuously being lebelled to build houses on it. We like it or not buildings are built on paddy land and the hills. Since paddy land soils are mostly silt with some clay and the hill soils are generally loose fine sand with a small percentage of silt and clay, engineers often had to go for costly foundation like deep foundation in these type of soils. Construction is risky in these soils due to uneven settlement, land slides and or shear failure. Deep foundations are, sometimes, beyond the financial capacity of average home builders trying to build a three or four story building to be claimed and taken pride of as their own house.

Therefore, a suitable and low cost alternative to deep foundation is to be identified for the average home owners going for a low rise building. Soil stabilization techniques might become the cheap alternatives against the conventional technique of deep foundation using pre cast or cast in situ piles. Improvements in engineering properties of soil such as increases in soil strength (shear resistance), stiffness (resistance to deformation) and

durability (wear resistance), reduction in swelling potential of wet clay soils can be done by soil stabilization(Sultan et al. 2014).

Soil stabilization involves the blending of natural soils with chemical agents such as lime, cement (OPC or PPC) and asphalt (Rogers et al.). These agents are generally potential binders which effectively bind together the soil aggregates. As a result, load carrying and stress distribution characteristics of soil improve; excessive shrinkage and swelling in soil come under control.. A very common and cheap technique to improve the soft clay soil is to add a certain percentage of lime with the soil (Farooq et al. 2011). Lime in the form of quicklime (calcium oxide – CaO), hydrated lime (calcium hydroxide – Ca[OH]2), or lime slurry can be used to treat the soils. Hydrated lime is created when the quicklime chemically reacts with water. It is hydrated lime that reacts with particles of clay and permanently transform them into a strong cementious matrix (Ajayi 2012) .

1.2 Chemistry of Lime Treatment

The chemical reactions between clay and lime particles can be grouped under two distinct types of changes; one is a short term change termed as modification and the other is a long term change termed as stabilization. In modification, the process of ion exchange makes the clay minerals flocculate and agglomerate leading to a reduction in plasticity, swell and moisture content. In stabilization, pozzolanic reaction takes place over a long period of time that creates cementitious products which are responsible for long-term gain in strength (Bozbey et al. 2016).

1.3 **Drying**:

If quicklime is used, it immediately hydrates (i.e., chemically combines with water) and releases heat. As a result, soil dries quickly, because part of the water present in the soil participates in the reaction, and the rest evaporates due to heat of hydration. The hydrated lime produced thus will subsequently react with clay particles. These subsequent reactions will slowly cause additional drying because of a reduction in soil's moisture holding capacity by way of modification in soil structure known as floculation. Floculation increases drainage capability of the soil and reduces the soil's moisture holding capacity. If hydrated lime or hydrated lime slurry is used instead of quicklime, drying occurs only through changes in the soil structure. This, in fact, increases the draining capability of of the soil; reduces the water holding capacity of the soil and increases its stability. In fig.1, it can be seen that water content Wn is reduced to W'n after treatment with lime.

1.4 **Modification**:

After initial mixing, the calcium ions (Ca++) from hydrated lime migrate to the surface of the clay particles and displace water and other ions. The soil becomes friable and granular, making it easier to work and compact. At this stage the Plasticity Index of the soil as shown in Figure 1 decreases dramatically, as does its tendency to swell and shrink. The process, which is called "flocculation and agglomeration," generally occurs in a matter of hours.

(Kerni, Sonthwal, and Jan 2015)

Figure 1**:** Effect of lime addition on the consistency of soil

1.5 Stabilization:

When adequate quantities of lime and water are added, the pH of the soil quickly increases to above 10.5, which enables the clay particles to break down. Silica and alumina are released and react with calcium from the lime to form calcium-silicate-hydrates (CSH) and calcium-aluminate-hydrates(CAH). Both CSA and CAH are cementitious products similar to those formed in Portland cement. They form the matrix that contributes to the strength of lime-stabilized soil layers. As this matrix forms, the soil is transformed from a sandy, granular material to a hard, relatively impermeable layer with significant load bearing capacity. The process begins within hours of lime addition and can continue for years in a properly designed system. The matrix formed is permanent, durable, and significantly impermeable, producing a structural layer that is both strong and flexible.

Therefore the purposes of binder addition to soft clays can be stated briefly (Bozbey et al. 2016) as:

- To increase the strength and stiffness of soft soil
- To improve the differential deformation properties of the soft soil
- To increase dynamic stiffness of the soft soil
- To remediate contaminated soil

The aim of this study is to determine the engineering properties and unconfined compressive strength of paddy land soil and hill soil. Additionally, this study investigates the improvement of the unconfined compressive strength of soil by mixing different percentages of lime with soil. Finally, it gives information about optimum lime content for this particular types of soil for improving the unconfined compressive strength of the soil . Four different time periods for curing were considered.

2. LITERATURE REVIEW

Soil stabilization is a procedure where natural or synthesized additives are used to improve the engineering properties of weak soil. Several reinforcing methods are available for stabilizing soils. Therefore, the techniques of soil stabilization can be classified into a number of categories such as physical stabilization, chemical stabilization and mechanical stabilization. There is a rich history of the use of soil stabilization admixtures to improve poor sub grade soil. Improvement in performance by controlling volume change and by increasing strength was in practice (Navale et al. 2016).

Tedesco (2006) studied soil compressibility before and after lime treatment with respect to the effects of initial moisture content of compacted soil sample, the curing time and the test procedure. He used a unique percentage of lime equal to 3% by weight of soil for all soil specimens. Using standard and modified Proctor tests, the samples were prepared with moisture content corresponding to optimum water content. In addition to the odometer, he developed a delayed procedure, which involved tests with constant curing time of 7 and 28 days. He pointed out that the lime-treated soil samples exhibited lower compressibility; particularly for samples compacted on the dry side and that dramatic over consolidation was obtained by dynamic compaction.

4% addition of lime with Gazipur clay soil increased the unconfined compressive strength at different curing period by four to six times. Strengths with 4% lime were, also, found to be 1.5 to 2 times higher compared to the addition of lime in the range of 2, 6 and 8%.(Farooq et al. 2011). Better strength was recorded when Gazipur soil was combined with 4% lime

By adding 6% lime with sandy clay maximum strength found was 198.44 KPa for 6% addition of lime (Jawad et al. 2014).

It is evident from literature review that lime stabilization is one of the most practical and cost effective techniques of sub grade stabilization. However, it is to be noted that in cold weather, lime stabilization could not give the desired strength in soil. The goal of this research is to clearly understand the behavior of lime in increasing compressive strength of locally available soil.

3. METHODS & PROCEDURES

The soils used in this study were classified according to Unified Soil Classification System (USCS). For the classification Atterberg limit test, Sieve Analysis test as well as Hydrometer Analysis test was conducted. The consistency limit test includes liquid limit and plastic limit tests of soil by using the Casagrande apparatus in accordance with ASTM specification. The ASTM standard procedure was followed in performing particle-size analysis of fine grained soil which was based on the principle of sedimentation of particles, and is measured by flotation of hydrometer for 36 hours. The results associated with the classification of both soil samples were showed in the tabular format in Table 1.

Table1: Classification and Engineering Properties of Soil

Soil Properties (Paddy Land Soil)		
Parameter		Percentages (%)
As Per Unified Soil Classification System(USCS) Group Symbol SM	Sand	68
	Silt & Clay	32
Liquid Limit		47
Plastic Limit		43.5
Plasticity Index		3.5
Optimum Moisture Content(OMC)		16
Salinity		Nil
Soil Properties (Hilly Soil)		
As Per Unified Soil Classification System(USCS) Group Symbol SC	Sand	59
	Silt & Clay	41
Liquid Limit		30.5
Plastic Limit		20
Plasticity Index		10.5
Optimum Moisture Content(OMC)		12
Salinity		Nil

Lime in the form of Lime-stones (CaCo3), quicklime (calcium oxide – CaO), hydrated lime (calcium hydroxide – Ca $(OH)_2$, or lime slurry can be used to treat soils. Quicklime is manufactured by chemically transforming calcium carbonate (limestone – CaCO3) into calcium oxide. Hydrated lime is created when quicklime chemically reacts with water. In our case, lime-stones were collected from the local market. Properties of lime-stones procured from the local market are given in Table-2.

Table 2: Properties of Lime-stones procured from local market

Lime Properties.		
SL No.	Parameter	Percentages (%)
1	Calcium oxide – CaO	63.2
2	Moisture	22.9
3(1+2)	Calcium Hydroxide $Ca(OH)_2$	86.1
4	Residual Materials	13.9

In this research, performance of lime with two different types of soils: hilly soil from Khulshi area and paddy land soil from South Salimpur within the city were assessed. For the ease of measurement, it was converted into powder by sprinkling water on it. It was found that the lime stone procured from the local market had a lime content of 63.2%(Table 2). Lime-powder in variable percentages of 0%, 2%, 4%, 6%, 8%, 10%, 12%, and 14% were used as binder/stabilizer. The unconfined compressive strengths of lime stabilized soil were evaluated for different curing period: 7 days, 14 days, 28 days and 60 days. The overall working framework is shown in Figure 2.

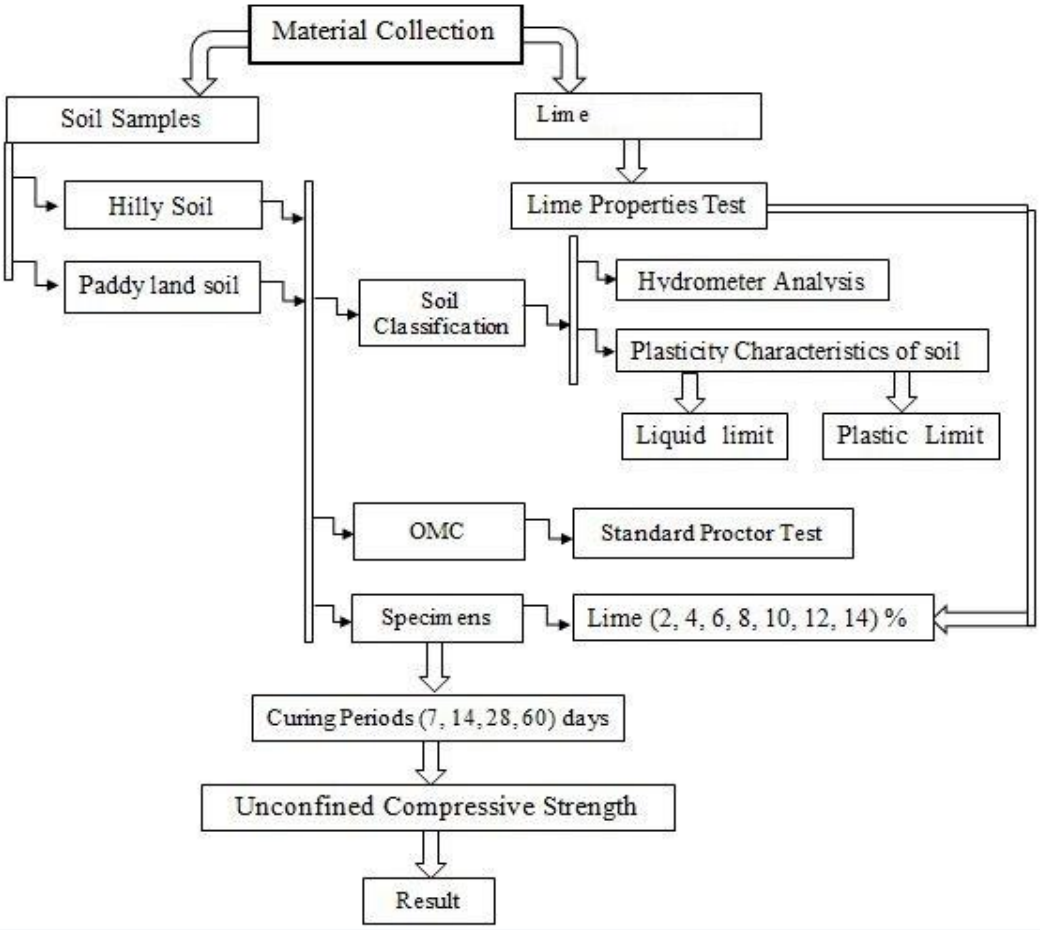

Figure 2: Flowchart of Methods and Procedures

4. RESULTS AND DISCUSSIONS

The results of the unconfined compressive strength tests are given in this section. Unconfined compressive strengths were estimated from stress strain diagram and plotted against eight different percentages of lime content for four different curing periods and are shown in figure 3**.** It shows that unconfined compressive strength increases as the curing period increases for all the hilly soil samples tested in this study. It also shows that unconfined compressive strength increases for (0% - 6%) lime content and decreases for further increment of lime content in the samples. The initial increment of unconfined compressive strength for using (0%-6%) percent of lime is due to the hydration of lime in the hilly soil sample and the later decrement of unconfined compressive strength for using (8 to 14 %) percent of lime is due to the presence of excessive lime, having less compressive strength compared to soil, in the hilly soil sample. It is clear from the Figure that 6% lime content in the hilly soil gives highest unconfined compressive strength after each curing period. The compressive strength is highest after a curing period of sixty days. It is clear that compared to cement lime takes more time in curing for gaining adequate strength.

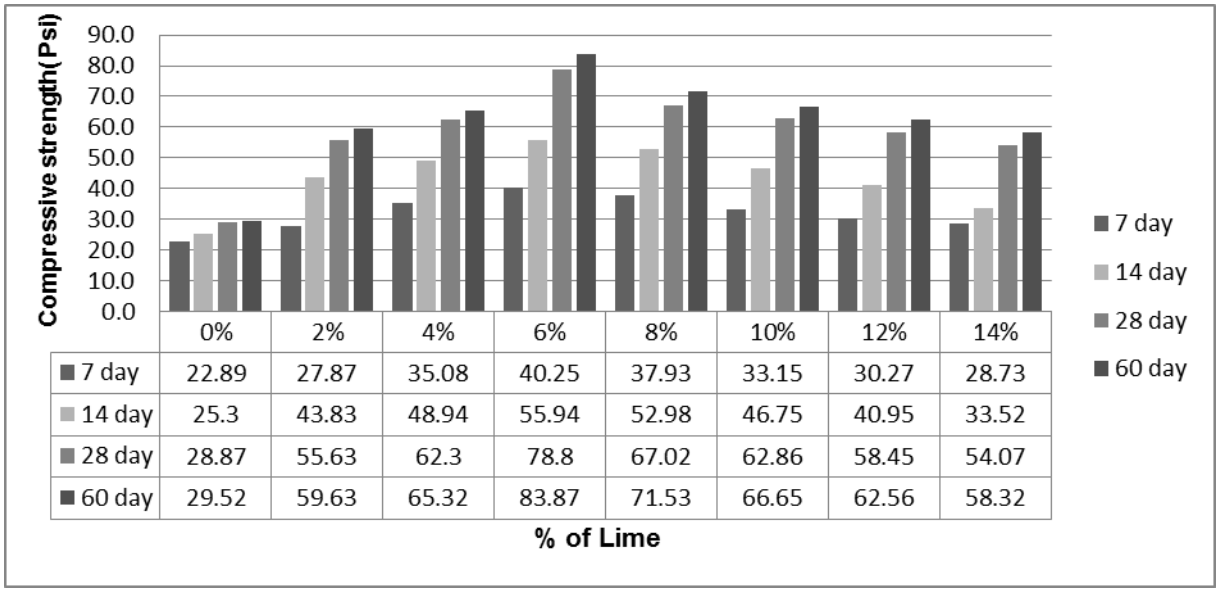

	0%	2%	4%	6%	8%	10%	12%	14%
7 day	22.89	27.87	35.08	40.25	37.93	33.15	30.27	28.73
14 day	25.3	43.83	48.94	55.94	52.98	46.75	40.95	33.52
28 day	28.87	55.63	62.3	78.8	67.02	62.86	58.45	54.07
60 day	29.52	59.63	65.32	83.87	71.53	66.65	62.56	58.32

Figure 3**:** Unconfined Compressive strength (UCS) of hilly Soil with different percentages of lime and different curing period

Figure 4 shows that unconfined compressive strength against four different curing periods for eight different percentages of lime soil mixture. It showed that that with 0% limes content, unconfined compressive strength is almost similar for all four curing periods. That means when no lime is used, increase in curing period will have no appreciable effect on the strength of soil. However, for varying percentages of lime in lime soil mixture, considerable variations of unconfined compressive strengths were observed. The optimum lime content required to produce maximum strength depends on curing temperature and curing period. From the figure:4, it is also found that soil without lime gives the lowest unconfined compressive strength and addition of 6% lime content with hilly soil showed largest values of unconfined compressive strength for all curing periods.

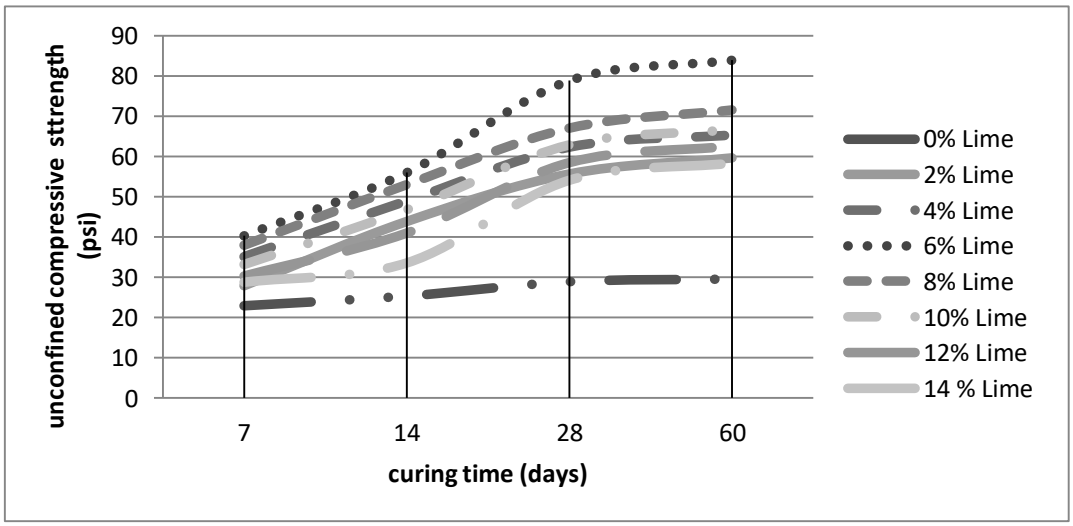

Figure 4**:** Unconfined compressive strength of Hilly soil as a function of curing period for eight different lime soil mixtures

In figure 5 it is shown that unconfined compressive strength increases with the increase in the length of curing period, even when the percentage of lime remained unchanged. It also showed that with further increase in lime, in all curing periods, strength decreases.

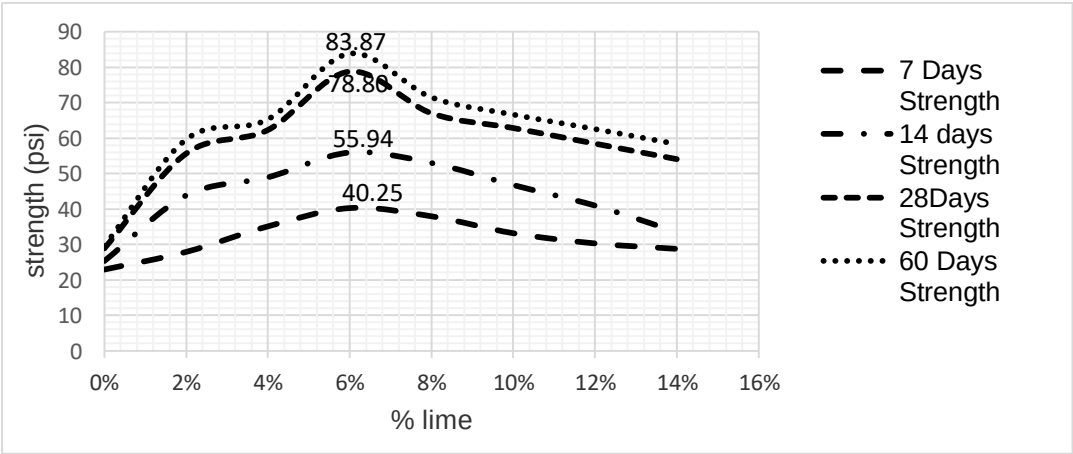

Figure 5: Unconfined compressive strength of hilly soil against percentages of lime for 7, 14, 28, 60 days of curing period.

Unconfined compressive strength was estimated from stress strain diagram and plotted against eight different percentages of lime content for four different curing periods. In figure 6, it shows that unconfined compressive strength increases as the curing period increases for all the paddy land soil samples tested in this study. It also shows that unconfined compressive strength increases for (0% - 8%) lime content and decreases for further increment of lime in the samples. The initial increment of unconfined compressive strength for using (0%-8%) percent of lime is due to the hydration of lime in the paddy land soil sample and the later decrement of unconfined compressive strength for using (10 to 14 %) percent of lime due to the presence of excess lime (having less compressive strength compared to soil) in the paddy land soil sample. It is clear from the Figure that 8% lime content in the paddy land soil gives highest unconfined compressive strength at each curing period used in this study.

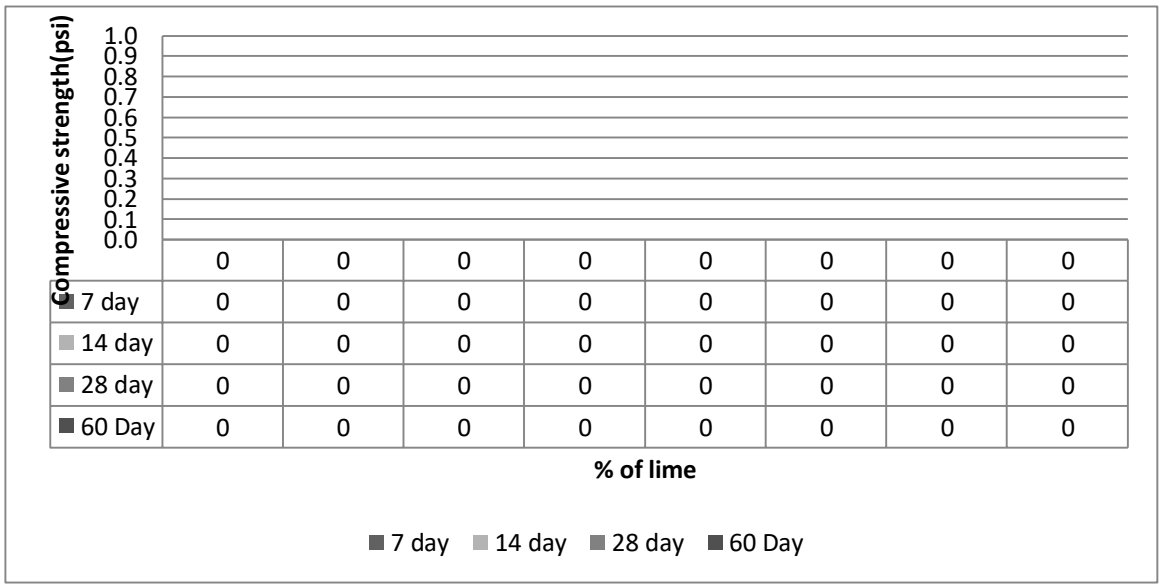

Figure 6: Unconfined Compressive strength (UCS) of Paddy Land Soil with the different percentages of lime

Figure 7 shows the plotting of unconfined compressive strength against four different curing periods for eight different percentages of lime soil mixture. It shows that (0% lime content) unconfined compressive strength is almost similar for all four curing periods indicating no effect of curing period on unconfined compressive strength for 100 percent sample soil. However, for other cases (lime soil mixture) considerable variation of unconfined compressive strength was observed with varying percentage of lime content in soil indicating the effect of lime content on unconfined compressive strength. From the Figure 7**,** it is also found that soil without lime gives the lowest unconfined compressive strength and 8% lime content in paddy land soil gave largest values of unconfined compressive strength for all curing periods. Therefore, adding only 8% of lime with paddy soil gives considerable improvement in the strength of soil.

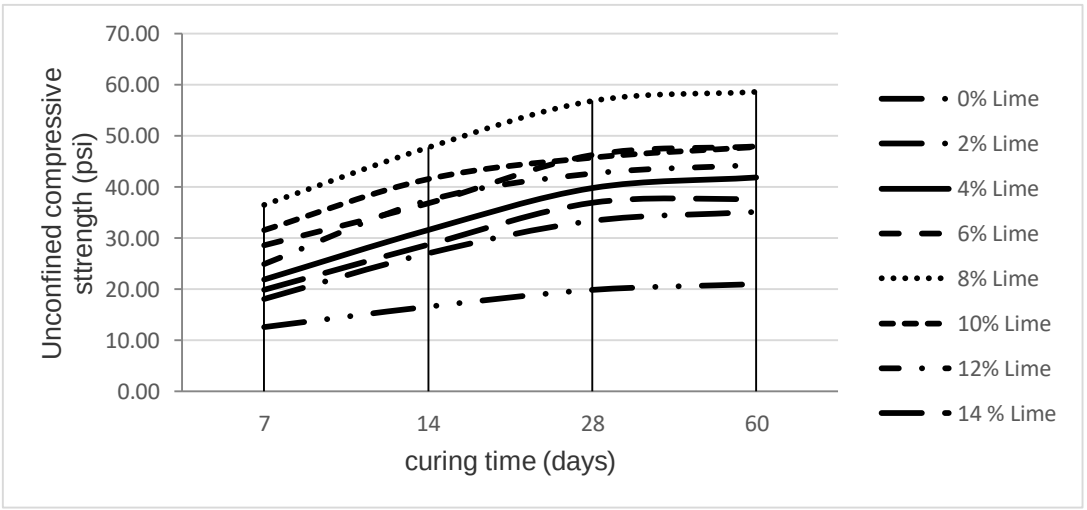

Figure 7: Unconfined compressive strength of Paddy Land Soil as a function of curing period for eight different lime soil mixtures

In figure 8 it is shown that the unconfined compressive strength increases in respect of curing period when the percentage of lime is constant. It also showed that with further increase of lime in all curing period, strength decreases.

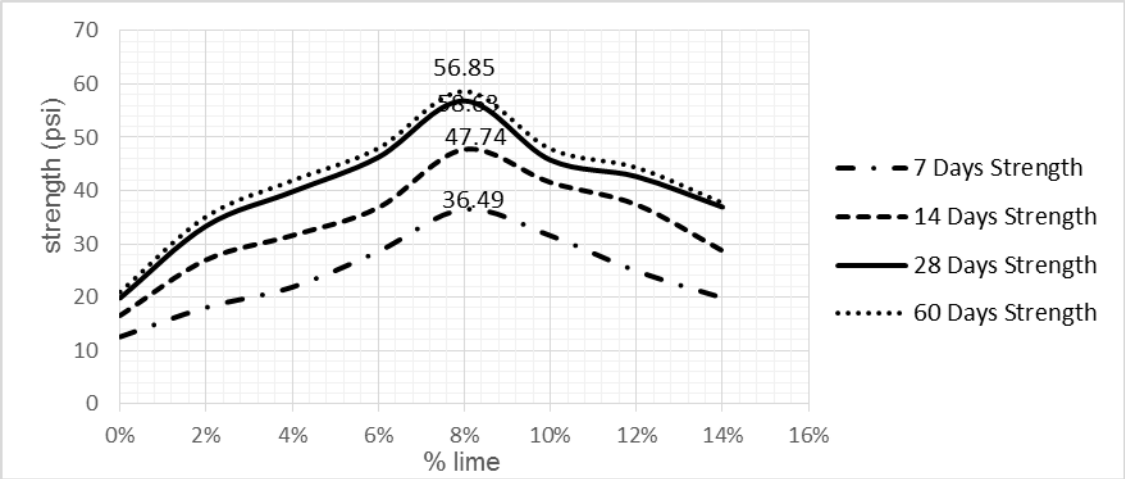

Figure 8: Unconfined compressive strength of Paddy Land Soil against percentages of lime content for 7, 14 and 28 days curing period.

5. CONCLUSIONS

It was found that the soil strength increased with the increase in percentage of lime to a certain limit. It was, also, found that strength increases with the increase in curing period. At 8% lime content, maximum compressive strength was found in paddy land soil while at 6 % lime content maximum compressive strength was found in hilly soil. Hilly soils are generally sandy while the paddy land soils are silty/clayey. It was found that less limes were necessary for stabilizing sandy hilly soil compared to silty paddy land soil.

RECOMMENDATIONS

The following recommendations are suggested for further research work.

- Different varieties of soil sample, especially soils frequently found and used in the locality, can be analyzed for same and similar percentages of lime used in this study.
- Impact of cyclic wetting–drying on swelling behavior of lime-stabilized soil is to be investigated.

ACKNOWLEDGEMENTS

Southern University Bangladesh Civil Engineering Laboratory and its resources were used during this research work.The authors thank the laboratory technicians for their help during the investigations.

REFERENCES

Ajayi, Emmanuel Sunday. 2012. “Int . J . Forest , Soil and Erosion , 2012 2 (4): 165-168 ISSN 2251-6387 [PRINT] 2251-824X [Online] © November 2012 , GHB â€™ S Journals , IJFSE , Shabestar , Iran Effect of Lime Variation on the Moisture Content and Dry Density of Lateritic Soil in Ilorin , Nigeria . Received : 2012-01-29 Accepted : 2012-03-22 Shabestar , Iran | 165.” 2(November): 165–68.

Bozbey, Ilknur et al. 2016. “Importance of Soil Pulverization Level in Lime Stabilized Soil Performance.” *Procedia Engineering* 143(Ictg): 642–49. http://dx.doi.org/10.1016/j.proeng.2016.06.091.

Farooq, S M, M A Rouf, S M A Hoque, and S M A Ashad. 2011. “Effect of Lime and Curing Period on Unconfined Compressive Strength of Gazipur Soil , Bangladesh.” : 4–8.

Jawad, Ibtehaj Taha, Mohd Raihan Taha, Zaid Hameed Majeed, and Tanveer A. Khan. 2014. “Soil Stabilization Using Lime: Advantages, Disadvantages and Proposing a Potential Alternative.” *Research Journal of Applied Sciences, Engineering and Technology* 8(4): 510–20.

Kerni, Vipul, Vinod Kumar Sonthwal, and Umar Jan. 2015. “Review on Stabilization of Clayey Soil Using Fines Obtained From Demolished Concrete Structures.” *International Journal of Innovative Research in Science, Engineering and Technology* 4(5): 296–99.

Navale, A V, B E Gite, M D Mundada, and S B Kolhe. 2016. “SOIL STABILISATION USING FLY-ASH & LIME.” (3): 4588–96.

Rogers, C. and S. Glendinning, 1996. Modification of clay soils using lime. Proceeding of Seminar on Lime Stabilization, pp: 99-114.

Sultan, T et al. 2014. “Experimental Study of Silty Clay Stabilization With Cement and Lime in Multan , Pakistan.” 19(Iii): 28–33.

Tedesco, D.V., 2006. Hydro-mechanical behaviour of lime-stabilised soils. Ph.D. Thesis, University of Cassino. Cassino, Italy.

THE EFFECT OF EMBEDMENT DEPTH ON BEARING CAPACITY OF STRIP FOOTING IN COHESIVE FRICTIONAL MEDIUM

Hasinur Rahman Nur[1], Md. Shafiqul Islam[2] and Md. Rokonuzzaman[3]

[1] Undergraduate Student, Dept. of Civil Engineering, Khulna University of Engineering and Technology, Bangladesh, e-mail: h.r.nur2k12@gmail.com
[2] Assistant Professor, Dept. of Civil Engineering, Khulna University of Engineering and Technology, Bangladesh, e-mail: sumon2k8@yahoo.com
[3] Professor, Dept. of Civil Engineering, Khulna University of Engineering and Technology, Bangladesh, e-mail: rokoncekuet@yahoo.com

ABSTRACT

In this study, two-dimensional finite-element models incorporating a Mohr-Coulomb elasto-plastic material model were validated for the evaluation of the bearing capacity factors for rough strip footings under vertical loading in c-φ soil. Earlier proposals are based on empirical data for surface condition in non-frictional medium, whereas a new suggestion for these factors presented in this paper is based on the elasto-plastic model of the soil in cohesive frictional medium considering variable friction angle and embedment depth. All the finite element analyses of this study were carried out using the finite element system ABAQUS. Finally, an attempt is made to propose a more accurate solution to estimate the bearing capacity factors of rough strip footing with equations fitted by simple functions of the soil friction angle and footing embedment depth.

Keywords: *Foundation, Bearing capacity, Strip footing, Finite element analyses (FEM).*

1. INTRODUCTION

The bearing capacity of foundations has become a fundamental problem in geotechnical engineering. For all structures placed on a soil foundation, geotechnical engineers must ensure that the soil has sufficient load carrying capacity so that the foundation does not collapse or become unstable under any conceivable loading (Zhu & Michalowski, 2005). A lot of research have been done which proposed approximate techniques for the estimation of bearing capacity of foundation and generally the conventional bearing capacity theory used which is suitable for strip footing but no exact solution has been established. (Terzaghi, 1943) proposed the following formula to calculate the ultimate bearing pressure of soil beneath a strip footing, where the influence of soil cohesion (c), surcharge (q) and the weight of soil (g) are considered independently:

$$Q_{ult} = cN_c + qN_q + \frac{1}{2}\gamma BN_\gamma \quad (1)$$

Where, Q_{ult}= ultimate pressure; B= footing width; D= depth of embedment; γ= unit weight of the soil; c= soil cohesion; N_c, N_q and N_γ= bearing capacity factors dependent only on the angle of the internal friction of soil. Terzaghi calculated all three components in Eq. (1) based on limit equilibrium. Also, (Terzaghi, 1943), (Reissner, 1924), and (Chen, 1975) among others, calculated the bearing capacity factors as follows:

$$N_q = K_p * \exp(\pi \tan\varphi)$$
$$N_c = (N_q - 1)\cot\varphi \quad (2)$$
$$\text{and,} \quad Kp = \frac{1+\sin\varphi}{1-\sin\varphi} \quad ; \quad \text{Where, } \varphi\text{=internal friction angle.}$$

There are several suggestions in different literature for factor N_γ (Meyerhof, 1963);(Hansen, 1970);(Vesic, 1973). A newer proposal was derived based on the strict upper bound approach of limit analysis (Michalowski, 1997).

$$N_\gamma = e^{0.66+5.11\tan\varphi}\tan\varphi \quad (3)$$

The factor in Eq.(3) is a closed-form approximation from the numerical results for the analysis of Coefficient N_γ for Rough and Smooth Strip Footings (Michalowski, 1997).

In recent years, both theoretical and experimental investigation of the ultimate bearing capacity of square and circular footings received the attention of many researchers. For example, (Cerato & Lutenegger, 2007) experimentally investigated the bearing capacity factor N_γ on sand for both square and circular footings. He found that the square footing provides higher bearing capacity than the circular footing. Similar results were found for the footing resting on sand by (Lavasan, A. A., & Ghazavi, 2012) and (Kiran, M., & Bacha, 2015). These investigations are significant for footings placed on sand, but they do not provide any information in the case of footings resting on frictional-cohesive (c-φ) soil. Only few numerical studies (Zhu & Michalowski, 2005); (Kumar & & Khatri, 2011) were performed on (c-φ) soil. This study involved numerical investigation of the ultimate bearing capacity with finite element analysis of (c-φ) soil for rough strip footings subjected to vertical loading and compared with previous studies through graphical presentation.

2. METHODOLOGY

ABAQUS is a software application used for both the modelling and analysis of mechanical components and assemblies (pre-processing). It is most suitable for analyzing the nonlinear behavior of material, failure phenomena and visualizing the finite element analysis result. All the finite element analyses of this study were carried out using the software ABAQUS. Two dimensional model was developed for strip footing analysis for different frictional angles and embedment depth. Simple soil conditions were modelled representing an isotropic linear elastic-perfectly plastic material considering embedment depth H/B= 0, 0.1, 0.3, 0.5, 0.75, 1.0, 1.5, 2.0 and frictional angle from zero degree to 40 degree. Meshing and displacement were applied to the model and ABAQUS was used to arrive at the limit loads (bearing capacity) of rough strip footings.

2.1 Element Size Study

On surface footing element size analysis was carried out to fix the element size and meshing as well as displacement. The fixation of mesh element size is an important part of modelling because it determines the amount of element number and time required for the analysis of the model. After fixation of the element size, the type of element was also selected whether it is linear, quadratic or triangular. The quadratic element shows more accurate result and load-displacement curve become constant very quickly. Although triangular element shows more accurate result compared to quadratic but to avoid huge time for the analysis quadratic element were used.

2.2 Modelling

Finite element system ABAQUS was used to arrive at the limit loads (bearing capacity) of rough strip footings and different meshing and displacement applied for two dimensional modelling. The model is created in four steps. In the first step which is the initial condition, all boundary conditions are defined as described previously. In the second step, surcharge load is applied on top of the model and gravity load is applied to the whole model. In the third step, a downward movement is applied on top of the soil under footing area where δ is vertical displacement and B is the width of footing. It should be noted that the duration for this l step is 100 seconds to avoid sudden collapse of soil body. Moreover, it is assumed that relative movement between soil and footing is impossible. The boundary conditions ensures no lateral movement will occur. For rough footing lateral displacement are restrained to zero and only vertical displacement occurred.

2.2.1 Materials

Simple soil conditions were modelled representing an isotropic linear elastic-perfectly plastic material with uniform undrained shear strength and depth,S_u. A fine grained material subjected to a period of loading sufficiently short such that no drainage will take place. Poisson's ratio v=0.3, modulus of elasticity was 10 MPa, cohesion was 10Kpa for the calculation of N_c. The cohesion varies in between $4E^3$ to $6E^3$ for N_γ & N_q. The angle of friction and dilation angle was varying from zero degree to 40 degree. The analysis was done at different embedment depth including surface considering a rough condition for strip footing.

2.2.2 Meshing

The two-dimensional finite element mesh used for analysis of a strip footing of width B and Length zero considered. The mesh extended 15B from the edges of the footing and 10B beneath the footing (shown in figure-1). A number of mesh densities were investigated to achieve a time efficient model and mesh element type was a 8-node linear plane strain quadrilateral, reduced integration and hourglass control. Meshing was done for linear, quadratic element to fix the element for the model and to determine which provide more accurate results.

Different type of meshing was tested and finally quadratic meshing was chosen to get more accurate result from the analysis. Meshing is shown in the figure-1 where the footing area contains finer meshing than the outer edge. This was done to reduce the number of elements so that the time of every analysis could be reduced.

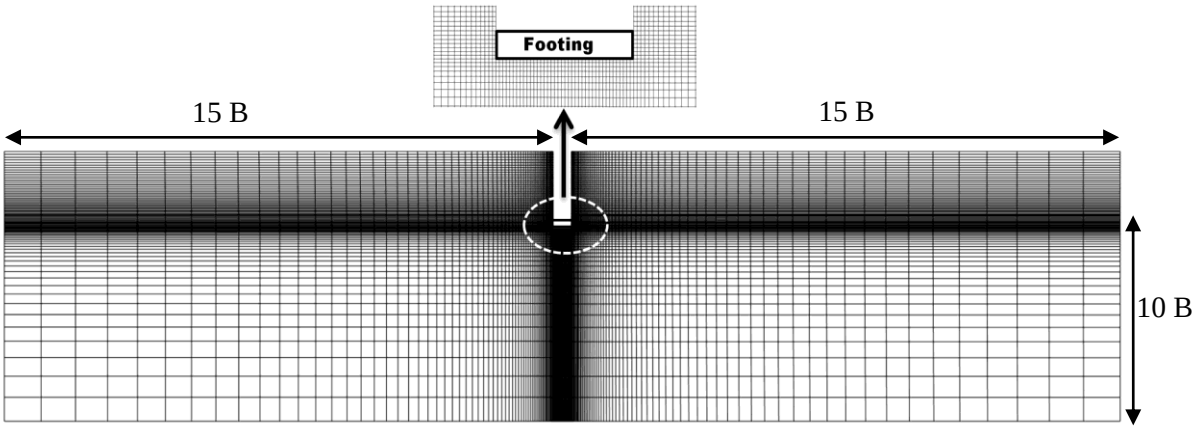

Figure 1: Meshing with quadratic element for two-dimensional strip footing

3. RESULT AND DISCUSSION

3.1 Validation of Study

Earlier proposals of evaluating bearing capacity factors were investigated thoroughly and numerical values were obtained from the previous empirical solutions for estimating bearing capacity factors for bearing capacity factors. Again, values from numerical analysis were obtained from finite element analysis. Both empirical and numerical values were compared through graphical presentations.

Table 1: Calculation of bearing capacity factors of previous study and FEM study

Angle	K_p	Previous study			FEM study		
		N_q	N_c	$N\gamma$	N_q	N_c	$N\gamma$
0	1	1	0	0	0	5.22	0
10	1.42	2.47	8.34	0.83	1.50	8.52	1.31
20	2.03	6.39	14.83	4.52	5.53	15.16	5.77
25	2.46	10.66	20.72	9.77	9.94	21.36	11.63
30	3.00	18.40	30.13	21.34	17.89	30.88	26.49
35	3.69	33.29	46.12	48.50	33.26	47.93	56.86
40	4.59	64.19	75.31	118.19	65.43	77.49	131.27

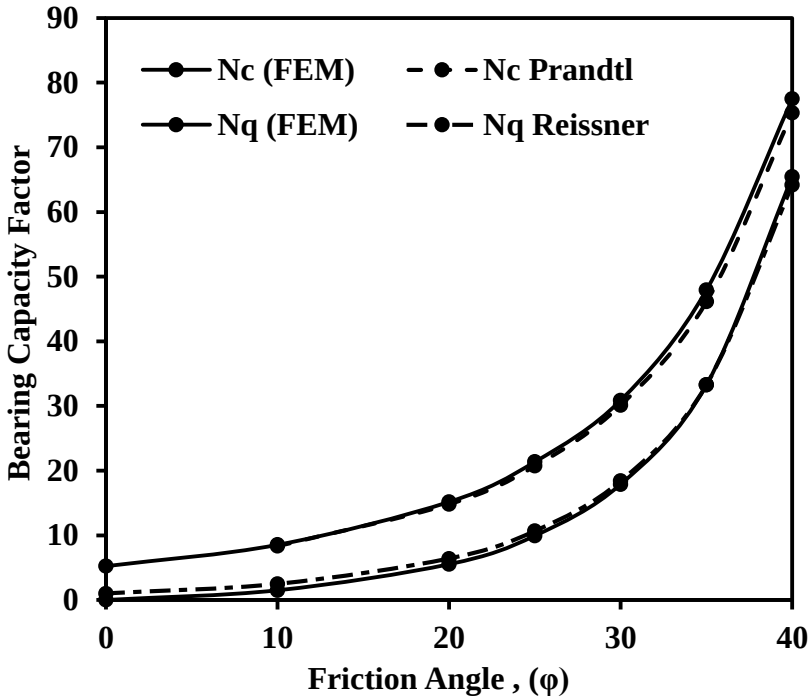

Figure 2: Comparative study of Surcharge and cohesion bearing capacity coefficients

The results for the two bearing capacity coefficients, as a function of the friction angle,ϕ, can be found in Figure-2 The analytical solutions of Prandtl and Reissner (short dashed lines) are also shown. The FEM study and analytical solutions for the two bearing capacity factors, N_q and N_c are found to be identical.

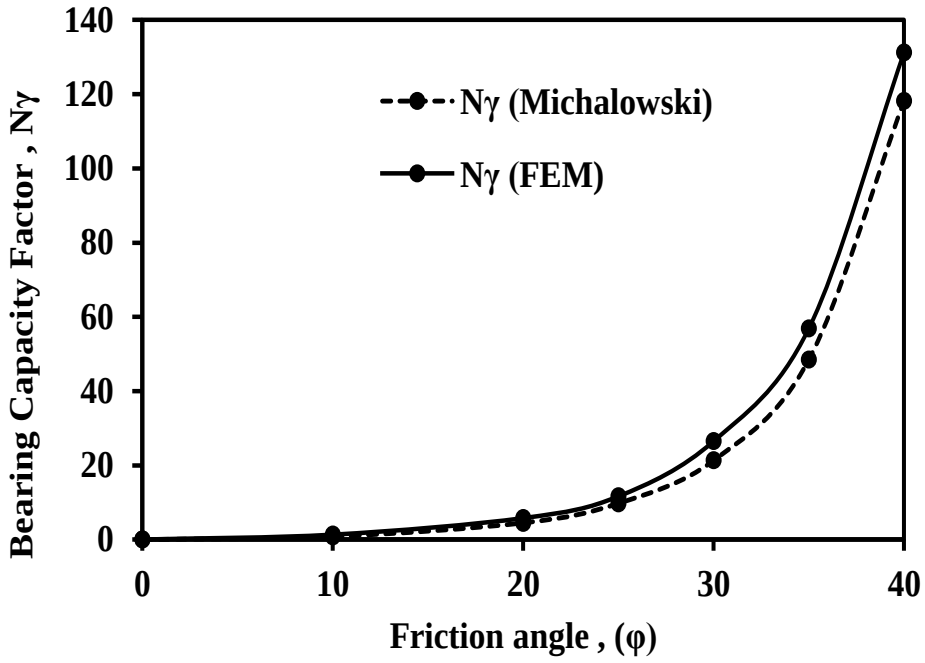

Figure 3: Comparative study of bearing capacity coefficient, Nγ

The result for the bearing capacity coefficient Nγ, as a function of the friction angle,ϕ, can be found in Figure-3 The analytical solutions of Michalowski is also shown as short dashed lines. The FEM study shows slightly upper values than the previous study. The variation of obtained values from FEM study with previous theoretical study is negotiable.

3.2 Variation of N_c in Cohesive Frictional Medium

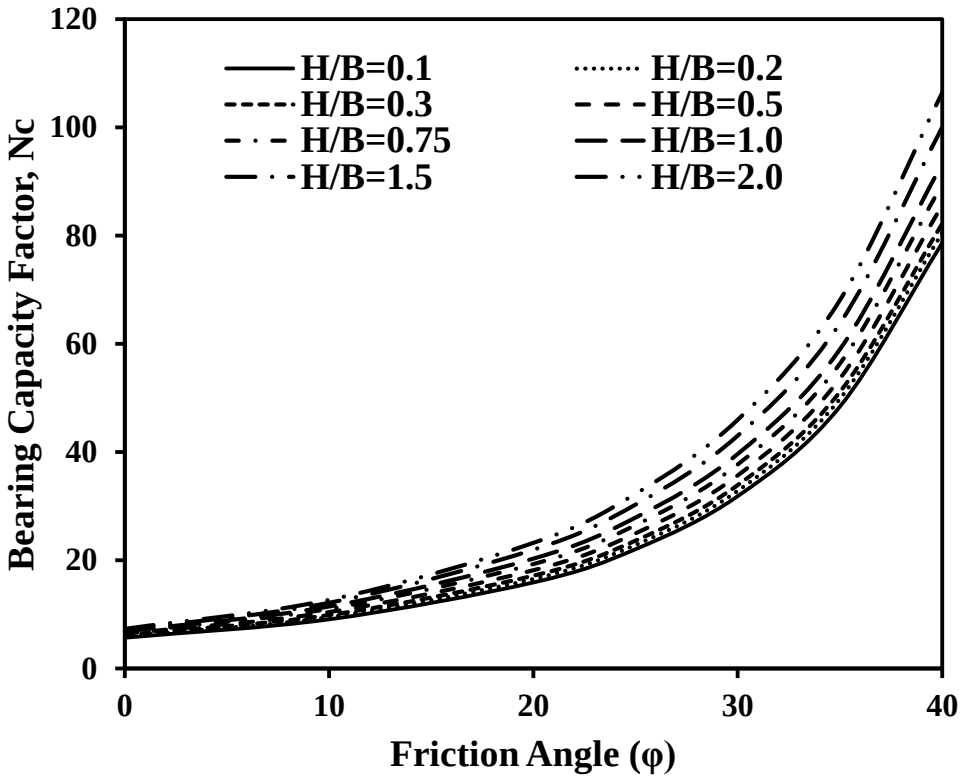

Figure **Error! No text of specified style in document.**: Variation of N_c in cohesive frictional medium

Figure-4 shows the graphical representation of bearing capacity factor, N_c at different embedment depth in cohesive frictional medium. Here, value of N_c increases with the embedment depth. The higher the value of embedment depth, the value of bearing capacity factor, N_c also increases accordingly. The nature of increase in different depth is quite similar. Again, value of N_c increases with friction angle and dilation angle but rate of change is not similar here. The rate of increasing the value of bearing capacity factor, N_c is slow at first. When it crosses 30 degree, the value of rate of change is much higher than before. Rapid change is observed in between 30 degree and 40 degree.

3.2.1 Variation of Depth Factor for N_c in Cohesive Frictional Medium

The depth factor of N_c is calculated by, $N_c = \frac{N_{c\,(STRIP\ AT\ D\neq 0)}}{N_{c\,(STRIP\ AT\ D=0)}}$

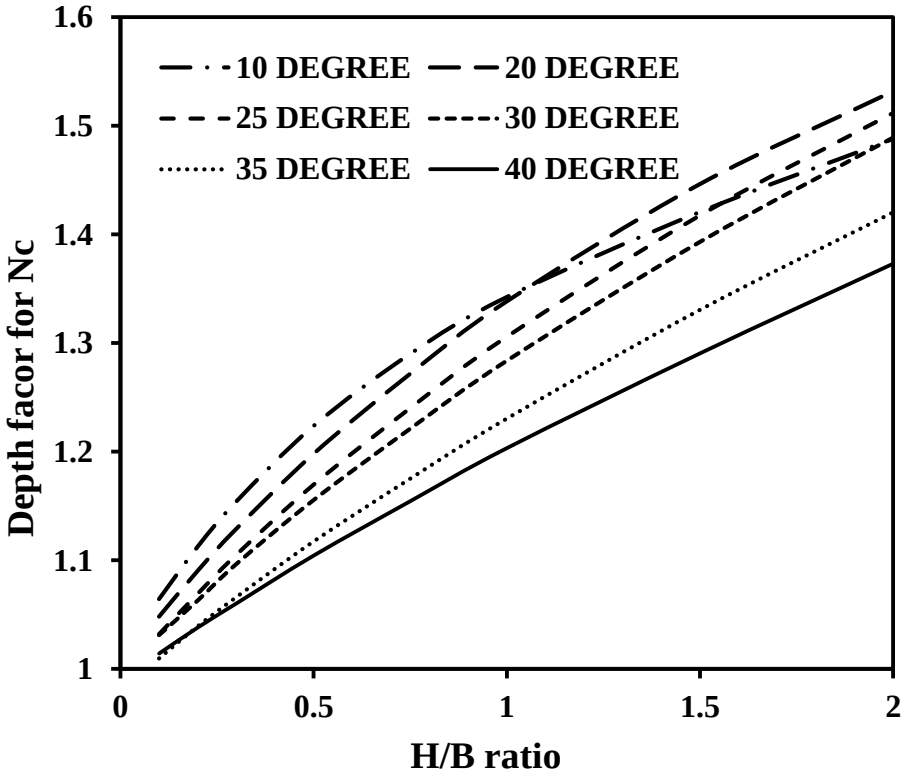

Figure 5: Variation of depth factor for N_c in cohesive frictional medium

Figure-5 shows the graphical representation of depth factor for N_c at different embedment depth in cohesive frictional medium. Value of H/B ratio is plotted along X-axis and depth factor for N_c is plotted along Y-axis. Here, value of depth factor increases with the embedment depth. The nature of increase in different depth is quite different. Rate of change for the first two curvature were quite faster than the others. Value of depth factor increases with friction angle but rate of change is not similar here.

3.3 Variation of N_q in Cohesive Frictional Medium

Figure-6 shows the graphical representation of bearing capacity factor, N_q at different embedment depth in cohesive frictional medium. Value of friction angel is plotted along X-axis and bearing capacity factor, N_q is plotted along Y-axis.

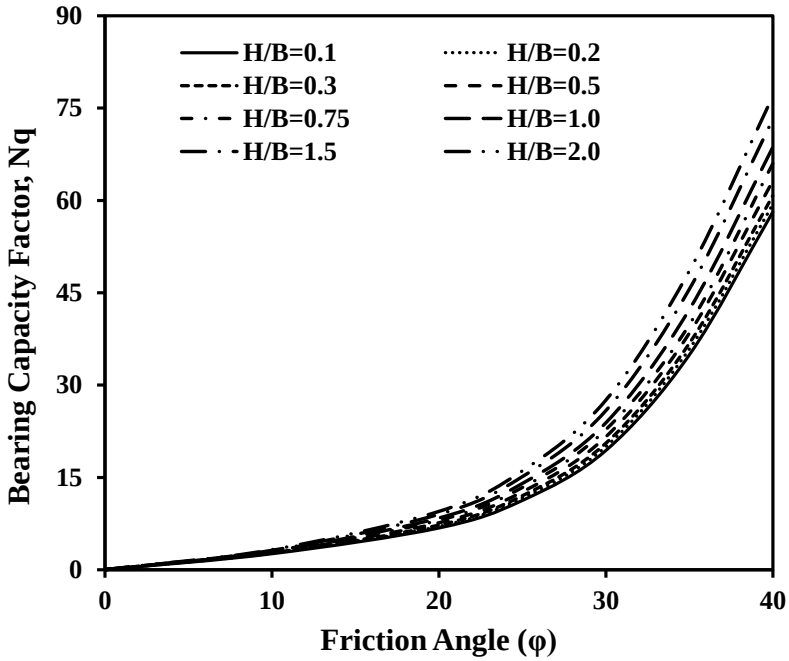

Figure 6: Variation of N_q in cohesive frictional medium

Here, value of N_q increases with the embedment depth. The higher the value of embedment depth, the value of bearing capacity factor, N_q also increases accordingly. The nature of increase in different depth is quite similar. Again, value of N_q increases with friction angle and dilation angle but rate of change is not similar here. The value of rate of increasing of bearing capacity factor, N_q was slow at first. When it crosses 30 degree, the value of rate of change is much higher than before. Rapid change is observed in between 30 degree and 40 degree.

3.3.1 Variation of Depth Factor for N_q in Cohesive Frictional Medium

The depth factor of N_q is calculated by, $N_q = \frac{N_{q\ (\text{STRIP AT } D \neq 0)}}{N_{q\ (\text{STRIP AT } D = 0)}}$

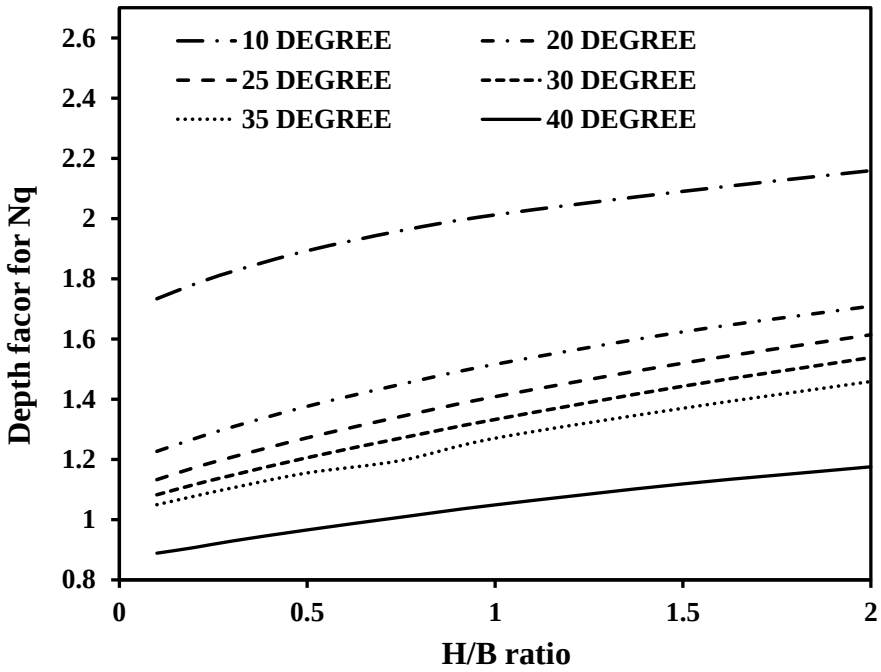

Figure 7: Variation of depth factor for N_q in cohesive frictional medium

Figure-7 shows the graphical representation of depth factor for N_q at different embedment depth in cohesive frictional medium. Value of H/B ratio is plotted along X-axis and depth factor for N_q is plotted along Y-axis. Here, value of depth factor increases very slowly with the embedment depth. The nature of increase in different depth is quite slow. Curvature slope is not steep at all and they are about to be horizontal. Huge gap is observed between first and second curvature and similar phenomena found for last curvature too. Value of depth factor increases with friction angle and but rate of change is quite similar here.

3.4 Variation of Nγ in Cohesive Frictional Medium

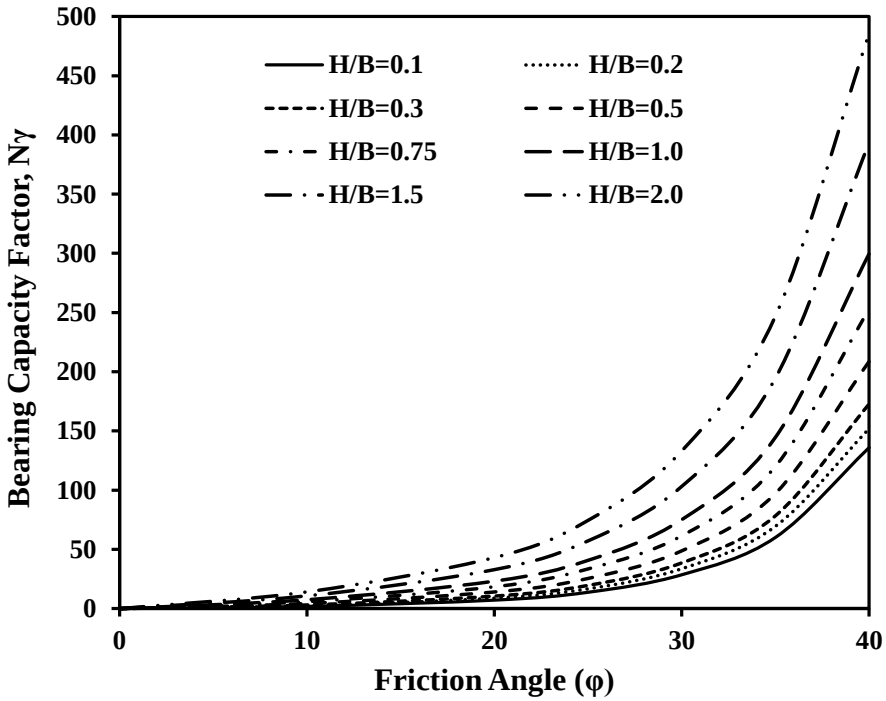

Figure 8 : Variation of Nγ in cohesive frictional medium

Figure-8 shows the graphical representation of bearing capacity factor, Nγ at different embedment depth in cohesive frictional medium. Value of friction angel is plotted along X-axis and bearing capacity factor, Nγ is plotted along Y-axis. Here, value of Nγ increases with the embedment depth. The nature of increase in different depth is quite similar. Again, value of Nγ increases with friction angle and dilation angle but rate of change is not similar here. The rate of increasing the value of bearing capacity factor, Nγ is slow at first. When it crosses 30 degree, the value of rate of change is much higher than before. Rapid change is observed in between 30 degree and 40 degree.

3.4.1 Variation of Depth Factor for Nγ in Cohesive Frictional Medium

The depth factor of Nγ is calculated by, $N\gamma = \frac{N_{\gamma\,(\text{STRIP AT } D\neq 0)}}{N_{\gamma\,(\text{STRIP AT } D=0)}}$

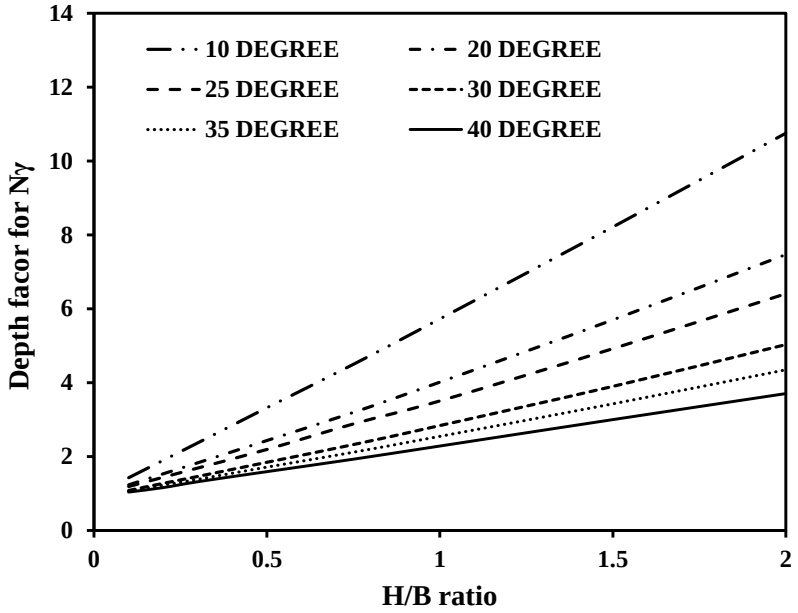

Figure 9 : Variation of depth factor for Nγ in cohesive frictional medium

Figure-9 shows the graphical representation of depth factor for Nγ at different embedment depth in cohesive frictional medium. Value of H/B ratio is plotted along X-axis and depth factor for Nγ is plotted along Y-axis. Here, value of depth factor increases with the embedment depth. The nature of increase in different depth is quite similar. The speciality for the depth factor of Nγ, straight lines are obtained instead of curvature. Thus, depth factor of Nγ shows some different graphs. Value of depth factor increases with friction angle But rate of change is quite similar here.

3.5 Soil Failure Mechanism

Here, Figure-10 shows the line contours of resultant soil displacement at failure for each of the footings modeled at surface (H/B=0) and at different embedment ratios (fig.(b) through fig.(i)). Under plane strain conditions a distinct Prandtl –type (1921) mechanism is observed in the finite element analyses Fig.(a). The contours (fig.(b) through fig.(f)) show the failure mechanism of footing in clay soil (ϕ=0). These illustrate the variation in nature of the soil displacement de-pending on embedment ratios. The footings are subjected to a uniform vertical displacement; the contours of resultant displace-ment beneath the rough footing show that the soil moves uni-formly vertically downwards with no relative soil movement on the underside of the footing. The line contours of soil displacement extend in surface upto shallow embedment ratios (i.e., H/B=2). For deep footing (H/B>2), contours start at the corner of footing and do not extend into the surface. Fig.6g through fig. 6j represents the variation of failure mechanism for sandy soil (c=0 and ϕ=30°) at surface (fig.6g) and different embedment ratios (Ffig.6.h through fig.6j). In all embedment ratios contour line extend to the surface and a triangular wedge zone is observed beneath the footing. A triangular zone is started at the corner of footing and extended to the surface. This zone is also observed at all embedment ratios for frictional soil but, it does not exist in clay soil.

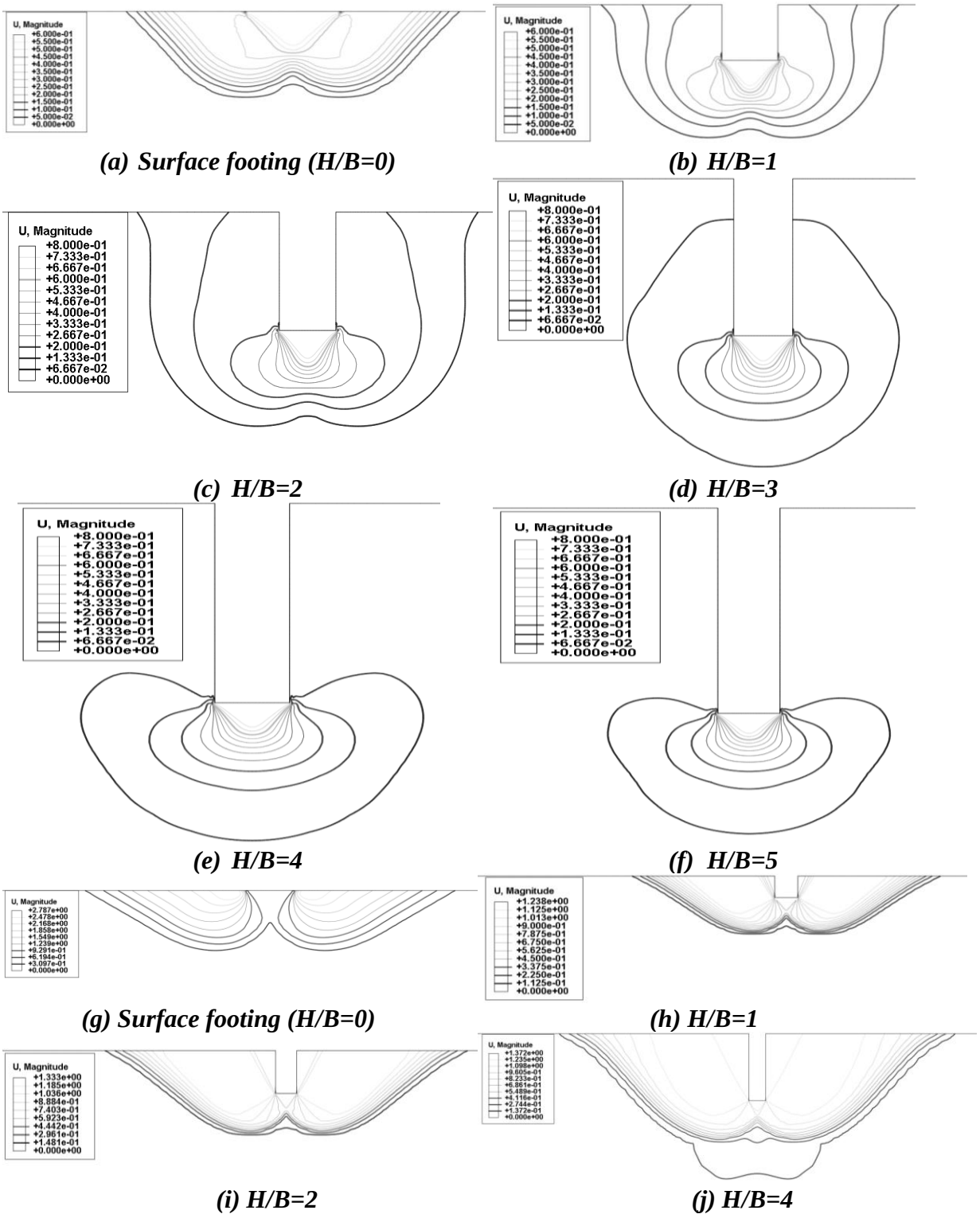

(a) Surface footing (H/B=0) ***(b) H/B=1***

(c) H/B=2 ***(d) H/B=3***

(e) H/B=4 ***(f) H/B=5***

(g) Surface footing (H/B=0) ***(h) H/B=1***

(i) H/B=2 ***(j) H/B=4***

Figure-10: Soil displacement at failure

3.6 Parametric Study

In this section, the validated solution of numerical models are used to calculate the ultimate bearing capacity factors of rough strip footings. Here, an attempt is made to propose a more accurate solution to estimate the bearing capacity factors of rough strip footing with equations fitted by simple functions of the soil friction angle and footing embedment depth. These best fitted equations are obtained using the data from numerical analysis of finite

element system Abacus. Hence, estimating the ultimate bearing capacity will be much more accurate and easier than previous empirical equations.

Proposed equations for bearing capacity factors are:

$N_c = 3.15 * \exp(4.56*\varphi + 0.17*H/B)$ (1)

$N_q = 0.88 * \exp(6.00*\varphi + 0.15*H/B)$ (2)

$N\gamma = 0.4 * \exp(7.75*\varphi + 1.23\sqrt{H/B})$ (3)

4. CONCLUSIONS

- Frictional angle and embedment depth has huge impact over bearing capacity factors.
- All the bearing capacity factors are proportional to embedment depth. When embedment depth increases, value of bearing capacity factors also increase.
- All the bearing capacity factors are also proportional to the friction angle of the medium. When friction angle increases, bearing capacity also increases.
- Footing at higher embedment depth and higher frictional medium will ensure higher bearing capacity.

REFERENCES

Cerato, A. B., & Lutenegger, A. J. (2007). Scale effects of shallow foundation bearing capacity on granular material. *Geotechnical and Geoenvironmental Engineering*, *133(10)*, 1192–1202.

Chen, W. F. (1975). *Limit analysis and soil plasticity*. Elsevier.

Hansen, J. B. (1970). A revised and extended formula for bearing capacity. *Geoteknisk Inst., Bulletin 28*, 5–11.

Kiran, M., & Bacha, N. (2015). An Experimental Study on Behaviour of Bearing Capacity and Settlement of Circular and Square Footing Resting on Reinforced Sand Bed Stratified with Lateritic Soil. *In International Journal of Engineering Research and Technology*, *(Vol. 4*, *N*(ESRSA Publications.).

Kumar, J., & & Khatri, V. N. (2011). Bearing capacity factors of circular foundations for a general c–ϕ soil using lower bound finite elements limit analysis. *International Journal for Numerical and Analytical Methods in Geomechanics*, *35(3)*, 393–405.

Lavasan, A. A., & Ghazavi, M. (2012). Behavior of closely spaced square and circular footings on reinforced sand. *Soils and Foundations*, *52(1)*, 160–167.

Meyerhof, G. G. (1963). Some recent research on the bearing capacity of foundations. *Canadian Geotechnical Journal*, *1*(1), 16–26.

Michalowski, R. L. (1997). An estimate of the influence of soil weight on bearing capacity using limit analysis. *Soils Found.*, *37*(4), 57–64.

Reissner, H. (1924). Zum erddruckproblem. In *Proc. 1st Int. Congress for Applied Mechanics* (pp. 295–311). Delft,The Netherlands.

Terzaghi, K. (1943). *Theoretical soil mechanics*. New York: Wiley.

Vesic, A. S. (1973). Analysis of ultimate loads of shallow foundations. *J. Soil Mech. Found. Div.*, *99*(1), 45–76.

Zhu, M., & Michalowski, R. L. (2005). Shape factors for limit loads on square and rectangular footings. *Journal of Geotechnical and Geoenvironmental Engineering*, *131*(2), 223–231.

Proceedings of the 4th International Conference on Civil Engineering for Sustainable Development (ICCESD 2018), 9~11 February 2018, KUET, Khulna, Bangladesh (ISBN-978-984-34-3502-6)

EFFECTIVENESS OF SAND COLUMN AS A GROUND IMPROVEMENT TECHNIQUE

Md.Ikramul Hoque[1] and Rana Sharmila Sheba[2]

[1]Assistant Professor, Department of Building Engineering and Construction Management, Khulna University of Engineering & Technology, Bangladesh, e-mail: ikramul3300@gmail.com.
*[*2]Student, Department of Building Engineering and Construction Management, Khulna University of Engineering & Technology, Bangladesh, e-mail: shebabecmzs@gmail.com,*

ABSTRACT

Soil strata is highly varying in nature and it is a challenging task for Geotechnical engineers to come up with the most suitable foundation system that is safe during static and dynamic loadings. In this paper, a case study on ground improvement using sand columns at a selected site of South-West region of Bangladesh is discussed. Ground improvement by granular piles is considered as one of the versatile and cost effective ground improvement method. This technique is suitable for very soft cohesive soil to loose deposits. Granular piles have already been installed in the soft soil regions of Bangladesh for the improvement of marginal sites. There is a record of successful application of rammed-displacement method in the installation of granular piles in the soft ground of Bangladesh. In this study, load tests were conducted on 0.30 m diameter plate resting a depth of 0.90 m from the existing ground surface on both the natural and improved ground. The plate load test was conducted on the natural ground at the foundation depth and on the top of sand piles after one month and one year of installation of granular pile. The results express that the bearing capacity of the normal ground was increased significantly by the installation of granular piles significantly. Comparing the natural ground, the bearing capacity of improved ground was increased by 200% and 250% for sand piles, respectively. The sub soil bore hole shows that the N-values increased by 2-3 fold than of natural ground. Thus this paper will include the soft ground improvement using granular piles technique which is a fast, economical and an efficient method to improve weak soil.

Keywords: *Sand column, rammed-displacement, soft ground, bearing capacity, improved ground.*

1. INTRODUCTION

This study deals with a particular improvement technique, namely granular piles, used to improve the soft ground condition. Amongst the various ground improvement techniques, construction of granular piles is considered as one of the foundation solution for its proven records of effectiveness in improving soft soil deposits. At the present time, more granular pile projects in the U.S.A have been constructed in silty sands rather than cohesive soils. World wide the reverse is true. Improvement of soft cohesive soils for construction purposes by means of vibro-displacement i.e. granular piles have been established for the last few decades (Engelhardt and Golding 1975, Barksdale and Bachus 1983, Shin et al. 1991, Okiawa et al. 1992, Bergado and Miruia 1994 and Alamgir 1996). Granular piles such as stone columns, sand compaction piles etc, have been used as a ground improvement technique to increase the bearing capacity, reduce settlement, increase the rime of consolidation, improve stability and resistance to liquefaction of soft ground. Granular piles with different types of granular materials were constructed in a typical soft ground of south western region of Bangladesh. Load tests were done over the constructed granular piles and the results show that the bearing capacity of the improved ground increased by 1.44 to 1.77 times than that of the natural ground. So it is termed as an essential component of ground improvement method. The main objectives of this research work is to study the improvement of the ground along the depth by comparing strength profiles of the ground before and after improvement and evaluate the response of ground improvement with elapsed period after the construction of sand pile. It can also evaluate the effectiveness of

locally available installation method for the condition of sand compaction pile in soft soil condition and determine the degree of improvement of the bearing capacity of soil due to the installation of granular piles by comparing the load settlement response obtained in the natural and the treated grounds.

2. METHODOLOGY

The granular piles were constructed here by vibro-displacement method in dry process. The dry method is frequently used to construct columnar inclusions through weak soils in developed areas because of the problems associated with the acquisition, retention and disposal of significant amount of water. The dry technique is suited for partially saturated soils that can stand unsupported, especially those that will density as a result of lateral vibration.

A 1500rpm traditional rig machine and a two end open casing pipe 8mm thickness and 300mm in diameter and 7m long with a vibro-hammer of weight 1000kg. The vibro-hammer was 250mm in diameter and 3.00 m long. The construction sequences are described in the following statements. The schematic diagram is shown in Figure.1.

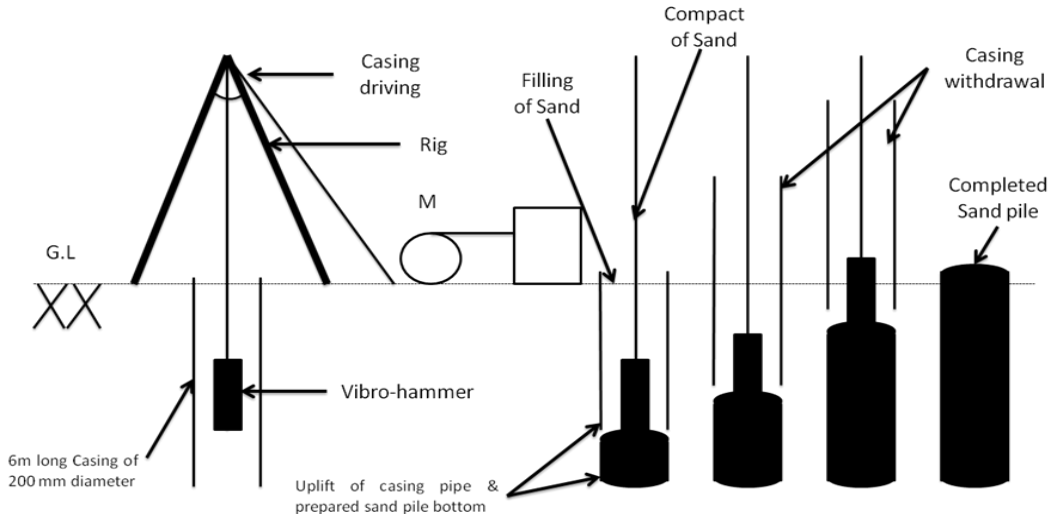

Figure 1: Schematic diagram of installation procedures of granular piles

i. A two end open casing pipe, 300mm in diameter and 7m long was placed vertically at the designed point on the natural ground surface for sand pile construction.

ii. The casing pipe was then inserted vertically into the ground about 300mm to 450mm depth at its own weight just by applying some pressure manually. At first a plug is made by the designated sand up to 750mm of casing pipe at bottom level.

iii. The vibro-hammer 250mm in diameter and 3.0m long, weighting 1000kg was placed inside the casing pipe. The vibro-hammer displaced the soil from beneath the casing pipe hence the casing pipe was driven by its own weight till reached the designated position (depth) into the ground. Here one casing pipe of 7m long was driven inside the ground.

iv. After reaching the designated depth, the sand plug is broken by providing excess energy then the vibro-hammer is withdrawn from the casing pipe.

v. Casing pipe was then lifted up by about 1m from its original bottom position. The designated granular materials were poured into the hole about 1m layer thickness measured from the bottom. The poured granular materials was then densified by vibro-hammer till the required compactness achieved.

vi. Casing pipe was then withdrawn from inside the ground that left the bottom portion of the hole unsupported and the top portion supported by the casing pipe. It was observed that the bottom portion of the hole standing safely without any lateral support.

vii. Then hole was poured by the selected granular materials in layers and hence 10 to 15 drops compacted each layer was densified by vibro-hammer till the designated compactness was reached.

viii. After the top of granular piles were reached about 1.0m to 1.5m below the ground surface the casing pipe was withdrawn and left the remaining hole unsupported.

ix. Then step five (v) was continued until the granular piles were constructed up to the ground level.

The plate load test was done on the natural ground at the project site to determine the load settlement response of the untreated ground. The ground improved by granular piles was also investigated by performing Standard Penetration Test. The effectiveness of granular piles in improving soft ground is justified by comparing N-values obtained for natural ground and improved ground.
Observations and recording system made a great contribution to ensure the quality control of the constructed granular piles. The careful site observation is the main requirement to construct the granular pile as per desire.

3. RESULTS AND DISCUSSIONS

3.1 Summary of The Plate Load Test Result

The plate load test reveal that the bearing capacity of the improved ground increased significantly due to the installation of granular piles. The arrangement of granular piles, installation pattern and the ratio of bearing capacity of treated (q_t) and natural ground (q_n) are shown in Table 3.1.

Table 3.1 Measured load carrying capacity of sand pile yields the largest increment of load carrying capacity which is 2.50 times than that of natural ground.

No. of Test	Description of granular piles	Load test after sand pile installation	Location of plate	q_t/q_n (Corresponding to 7mm settlement)
1	Sand piles	Immediately	Top of pile	2.00
2	Sand piles	After one year	Top of pile	2.50

3.2 Comparison of Result Obtained from SPT

Standard Penetration Test were performed on the improved ground for different conditions. There are (i) The boring immediately after sand pile installation and (ii) The boring one year after sand pile installation. The Standard Penetration Test results are given in the following sections for different improved conditions.

3.2.1 Immediately After Sand Pile Installation

Standard Penetration Test was performed in two bore hole of improved ground to depict the improvement of soft ground along the depth due to the penetration installation of granular piles. The penetration resistance i.e. N-values obtained in two boreholes are compared with those of natural ground before granular piles installation. The comparison is shown in fig. 2. This figure shows that N-values ranges 3 to 9. for the natural ground, while the values increases to 4 to 15 and 5 to 24 for the bore holes one and two respectively, in case of improved ground.

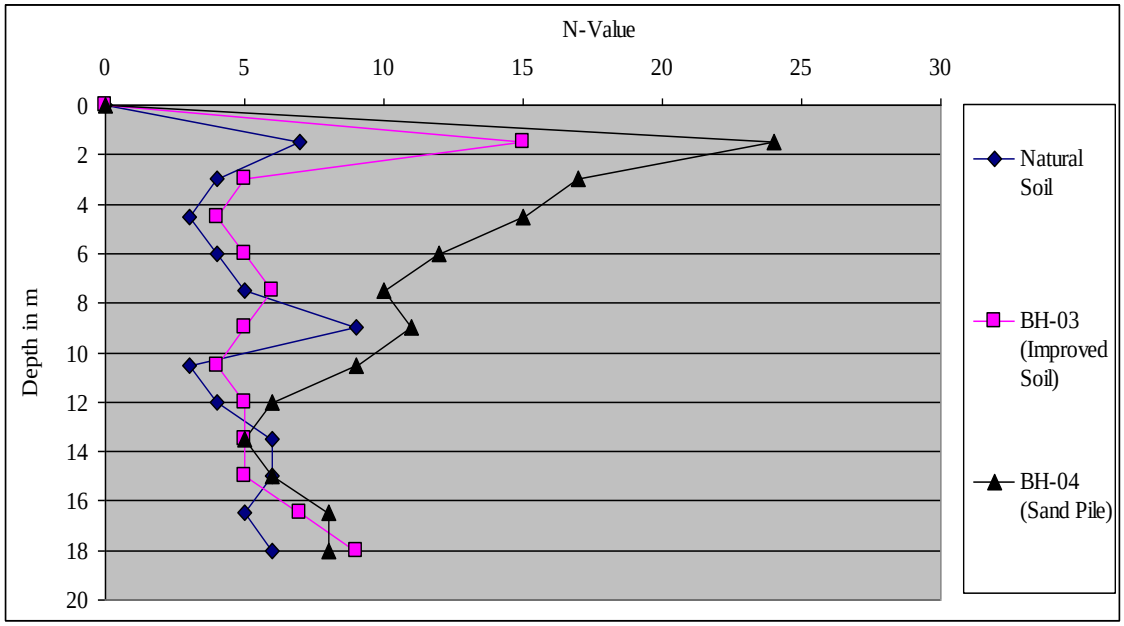

Figure.2 Comparison of SPT result, treated and natural ground (Immediately after sand pile installation

3.2.2 One Year After Sand Pile Installation

Standard Penetration Test was performed in two bore hole of improved ground to depict the improvement of soft ground along the depth due to the penetration installation of granular piles. The penetration resistance i.e. N-values obtained in two boreholes are compared with those of natural ground before granular piles installation. The comparison is shown in fig.3. This figure shows that N-values ranges 3 to 9. for the natural ground, while the values increases to 4 to 12 and 5 to 19 for the bore holes one and two respectively, in case of improved ground.

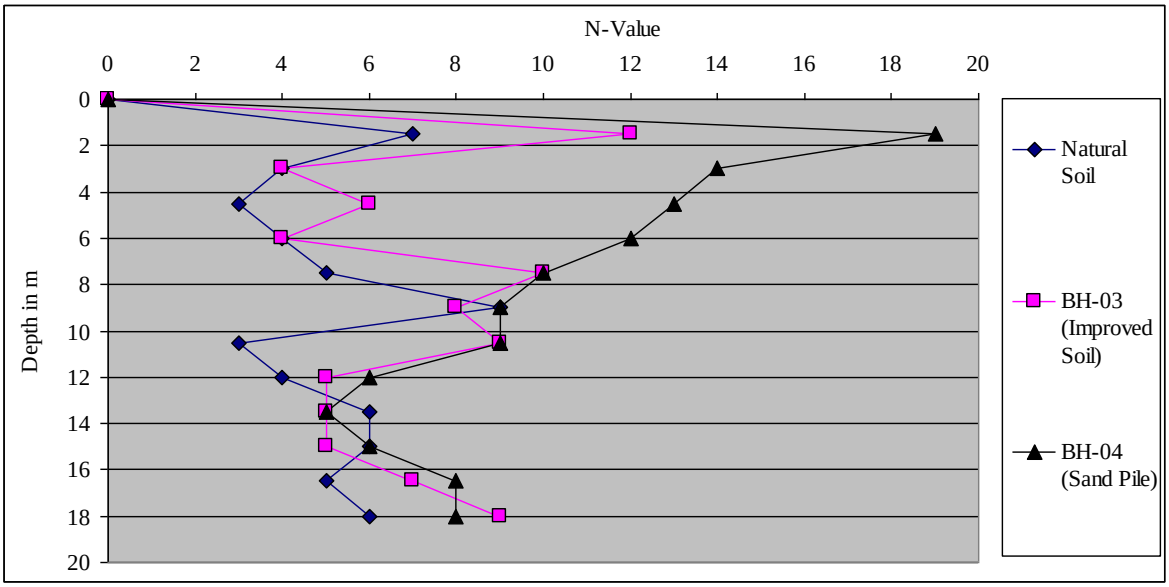

Figure.3 Comparison of SPT result, treated and natural ground (one year after sand pile installation)

4.CONCLUSIONS

Based on the construction of granular piles and the related test reported in this study, we can say that amongst the various ground improvement techniques for improving soft ground conditions, granular piles are considered as one of the most versatile and cost effective method. The simple construction procedures and the related equipment adopted in this project for the installation of the desired granular piles were found to provide high degree of effectiveness. The better increment of bearing capacity by granular pile are observed than that of natural soil. Standard Penetration Test (SPT) results also reveal that the significant improvement of the ground can be achieved along the depth due to the installation of granular piles. The practicing engineer can get help from this study and experience to improve the soft ground by the installation of granular piles.

REFERENCES

Md. Ikramul Hoque (2012) “Effectiveness of Sand Column as a Ground Improvement Technique” MSC Thesis, Dept. of Civil Engg., KUET.

Alamgir, M. 1996. "Deformation Analysis of soft ground reinforced by columnar inclusions " Ph.D. Thesis, Dept. of Civil Engg., Saga University, Japan.

Alamgir, M., Miura, N. and Poorooshasb, H.B. (1996) “Effect of Granular Fill on Settlement of Column-Reinforced Ground.”31st Annual Conf. of Japanese Geotechnical Society, pp.1505-1506.

Alamgir, M., Miura, N. and Poorooshasb, H.B. and Madhav, M.R. (1996). Deformation analysis of soft ground reinforced by columnar inclusions. Computer and Geotechnics, 18:267-290.

Barksdale, R.D. July (1981), Site Improvement in Japan Using Sand Compaction Piles, Georgia Institute of Technology, AQtlanta.

Bergado, D.T. and Lam, F.L. 1987. Full scale load test of granular piles with different densities and different proportions of gravel and sand in the soft Bankok clay. *Soils and Foundations, Vol.27, No. 1, pp*.86-93.

Bowles, J.E. (1988). *Foundation design and analysis*. McGraw-Hill International Edition: Civil Engineering Series, 4th Edition, Singapore

Zaher, S.M. (2000). "Effectiveness of granular Piles Installed by Vibro- displacement Method in Improving Soft Soil." M. Engg. Thesis, Department of Civil Engg., KUET.

Proceedings of the 4th International Conference on Civil Engineering for Sustainable Development (ICCESD 2018), 9~11 February 2018, KUET, Khulna, Bangladesh (ISBN-978-984-34-3502-6)

NUMERICAL STUDY ON STABILITY OF PLATE ANCHOR IN SLOPING GROUND

Shishir Chandra Das[1], Mst. Rahanuma Tajnin[2], Md. Shafiqul Islam[3] Grytan Sarkar[4] and Md. Rokonuzzaman[5]

[1] Undergraduate Student, Dept. of Civil Engineering, Khulna University of Engineering & Technology, Bangladesh, e-mail: shishircivil13@gmai.com
[2] Assistant Engineer, Public Works Department (PWD) Division-2, Bangladesh, e-mail: rtajnin@gmail.com
[3] Assistant Professor, Dept. of Civil Engineering, Khulna University of Engineering & Technology, Bangladesh, e-mail: shafiq0837@gmail.com
[4] Assistant Professor, Dept. of Civil Engineering, Khulna University of Engineering & Technology, Bangladesh, e-mail: grytan_ce04@yahoo.com
[5] Professor, Dept. of Civil Engineering, Khulna University of Engineering & Technology, Bangladesh, e-mail: rokoncekuet@yahoo.com

ABSTRACT

This study focuses on the uplift capacity of strip plate anchor placed in homogeneous clay for both the horizontal and sloping ground. The effect of anchor embedment ratios and inclination angle of sloping ground have been studied by finite element analysis. From the analyses results, the uplift capacity of plate anchor was found to be decreased linearly in relation to the increasing of inclination angle of slope. It is clear that, the slope angle is an important factor for computing uplift capacity of strip plate anchor embedded in sloping ground and should considered in design.

1. INTRODUCTION

The layout of many engineering systems calls for the foundation system to resist pullout forces. Plate anchors are often used as an economical solution for the foundation system of transmission towers, dry docks and pipelines under water, etc. In the previous times several studies have been done on the uplift capacity of plate anchors embedded in horizontal ground surface (Das, 1978;Rowe and Davis,1982; Murray and Geddes, 1987; Merifield et al., 2001; Merifield et al., 2006; Dickin and Laman 2007, Song et al., 2008, Hanna et al., 2011, Rokonuzzaman and Sakai 2012, Kumar and Sahoo 2012; Sahoo and Kumar 2014). Surprisingly, the study on uplift capacity of plate anchors in sloping ground surface, especially clayey sloping ground is rare. A few studies have been done on sloping grounds. Lower Bound Solutions for Uplift Capacity of Strip Anchors adjacent to Sloping Ground in Clay is done by Sahoo and Khuntia (2017). Kumar (1997) analytically and experimentally (Dos and Singh, 1994, RAO and Prasad, 1992, Emirler et al., 2016) investigated the behaviour of anchor plates installed in a sloping ground. Sawwaf (2007) experimentally studied the uplift behavior of horizontal anchor plates located near sandy earth slopes with and without geo synthetic reinforcement. Bildik et al.(2013) analysed the uplift capacity of a strip anchor buried in sandy soil near a sloping ground using finite element method. Based on the interaction between anchor and underlying soil two cases are observed, called immediate break way (unbounded) and no break way conditions. In immediate break way case, it is assumed that there remains no adhesion or suction force between the anchor and the soil. But, in no break way condition, adhesion force developed between the anchor and the soil at the time of loading. Das et al., (1994) observed that the suction force is dependent on the embedded depth of anchor, permeability of soil, and rate of loading. In this study, the uplift behavior of anchor plates in clayey sloping ground has been investigated by finite element analyses. The effects of several factors, such as embedment ratio of anchor plate, inclination angle of slope, have been investigated by using ABAQUS. The results of these

analyses are summarized, compared with existing published results and presented in the familiar form of pullout capacity factor N_c.

2. PROBLEM DEFINITION

A rigid strip plate anchor of width (B) and thickness (t=B/20) is placed in a clayey sloping ground. The ground surface having inclination angle, β. Height from the top surface of the anchor to the sloping ground is H as illustrated in Figure1.The embedment ratio varied over a large range(H/B=1 to 10). The uplift capacity factors N_c is computed by the equation;

$$N_c = q_u/C_u*B; \quad (1)$$

Where, C_u is the cohesion of cohesive soil. The collapse load (qu) per unit length of the plate anchor is computed for both the immediate breakaway (vented) and no break-way (attached) cases. The effect of different embedment ratios and ground surface inclination (0º to 45º) has been studied.

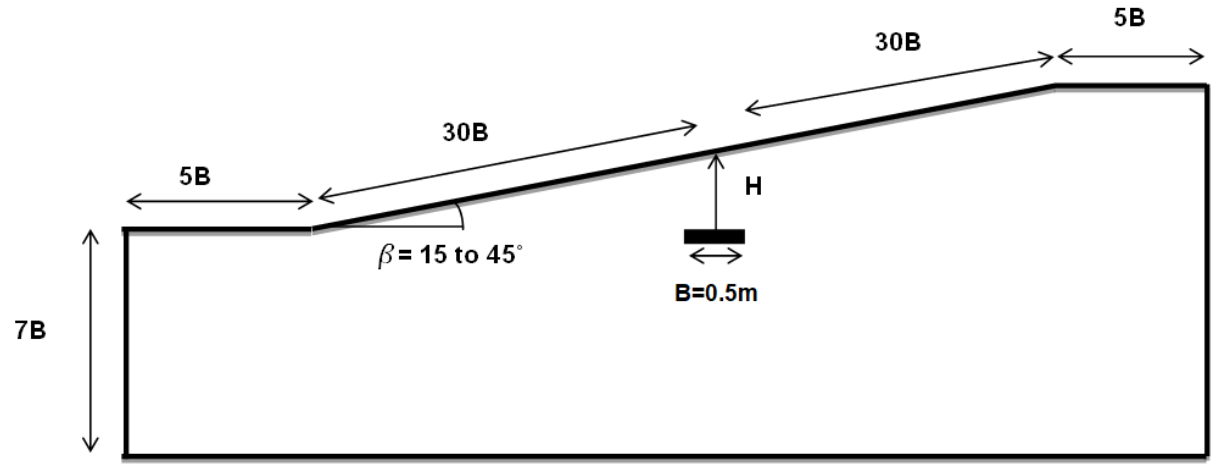

Figure1: Definition of the problem

3. FINITE ELEMENT MODEL

The analysis type was elasto-plastic finite element (FE) analysis over a wide range conducted using ABAQUS to find out the ultimate pull-out load of the strip plate anchor. The soil is assumed to be isotropic and homogenous and Mohr-Coulomb yield criterion is specified by cohesion value c, angle of internal friction ϕ. The strip rigid plate anchor is made contact with the soil and it is made displaced through the pullout direction. The interface between the soil and anchor is defined by (i) tangential behavior and (ii) normal behavior. In no break way case (Attached/fully bonded) the tangential behavior is defined by 'Rough' friction formulation and normal behavior is specified by 'Hard contact' for pressure over-closure. In immediate break-way (vented) case the tangential behavior is defined by 'penalty' friction with a friction coefficient 1.0 and the normal behavior is specified by 'Hard contact' with separation occurs immediately when tension develops. The analyses are conducted on six-nodded modified quadratic element. Figure 2 shows a typical two-dimensional finite-element mesh for a strip plate anchor embedded at H/B=4 and B=0.5m.

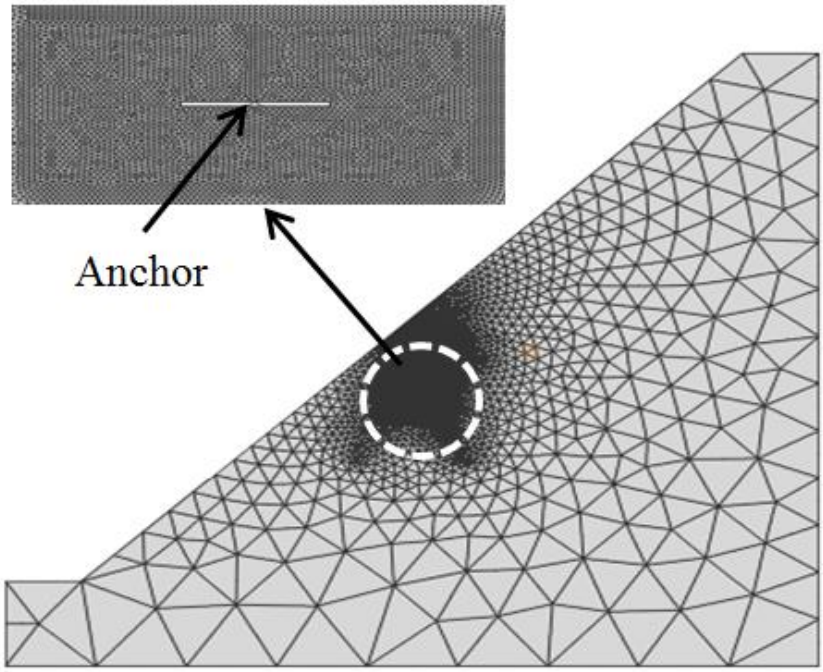

Figure 2: Typical two-dimensional finite-element mesh for H/B=4

The anchor is assumed to be perfectly rigid and displacement is applied to reference point (RP) anchor node with the contact of soil. In case of horizontal ground surface (surface inclination angle zero degree) the soil domain is extended to 20*B* from the edge of anchor. Amount of extended soil domain in the crest is 5B in horizontal directions both sides. Soil domain is extended 7B in vertical direction from the bottom crest. Two vertical edges are made hinged and the base of the mesh is fixed in all three coordinate directions. The element size near the plate is kept smaller and increasing steadily with the increase of distance from the anchor. Displacement based analyses are performed to obtain collapse load. The gravity loads on soil was assigned after initial step. The total displacement has been then applied and the collapse load has been calculated from the load-displacement curve.

4. RESULTS AND DISCUSSIONS

The finite element (FE) models have been first validated against existing studies. The pull-out capacity factor of horizontal ground (C_u=20kPa,γ= 0) has been computed and compared with the results of Rowe & Davis (1982), Merifield et.al., (2001) and Yu et al., (2011). The validity of the numerical results for the horizontal anchor is established through verification against published results before conducting the detailed parametric study. The designed FE model is validated for the pullout capacity factor N_c of a strip anchor in weightless soil (γ=0). It can be seen in Figure 3a and 3b that N_c for horizontal anchor agrees well with the numerical solution obtained by Yu et al. (2011) and Merifield et al. (2001).N_c values for horizontal are closer with the upper bound solution upto a embedment ratio of 3 then deviates and maximum differences are found 6.6% for horizontal anchor. Note that, the current FE results, Yu et al. (2011), Merifield et al. (2001) and Rowe & Davis (1982) stay close together for shallow embedment ratio (H/B=2). FE result of Rowe & Davis (1982) shows lower values and almost constant at large embedment ratio (H/B>3). These differences may be due to truncation criterion, where the pullout capacity

was taken at a displacement as 15-20 % of anchor width, rather than the ultimate capacity for large embedment ratio

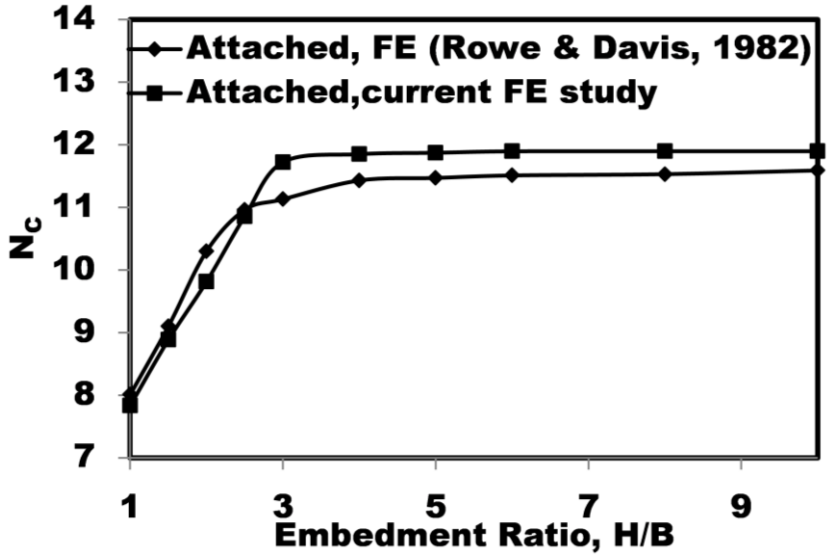

(a)

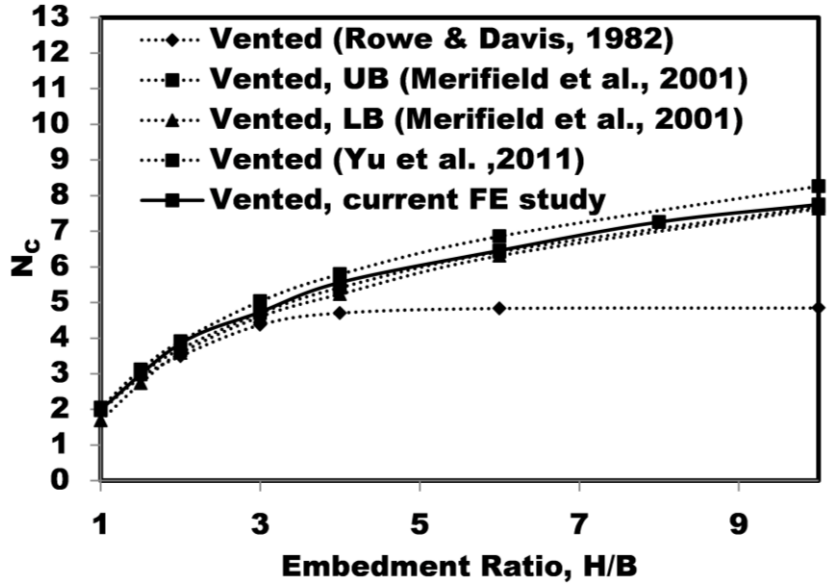

(b)

Figure 3: Comparison of the bearing capacity factors for plate anchors in weightless uniform clay: (a) Attached case; (b) Vented case

4.1 The Effect of Slope

The present study concentrated on the effect of sloping ground upon the uplift capacity of plate anchor. Subsequently, finite element (FE) models for inclination angle β=15º, 30º and 45º have been analyzed for embedment ratios (H/B) 1,1.5, 2, 2.5, 3, 4, 5, 6, 8 and 10. The analyses have been conducted for both attached and vented cases. The analyses results show that the uplift capacity of plate anchor decreases with the increase of ground surface inclination. In attached (no break-way) case, for small inclination (15º) of ground surface the value of N_c has been found to be increasing up to embedment ratio (H/B) 4.0 and then it becomes constant. The value of N_c for both ground surface inclination 30º and 45º have been found to be increasing up to embedment ratio (H/B) 6.0 and 8.0 respectively, and then it becomes constant and found same as the ultimate capacity of deep anchor (H/B≥3).

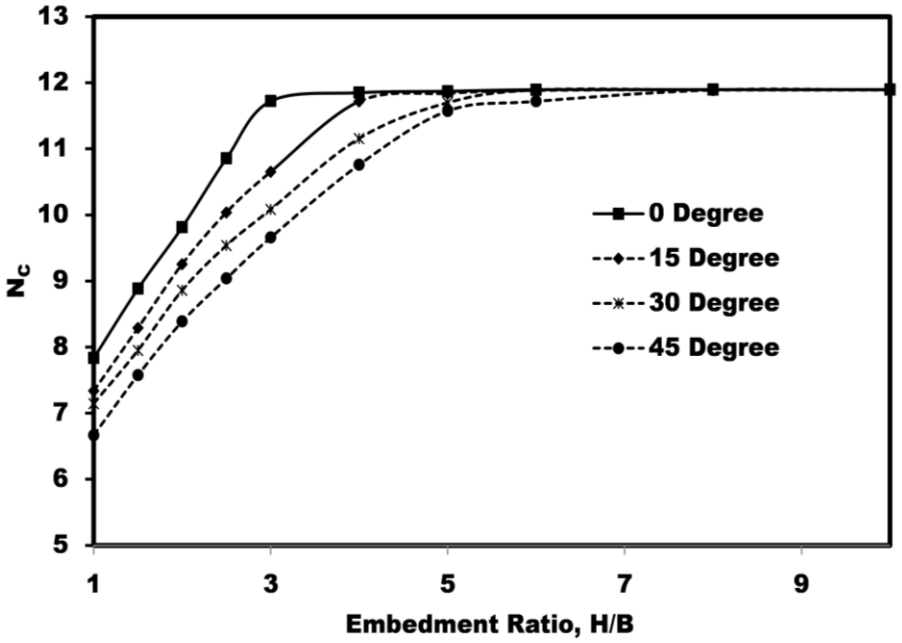

(a)

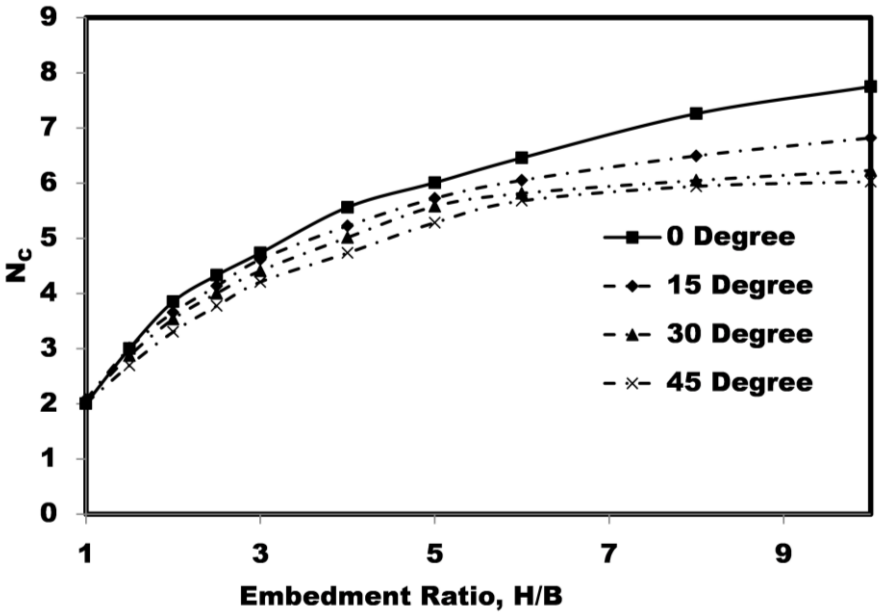

(b)

Figure 4: Effect of slope on N_c at different embedment ratios (H/B) (a) Attached case (b) Vented case

In case of immediate break-way(vented), of the pullout capacity factor (N_c) decreases at all H/B ratios. For 15º inclination of ground surface, the deviation of N_c value is small for shallow anchor but, increases with the anchor embedment ratios (H/B). The maximum value of N_c is 7.75 (H/B=10) in horizontal ground surface whereas, for 15º inclination of ground surface the N_c value shows 6.82. The maximum value of N_c decreases almost 12%. For 30º

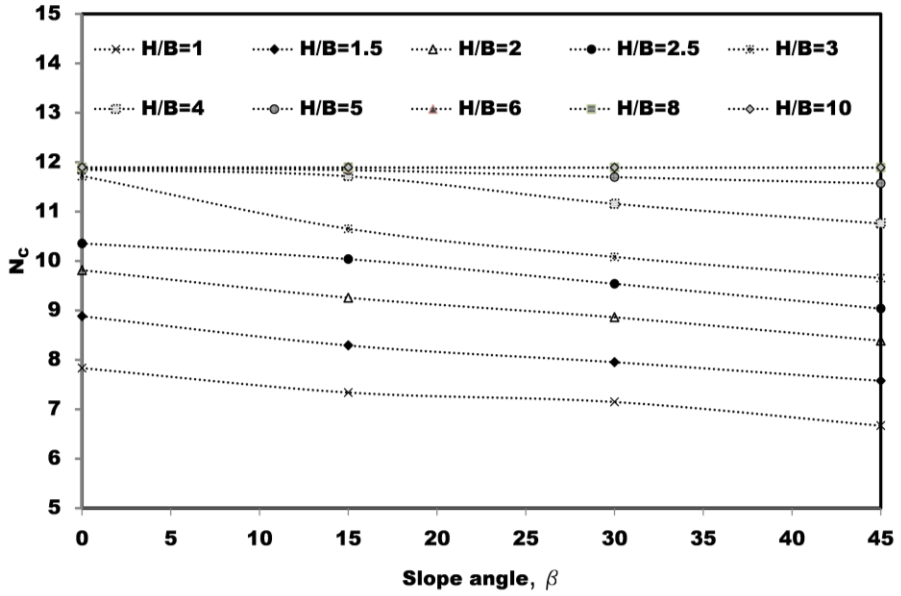

(a)

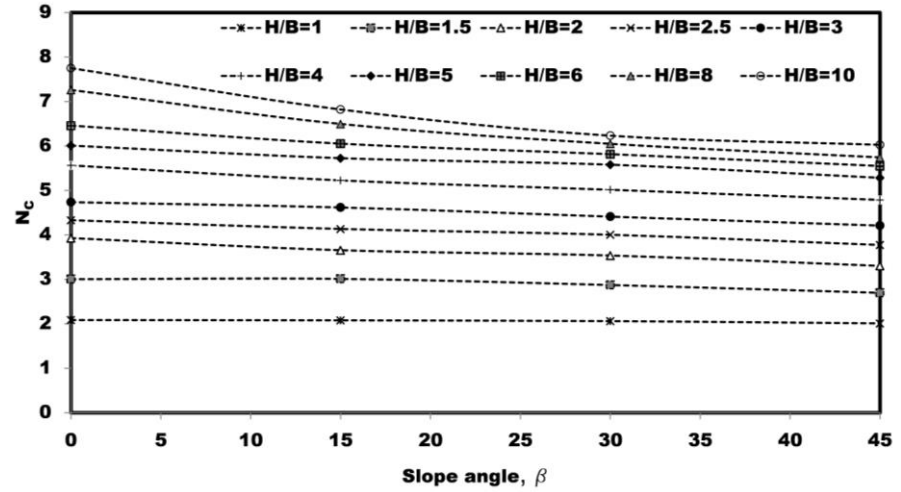

(b)

Figure 5: Variation of N_c with slope angles, β at different embedment ratios (a) Attached case (b) Vented case

Inclination of ground surface the maximum value of N_c decreases almost 19.61%. The maximum value of N_c decreases almost 22.24% (for β=45°) from the maximum value of N_c (H/B=10) in horizontal ground surface. From this finite element (FE) study, two different behaviors of the change of the value of N_c are observed. At any slope angle, for example 15° (see Fig-4a), the N_c value increases up to certain embedment ratio (H/B=4 for 15°), then it becomes constant. On the other hand in vented case, the value of N_c in sloping ground gradually decreases also with the increase of slope angles. But, for a certain slope angle the value of N_c tends to increase with the increase of embedment ratios and it is not found to be constant. At 15º inclination the deviation from the value of N_c in horizontal ground surface starts from 0.32% (H/B=1) to 12% (H/B=10). Figure5a and Figure 5b shows the variation of uplift capacity factor (N_c) with ground surface inclination angles at different embedment ratio

(H/B) for both attached and vented cases. It is seen that, the variation of the uplift capacity factor (N_c) with ground surface inclination angles is more or less linear.

4.2 Soil Failure Mechanism

Fig. 6 shows the line contours of resultant soil displacement at failure for each of the anchors modeled at different embedment ratios on horizontal (Fig-6a through Fig-6c) and sloping ground (Fig-6d through Fig-6j). Under plane strain conditions, the contour shows the failure mechanism of anchor in clay soil (ϕ=0°) for both attached (Fig: 6a and Fig: 6b) and vented case (Fig-6c). These illustrate the variation in nature of the soil displacement depending on interface conditions. When the anchor is attached to the soil then the local failure mechanism occurs and contours do not extend to the surface. These type of failure mechanism is also observed when embedment ratio (H/B)>8 at slope 45°. This trend is also observed as shown in fig-6(j) so, it can be concluded that, the effect of slope on vertical uplift capacities is negligible after at H/B>8. At a lower inclination angle, for example β=15°, β=30° uplift capacity is found constant at lower embedment ratios (H/B=4~5) than the higher sloping angle.

In vented case, failure mechanism extending to the soil surface (see Fig.6c). A vertical shear plane can be seen extending upward from the edge of the anchor, and soil is drawn in behind the anchor. This type of soil failure mechanism is also observed in all vented case of sloping ground and attested case of sloping ground at embedment ratios <8. Hence, it is clear that the uplift capacity of anchor decreases at all embedment ratios in vented cases.

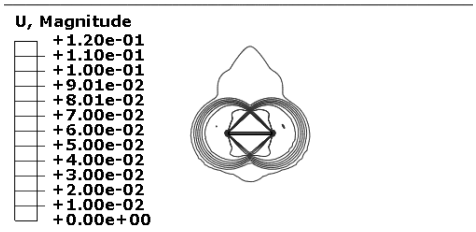

(a) H/B=3 Attached Case, β=0°

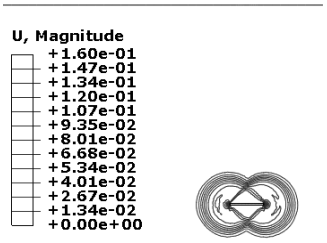

(b) H/B=6 Attached Case, β=0°

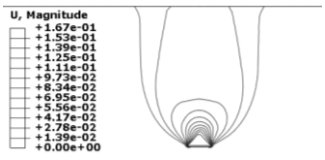

(c) H/B=6 vented Case, β=0°

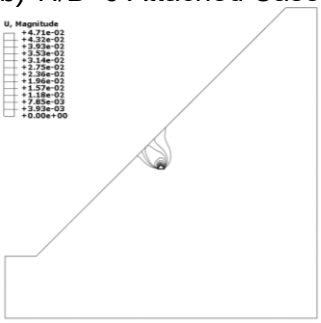

(d) H/B=6 Vented Case , β=45°

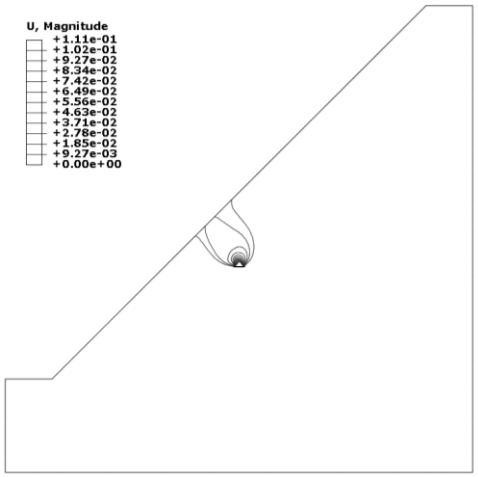

(e) H/B=8 Vented Case , β=45°

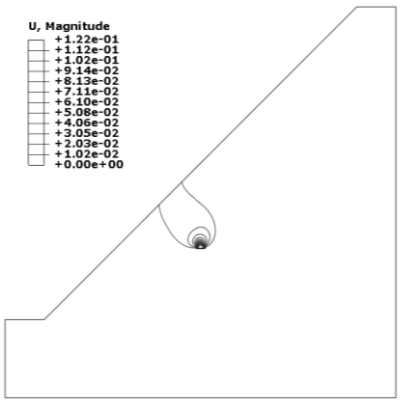

(f) H/B=10 Vented Case , β=45°

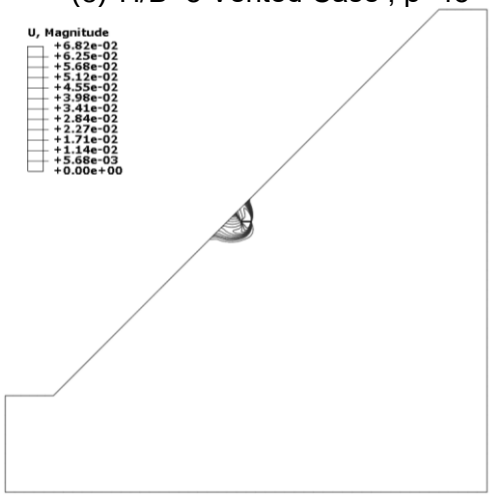

(g) H/B=2 Attached Case , β=45°

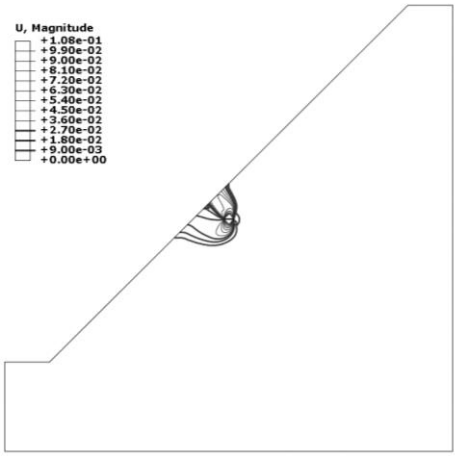

(h) H/B=4 Attached Case , β=45°

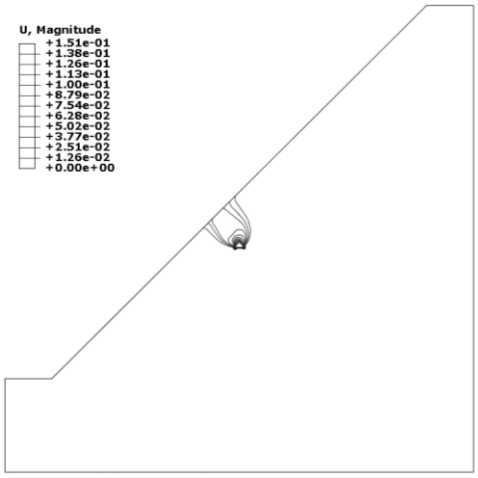

(i) H/B=6 Attached Case , β=45°

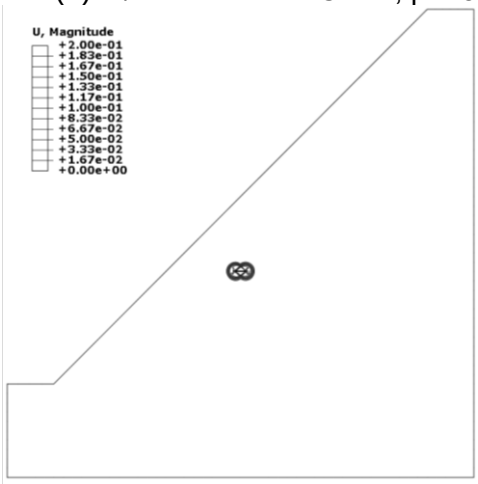

(j) H/B=8 Attached Case , β=45°

Figure 6: Soil failure mechanism for both attested and vented case

5. CONCLUSIONS

In this study finite element analysis has been performed using ABAQUS to investigate the uplift capacity of strip plate anchor embedded in clayey horizontal and sloping ground. Result reveals that the uplift capacity of plate anchor increases in relation to the increasing of embedment ratio for vented case for both horizontal and sloping ground. In addition, the uplift capacity decreases almost linearly with the rotation angle for vented case at all embedment ratios. In attested case, uplift capacities found constant and equal to 11.89 at H/B≥8,H/B≥6 and H/B≥4, for slope angle 45°,30° and 15°. Hence it can be conclude that the effect of slope is negligible at H/B≥8,H/B≥6 and H/B≥4, for slope angle 45°,30° and 15°.

REFERENCES

Bildik, S., Laman, M., & Suleiman, M.T. (2013). "Uplift behavior of anchor plates in slope." *In Geo-Congress : Stability and Performance of Slopes and Embankments III*, pp. 1795-1803.

Das, B.M. (1978). "Model tests for uplift capacity of foundations in clay." *Soils and Foundations*, 18(2), 17–24.

Dickin, E.A., and Laman, M. (2007). "Uplift response of strip anchors in cohesionless soil." *Advances in Engineering Software*, 38(8), 618–625.

Dos, B.M., & Singh, G. (1994). "Uplift capacity of plate anchors in clay." *In The Fourth International Offshore and Polar Engineering Conference*, International Society of Offshore and Polar Engineers.

Emirler, B., Tolun, M., & Laman, M. (2016). "Experimental investigation of the uplift capacity of group anchor plates embedded in sand." *GEOMECHANICS AND ENGINEERING*, 11(5), 691–711.

Hanna, A., Rahman, F., and Ayadat, T. (2011). "Passive earth pressure on embedded vertical plate anchors in sand." *Acta Geotechnica*, 6(1), 21–29.

Kumar, J. (1997). "Short Communications Upper Bound Solution for Pullout Capacity of Anchors on Sandy Slopes." 21(January 1996), 477–484.

Kumar, J., and Sahoo, J.P. (2012). "Vertical Uplift Resistance of a Group of Two Coaxial Anchors in Clay." 138(March), 419–422.

Merifield, R. S., Sloan, S. W., and Lyamin, A. V. (2006). "Three-dimensional lower-bound solutions for the stability of plate anchors in sand." *Géotechnique*, 56(2), 123–132.

Merifield, R. S., Sloan, S. W., and Yu, H. S. (2001). "Stability of plate anchors in undrained clay." *Geotechnique*, 51(2), 141–153.

Murray, E. J., and Geddes, J. D. (1987). "Uplift of anchor plates in sand." *Journal of Geotechnical Engineering*, 113(3), 202–215.

RAO, S. N., & Prasad, Y. V. S. N. (1992). "Uplift capacity of plate anchors in sloped clayey ground." *Soils and Foundations*, 32(4), 164–170.

Rokonuzzaman, M., and Sakai, T. (2012). "Model Tests and 3D Finite Element Simulations of Uplift Resistance of Shallow Rectangular Anchor Foundations." *International Journal of Geomechanics*, 12(2), 105–112.

Rowe, R. K., and Davis, E. H. (1982). "The behaviour of anchor plates in clay." *Geotechnique*, 32(1), 9–23.

Sahoo, J. P., and Khuntia, S. (2017). "Lower bound solutions for uplift capacity of strip anchors adjacent to sloping ground in clay." *Marine Georesources & Geotechnology*, 618(April), 1–12.

Sahoo, J. P., and Kumar, J. (2014). "Vertical Uplift Resistance of Two Interfering Horizontal Anchors in Clay." *Journal of Geotechnical and Geoenvironmental Engineering*, 140(4), 6013007.

Sawwaf, M. A. (2007). *Uplift behavior of horizontal anchor plates buried in geosynthetic reinforced slopes.*

Song, Z., Hu, Y., & Randolph, M. F. (2008). "Numerical Simulation of Vertical Pullout of Plate Anchors in Clay." *Journal of Geotechnical and Geoenvironmental Engineering*, 134(6), 866–875.

YU, L., LIU, J., KONG, X.-J., and HU, Y. (2011). "Numerical study on plate anchor stability in clay." *Géotechnique*, 61(3), 235.

Proceedings of the 4th International Conference on Civil Engineering for Sustainable Development (ICCESD 2018), 9~11 February 2018, KUET, Khulna, Bangladesh (ISBN-978-984-34-3502-6)

PURE HORIZONTAL, VERTICAL AND MOMENT CAPACITY OF PLATE ANCHOR IN SAND

Jagobandhu Sarkar[1], Mst. Rahanuma Tajnin[2], Md. Shafiqul Islam[3] Grytan Sarkar[4] and Md. Rokonuzzaman[5]

[1] *Undergraduate Student, Dept. of Civil Engineering, Khulna University of Engineering & Technology, Bangladesh, e-mail: jagobandhu.01950@gmail.com*
[2]*Assistant Engineer, Public Works Department(PWD) Division-2, Bangladesh, e-mail: rtajnin@gmail.com*
[3] *Assistant Professor, Dept. of Civil Engineering, Khulna University of Engineering & Technology, Bangladesh, e-mail: shafiq0837@gmail.com*
[4]*Assistant Professor, Dept. of Civil Engineering, Khulna University of Engineering & Technology, Bangladesh, e-mail: grytan_ce04@yahoo.com*
[5] *Professor, Dept. of Civil Engineering, Khulna University of Engineering & Technology,Bangladesh, e-mail: rokoncekuet@yahoo.com*

ABSTRACT

The pullout capacity of plate anchor subjected to general (horizontal, vertical and moment) loading is of interest to the geotechnical engineer. Literature reveals that no precious design method is available that can be used to determine the pullout capacity of plate anchor in the sand under such loading. Therefore, a two-dimensional finite element analysis (2D-FE) is used to investigate the pullout capacity of a strip horizontal plate anchor in sand subjected to vertical, horizontal and moment loading. The effects of the embedment ratio and friction angle on the pullout capacity factor is also investigated. It is seen that both the embedment ratio and friction angle significantly affects the pullout capacity of plate anchor. Both the horizontal and moment capacity increases nonlinearly, while the vertical pullout capacity increases linearly with the friction angle of sand for every embedment depth of anchor. The horizontal pullout capacity is found lower compared to vertical capacity for small friction angle (10° to 30°), while for higher friction angle (>30°) the horizontal capacity is higher than that of the vertical capacity of horizontal strip plate anchor embedded in the sand. Therefore, for compacted dense sand the horizontal capacity is higher than vertical capacity.

Keywords: *plate anchor, pullout capacity, general loading, sand, numerical analysis*

1. INTRODUCTION

Plate anchors are commonly used cost-effective and geotechnically efficient anchoring system widely used in transmission tower, sheet piles, retaining wall, deepwater offshore developments, and mooring system for floating structure (Hanna et al. 2014; Merifield and Smith 2010; Sutherland et al. 1983). However, Yang et al. (2010) mentioned that it cannot be preferred for permanent mooring system due to the uncertainties have arisen in predicting anchor performances. Because the available design approach is reasonable for the normal loading (in-plane) conditions. But this anchor may be subjected to the horizontal and overturning moment (out-of-plane line) loadings due to the movement of wind, wave, and many other environmental loadings. This out-of-plane loads can significantly reduce the pullout capacity of the anchor embedded in a particular location and for a particular soil. Literature reveals that very few studies are available that can be used to determine the pullout capacity of the anchor in clay subjected to in-plane and or out-of-plane loading. The study on the pullout capacity of strip anchor subjected to general loading (combined vertical, horizontal and moment) have been first stated by (O'neill et al., 2003). The results obtained from their study for both the upper bound and small strain FEM techniques showed that the horizontal and moment pullout capacity of a horizontal plate anchor in clay is about one-third and one-eighth of the vertical capacity. The similar results are found from small strain FEM

(Yang et al. 2010) and Eulerian FEM (Nouri et al., 2017). Gilbert et al. (2009) conducted both the experimental and analytical method to determine the rectangular and square plate anchors with zero thickness in terms of plastic envelopes subjected to multiaxial loading. Gilbert et al. (2009) investigated the effect of plate-soil interface friction and plate thickness on the pullout capacity of drag anchor using FEM. According to the author knowledge, there is no established technique for predicting pullout capacity of plate anchor under general loading. Therefore, it is required to develop design methods and or charts for the practitioner to understand the performance of plate anchor subjected to general loading.

In the current study, a two-dimensional finite element analysis (2D-FE) is used to investigate the pullout capacity of a strip horizontal plate anchor in sand subjected to general loading. The effects of the embedment ratio and friction angle on the pullout capacity factor is also investigated.

2. METHODOLOGY

2.1 Finite Element Analysis

The objectives of this study are to improve the understanding of the fundamental mechanism of the continuous pullout of horizontal anchor under combined loading condition (V, H, M). The two-dimensional finite element analysis (FEM) is carried out by commercial software ABAQUS is used in this study. The strip plate anchor of width B is assumed to be deeply embedded, with localized plastic flow forming around the plate anchor and not extending to the surface, resulting in capacity factors that are not affected by overburden and soil weight (Song et al. 2008; Wang et al. 2010). Conventional small strain analysis is carried out to determine the pullout capacity of the embedded anchor, where the anchor movement is limited to 0.1 times to the anchor length. The contact between the anchor and the soil is assumed to be rough. In order to ensure the rough condition, the interfaces between the anchor plate and soil domains are defined as (i) tangential behaviours and (ii) normal behaviour. In tangential behaviour is assumed to be rough and normal behaviours is defined as hard contact with separation between soil and anchor when tension develops.

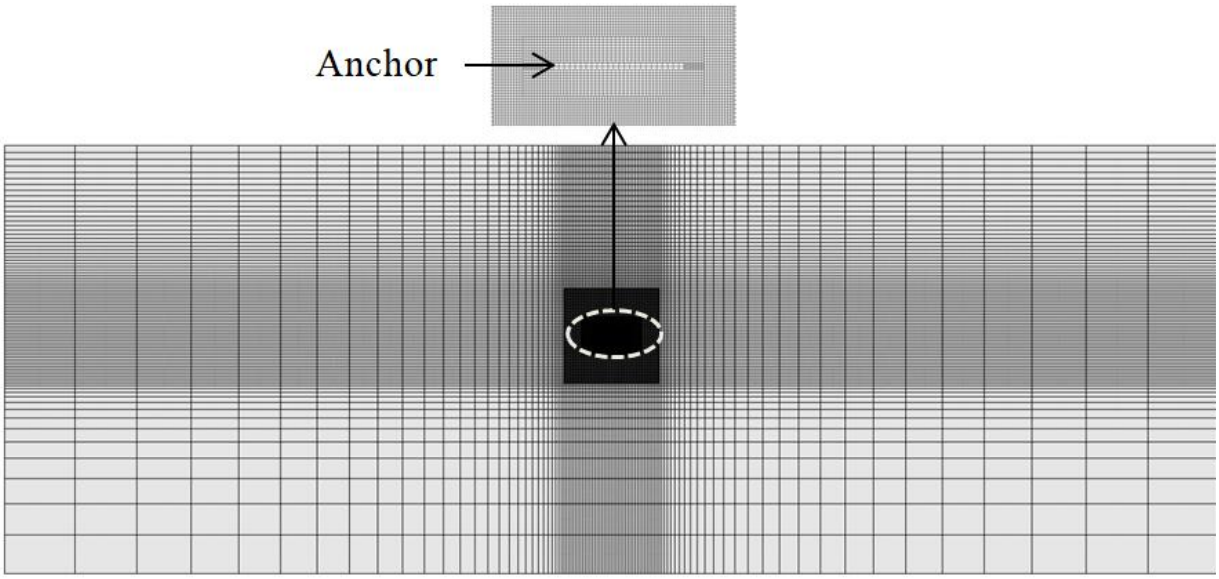

Figure. 1: Finite element model used for numerical analysis

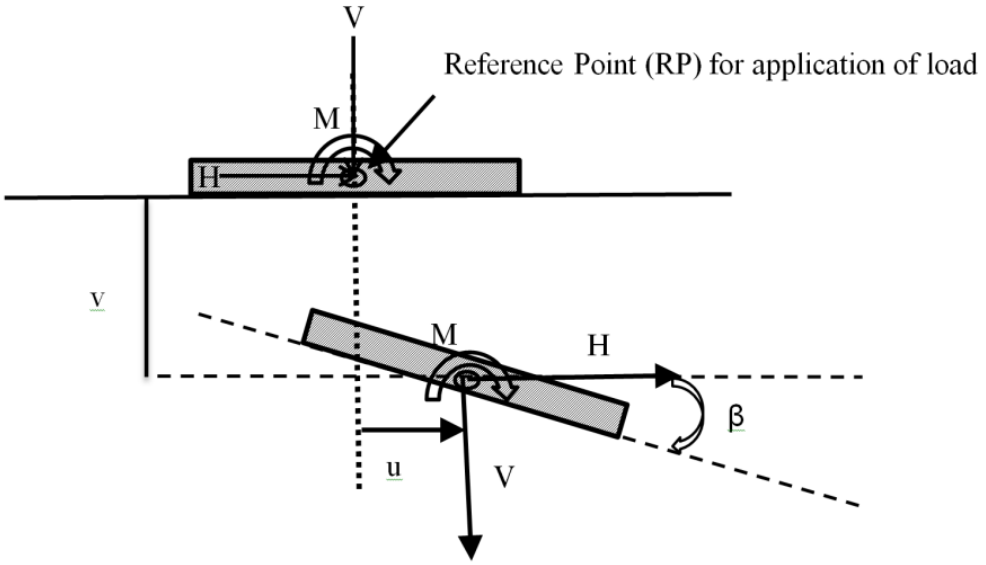

Figure. 2. Load and displacement convention adopted

An elastic-perfectly plastic associative Mohr-Coulomb material model is used for purely cohesive soil with cohesion c=3 kPa, modulus of elasticity E=30 Mpa and the Poisson's ratio 0.33. The anchor is modeled as a rigid body with Young's modulus 10^7 times that of soil and Poisson's ratio 0.15(Andersen et. al, 2003). The FE analyses are based on 8-noded quadrilateral elements of type CPE8R with reduced integration. Figure 1 presents a typical two-dimensional finite-element mesh for a strip plate of width B=0.5m and thickness t=L/7=0.071m. The soil domain is extended to 25B in horizontal and 10B in vertical directions, respectively. Zero-displacement boundary conditions are applied to prevent out-of-plane displacements of the vertical boundaries and the base of the mesh is fixed in both horizontal and vertical coordinate directions. To obtain more accurate results, elements are kept very small (L/60) near the plate, increasing gradually in size and moving away from the plate (Nouri et al., 2017). To determine the collapse load of the footing, displacement-based analyses are performed. The total displacement is applied over a number of sub-steps in the reference point (RP) of the anchor as shown in Figure 2. All the nodes defining the soil anchor interfaces are forced to move together either parallel to the anchor (sliding), perpendicular to the anchor (normal) and in a path corresponding to the rotation of anchor plate about the centre. All results are presented here as non-dimensional forms using the factors defined as

$$N_v = \frac{F_V}{B\gamma H};\ N_s = \frac{F_H}{B\gamma H};\ N_m = \frac{M_m}{B^2\gamma H} \tag{1}$$

2.2 Sign Convention for Load and Displacement

The centroid of the anchor is used as the reference point (RP) for application of combined load components V, H and M**.** The V, H, and M loads, as well as the corresponding footing movements' v, u and β, are illustrated in Figure. 2, following the convention of Butterfield et al. (1997).

3. RESULTS AND DISCUSSIONS

3.1 Vertical Pullout Capacity

The variation of vertical pullout capacity factor ($N_{v,\ Vertical}$) due to the contribution of soil weight with the soil friction angle for different embedment ratio is shown in Figure 3. It is seen that

the vertical pullout capacity factor of strip plate anchor embedded in sand shows nearly linear behaviour with the friction angle. Similar to the horizontal pullout capacity factor, the vertical pullout capacity factor increases gradually up to the embedment ratio of 4 and increases steeply for embedment ration greater than 4.

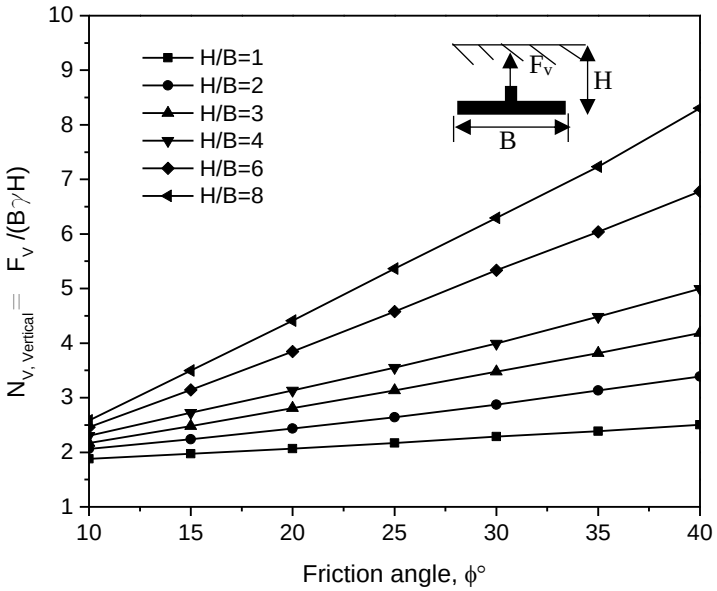

Figure 3: Vertical pullout capacity factor of horizontal strip anchor embedded in sand

3.2 Horizontal Pullout Capacity

It is seen that the horizontal pullout capacity factor ($N_{s,\ Horizontal}$) due to the contribution of soil weight increases gradually with the increases of friction angle for embedment depth up to 4 as shown in Figure 4. While the horizontal pullout capacity factor for the deep anchor (embedded ratio>4) varied steeply with the friction angle. It is also seen that the horizontal pullout capacity factor shows nonlinear behavior with the friction angle of soil.

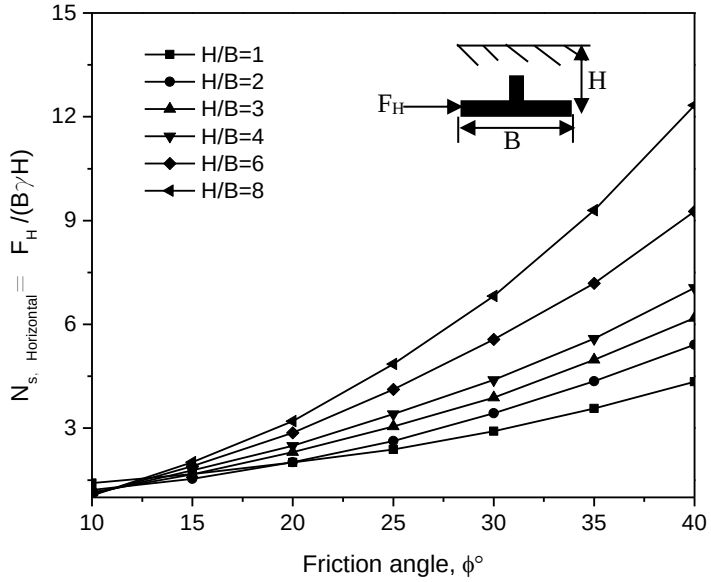

Figure 4: Horizontal pullout capacity factor of horizontal strip anchor embedded in sand

3.3 Moment Capacity

The moment capacity of plate anchor embedded in the sand for different embedment ratio and the frictional angle is shown in Figure 5. It is seen that similar to horizontal capacity factor the moment capacity factor ($N_{m,\ Horizontal}$) of strip anchor embedded in sand shows

nonlinear behaviour with the friction angle. The moment capacity factor of strip plate anchor increases with both the friction angle and embedment ratio.

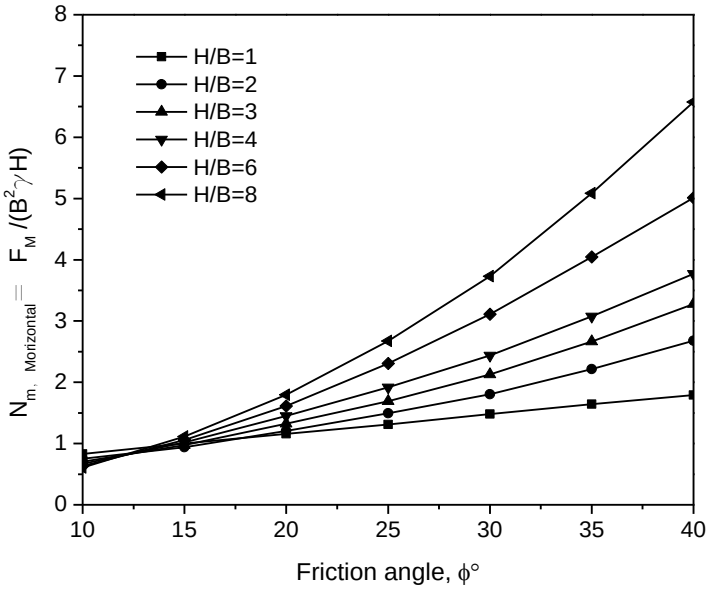

Figure 5: Moment pullout capacity factor of horizontal strip anchor embedded in sand

3.4 Comparison with the previous study

A detailed comparison study on the vertical pullout capacity factor of strip anchor in the sand is shown in Figure 6. It is found that the vertical pullout capacity factor of strip plate anchor in the current shows higher value compared to Merifield and Sloan (2006).

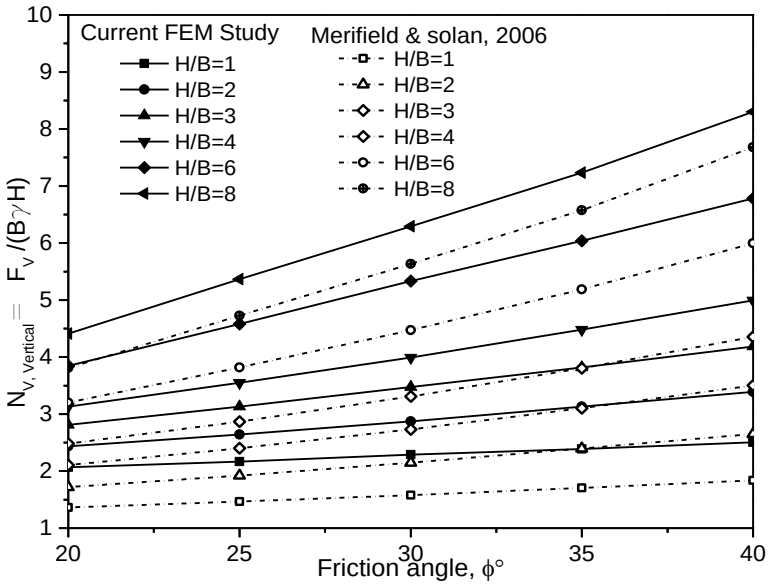

Figure 6: Comparison of vertical pullout capacity factor of horizontal strip anchor embedded in sand

3.5 Comparison of Horizontal and Vertical Pullout Capacity

A detailed comparison between the vertical and horizontal pullout capacity of strip horizontal plate anchor are also conducted. It is seen that for lower friction angle (10° to 30°), the vertical pullout capacity is higher than that of horizontal capacity as shown in Figure 7. But for friction angle above 30°, the horizontal pullout capacity is higher than the vertical capacity of horizontal strip anchor.

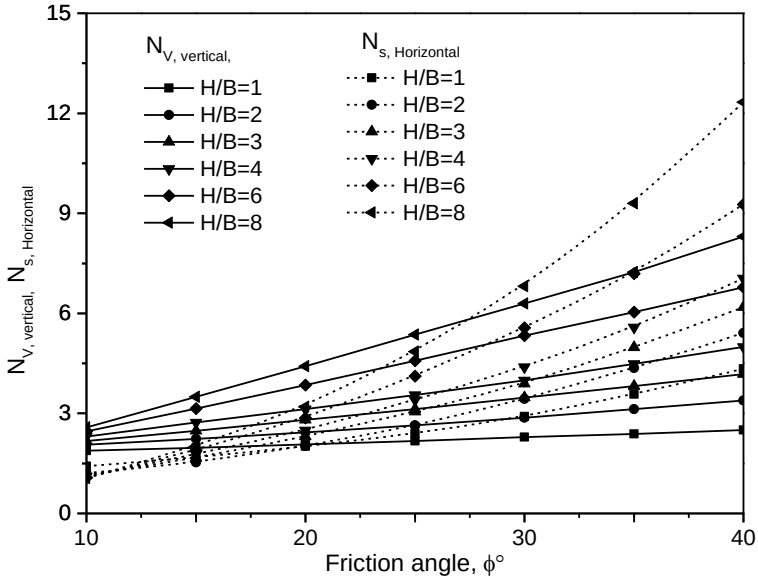

Figure 7: Comparison of vertical and horizontal pullout capacity factor of horizontal strip anchor embedded in sand

4. SOIL FAILURE MECHANISM

Figure 8 shows the contours of resultant soil displacement at the failure of anchors modeled at an embedment ratios of H/B=6 and H/B=8 for pure vertical, horizontal and moment. Under plane strain conditions, the contour shows the failure mechanism of the anchor in sandy soil (ϕ=30°). In all cases, displacement contours extend to the soil surface (see Figure 8a and Figure 8d) and symmetrical about vertical axis due to vertical loadings. A vertical shear plane can be seen extending upward from the edge of the anchor, and soil is drawn in behind the anchor. This type of soil failure mechanism is also observed in all embedment ratios. But, for shear and moment loading symmetry does not exist about vertical axis. Failure surface becomes larger due to the increase of embedment ratios.

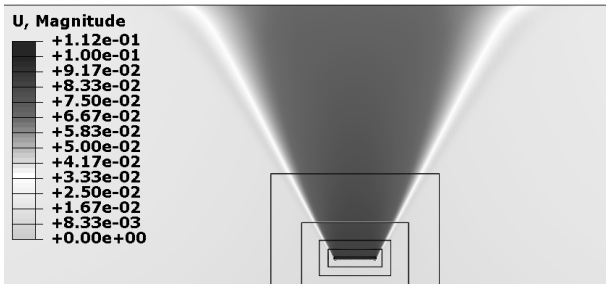

(a) Pure Vertical at H/B=6

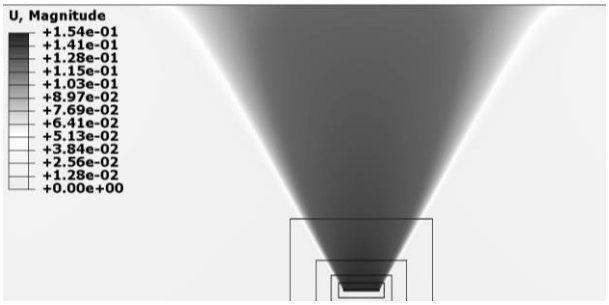

(b) Pure Vertical at H/B=8

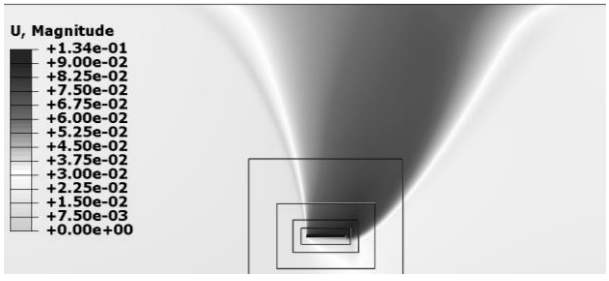

(c) Pure Horizontal at H/B=6

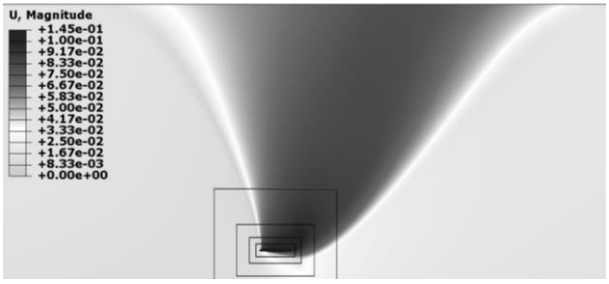

(d) Pure Horizontal at H/B=6

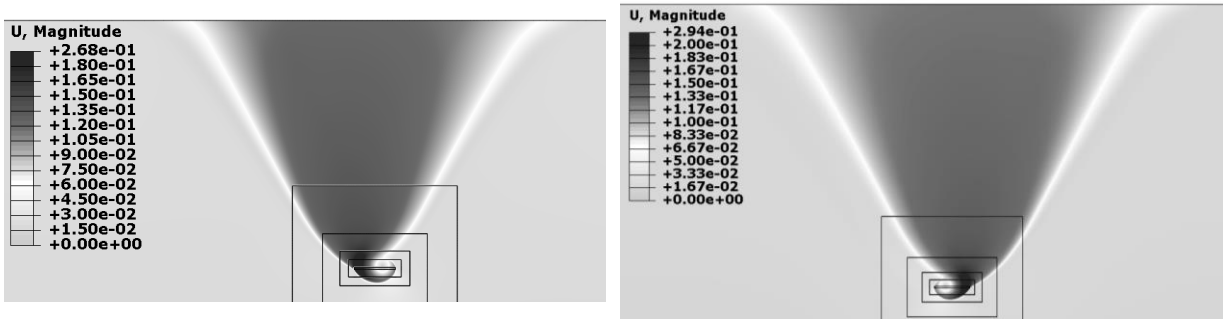

(e) Pure positive moment at H/B=6 (f) Pure negative moment at H/B=8

Figure 8: soil failure mechanism

5. CONCLUSIONS

A detailed FEM analysis on the vertical, horizontal and pure moment pullout capacity of strip horizontal plate anchor in the sand is studied. The following conclusions can be drawn from the results presented in this paper.

(a) The embedment depth and friction angle have a significant impact on the horizontal, vertical and moment pullout capacity of horizontal plate anchor in sand. Both the horizontal and moment capacity increases nonlinearly, while the vertical pullout capacity increases linearly with the friction angle of sand for every embedment depth of anchor.
(b) The horizontal pullout capacity is found lower compared to vertical capacity for small friction angle (10° to 30°), while for higher friction angle (>30°) the horizontal capacity is higher than that of the vertical capacity of horizontal strip plate anchor embedded in the sand. Therefore, for compacted dense sand the horizontal capacity is higher than vertical capacity.
(c) The current FEM study on the vertical pullout capacity of horizontal anchor showed higher value compared to the results obtained from Merifield and Sloan (2006).

REFERENCES

Butterfield R, Houlsby GT, G. G. (1997). “Standardized sign conventions and notation for generally loaded foundations.” *Geotechnique*, 47(5), 1051–4.

Gilbert, R. B., Lupulescu, C., Lee, C. H., Miller, J., Kroncke, M., Yang, M., Aubeny, C. P., and A, J. D. M. T. (2009). “Analytical and Experimental Modeling for Out-of-Plane Loading of Plate Anchors.” *OTC 20115*, 1–15.

Hanna, A., Foriero, A., and Ayadat, T. (2014). “Pullout Capacity of Inclined Shallow Single Anchor Plate in Sand.” *Indian Geotechnical Journal*, 45(1), 110–120.

Merifield, R. S., and Sloan, S. W. (2006). “The ultimate pullout capacity of anchors in frictional soils.” *Canadian Geotechnical Journal*, 43(8), 852–868.

Merifield, R. S., and Smith, C. C. (2010). “Computers and Geotechnics The ultimate uplift capacity of multi-plate strip anchors in undrained clay.” *Computers and Geotechnics*, Elsevier Ltd, 37(4), 504–514.

Nouri, H., Biscontin, G., Aubeny, C. P., and Asce, M. (2017). “Numerical prediction of undrained response of plate anchors under combined translation and torsion.” *Computers and Geotechnics*, 81, 39–48.

O’neill, M. P., Bransby, M. F., and Randolph, M. F. (2003). “Drag anchor fluke – soil interaction in clays.” *Canadian Geotechnical Journal*, 40(1), 78–94.

Song, Z., Hu, Y., and Randolph, M. F. (2008). “Numerical Simulation of Vertical Pullout of Plate Anchors in Clay.” *Journal of Geotechnical and Geoenvironmental Engineering*, 134(6), 866–875.

Sutherland, H. B., Finlay, T. W., and Fadl, M. O. (1983). “Uplift capacity of embedded anchors in sand.” *Int Conf Behav Offshore Struct*, 451–463.

Wang, D., Hu, Y., and Randolph, M. F. (2010). “Three-Dimensional Large Deformation Finite-Element Analysis of Plate Anchors in Uniform Clay.” *Journal of Geotechnical and Geoenvironmental Engineering*, 136(2), 355–365.

Yang, M., Ph, D., Murff, J. D., Ph, D., Asce, D. M., Aubeny, C. P., Ph, D., and Asce, M. (2010). “Undrained Capacity of Plate Anchors under General Loading.” *Journal of Geotechnical and Geoenvironmental Engineering*, 136(10), 1383–1393.

Proceedings of the 4th International Conference on Civil Engineering for Sustainable Development (ICCESD 2018), 9~11 February 2018, KUET, Khulna, Bangladesh (ISBN-978-984-34-3502-6)

EARTHQUAKE GROUND RESPONSE ANALYSIS OF BANASREE RESIDENTIAL AREA USING SHAKE 2000.

Shahana A Esha[1], A. S. M F Hossain[2] and Md A Habib[3], Md. B Hossain[4] and Md. Al N Islam[5]

[1] Graduate Student, Bangladesh University of Engineering and Technology, Bangladesh, e-mail: eshace6@gmail.com
[2] Assistant Professor, Ahsanullah University of Science and Technology, Bangladesh, e-mail: fahad.ce@aust.edu
[3,4,5] Graduate Student, Ahsanullah University of Science and Technology, Bangladesh.

ABSTRACT

The study attempted in performing one dimensional ground response analysis by the use of program SHAKE 2000 for assessing the potential amplification of earthquake ground motions with respect to different characteristic parameters in different types of soil conditions in Banasree residential area, Dhaka. A definite earthquake motion from the earthquake record database was taken as input motion for the soil profiles. Simplified relations relating only to the SPT-N value was used for determining maximum shear modulus and damping of 5% was considered for all the locations. From the database of dynamic material properties, G/Gmax and Damping curves were adopted for the layers. Characteristic graphs of Strain Compatible Damping, Strain Compatible Shear Modulus, Maximum Shear Strain& Stress, Peak Acceleration, Acceleration Time History, Amplification Ratio, etc. were obtained for each location. From the seismic response analysis ,relatively dense stratum range of the shear modulus was much lower with a gradual rise within the sandy layers. The range of shear modulus was relatively low within the sand layers in dense soil. In hard soils within the sand layers the range of shear strains were low but with the densification of layers the shear strain gradually increased. Again peak ground acceleration was high in soft soil areas indicating site amplification in soft soil. The highest acceleration occurred at 22 seconds and at 31 seconds about 0.19g for the input motion acceleration of 0.051g at 21 seconds. Cyclic stress ratio decreased with depth for all types of soil. Spectral acceleration and Fourier amplitude spectrum was found highest.

Keywords: *Shake 2000, Ground Response, Shear waves, Peak acceleration, Damping*

1. INTRODUCTION

Earthquake is such a natural disaster that mankind has been combating with since its origin. The intensity of earthquake threat is not uniform in all the regions of the world. So, regions within the earthquake threat demands their careful consideration in the design of structures and facilities. But on the context of Bangladesh, in spite of being a region of high seismic activity, earthquake resistant design considerations are given least importance. But over the years few of the major earthquakes as, The Great Indian earthquake with magnitude of 8.7 on surface wave magnitude scale, one of the world's strongest, had its epicentre only about 230 km from the capital city Dhaka (Ali and Chowdhury,1992) and most recently the earthquake. Past studies, such as by Ansary et al. (2004), Ashford et al, (2005), Ranjan (2005) and Abe et al. (1996) have demonstrated the role played by the surface geology in altering the observed seismic motion. Most of the methods are based on the assumption that the main response in a soil deposit is caused by the upward propagation of shear waves from the underlying rock formation. Determining the characteristics of the motions likely to develop in the rock formation underlying the site, and selecting an accelerogram with these characteristics is used in the analysis. The maximum acceleration, predominant period, and effective duration are the most important parameters of an earthquake motion. Empirical relationships between these parameters and the distance from the causative fault to the site have been established for different magnitude earthquakes (Gutenberg and Richter, 1956;

Seed et. al., 1969; Schnabel and Seed, 1972). A design motion with the desired characteristics can be selected from the strong motion accelerograms that have been recorded during previous earthquakes (Seed and Idriss,1969) or from artificially generated accelerograms (Housner and Jennings,1964).Average relationships between the dynamic shear moduli and damping ratios of soils, as functions of shear strain and static properties; have been established for various soil types (Hardin and Drnevich,1970; Seed and Idriss,1970).A one dimensional method of analysis can be used if the soil structure is essentially horizontal (Kanai, 1951; Matthiesen et al., 1964; Roesset and Whitman,1969; Lysmer et al.,1971). In this study, As a method of assessment the one dimensional analysis by the program SHAKE 2000 is followed for the local soil conditions at five locations of Banasree residential area to know about the amplification effects on the structures made at that locations based on the soil testing information for a particular damping and a generalized earthquake data .

2. STUDY AREA

Here, study area as Block A, B , D, E, F; shown in the Figure 1, is referred as site 1, site2, site 3, site 4 and site 5 .

Figure 1: Working map locations.

3. METHODOLOGY

The program models the nonlinear variation of the soil Shear Module and Damping as a function of shear strain. The hysteretic stress-strain behavior of soils under symmetrical cyclic loading is represented by an equivalent modulus, G corresponding to the secant modulus through the end points of the hysteresis loop and equivalent linear damping ratio, β which is proportional to the energy loss from a single cycle of shear deformation. For a given soil layer, G and β are assumed to be constant with time during the earthquake shaking. The soil types present on the actual bore log data were made to match the default soil profiles present within the program to get the Shear Modulus and Damping values considering the

soil type anvarious strata. The Maximum Shear Modulus for Sandy Soil and Clayey Soil was determined following the simplified formulae (Imai and Tonuchi,1982; Seed and Idriss 1970; Egan and Ebeling, 1985) which consider the SPT value only. They are shown in the Table1.

Table 1: Equations for Maximum Shear Modulus

Soil Type	Formulae	Variables	Unit	References
Sand	$G_{max}= 325N_{60}^{0.68}$	N_{60}= SPT value	Kip/ft^2	(Imai and Tonuchi,1982) Table A. 2
Clay	$G_{max}= 2000S_u$ $S_u = 6\ N_f$	Su= Undrained Shear Strength, Nf= Field SPT Value	KN/m^2	(Seed,H.B and Idriss, I.M 1970); Egan, J.A and Ebeling R.M ,1985)

The shear wave velocity at the bottom of the bedrock was considered to be of 700 m/s. for all types of soil profiles. A default earthquake source was considered for the analysis for knowing the change in the characteristic curves in the soil profiles.

2.1 Damping Provided

It is a common practice to specify a design spectrum for a 5% damping ratio. So 5% damping was taken for the analysis. However, depending on the structural material behavior and the level of ground motion excitation, a design spectrum for other damping values may be needed.

2.2 Input Motion Provided

Due to unavailability of an earthquake source that influenced a significant amplification in the cities of Bangladesh; the earthquake at Southeastern, Alaska, 1979 - M: 7.3 R: 166 km - N279E Component - Yakutat Station shown in Figure 2, was taken for input motion for the analysis for all types of soil profiles.

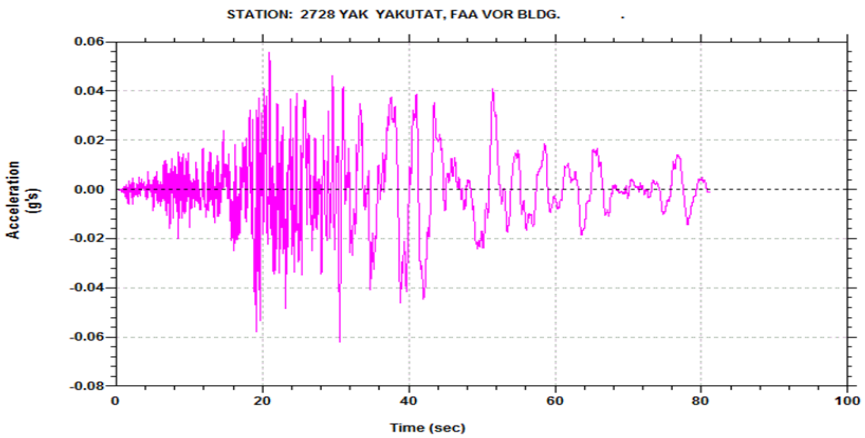

Figure 2: Acceleration Time HistoryRecorded at Yakukat Station For South Eastern Alaskan Earthquake, 1979

3. OUTCOMES OF ANALYSES

The results of analyses are obtained by the program SHAKE 2000 in the form of characteristic curves. The curve induces the following important defining parameters based on which relative discussions on response analysis over the soil profile are provided.

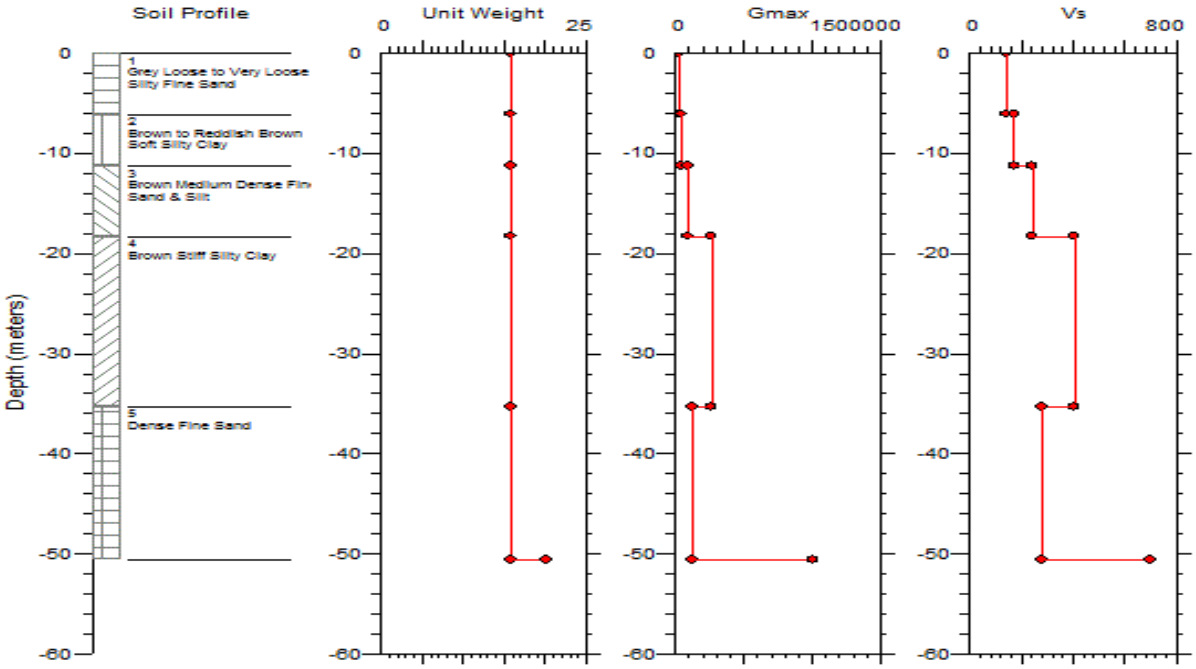

(a) Site-1

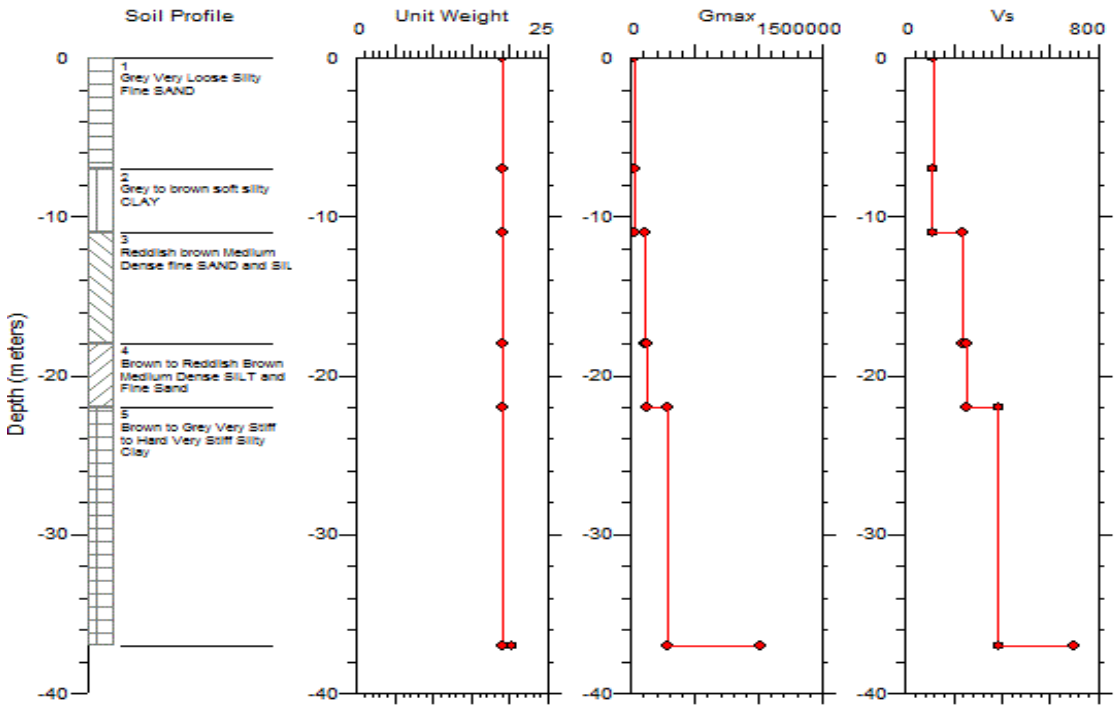

(b) Site-2

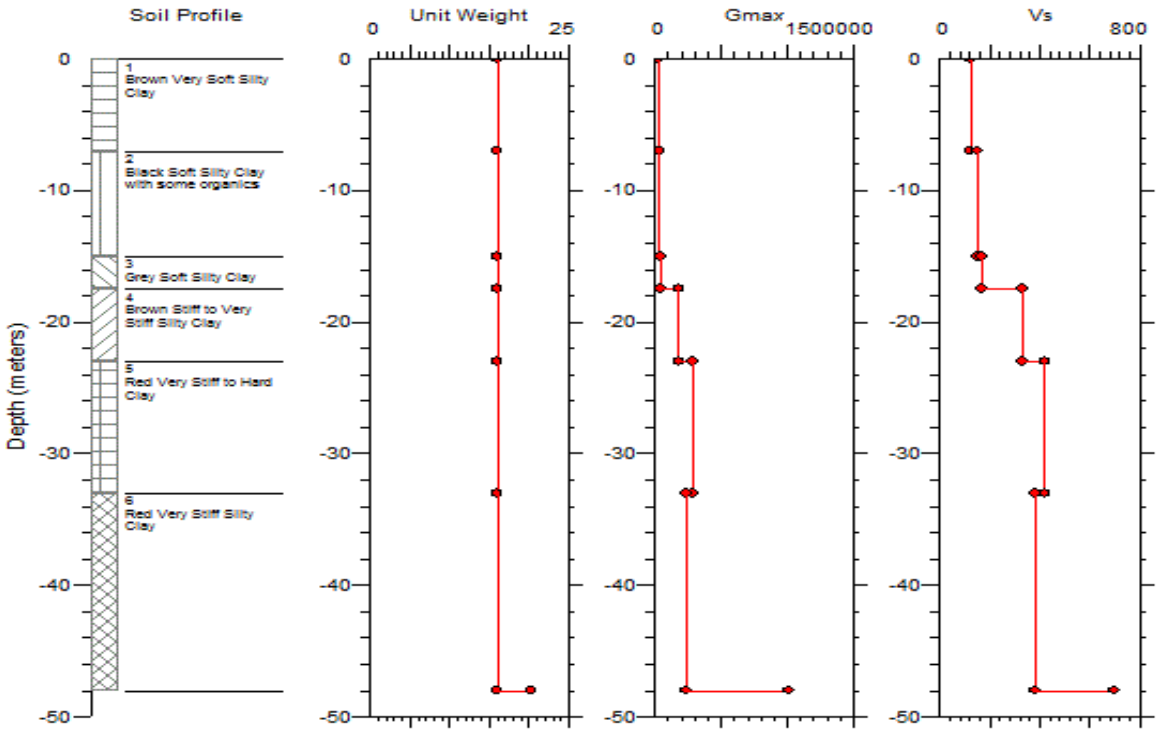

(c) Site-3

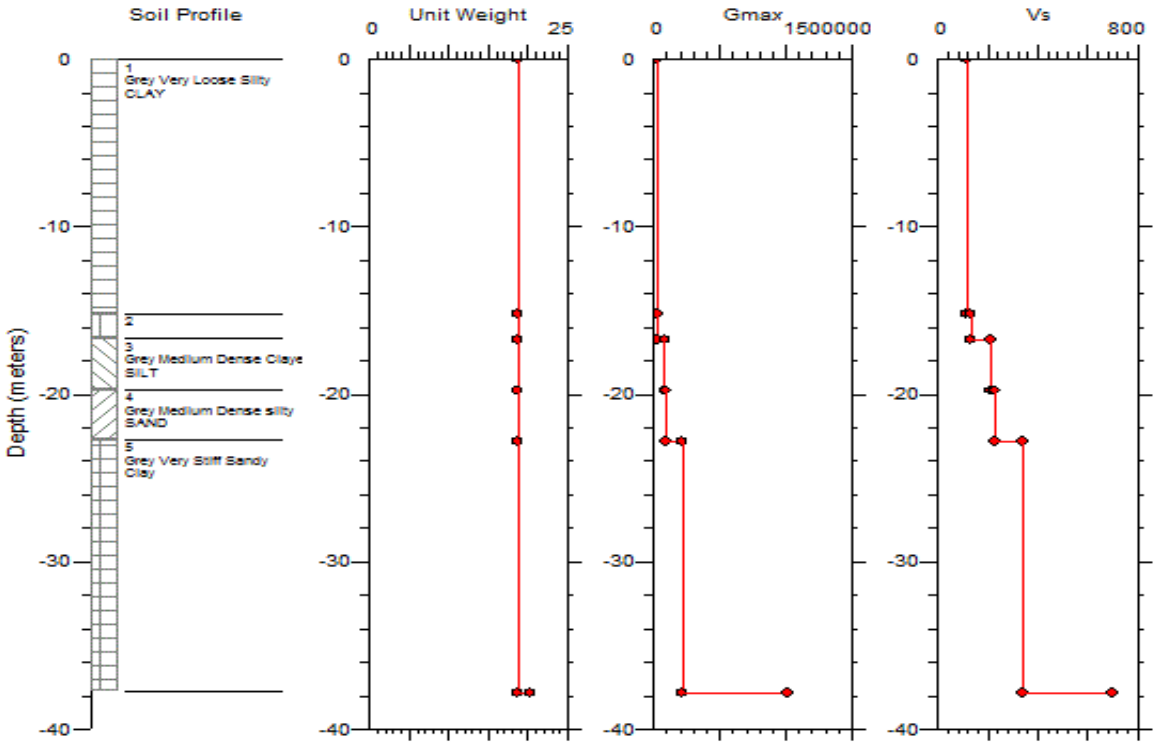

(d) Site-4

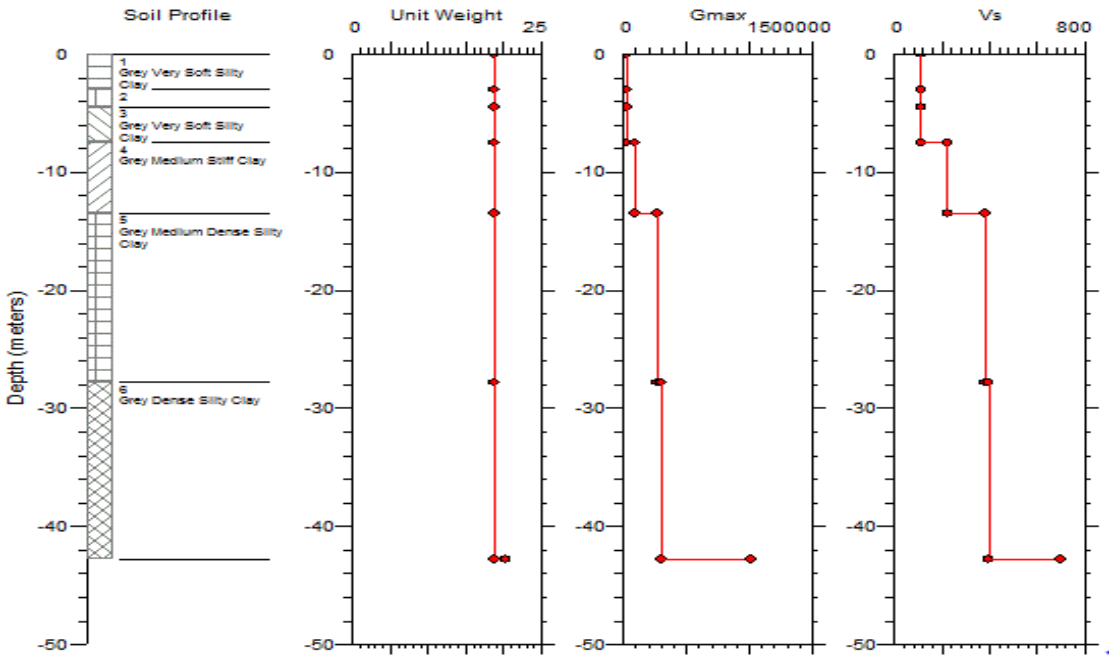

(e) Site-5

Figure 3: Soil profile of study locations depicting variation of Unit Weight (KN/m^3), G_{max} (KN/m^2), Velocity (m/s) with depth.

3.1 Peak Acceleration

Peak ground acceleration (PGA) is equal to the maximum ground acceleration that occurred during earthquake shaking at a location. PGA is equal to the amplitude of the largest absolute acceleration recorded on an accelerogramat a site during a particular earthquake. Earthquake shaking generally occurs in all three directions. Therefore, PGA is often split into the horizontal and vertical components. Horizontal PGAs are generally larger than those in the vertical direction but this is not always true, especially close to large earthquakes. Peak acceleration is highest at the top surface but relatively less in hard stratum compared to loose stratum shown in Figure 3. Among all the locations the highest acceleration occurs in Site-2 at 22 seconds and at 31 seconds about 0.19g for the input motion acceleration of 0.051g at 21 seconds. Peak spectral velocity is almost constant at 1.1 m/s over all the five locations. Figure 3 represents the outputs from the several parameters.

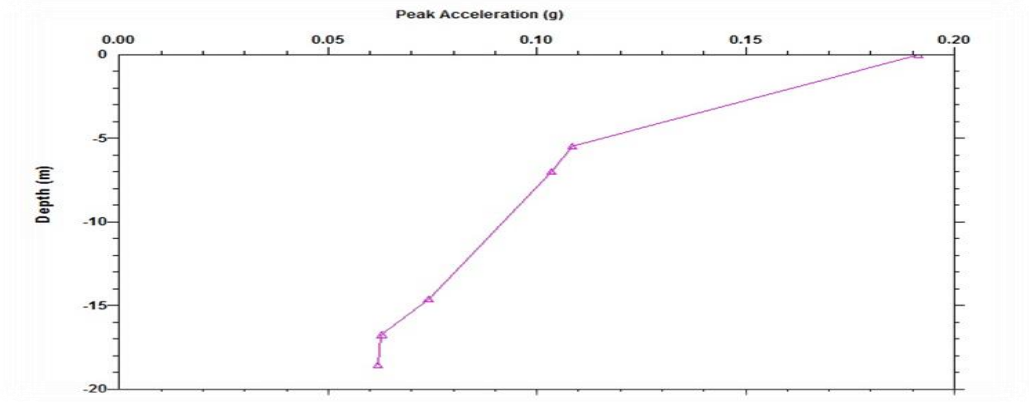

(a) Depth vs Peak Acceleration

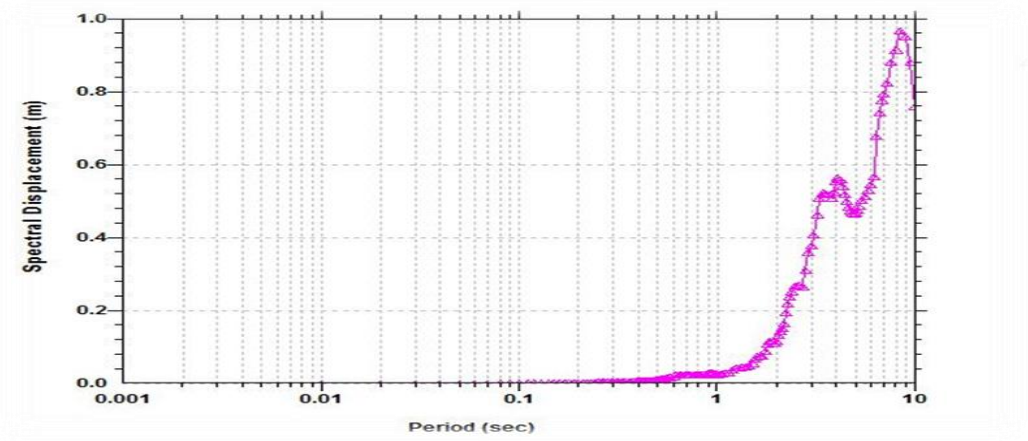

(b) Spectral Displacement Vs Period

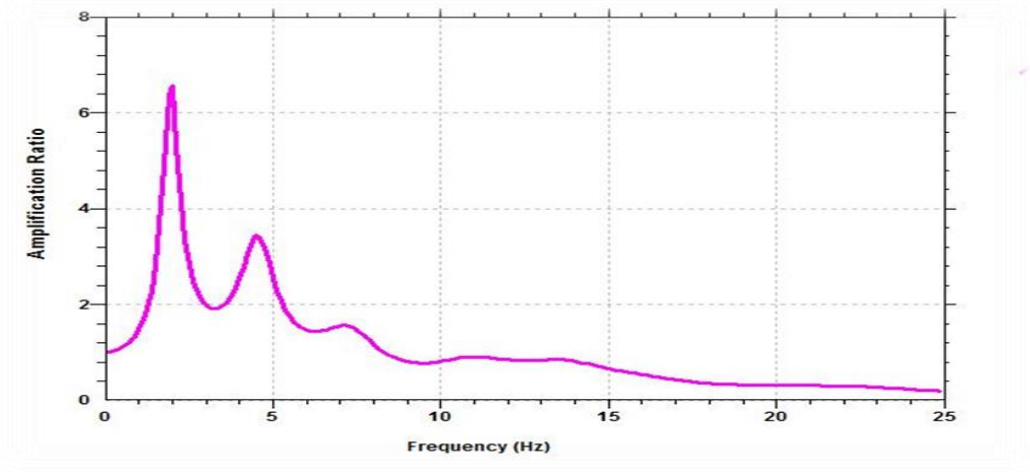

(c) Amplification Ratio Vs Frequency

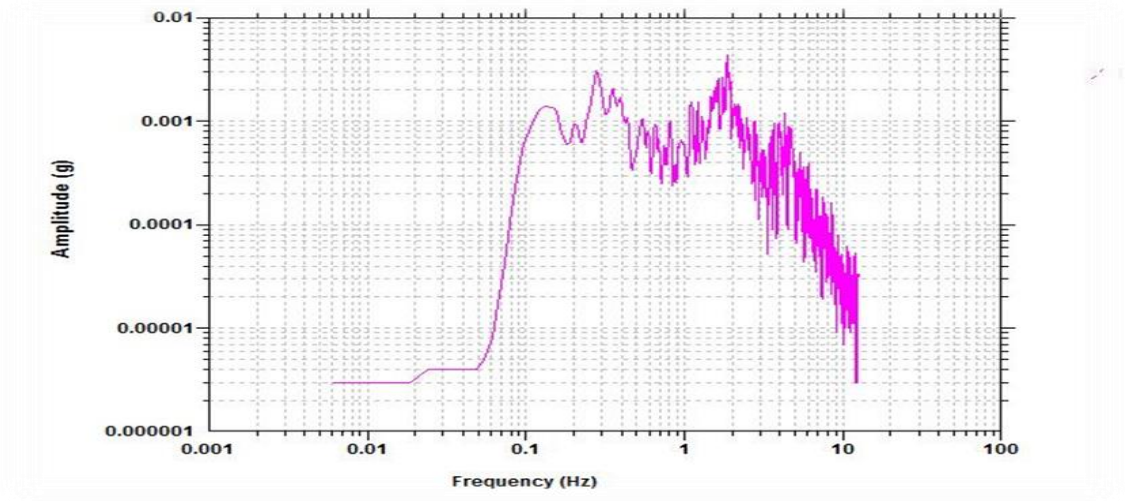

(d) Amplitude vs frequency

Figure 4: Analysis result of Site-

3.2 Shear Modulus

The strain compatible shear modulus curve, it can be concluded that within the loose stratum where both clay and sandy layers are present, shear modulus increases from sand to clay layers, where organic material was present shear modulus was low at that layers and when a hard clay layer is present between the soft clay layers an increase in shear modulus occurs in those layers. In case of relatively dense stratum range of the shear modulus was much lower with a gradual rise within the sandy layers. The range of shear modulus was relatively low within the sand layers in dense soil. In hard soils within the sand layers the range of shear strains are low but with the densification of layers the shear strain gradual increases. With the increase in depth of bedrock from ground surface higher shear stress was obtained in the adjacent layer of soil. The shear wave velocity was low within the hard stratum of soil and with the densification of soil the shear wave velocity increases. Shear stress was comparatively high in Site-2 locations shown in Figure 5.

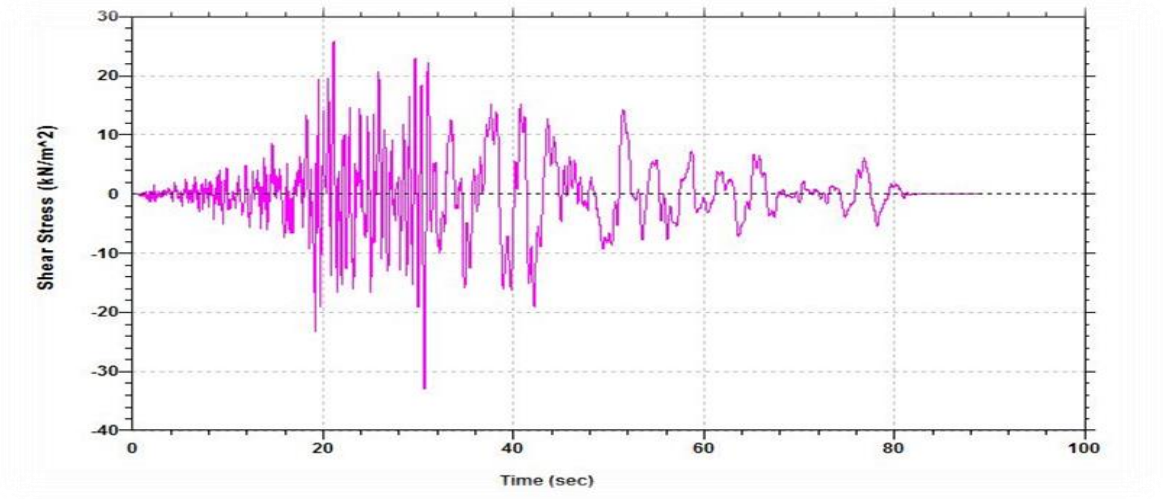

(a) Shear Stress vs Time

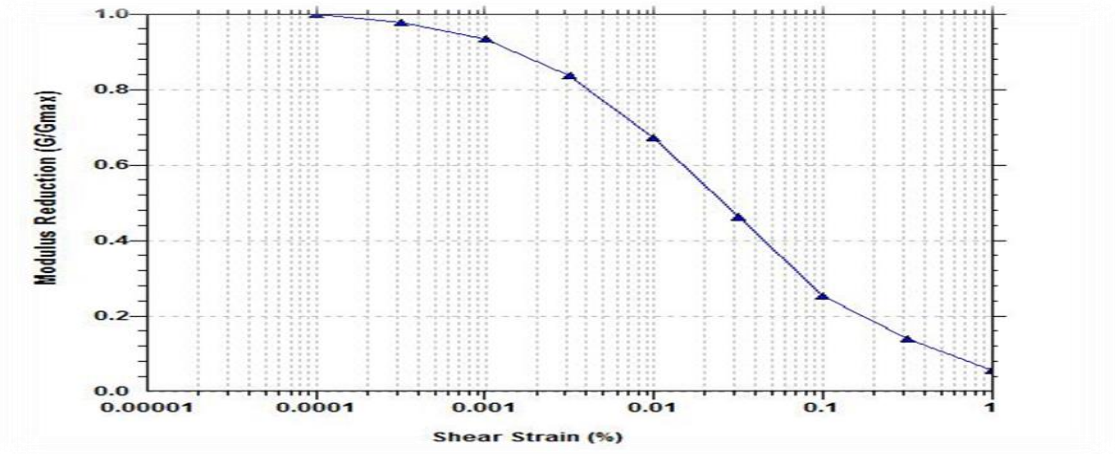

(b) Modulus Reduction vs Shear Strain

Figure 5: Analysis result of Site-2

4. CONCLUSIONS

The ground response analysis by the program SHAKE 2000 was done on the five study locations in Banasree where the soil testing data of a particular site in that location was used to determine the characteristics of response analysis parameters. The study focused on locally available dry sand. The range of damping and shear modulus was relatively low within the sand layers in dense soils. Shear wave velocity was considerably low within the

hard stratum of soil and with the densification of soil the shear wave velocity increases. Shear stress and Peak spectral acceleration was comparatively high in Site-2 locations. Peak acceleration is highest at the top surface but relatively less in hard stratum compared to loose stratum. Peak spectral velocity was almost constant at 1.1 m/s over all the five locations. Gradual decrease in CSR occurs with depth in all of the locations but the variation of CSR with top and the underlying layers is less in hard stratum. For the case of simplicity, number of assumptions and simplified relations was used for the analysis. The results may vary with the change in the earthquake intensity and with the attenuation relations used in the analysis for the program. So, further research can be focused on attenuation relations for peak ground acceleration, peak ground velocity, acceleration spectrum and the velocity spectrum both in the horizontal and vertical direction.

REFERENCES

Abe, K. and Watanabe, H. (1996).A Study on Amplification factors of earthquake motions observed at a granite site and relationships between their vertical and horizontal motions.11th World Conference on Earthquake Engineering, 1242.

Ali, M.H .and Choudhury, J.R. (1992). “Tectonics and earthquake occurrence in Bangladesh”. 36th Annual Convention, IEB, Dhaka.

Ansary, M. A. , Noor, M. A. and Rashid, A. (2004). Site Amplification Characteristics of Dhaka City. Journal of Civil Eng.(IEB), 32 (1) (2004) 1-16

Ashford, S. A. ; Jakrapiyanun, S. A. and Lukkunaprasit, P.(2005).Amplification of Earthquake Ground Motions in Bangkok. 12 WCEE 200, 1466.

Egan, J.A and Ebeling, R.M (1985). “Variation of Small Strain Shear Modulus with Undrained Shear Strength of Clays.” Second International Conference on Soil Dynamics & Earthquake Engineering on Board The Liner Queen Elizabeth 2 , June.

Gutenberg, B. Richter & C. F (1956) "Earthquake Magnitude and Energy," Annual Geophysics Vol 9

Hardin, B and Drnevich, V (1972). “Shear Modulus and Damping in Soils : Design Equations and Curves,” Journal of the Soil Mechanics and Foundation Division , American Society of Civil Engineers, Vol 98, No. 7, pp 667-691

Imai, T. and Tonouchi, K. (1982). “Correlation of N-value with s-wave velocity and shear modulus”. Proceedings, 2nd European Symposium on Penetration Testing, Amsterdam, pp 57-72.

Kanai, K. (1951). “Relation between the Nature of Surface Layer and the Amplitude of Earthquake Motions”. Bulletin Tokyo Earthquake Research Institute.

Lysmer, J., Seed, H.B. and Schnabel, P.B. (1971).“Influence of Base-Rock Characteristics on Ground Response.” Bulletin of the Seismological Society of America, Vol. 61, No. 5, October, pp. 1213-1232.

Matthiesen, R.B., Duke, C.M., Leeds, D.J. and Fraser, J.C. (1964). “Site Characteristics of Southern California Strong-Motion Earthquake Stations”, Part Two. Report No. 64-15, Dept. of Engineering, University of California, Los Angeles, August.

Ranjan, R. (2005).Seismic Response Analysis of Dehradun City, India Thesis submitted to the International Institute for Geo-information Science and Earth Observation, Dehradun, India

Roesset, J.M. and Whitman, R.V. (1969). “Theoretical Background for Amplification Studies”. Research Report No. R69-15, Soils Publication No. 231, Massachusetts Institute of Technology, Cambridge.

Seed, H.B., Idriss, I.M. and Kiefer, F.W. (1969). “Characteristics of Rock Motions During Earthquakes”. Journal of Soil Mechanics and Foundations Division, ASCE, Vol. 95, No. SM5, September.

Seed, H. B and Idriss I, M. (1970), “Soils Moduli and Damping Factors for Dynamic Response Analyses”, UC. Berkeley, Earthquake Engineering Research Center, Report No EERC 70-10

Proceedings of the 4th International Conference on Civil Engineering for Sustainable Development (ICCESD 2018), 9~11 February 2018, KUET, Khulna, Bangladesh (ISBN-978-984-34-3502-6)

NUMERICAL MODELLING OF ANCHOR FOUNDATION IN DENSE SAND

A.S.M. Riyad[1] and Md. Rokonuzzaman[2]

[1] *Lecturer, Khulna University of Engineering & Technology, Bangladesh, e-mail: riyadtowhid@yahoo.com*
[2] *Professor, Khulna University of Engineering & Technology, Bangladesh, e-mail: rokoncekuet@yahoo.com*

ABSTRACT

Anchors and anchoring systems are widely used in different structures with different embedment, size, and shapes. The Finite Element Method has the ability to handle complex soil stratigraphy and it also has the potentiality of solving different soil-structure interaction problems. Presently evolved, almost all of the prevailing sophisticated models are very complex and incomplete in the sense that they do not define important factors such as strain localization, strain softening, etc. Above important factor overlooked in most of the current geotechnical models is a strong link between the model and a reliable set of experimental data. Mohr-Coulomb failure surface has corners or singularities, and therefore it is not mathematically convenient to use particularly for 3D problems because of discontinuties of gradient occur at edges and tip of the hexagonal shape yield surface pyramid. In this study, different approximation models are used to determine the appropriate models with respect to experiment. Furthermore, parametric studies are done on peak frictional and dilatancy angles. This study validated the rigorous 3D FE models, incorporating simple strain softening law for anchor foundation in dense sand using in-house finite element program. DP compromise cone predictions are found to be in better agreement with the experimental results. Dilatancy of sand makes significant effect on the uplift behavior of anchors. The greater dilation angle is resulted from the higher collapse load and displacement. With the increase of friction angle and embedment ratio, the effecet of dilatancy is more remarkable.

Keywords: *Anchors, approximation, dilatancy, finite element method, frictional angle*

1. INTRODUCTION

Anchors are foundation systems that are designed primarily to resist uplift (tensile) loads. Anchor usage was started in early 1930's and with a boom after the Second World War and today, anchoring is a well-established branch of Geotechnical engineering. Different types of anchors and anchoring systems are being used widely all over the world and engineers are showing more enthusiasm on anchor usage techniques, their behaviour, and design. Anchor problems are related to different types of geotechnical and civil engineering constructions such as retaining walls, television and transmission towers, anchor bulkheads, submerged pipelines, offshore platforms, free-standing and guyed lattice towers, tension cables for suspension bridges, tent type roofs, and tunnels with different embedment, size, and shapes. Due to lack of proper installation technology and practical designers and/or engineers do not accept new technology; there is limited use of anchor foundations in Bangladesh. Anchor foundations have good potential in Bangladesh which can be used as tension members, earth reinforcement, and so on, which can reduce the cost of foundation of different structures significantly. Various studies of anchors have been conducted by numerous researches (Baker & Konder, 1966; Ball, 1961; Clemence & Veesaert, 1977; Davie & Sutherland, 1977; Deshmukh et al., 2010; Dickin, 1988; Hanna et al., 1972; Majer, 1955; Matsuo, 1967; Merifield & Sloan, 2006; Meyerhof & Adams, 1968; Mors, 1959; Murray & Geddes, 1987; Ovesen, 1981; Rokonuzzaman & Sakai, 2011; Rowe & Booker, 1979; Rowe & Davis, 1982; Sakai & Tanaka, 1998, 2007, 2009; Vermeer & Sutjiadi, 1985; Vesic, 1969). Some of the researchers are widely used limit state theories, which are based on a rigid elastic-perfectly plastic assumption which cannot adopt the failure in the real soil which

is highly progressive. So, the displacement based elastoplastic finite element method (FEM) is widely being used by the geotechnical researchers and engineers to find the load-displacement relationship and, thus, the collapsed load, due to its robust ability to deal with the complicated geometry and loadings, nonlinear constitutive law, anisotropic nature of soils, etc. The widely used model in elastoplastic geotechnical analysis is Mohr-Coulomb yield criterion. While this yield criterion is superseded by more complicated soil models for advanced applications, is widely used in the geotechnical analysis. The most important advantages of this model are its simplicity and the finite element solutions can be compared with different classical plasticity equations which is more useful for validating finite element codes (Abbo & Sloan, 1995). Rowe and Davis (1982) applied elasto-plastic FEM with Mohr-coloumb failure criteria and continuous dilatancy, producing highly conservative design charts. Vermeer and Sutjiadi (1985) used non-associated elasto-perfectly plastic FEM model (Borst & Vermeer, 1984) to validate their proposed design equations. Merifield and Sloan (2006) used elasto-perfectly plastic FEM with Mohr-Coulomb yield criteria to compare their results obtained by limit state theories. Mohr-Coulomb failure surface has corners or singularities, and therefore it is not mathematically convenient to use particularly for 3D problems because of discontinuties of gradient occur at edges and tip of the hexagonal shape yield surface pyramid. It is well known that these singularities often cause stress integration schemes to perform inefficiently or fail. Originally the corners and the apex of the Mohr-Coulomb yield surface caused problems in the numerical implementation, so an approximate yield surface with smoothed or rounded corners has to be used. The singularities in the yield surfaces, where the gradient with respect to the stresses is undefined, occur at $\theta = \pm 30^0$. To deal with these singularities which are often encountered in finite element analysis, a satisfactory method is needed under the conditions of axial symmetry (Sloan & Booker, 1986). Nowadays, methods for implementing the corners explicitly exist, but the use of the rounded surfaces is still widespread. The implications of using these approximations, however, are not documented in the literature. Various techniques for dealing with these corners have been discussed by Hinton and Owen (1986); Sloan and Booker (1986); Zienkiewicz and Pande (1977). Drucker-Prager model has been proposed by Drucker and Prager (1952) as a smooth approximation to the Mohr-Coulomb law. The Drucker Prager model can also be made either more or less conservative than the Mohr-Coulomb law by fitting it to the inner or outer apices (Mijangos & O'Kelly, 2009). For non-associative flow rule, the major symmetry of the consistent tangent operator is lost. Further, cone apex is singular, and the normal to the potential surface is not defined. Special algorithmic treatment is needed around this region (Hofstetter & Taylor, 1991). In order to approximate the Mohr-Coulomb hexagon on the deviatoric stress plane (π plane), several strategies are available for determining Drucker-Prager cone parameters. According to author knowledge, no researcher has proposed a rigorous numerical model which can consider the combined effect of peak frictional angle, dilatancy, and singularities for the rectangular anchor foundations buried in the dense sand. So, in this study, an elasto-plastic 3D FEM model, incorporating non-associated simple stain softening constitutive law with shear-band, is validated against model tests to simulate uplift load-displacement relationships of rectangular anchor foundations and also determine the effect of peak frictional angle, dilatancy and Drucker-Prager approximation on the uplift behaviour of the shallow rectangular anchor in sand.

2. METHODOLOGY

In this study, an in-house finite element programs written in FORTRAN which is coded by Professor Tanaka is used. 3D FEM model is validated using simple strain softening law, for the vertically uploaded rectangular anchor foundations embed in dense sand for clearly understanding the related failure mechanisms. Furthermore, different approximate models to the exact Mohr-Coulomb model in the in-house finite element programs are implemented.

Besides, design graphs are developed for the practical design based upon detailed parametric studies on peak frictional and dilatancy angles.

2.1 Physical Modeling

The experimental setup, which is used for the experiments, is shown in Figure 1. The experimental results are used in this study with taking the permission from Sakai and his research group conducted at Mie University. The detailed procedure can be found from Rokonuzzaman and Sakai (2011).

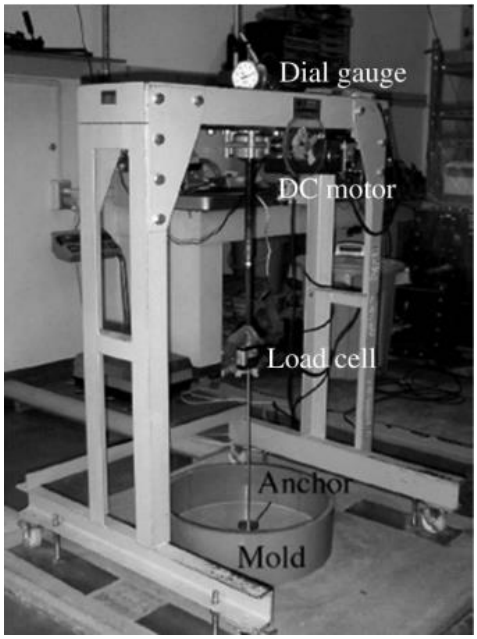

Figure 1: Setup for the anchor pullout experiment (Rokonuzzaman & Sakai, 2011)

2.1.1 Numerical Modeling

The 3D FE model uses the nonlinear elasticity (Hardin & Black, 1968), non-associated flow rules (Drucker-Prager potential and Mohr-Coulomb yield surface), simple strain softening constitutive law (Walters & Thomas, 1982) in an elasto-plastic framework. The dynamic relaxation method devised with return mapping algorithm (Sakai & Tanaka, 2009; Tanaka & Kawamoto, 1988) is used for the fast solution of highly nonlinear equations (e.g. dense Toyoura sands with the high frictional angle of 45°), which is very essential for 3D problems to save computational time. The standard FE solutions of strain-softening material are strongly meshed size-dependent. Several techniques have been proposed to resolve the mesh-dependent pathology of FE solutions; Pietruszczak and Mroz (1981) proposed the idea of employing a softening modulus scaled by the element size, which is used here.

A characteristic photograph of the ground surface is shown in Figure 2. It has two symmetrical vertical planes passing through the center of the foundation, validating the necessity of 3D design consideration. Also, taking the benefits of this symmetry, one-quarter of the domain is discretized into finite elements; some meshes are shown in Figure 3. The mesh extends following the recommendation of Bray et al. (1989). Zero-displacement boundary conditions are applied to prevent the out of plane displacements of the central vertical symmetrical boundaries and the base of the mesh was fixed in all three coordinate directions, except the anchor plate area. The differential quasi-elastic displacements are applied along the anchor boundary in small consecutive increments till to the failure, and the corresponding nodal forces were averaged over the displacement control nodes to find the uplift load. To construct the mesh, the same type of element, and the equivalent boundary conditions, soil conditions, and analysis procedure are maintained. Following the

recommendations of Lindsay (1980), the displacement (δ) and the uplift load (P) are normalized as the displacement factor, δ/B, and the pullout resistance factor, N_p (=P/γ_dHBL), respectively. The material parameters are used for the analysis is shown in Table 1.

Table 1: Parameters for Simple Strain Softening Material Models

Parameters	**Properties**
Density (g/cm^3)	1.63
Void ratio, e	0.62
Relative density, D_r	0.95
Coefficient of shear modulus, G_0	500
Peak frictional angle, ϕ_p	45
Dilatancy angle, ψ	20
Residual frictional angle, ϕ_r (degrees)	33
Poisson's ratio	0.3
B	0.5
C	0.5
D	0.5

Such a numerical model incorporating softening law must be verified before to apply for the analysis of anchor foundations, as the FE solutions can be sensitive to mesh size. For this purpose, cubic hexahedral elements finite elements of 14208 (Figure 3a) and 6525 (Figure 3b) with the size of 5 mm and 6.25 mm in the central zone, respectively, are used for an anchor foundation (H/B=2, L/B=2, B=50 mm). The curves in the Figure 3c depict the relationship between the numerical pullout resistance and displacement factor, and it is shown that the numerical solutions are not susceptible to the mesh size effect.

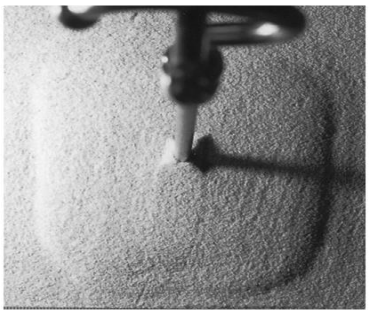

Figure 2: Characteristic photograph of heave on ground surface (square anchor)

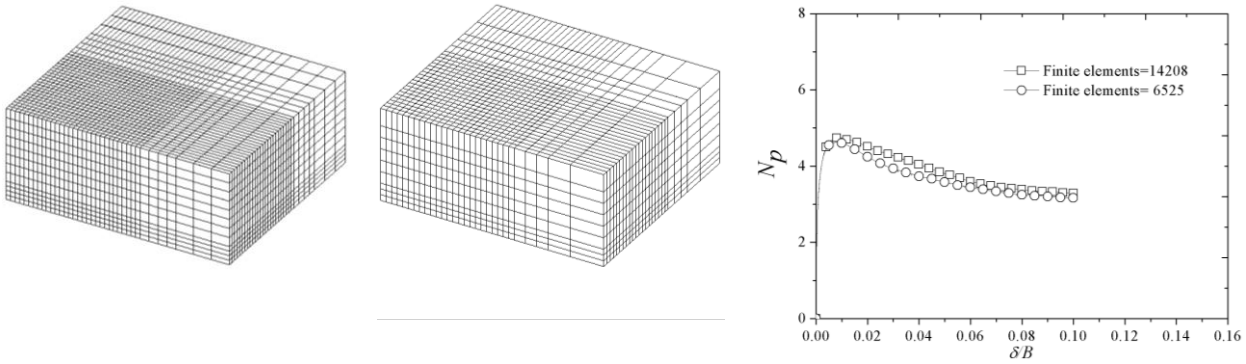

(a) **(b)** **(c)**

Figure 3: Mesh-size effect (*H/B*=2, *L/B*=2, *B*=50 mm): (a) fine mesh (elements=14208), (b) course mesh (elements=6525), and (c) uplift resistance-displacement factor relationship

3. RESULTS AND DISCUSSIONS

3.1 Validation and Verification with Experiment

The curves are shown in Figure 4, depict the experimental and numerical relationships between the pullout resistance and displacement factor of the square and rectangular anchor foundations with L/B= 1, 2, 3, 4, 5 and 6 (B = 50 mm and H/B= 2). The experimental and numerical results show close agreement. All the curves show three distinct phases: the initial phase with the sharp increase in pullout resistance with the anchor displacement, followed by a softening nature of decreasing the pullout resistance with anchor displacement, and, finally, the pullout resistance remains unchanged with the further uplifting of the anchor, defining the residual phase. The overall shape of load-displacement curves is attributed to the progressive failure. The rate of softening after the peak uplift resistance factor is decreasing with the increase of L/B.

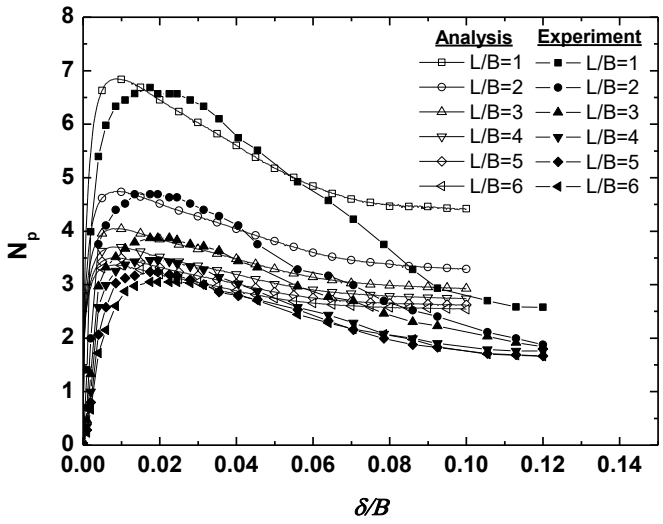

Figure 4: Uplift resistance-displacement factor relationships at H/B=2

3.2 Effect of Peak Frictional Angle and Dilatancy

Geotechnical material is non-associated material in apply, so non-associated flow rule ought to be adopted in soil model. Sand dilatancy depends on density and stress level. Dense sand with low-stress level exhibits shear dilation and loose sand with high-stress level

usually behaviors shear contraction. The dilation angle of zero degree corresponds to a soil that deforms plastically with zero volume change. This can be an affordable assumption for loose sands (Rowe & Davis, 1982). The uplift behavior of horizontal circular anchors with H/B varying from 1 to 3 have been simulated where φ ranges from 25° to 45°, ψ from 0° to 25°. Figure 5 show the values of N_{pu} for H/B= 1, 2, 3 and various sand properties. The uplift capacity increases with dilation angle significantly and the effect of dilatancy become greater with the increase of friction angle and embedment ratio. When H/D=1, $\phi=25^0$ and 45^0, the uplift capacity for the case that $\psi= 25^0$ are about 1.1 and 1.3 times of the values for the case that $\psi= 0^0$, respectively. When H/D=3, $\phi= 25^0$ and 45^0, the uplift capacity for the case that $\psi= 30^0$ are about 1.2 and 1.5 times of the values for the case that $\psi=0^0$, respectively.

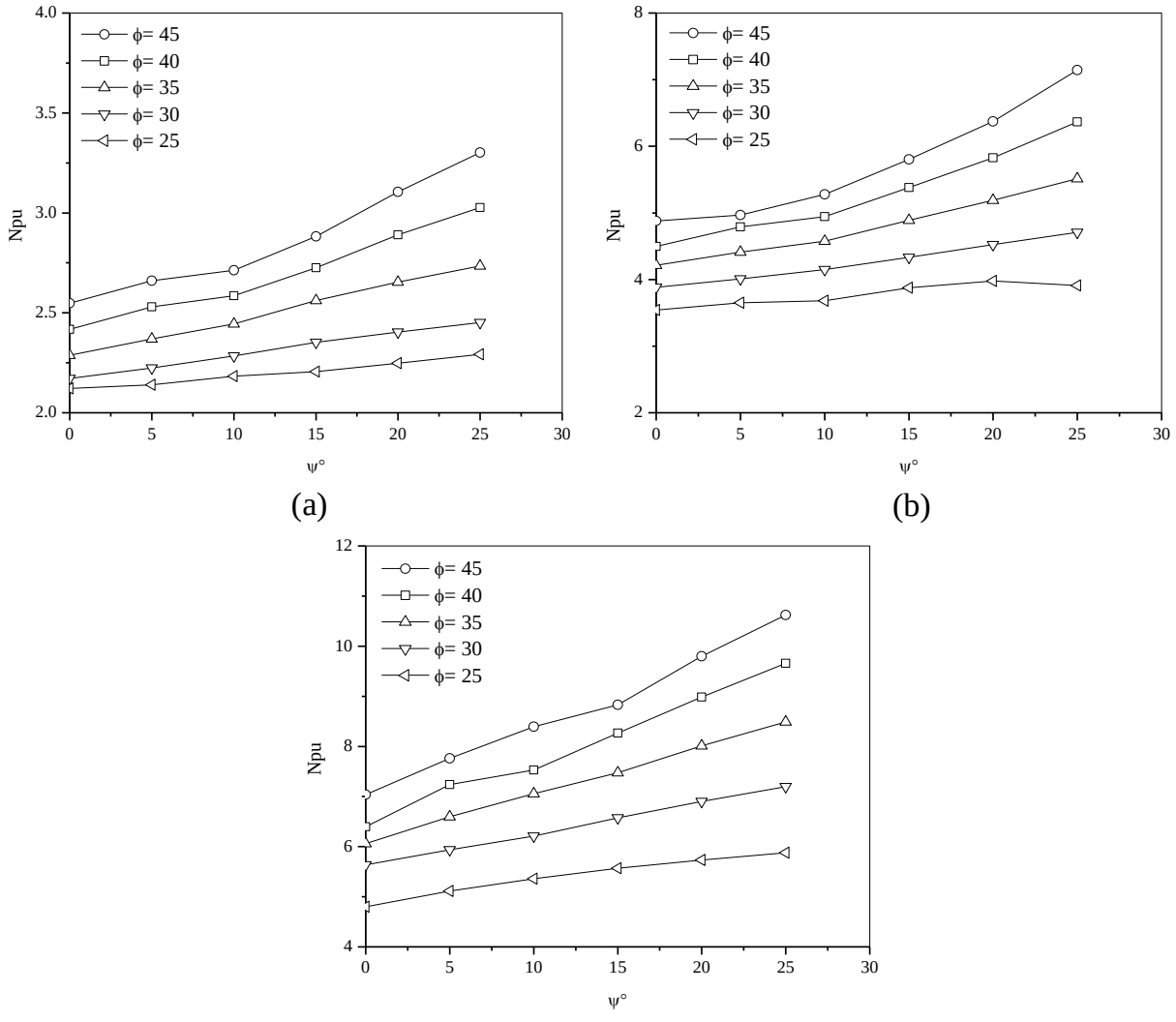

Figure 5: Breakout factors for various H/B and sand properties: (a) H/B=1, (b) H/B=2, and (c) H/B=3

The increases in uplift capacity due to the effect of dilatancy are approximately linear for various embedment ratio and friction angles. Therefore, the breakout factor Npu for a certain value of dilation angle may be determined conveniently by linearly interpolating between the values of Npu for the cases that $\psi=0^0$ and 25^0. The interpolation results are lower than numerical results and the differences are less than about 10%, which is safe for practical engineering. For the convenience of application, the breakout factors are presented in Figure 6, when $\psi=0^0$ and 25^0 for various friction angles and embedment ratios.

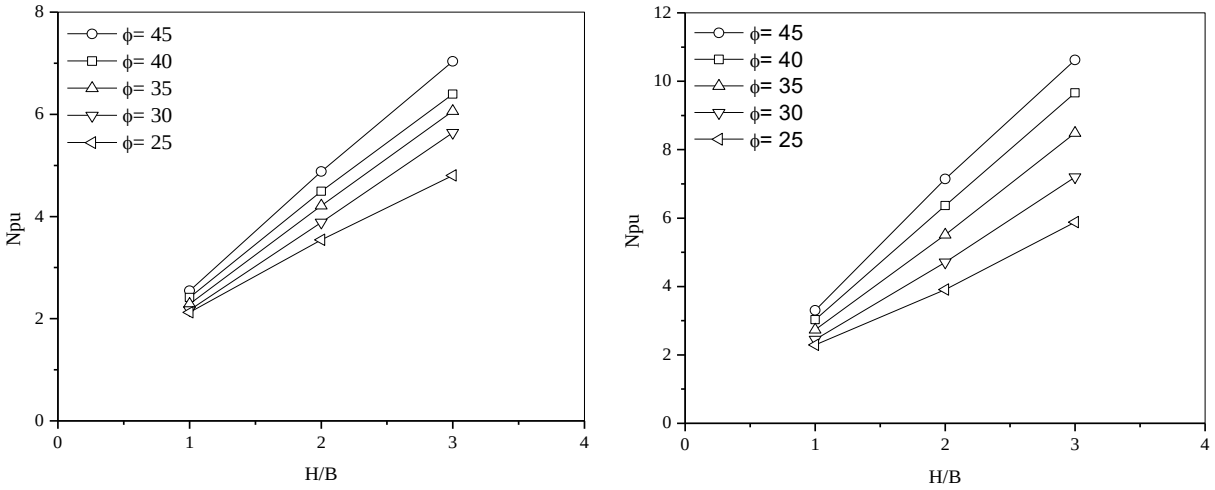

Figure 6: Relationships of H/B and N_{pu} for various ϕ:(a) ψ= 0^0, and (b) ψ= 25^0

3.3 Drucker Prager Approximation

The material parameters are used for the analysis is shown in Table 1. In the M–C criterion, the predicted failure strength is independent of the intermediate principal stress σ_2, which disagrees with the fact that the biaxial compressive strength is always higher than the uniaxial compressive strength for geomaterials. However, the D–P criterion takes into account the influence of σ_2. From all the curves of Figure 7, it is evident that, Mohr-Coulomb model predicts lower strength at greater strains at all stages of loading compares to Drucker-Prager model. The uplift resistance predicted by the DP compromise cone model is in agreement with the experimental results, though the strength value matches well with the Mohr-Coulomb model predictions. As noted before the strains predicted by Mohr-Coulomb model are conservative. These models do not capture the strain softening behaviour which is found in natural soils according to figure.

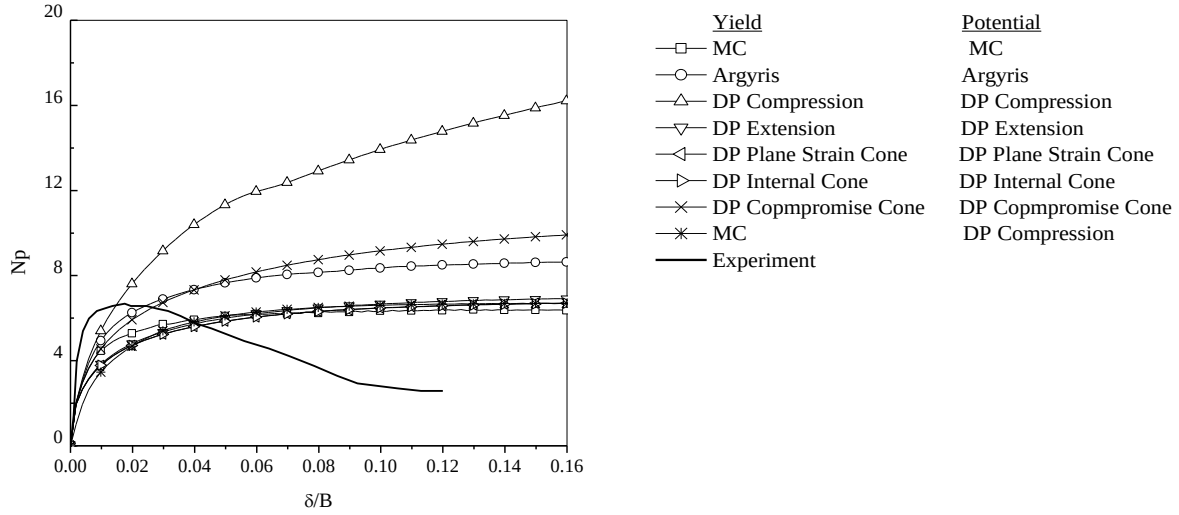

(a) L/B=1

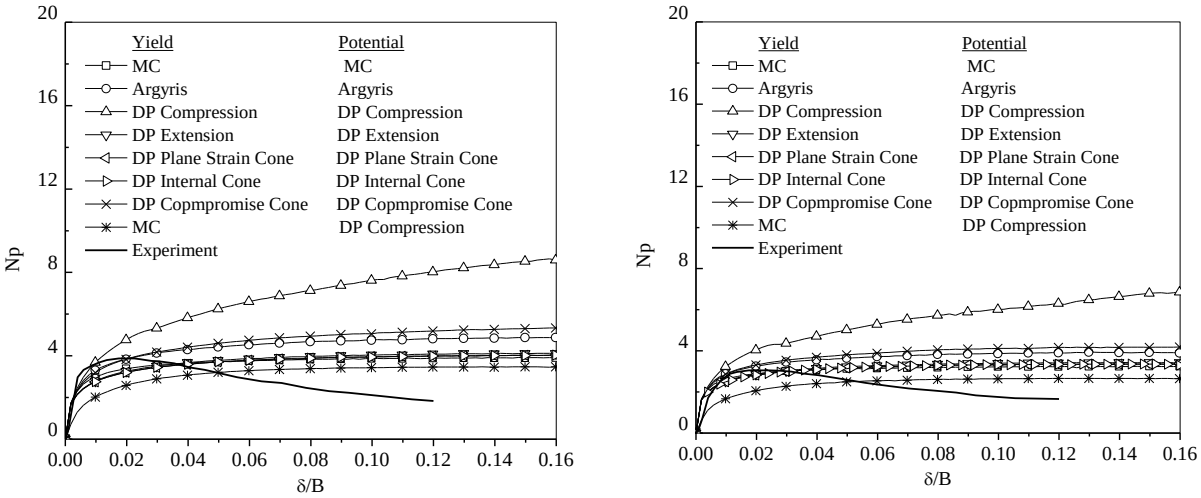

(b) L/B=3 (c) L/B=6

Figure 7: Approximation to Mohr-Coulomb Material Model using 3D FEM

4. CONCLUSIONS

The effects of peak frictional angle, dilatancy, and approximation on the pullout capacity of rectangular anchor foundations buried in dense Toyoura sand is studied through model tests and/or extensive 3D FEM analysis. Dilatancy of sand makes significant effect on the uplift behavior of anchors. The greater dilation angle is resulted from the higher collapse load and displacement when embedment ratio and friction angle are the same. With the increase of friction angle and embedment ratio, the effect of dilatancy is more remarkable. The relationships of dilatancy angles and breakout factors are approximately linear for the same embedment ratio and friction angle. From observations, the Drucker-Prager compromise cone predictions are found to be in better agreement with the experimental results. The Mohr-Coulomb predictions are conservative and hence are in vague in many practical situations in engineering practice. The soils exhibiting post-peak softening, probably due to the presence of natural structure is not predicted by any of these models. Overall, the uplift resistance-displacement factor relationship, response stiffness, and peak uplift resistance factor are the functions of peak frictional angle and dilatancy. Thus, for the practical design and analysis of rectangular anchor foundations, it is necessary to use such a 3D FEM model to handle the issues of soil behavior, geometrical and so on factors.

REFERENCES

Abbo, A., & Sloan, S. (1995). A smooth hyperbolic approximation to the Mohr-Coulomb yield criterion. *Computers & structures, 54*(3), 427-441.

Baker, W. H., & Konder, R. L. (1966). Pullout load capacity of a circular earth anchor buried in sand. *Highway Research Record*(108).

Ball, A. (1961). *The resistance to breaking-out of mushroom foundations for pylons.* Paper presented at the Proceedings of 5th International Conference on SMFE.

Borst, R. D., & Vermeer, P. A. (1984). Possibilites and limitations of finite elements for limit analysis. *Geotechnique, 34*(2), 199-210.

Bray, J. D., Seed, R. B., & Seed, H. B. (1989). *The effects of tectonic movements on stresses and deformations in earth embankments*: Earthquake Engineering Research Center, University of California.

Clemence, S., & Veesaert, C. (1977). *Dynamic pullout resistance of anchors in sand.* Paper presented at the Proceedings of the Int. Symp. On Soil-Structure Interaction.

Davie, J. R., & Sutherland, H. B. (1977). Uplift resistance of cohesive soils. *Journal of the Geotechnical Engineering Division, 103*(9), 935-952.

Deshmukh, V., Dewaikar, D., & Choudhury, D. (2010). Analysis of rectangular and square anchors in cohesionless soil. *International Journal of Geotechnical Engineering, 4*(1), 79-87.

Dickin, E. A. (1988). Uplift behavior of horizontal anchor plates in sand. *Journal of Geotechnical Engineering, 114*(11), 1300-1317.

Drucker, D. C., & Prager, W. (1952). Soil mechanics and plastic analysis or limit design. *Quarterly of applied mathematics, 10*(2), 157-165.

Hanna, T. H., Sparks, R., & Yilmaz, M. (1972). Anchor behavior in sand. *J. Soil Mech. Found. Div., Am. Soc. Civ. Eng.;(United States), 98*.

Hardin, B. O., & Black, W. (1968). Vibration Modulus of normally consolidated Clay. *Proceedings of the American Society of Civil Engineers, 94*(SM2), 353-359.

Hinton, E., & Owen, D. R. J. (1986). *Finite elements in plasticity: Theory and practice*: Pineridge Press Limited.

Hofstetter, G., & Taylor, R. (1991). Treatment of the corner region for Drucker-Prager type plasticity. *Zeitschrift für angewandte Mathematik und Mechanik, 71*(6), T589-T591.

Lindsay, J. A. (1980). The use of physical models in design. *Design Parameters in Geotechnical Engineering, 4*, 324-326.

Majer, J. (1955). Zur berechnung von zugfundamenten. *Osterreichische Bauzeitschrift, 10*(5), 85-90.

Matsuo, M. (1967). Study on the uplift resistance of footing (I). *Soils and Foundations, 7*(4), 1-37.

Merifield, R., & Sloan, S. (2006). The ultimate pullout capacity of anchors in frictional soils. *Canadian geotechnical journal, 43*(8), 852-868.

Meyerhof, G., & Adams, J. (1968). The ultimate uplift capacity of foundations. *Canadian geotechnical journal, 5*(4), 225-244.

Mijangos, I., & O'Kelly, K. (2009). Drucker-Prager Finite Element Constitutive Model of Microindentation in Polycrystalline Alumina.

Mors, H. (1959). The behaviour of mast foundations subjected to tensile forces. *Bautechnik, 36*(10), 367-378.

Murray, E., & Geddes, J. D. (1987). Uplift of anchor plates in sand. *Journal of Geotechnical Engineering, 113*(3), 202-215.

Ovesen, N. (1981). *Centrifuge tests of the uplift capacity of anchors.* Paper presented at the Proceedings of the 10th International Conference on Soil Mechanics and Foundation Engineering, Stockholm.

Pietruszczak, S., & Mroz, Z. (1981). Finite element analysis of deformation of strain-softening materials. *International Journal for Numerical Methods in Engineering, 17*(3), 327-334.

Rokonuzzaman, M., & Sakai, T. (2011). Model tests and 3D finite element simulations of uplift resistance of shallow rectangular anchor foundations. *International Journal of Geomechanics, 12*(2), 105-112.

Rowe, R., & Booker, J. R. (1979). A method of analysis for horizontally embedded anchors in an elastic soil. *International Journal for Numerical and Analytical Methods in Geomechanics, 3*(2), 187-203.

Rowe, R., & Davis, E. (1982). Behaviour of anchor plates in sand. *Geotechnique, 32*(1), 25-41.

Sakai, T., & Tanaka, T. (1998). Scale effect of a shallow circular anchor in dense sand. *Soils and Foundations, 38*(2), 93-99.

Sakai, T., & Tanaka, T. (2007). Experimental and numerical study of uplift behavior of shallow circular anchor in two-layered sand. *Journal of geotechnical and geoenvironmental engineering, 133*(4), 469-477.

Sakai, T., & Tanaka, T. (2009). Uplift behavior of circular and square anchor foundations in dense sand. *Doboku Gakkai Ronbunshuu C, 131*, 137.

Sloan, S., & Booker, J. (1986). Removal of singularities in Tresca and Mohr–Coulomb yield functions. *International Journal for Numerical Methods in Biomedical Engineering, 2*(2), 173-179.

Tanaka, T., & Kawamoto, O. (1988). *Three-dimensional finite element collapse analysis for foundations and slopes using dynamic relaxation.* Paper presented at the Proc. of the 6th Int. Conf. on Numerical Methods in Geomechanics.

Vermeer, P. A., & Sutjiadi, W. (1985). The uplift resistance of shallow embedded anchors. *Int. J. Numer. and Anal. Methods in Geomech., 1*, 57-78.

Vesic, A. S. (1969). Breakout resistance of objects embedded in ocean bottom.

Walters, J. V., & Thomas, J. N. (1982). Shear zone development in granular materials. *Proceedings of 4th International Conference on Numerical Methods in Geomechanics*, 263-274.

Zienkiewicz, O., & Pande, G. (1977). Some useful forms of isotropic yield surface for soil and rock mechanics. *Finite elements in geomechanics*, 179-190.